

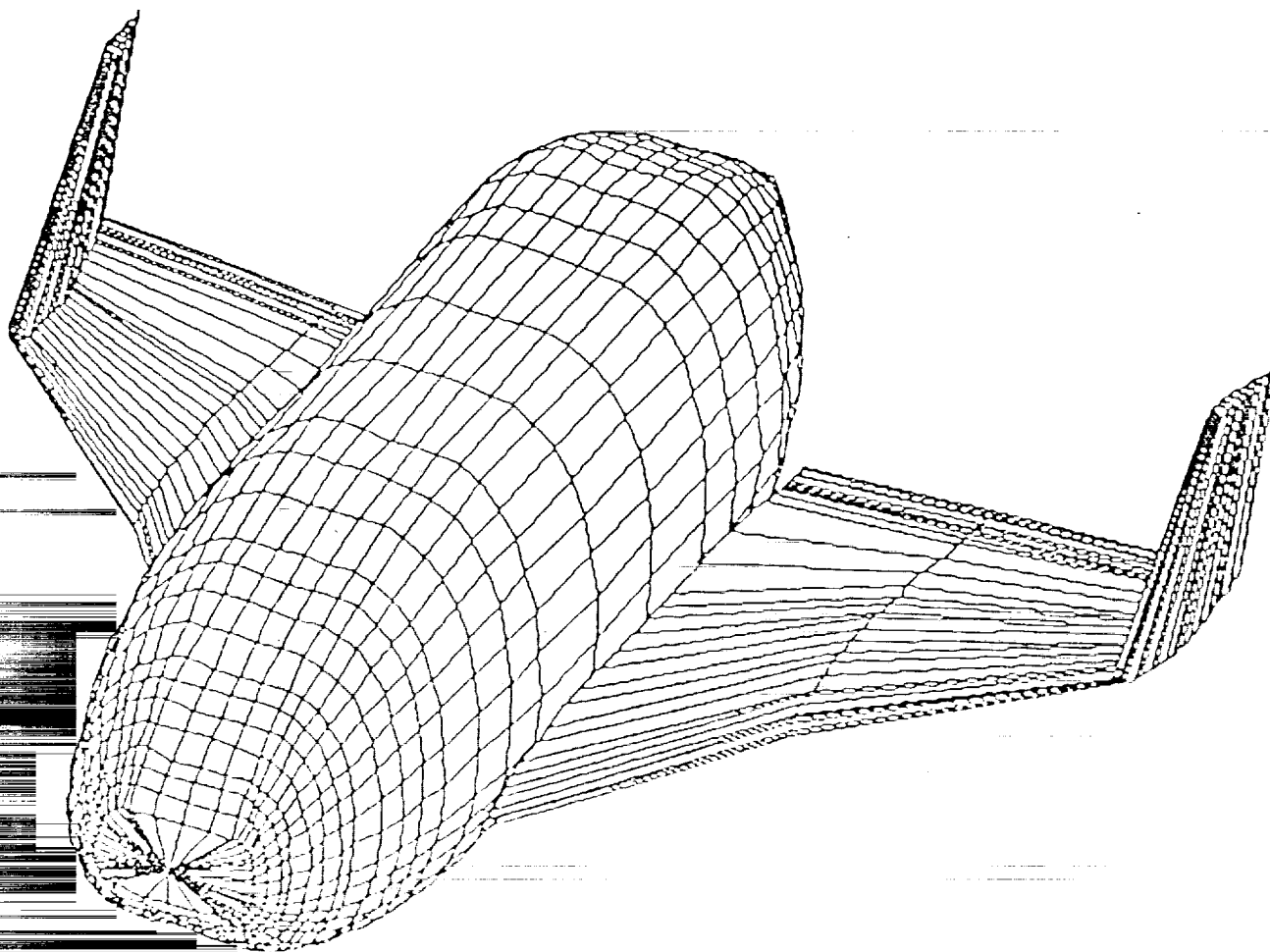
WINGED CARGO RETURN VEHICLE

P-270

Department of Aerospace Engineering & Mechanics
University of Minnesota
Minneapolis, MN

VOLUME I—CONCEPTUAL DESIGN

June 2, 1990



(NASA-CR-186823) WINGED CARGO RETURN
VEHICLE. VOLUME 1: CONCEPTUAL DESIGN
NASA/USRA Advanced Design Project
(Minnesota Univ.) 270 p

N90-26050

CSC 22B

Unclass

G3/18 0295006

NASA/USRA Advanced Design Project

TABLE OF CONTENTS

LIST OF FIGURES	IV
LIST OF TABLES	IX
LIST OF ACRONYMS	X
EXECUTIVE SUMMARY	XII
1.0 SYSTEM INTEGRATION	1
1.1 DESIGN TEAM ORGANIZATION	1
1.2 DESIGN RATIONALE	1
1.3 FINAL CONFIGURATION TRADE STUDY	3
1.4 CONFIGURATIONS CONSIDERED	6
1.5 FINAL CONFIGURATION/RECOMMENDATIONS	6
1.6 SUMMARY OF WINGED CRV	7
2.0 SYSTEMS LAYOUT	13
2.1 DESIGN LAYOUT	13
2.2 MASS PROPERTIES	20
3.0 MISSION OPERATIONS	29
3.1 ASSUMPTIONS, REQUIREMENTS AND DESCRIPTION OF SSF	29
3.2 GROUND OPERATIONS	33
3.3 ASCENT TO RENDEZVOUS WITH THE SSF	38
3.4 COMMAND AND CONTROL ZONE OPERATIONS	41
3.5 DESCENT AND DE-ORBIT	49
3.6 ALTERNATE MISSION PLAN (CRV HARD-DOCK)	53
3.7 ERROR IN PHASE ANGLE	55
3.8 MAN RATING THE CRV	57
3.9 SUMMARY	57
4.0 RE-ENTRY GUIDANCE AND DYNAMICS	59
4.1 FLIGHT PROFILES CONSIDERED	59
4.2 GUIDANCE AND NAVIGATION	65
4.3 PREDICTION OF G-LOADING ON VEHICLE	68
4.4 RANGE CALCULATIONS	70
5.0 AERODYNAMICS	71
5.1 GENERAL AERODYNAMIC CONSIDERATIONS	71
5.2 HABP GEOMETRY INPUT	77
5.3 ANALYSIS METHODOLOGY	81
5.4 SUBSONIC AERODYNAMICS	85
5.5 CANARDS	92
5.6 CONFIGURATIONS CONSIDERED	93
5.7 CONFIGURATIONS CONSIDERED	100
5.8 SUMMARY	111

6.0	STABILITY AND CONTROL	123
	6.1 STABILITY AXES	123
	6.2 EXPLANATION OF S.A.P. AND TECHNIQUES	125
	6.3 STABILITY AND CONTROL REQUIREMENTS	126
	6.4 CONTROLS	128
	6.5 PERFORMANCE ANALYSIS	132
	6.6 LAUNCH INTEGRATION	157
7.0	AVIONICS AND POWER SUBSYSTEMS	161
	7.1 POWER SUPPLY	161
	7.2 CONTROL ACTUATORS	164
	7.3 POWER VS. TIME	165
	7.4 ORBIT TIME AND POWER CONSUMPTION	165
	7.5 AVIONICS	166
	7.6 CAMERAS	170
	7.7 CLOCKS	171
	7.8 MAIN DATA HANDLING COMPUTERS	171
	7.9 ENVIRONMENT CONTROL SYSTEM	171
8.0	THERMAL PROTECTION SYSTEM	175
	8.1 AEROHEATING ANALYSIS	175
	8.2 THERMAL PROTECTION SYSTEM CHOSEN	179
	8.3 MATERIAL AND INSULATION DESCRIPTION	180
	8.4 TPS VEHICLE PLACEMENT	182
	8.5 TPS MOUNTING METHODS AND THERMAL SEALS	182
	8.6 WEIGHT AND COST OF THE TPS	187
	8.7 THERMAL CONTROL OF THE CRV	188
	8.8 DEBRIS PROTECTION SYSTEM	191
	8.8 CONCLUSIONS	191
9.0	PROPULSION	193
	9.1 ORBITAL MANEUVERING SYSTEM	193
	9.2 REACTION CONTROL SYSTEM	197
	9.3 FUEL USAGE AND BURN TIMES	200
	9.4 FUEL TANKAGE AND FEED SYSTEMS NEEDED	200
	9.5 POSSIBLE OMS ENGINE OUT	204
	9.6 NUMBER OF RCS THRUSTERS AND PLACEMENT	205
	9.7 ENGINE SELECTION, OMS, RCS AND COLD GAS	205
	9.8 LAUNCH SYSTEMS	206

10.0 STRUCTURAL ANALYSIS AND DESIGN	211
10.1 WING STRUCTURAL LAYOUT	211
10.2 FORWARD FUSELAGE STRUCTURAL LAYOUT	212
10.3 PAYLOAD BAY AND MID-FUSELAGE STRUCTURAL DESIGN	219
10.4 AFT FUSELAGE STRUCTURAL LAYOUT	223
10.5 THRUST STRUCTURE DESIGN	229
10.6 LANDING GEAR	231
10.7 CRV/LAUNCH VEHICLE INTERFACE DESIGN	231
10.8 DEBRIS PROTECTION SYSTEM	234
10.9 STRUCTURAL ANALYSIS	235
11.0 DESIGN OPTIMIZATION AND COST ANALYSIS	237
11.1 OPTIMIZING BACKGROUND	237
11.2 METHODS OF OPTIMIZING	237
11.3 OPTIMIZATION OF SYSTEMS	239
11.4 FUTURE OPTIMIZATION PROBLEMS	252
LIST OF REFERENCES	253

LIST OF FIGURES

Figure 1-1	Organization Chart	2
Figure 1-2	CRV on Launch Pad	10
Figure 1-3	PLOG and UnPLOG	11
Figure 2-1	Trade Study Configuration	14
Figure 2-2	Wing Drawing	16
Figure 2-3	RCS/OMS	17
Figure 2-4	Avionics Drawing/SPIDS	18
Figure 2-5	Structural Drawing	19
Figure 2-6	C.G. Envelope for UNPLOG (ft.)	25
Figure 2-7	C.G Envelope for UNPLOG (% M.A.C.)	25
Figure 2-8	C.G Envelope for PLOG (ft.)	26
Figure 2-9	C.G Envelope for PLOG (%M.A.C.)	26
Figure 2-10	Moment Of Inertia vs. Total Launch Weight	27
Figure 2-11	Moment Of Inertia vs. CRV Landing Weight	28
Figure. 3-1	Space Station Freedom	32
Figure. 3-2	Phasing Orbit	39
Figure. 3-3	Hohmann Transfer	40
Figure. 3-4	Mission Profile Ascent for Rendezvous	42
Figure. 3-5	Mission Profile Ascent for Rendezvous Alt.vs. Time	42
Figure. 3-6	Phase Angle Correction Time at 110NMI	43
Figure. 3-7	Phase Angle Correction Time at 210NMI	43
Figure. 3-8	Payload Disconnect Mechanism	47
Figure. 3-9	Reposition Orbit	50
Figure. 3-10	CRV Proximity Operations	51
Figure. 3-11	Mission Profile Descent to Re-entry	51
Figure. 3-12	Mission Profile Descent to Re-entry Alt.Vs.Time	52
Figure. 3-13	Ground Track	52
Figure. 3-14	Time Required Vs. Delta-V	56
Figure. 3-15	Correction Angle Vs. Delta-V	56
Figure 4-1	Landing Foot Print	59
Figure 4-2		
Figure 4-3		
Figure 4-4	Angle of Attack for Imp Simulations	61
Figure 4-5	Angle From Re-entry Point to Landing Sites	62
Figure 4-6	Latitude calculated Using IMP	63

Figure 4-7	Longitude calculated Using IMP	64
Figure 4-8	Atmospheric Re-entry	66
Figure 4-9	Beginning of S- Turns	67
Figure 4-10	Auto Land Sequence	69
Figure 4-11	Change in G-Loading During Banking	70
Figure 5-1	HABP Coordinate Axis-Isometric View	78
Figure 5-2	CRV Control Surface Neutral Position	80
Figure 5-3	Wedge Type Control Surface	80
Figure 5-4	Two-Airfoil Control Surface	80
Figure 5-5	Bent-Airfoil Control Surface	81
Figure 5-6	Surface Pressure Distribution Over A Parabola	83
Figure 5-7	Comparison Between Newtonian and Exact Results for Pressure Coefficients	84
Figure 5-8	Shadow Region on Leeward-Side of Body	84
Figure 5-9	ULTIMATE Models	87
Figure 5-10	Induced Drag vs. Angle of Attack	89
Figure 5-11	Lift/Drag vs. Angle of Attack	89
Figure. 5-12	Cl vs. Angle of Attack, CRV and Shuttle	91
Figure. 5-13	Cdi vs. Angle of Attack, CRV and Shuttle	91
Figure. 5-14	L/D vs. Angle of Attack, CRV and Shuttle	92
Figure. 5-15	Trade Study Configuration	97
Figure. 5-16	Baseline Configuration	98
Figure. 5-17	Fixed Canard Option	99
Figure. 5-18	Trade Study vs. HABP Body Shape	99
Figure. 5-19	Baseline Comparison - AIREZ vs. HABP	102
Figure. 5-20	Max. L/D vs, Mach -Baseline Config.	102
Figure. 5-21	Vertical Tail With Variable Winglets Configuration	103
Figure. 5-22	Vertical Tail Only Configuration -Split Rudder	106
Figure. 5-23,24	Configuration Comparisons	107
Figure. 5-25	Strake Vortex Shedding -Vortex Lift	110
Figure. 5-26	Max. L/D vs. Mach - Wingtip Fin Config.	112
Figure. 5-27	L/D vs AOA -Wingtip Fin Config.	112
Figure. 5-28,29	Strake Comparison - Wingtip Fin Config.	113
Figure. 5-30,31	AIREZ vs. HABP - Wingtip Fin Config.	114
Figure 5-32	Final Configuration - Isometric View	115
Figure 5-33	Final Configuration - Top View	116
Figure 5-34	Final Configuration - Side View	117

Figure 5-35	Final Configuration - Bottom View	118
Figure 5-36	Final Configuration - Front View	119
Figure 5-37	Final Configuration - Back View	119
Figure 5-38	CRV - No Strake	120
Figure 5-39	Final Configuration - Front View (Alpha = 35 deg.)	121
Figure 6-1	Generalized Configuration Geometry for Hypersonic Stability Derivative Approximation	124
Figure 6-2	Axes used for atmospheric stability analysis of the winged CRV.	125
Figure 6-3	Thrust location of RCS	130
Figure 6-4	On orbit Control Law	130
Figure 6-5	Ascent OMS Control Law	131
Figure 6-7	"Bang-bang" Control Law With Negative Feedback	132
Figure 6-8	Root Locus of Transfer Functions of Varying Gain	133
Figure 6-9	$C_{m\alpha}$ vs Mach	135
Figure 6-10	Location of Subsonic and Supersonic Vehicle Neutral and Maneuver Points	136
Figure 6-11	Angle of Attack Envelope vs. Mach Number	139
Figure 6-12		
Figure 6-13	Dihedral Effect (M = 2.8)	141
Figure 6-14	Dihedral Effect (M = 7.2)	142
Figure 6-15	Dihedral Effect (M = 8.2)	142
Figure 6-16	Dihedral Effect (M = 11.7)	143
Figure 6-17	C_{lB} vs. Alpha	143
Figure 6-18	Breakdown of C_{lB} Contributions	145
Figure 6-19	Weathercock Stability (M = 2.8)	146
Figure 6-20	Weathercock Stability (M = 7.2)	146
Figure 6-21	Weathercock Stability (M = 8.2)	147
Figure 6-22	Weathercock Stability (M = 11.77)	147
Figure 6-23	Weathercock Stability (M = 17.2)	148
Figure 6-24	Breakdown of C_{nB} Contributions	149
Figure 6-25	Variation of C_{yr} vs. M and Alpha	151
Figure 6-26	Effect of 6 Degree Toe-in	152
Figure 6-27	Body Flap Deflection	152

Figure 6-28	Side Slip Angle vs. Mach Number	153
Figure 6-29	Operational C.G. Envelope	155
Figure 6-30	Resultant Forces and Moments on Launch Assembly	159
Figure 6-31a,b	Flight Envelopes for the Integrated Launch Vehicle	160
Figure 7-1	Power Supply Decision Matrix	162
Figure 7-2	Power System Schematic	166
Figure 7-3	Avionic System Schematic	169
Figure 7-4	Cooling System Schematic	173
Figure 8-1	Angle of Attack vs. Time	177
Figure 8-2	Nose Temp. vs. Time	177
Figure 8-3	Leading Edge Temp. vs. Time	178
Figure 8-4	Bottom Wing Temp vs. Time	178
Figure 8-5	Wing Tip Temp vs. Time	179
Figure 8-6	Temperature Gradient	181
Figure 8-7	TPS Placement	183
Figure 8-8	Void-Free Laminate Construction	187
Figure 8-9	Forced Convection Concept	190
Figure 9-1	RCS/OMS Schematic	201
Figure 9-2	Side View Fore RCS	202
Figure 9-3	Cross-sectional view, aft sys.	202
Figure 9-4	Side View, Aft Systems	203
Figure 9-5	SSME Specifications	207
Figure 9-6	Launch System	209
Figure 10-1	Three Dimensional Wing Structure	213
Figure 10-2	Front Fuselage Side View	214
Figure 10-3	Skin/Stringer Combination	214
Figure 10-4	Front Fuselage Support Frame and Cross-Section	215
Figure 10-5	Modified Support Frame	217
Figure 10-6	Mid Fuselage Components	218
Figure 10-7	Payload Bay Truss Frame	220
Figure 10-8	T-Section and Tubular Truss Members	221
Figure 10-9	Sill Longeron and Corner Longeron Cross-Section	221
Figure 10-10	Forward Bulkhead and Base Heat Shield	225
Figure 10-11	Aft Fuselage Frames	227
Figure 10-12	Aft Fuselage Structural Dimensions	228

Figure 10-13	Aft Fuselage Frame and Thrust Structure	230
Figure 10-14	Bottom View Gear Placement	232
Figure 10-15	Front and Side Views Gear Deployed	232
Figure 10-16	CRV/Launch Vehicle Interface-Side View	233
Figure 10-17	CRV/Launch Vehicle Interface-Top View	233
Figure 10-18	Structural Analysis Model	236
Figure 11-1	Vertical Members of CRV/Booster Interface and Optimization Equation	240
Figure 11-2	CRV/Booster Interface(Titanium)	242
Figure 11-3	CRV/Booster Interface(Aluminum, Stainless Steel, & Titanium)	242
Figure 11-4	Propellant Tank	244
Figure 11-5	Dry Tank Weights	247
Figure 11-6	Feedlines	248
Figure 11-7	Dry Feedline Weights	251
Figure 11-8	Total Dry Weights of systems	251

LIST OF TABLES

Table 1-1	CRV Physical Characteristics	8
Table 1-2	Performance Characteristics	8
Table 2-1	CRV Preliminary Weight Statement	21
Table 2-2	CRV Finalized Weight Statement	22
Table 3-1	Mission Profile	44
Table 3-2	SPDS Rotation Time	48
Table 5-1	ULTIMATE Output	88
Table 5-2	AIREZ Trade Study and HABP L/D Data	101
Table 6-1	Dead Band Ranges	129
Table 6-2	Vehicle parameters used for analysis of the three configurations:	137
Table 6-3	Minnemac results	138
Table 6-4	Points for Analysis of Stability and Control	141
Table 6-5	Comparison of $C_{l\beta}$	144
Table 6-6	Summary of $C_{l\beta}$ contributions from Mach 2.8 to Mach 17.2	145
Table 6-7	Comparison of $C_{n\beta}$	148
Table 6-8	Minnemac Dynamic Analysis	150
Table 6-9	Aerodynamic Force and Moment Reference Dimensions	156
Table 8-1	Weight Breakdown of the TPS	187
Table 9-1	Cold Gas Data Table	194
Table 9-2	Reaction Control System	195
Table 9-3	Orbital Maneuvering System	196
Table 9-4	Cold Gas Comparison	198
Table 9-5	Fuel Usage and Burn Times	200
Table 9-6	Tank Specifications	204
Table 10-1	Front Fuselage Component Weights	219
Table 10-2	Mid Fuselage Component Weights	223
Table 11-1	OMS SYSTEM - tanks	245
Table 11-2	COLD GAS SYSTEM - tanks	246
Table 11-3	RCS SYSTEM - tanks	246
Table 11-4	OMS SYSTEM - feedlines	249
Table 11-5	RCS SYSTEM - feedlines	250
Table 11-6	COLD GAS SYSTEM - feedlines	250

LIST OF ACRONYMS

ACRV	ASSURED CREW RETURN VEHICLE
AOA	ANGLE OF ATTACK
AVF	ARTIFICIAL VISION FUNCTION TRACKING MODE
CCZ	COMMAND AND CONTROL ZONE
CRV	CARGO RETURN VEHICLE
DIU	DIGITAL INTEGRATING UNIT
DME	DISTANCE MEASURING EQUIPMENT
EAFB	EDWARDS AIR FORCE BASE
ECS	ENVIRONMENTAL CONTROL SYSTEM
EVA	EXTRA VEHICULAR ACTIVITY
GCC	GROUND CONTROL CONSOLES
GN2	NITROGEN GAS
GN&C	GUIDANCE, NAVIGATION AND CONTROL
GPS	GLOBAL POSITIONING SYSTEM
GSC	GROUND SUPPORT COMPLEX
GSFC	GODDARD SPACE FLIGHT CENTER
HABP	HYPERVELOCITY ARBITRARY BODY PROGRAM
H ₂	HYDROGEN
H/X	HEAT EXCHANGER
HYMAT	HIGHLY MANEUVERABLE AIRCRAFT TESTING
IMP	INTEGRATED MISSION PROGRAM
IMU	INERTIAL MEASURING UNIT
JSC	JOHNSON SPACE CENTER
KSC	KENNEDY SPACE CENTER
LAD	LIQUID ACQUISITION DEVICE
L/D	LIFT/DRAG
LDEF	LONG DURATION EXPOSURE FACILITY
l.e	LEADING EDGE
LM	LOGISTICS MODULE
LRB	LIQUID ROCKET BOOSTER
MA	MACH NUMBER
MCC	MISSION CONTROL CENTER
MLS	MICROWAVE LANDING SYSTEM
MMH	MONOMETHYL HYDRAZINE
MSBLS	MICROWAVE SCAN BEAM LANDING SYSTEM
MSS	MOBILE SERVICING SYSTEM
MTU	MASTER TIMING UNIT
NACA	NATIONAL ADVISORY COMMITTEE ON AERONAUTICS
N ₂ H ₄	HYDRAZINE

NTO	NITROGEN TETROXIDE
O ₂	OXYGEN
OMS	ORBITAL MANEUVERING SYSTEM
OMV	ORBITAL MANEUVERING VEHICLE
OMVCC	ORBITAL MANEUVERING VEHICLE CONTROL CENTER
OPF	ORBITER PROCESSING FACILITY
OPM	ORBITAL POSITIONING MECHANISM
OSC	OPERATION SUPPORT CENTERS
PDA	PAYLOAD DISCONNECT ASSEMBLY
PDM	PAYLOAD DISCONNECT MECHANISM
PLOG	PRESSURIZED LOGISTICS MODULE
POCC	PAYLOAD OPERATION CONTROL CENTER
PTZ	PAN-TILT-ZOOM
RCC	REINFORCED CARBON-CARBON
RCS	REACTION CONTROL SYSTEM
RGDM	REMOTE GRAPPLE DOCKING MECHANISM
ROEU	REMOTELY OPERATED ELECTRICAL UMBILICAL
SB	SECONDARY BURN
SLF	SHUTTLE LANDING FACILITY
SPDS	STABILIZED PAYLOAD DEPLOYMENT SYSTEM
SRB	SOLID ROCKET BOOSTER
SSF	SPACE STATION FREEDOM
SSP	SPACE STATION PROGRAM
SSRMS	SPACE STATION REMOTE MANIPULATOR SERVICER
SSSC	SPACE STATION SUPPORT CENTER
TACAN	TACTICAL AIR NAVIGATION STATION
TAEM	TERMINAL AREA ENERGY MANAGEMENT
t.e.	TRAILING EDGE
TI	INITIAL THRUST
TF	TERMINAL BRAKING MANEUVER
TPS	THERMAL PROTECTION SYSTEM
TDRSS	TRACKING DATA RELAY SATELLITE SYSTEM
TPDM	THREE POINT DOCKING MECHANISM
UPLOG	UNPRESSURIZED LOGISTICS MODULE
VAB	VERTICAL ASSEMBLY BUILDING

Executive Summary

The Advanced Design Project (ADP) allows an opportunity for students to work in conjunction with NASA and other aerospace companies on NASA Advanced Design Projects. The following volumes represent the design report:

- Volume 1 Conceptual Design
- Volume 2 Wind Tunnel Tests
- Volume 3 Structural Analysis
- Volume 4 Water Tunnel Tests

CRV Justification and Fleet Structure

The project chosen by the University of Minnesota in conjunction with NASA Marshall Space Flight Center for this year is a Cargo Return Vehicle (CRV) to support the Space Station Freedom. The vehicle is the third generation of vehicles to be built by NASA, the first two being the Apollo program, and the Space Shuttle program. The CRV is to work in conjunction with a personnel launch system (PLS) to further subdivide and specialize the vehicles that NASA will operate in the year 2000. The cargo return vehicle will carry payload to and from the Space Station Freedom (SSF).

1.0 SYSTEMS INTEGRATION

This conceptual design study concerns the design of a Winged Cargo Return Vehicle. The trade study concerning this vehicle was made in the fall of 1989 by the senior students of the University of Minnesota Design Class for the NASA/USRA Advanced Design Project. The projected vehicle is required to meet the logistics needs of the Space Station Freedom which will begin operation in the mid-nineteen nineties.

The intended mission for the cargo return vehicle (CRV) is to launch from Kennedy Space Center carrying cargo modules to a 220 nautical mile circular orbit and rendezvous with the Space Station, where it will transfer its payload. The CRV would then return to Earth with any payload or empty modules. Once inside the atmosphere the CRV would glide down and land at Kennedy Space Center, or any other runway which is at least 10,000 feet in length. The payload would then be off-loaded and the CRV reprocessed for another mission.

1.1 Design Team Organization

The Winged Aerospace Design Team was broken down into 11 different discipline groups. Each discipline group was responsible for their individual parts of the design and performance analysis of the CRV. The groups were organized under two headings Hardware and Performance (see Fig. 1-1).

1.2 DESIGN RATIONALE

With the planned operation of the Space Station Freedom beginning in the mid-nineteen nineties a logistics shortfall will occur in supporting a permanent manned contingency in orbit. This shortfall and the availability of new technologies have lead to investigations in third generation spacecraft. The Cargo Return Vehicle (CRV) was to fill the need for a reusable unmanned supply vehicle.

DESIGN TEAM ORGANIZATION

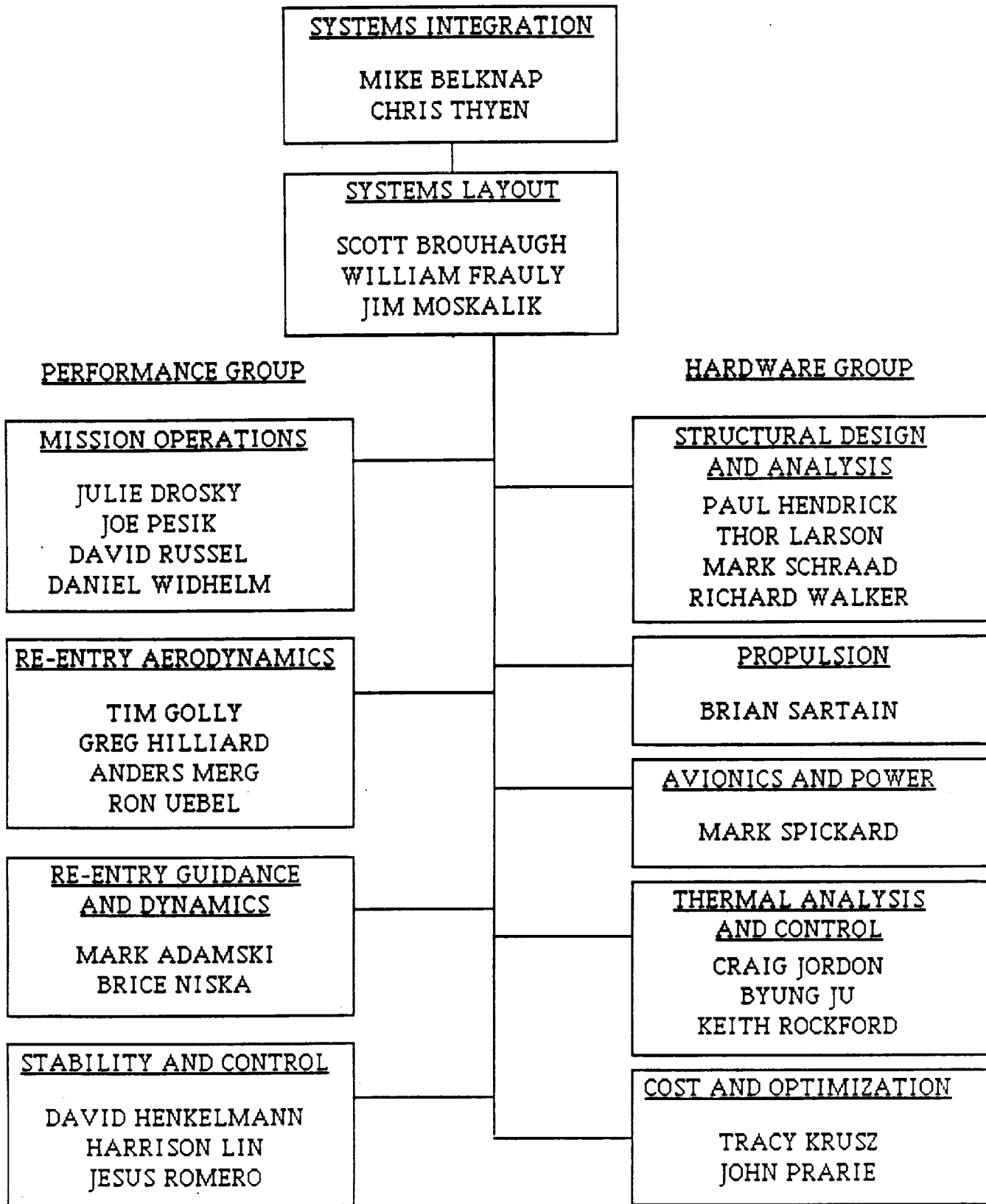


Fig. 1-1 Design Team Organization

DESIGN REQUIREMENTS

1. Years of service, 2000-2020
2. Must be able to perform its mission unmanned
3. The CRV must be dry land recoverable
4. The CRV must use Space Shuttle attachment methods
5. Must be a reusable vehicle
6. Must be capable of reaching SSF orbit of 220 x 220 nmi. with an inclination of 28.5 degrees.
7. Must have a minimum cross range of 1000 nmi
8. Minimum on orbit time is 34 hours
9. Minimum turnaround time is 172 hours
10. CRV must be able to maintain an internal temperature range of 40 to 90 degrees Fahrenheit
11. Must be able to land on a 10,000 foot runway
12. Primary landing site Kennedy Space Center
13. Must meet all NASA design requirements
14. Must be designed around military and/or industrial standards when applicable.
15. All payload must be carried in either the Pressurized Logistics Module (food, clothing, experiments, etc - docks with the Space Station) or the Unpressurized Logistics Module (fluids and dry cargo not needed within the space station).

1.3 FINAL CONFIGURATION TRADE STUDY

1.3.1 Configuration

The original basis of the vehicle was derived from the. The overall length was 76 feet, which was divided into three main sections: nose cone, cargo bay, and tail cone.

The nose cone length was set at twenty-seven feet using the AIREZ program. Keeping the body shape constant the nose cone length and droop was varied. A twenty-seven foot nose section with a two foot droop was chosen because it gave reasonable L/D performance at a minimum length.

The cargo bay was sized so as to fit one Pressurized Logistics Module (PLOG) and one Unpressurized Logistics Module (UNPLOG). The overall length of the cargo bay was set at 30 feet. The cargo bay is protected by a two bulkheads 2 feet in length, one in the front of the

bay and one behind the bay. The third major section of the winged CRV was the tail cone. The tail cone was designed to contain one Orbital Maneuvering System (OMS) engine to transfer the CRV from 110 nautical miles to rendezvous orbit with Space Station Freedom (SSF). The rear hardpoint will be located six feet up from the rear tip of the cone. The hardpoint is a structural mounting position for the single OMS engine. The general body cross-section shape is a circular top portion, with vertical sides and a flat bottom.

1.3.2 Avionics, Communications, and Power

The winged CRV is expected to be unmanned, have long mission times, and be reusable. These requirements call for a power supply that is reliable, versatile, and cost effective. The power for the CRV will be provided by two systems. Batteries will supply the energy to power the electro-servo actuators used on various control surfaces and the cargo bay doors. The other system to be used is Fuel Cells to power the avionics, communication and navigation systems. Current fuel cells produce a power supply of 7 KW continuous and 12 KW peak. The fuel cells are self cooling units with their own fuel and oxidizer supply.

Avionics would be placed in the forward bay and in the aft cargo bay in order to allow easy access. The avionics is subdivided into the systems: guidance, navigation, control, communications, and tracking. Most of these systems are similar to those employed on the Space Shuttle. Communications will be carried on S, KU, L, and C band frequencies. Telemetry data will be sent by the S band. Vehicle control information will be sent to the main computers during flight by ground control and by the Space Station Freedom when within its control zone. For inertial measuring, two Ring Laser Gyro inertial measurement units will be used. The Global Positioning System (GPS) will be used to find position and velocity with respect to the Earth. The Guidance and Navigation systems chosen include the Global Positioning System (GPS), Inertial Measuring Units (IMU), and a Star Tracker system. The Communications and Tracking will be provided by the Tracking and Data Relay Satellite System (TDRSS). The Flight Control systems chosen were; a Microwave Scan Beam Landing System (MSBLS) in order to allow the CRV to Auto Land, Radar Altimeter is to provide data for the landing system in case of an emergency override, and cameras for use in the SSF proximity operations, as well as, for an emergency manual landing.

1.3.3 Thermal Protection System

The Thermal Protection System (TPS) was chosen on the basis of thermal limits on the vehicle's inner structures, reusability, low cost, and low maintenance. The main materials used include: Reinforced Carbon/Carbon for high heating areas such as the nose and wing leading edges, Fibrous Refractory Composite Insulation for areas of lower heating, and Tailorable Advanced Blanket Insulation for the lowest heating areas such as the top and sides of the vehicle.

1.3.4 Propulsion Systems

The booster system will utilize a liquid rocket booster system consisting of a core, with two Space Shuttle Main Engines (SSME), and two boosters on either side. This will allow the CRV to deliver a payload of over 44,000 lbs and will deliver the CRV to a 100 nmi. insertion orbit. The design calls for this to be an in-line arrangement.

The on board propulsion consists of two main systems: Orbital Maneuvering System(OMS) and Reaction Control System(RCS). The OMS system consists of one OMS engine which is responsible for moving the CRV from the 110 nmi insertion orbit to the 220 nmi SSF orbit. The other main system is the RCS system which will be used for controlling the attitude of the CRV during re-entry, as well as, maneuvering in and around the SSF control zone. The RCS thrusters are broken down into two separate systems in order to accommodate the ability of the CRV to hard dock with SSF.: a cold gas N₂ is used for proximity operations to the SSF, and a system fueled by Nitrogen Tetroxide/Monomethyl Hydrazine(NTO/MMH) to maneuver outside the zone. The two systems consists of 24 and 28 thrusters respectively.

1.3.5 Control Systems

There are two different control systems used during the CRV's mission. The RCS thrusters are used during the on-orbit phase of the mission, as well as, the re-entry phase. The other system used consists of basic aerodynamic control surfaces which are powered by electro-servo actuators.

1.3.6 Structural Materials

The structure of the CRV consists of three main materials. TA2219 Aluminum was used for the major structural members of the vehicle (i.e., wing spars, cargo bay supports and bulkheads), and TA2024 Aluminum was used for the skin of the vehicle. Graphite/Epoxy composites are used for the Cargo Bay Doors.

1.4 CONFIGURATIONS CONSIDERED

The CRV was designed for the case of not having the Advanced Launch System which was down scaled due to lack of Federal funding. This change made the maximum allowable lift-off weight 108,000 lbs. Additionally, the availability of the Orbital Maneuvering Vehicle (OMV) was questioned.

The lack of the OMV changed the trade study mission operations from allowing standoff payload transfers to the need to hard-dock with SSF. This single change altered the CRV so that it had to fulfill NASA's requirements of operations within the sphere of influence of SSF. As a result, many systems were designed with options for use in either scenarios.

1.5 AREAS FOR FUTURE STUDY

Three main areas are open for future study, they include: Stability and Control, Cost and Optimization, and Structural Analysis.

The Structures group in the next phase of the study will use the NASTRAN computer program to analyze and optimize the design of the CRV sub-structure (see Volume 3). Up to this point only an elementary analysis has been performed.

The Optimizations group will be concerned with finding the fleet size of the Winged CRV.

Stability and Control will use data obtained from wind and water tunnel tests to obtain better estimates of the aerodynamic derivatives used in calculating the vehicles performance.

1.6 SUMMARY OF WINGED CRV

The Winged CRV has the following characteristics (Table 1-1 and Table 1-2):

Table 1-1, CRV Physical Characteristics

Body Length	76 ft
Wing Span	58.0ft
Winglet height	10.5 ft
Frame Materials	Aluminum TA-2219 Alloy
Nose Section Length	27.0 ft
Fuselage Section Length	30.0 ft
Tail Section Length	18.0 ft
Power System	
Type	Fuel Cells
Number	3
Peak Output	12 kw
Continuous Output	7 kw
Actuator Power System	
Type Actuator	Electro-Mechanical
Type of Power System	Nickel Cadmium Rechargeable Batteries
CRV Engines	
A. Orbital Manuevering System Eng.	1
Type	Aerojet AJ10-190
Thrust (vac)	6000 lbf
B. Reaction Control System Engines	52
1. Type	28-NTO/MMH 24-Cold Gas
Thrust (vac)	NTO/MMH (used on Space Shuttles)
2. Type	400 lbf
Thrust (vac)	Cold Gas 50 lbf

Table 1-1, CRV Physical Characteristics (cont.)

Cargo Bay and Payload

Cargo Bay Length	30 ft
Cargo Bay Diameter	9.8 ft
Dry Weight	61,596 lbs
Payload to LEO	44,416 lbs
Consumables	5,568 lbs
Landing Weight	106,012 lbs

Launch Vehicle

Description	2-LRB 1-Core Booster
CRV Mounting	Inline Mounting
A. Liquid Rocket Booster Engines	5
Type	Space Shuttle Main Engines
Thrust	
B. Core Booster Engines	2
Type	Space Shuttle Main Engines
Fuel	Liquid Hydrogen
Oxidizer	Liquid Oxygen
Payload to LEO	113,000 lbs
Max Load	4.00 g's

Table 1-2, Performance Characteristics

Wing Characteristics

Wing Modeled On	NACA-64010
L/D (Subsonic)	5.96
L/D (Supersonic)	1.58
L/D (Hypersonic)	1.49
Sweep Angle (Outboard)	54 deg.
Sweep Angle (Inboard)	70 deg.
S	1671 ft ²
Winglet toe-in	6 deg.
Fin Taper	0.34

Table 1-2 Performance Characteristics (cont.)

Stability Characteristics

Root Chord Length	46.95 ft
Mean Aerodynamic Chord	33.44 ft
Supersonic Neutral Point	53.40 ft aft of nose
Subsonic Neutral Point	45.05 ft aft of nose

Re-Entry Characteristics

Cross Range	1351 nmi
Downrange	5291 nmi
Bank Angle (Optimal)	47.8 deg.
Maximum G-Loading	2.4 g's
Angle of Attack	25 deg.

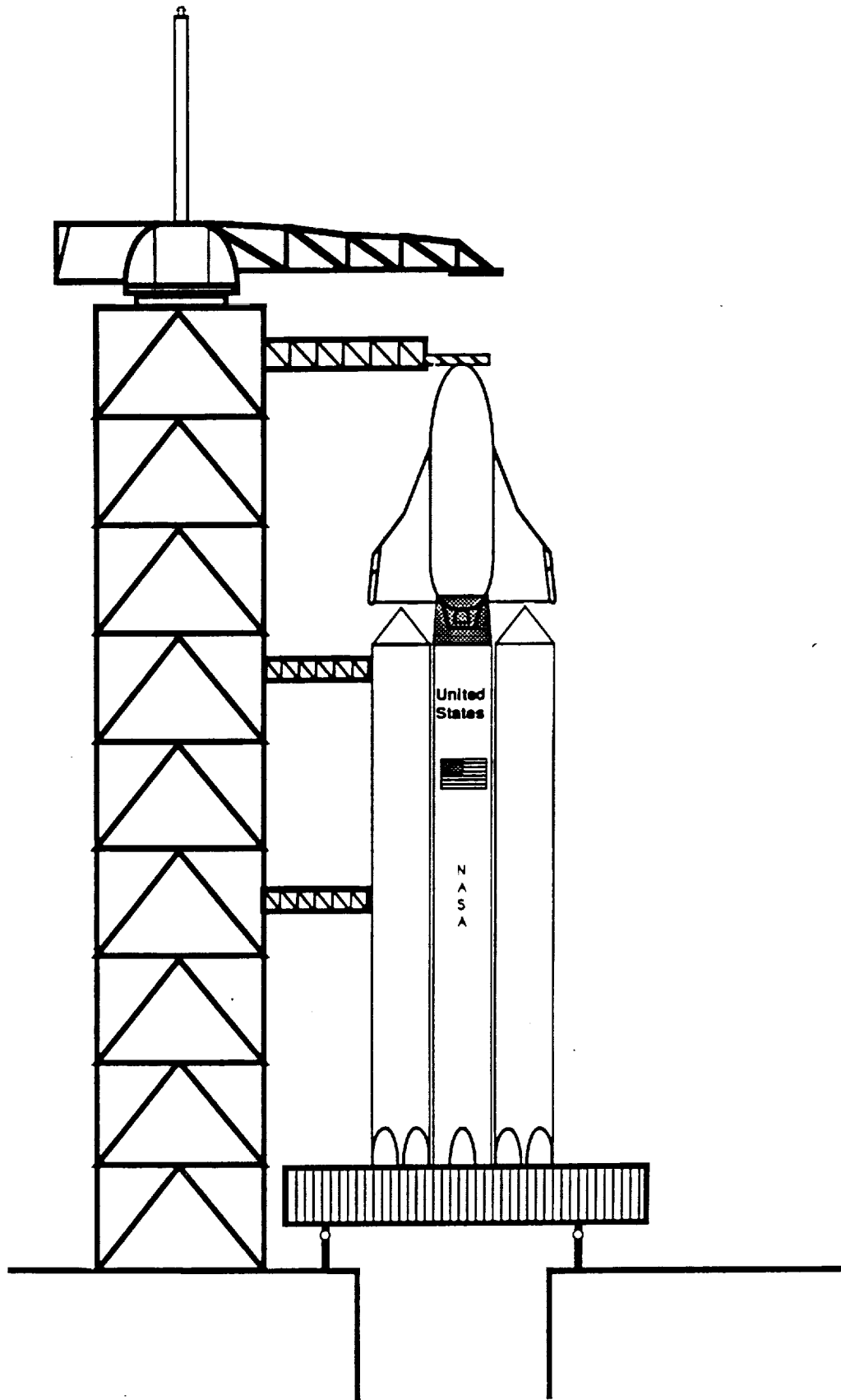
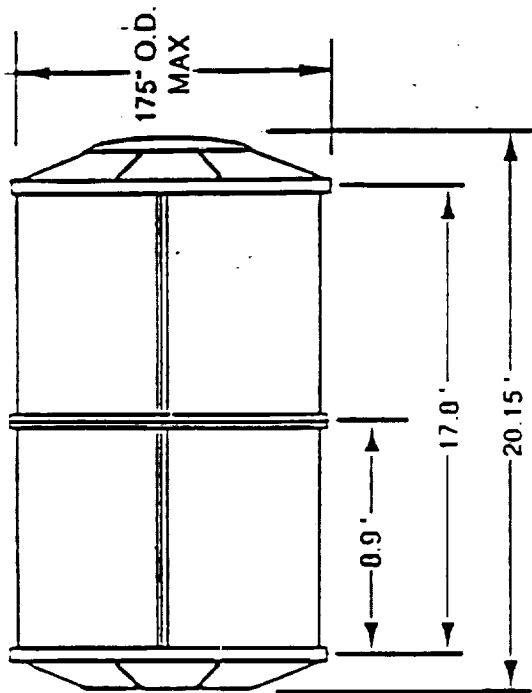
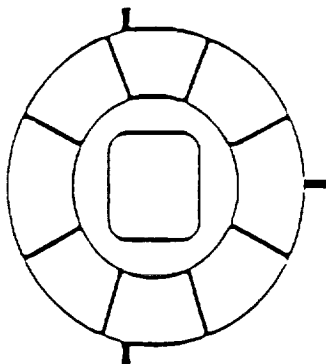


Figure 1-2 CRV on Launch Pad

Pressurized Logistics Module



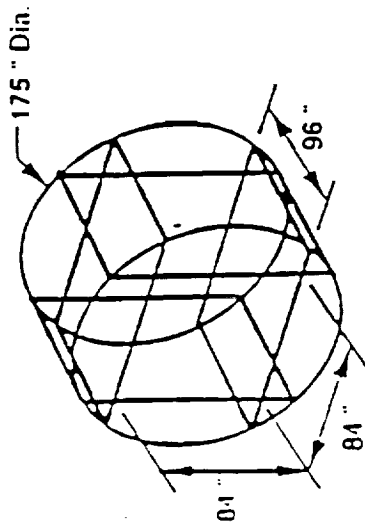
FWD

NOT TO SCALE

Empty Weight - 14,590 lb
Cargo Capacity - 22,600 lb

Unpressurized Logistics Modules

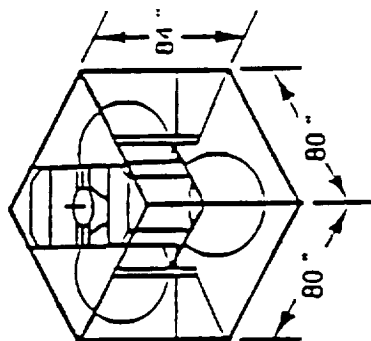
Basic Carrier



Note: This is a frame on which the subcarriers are mounted

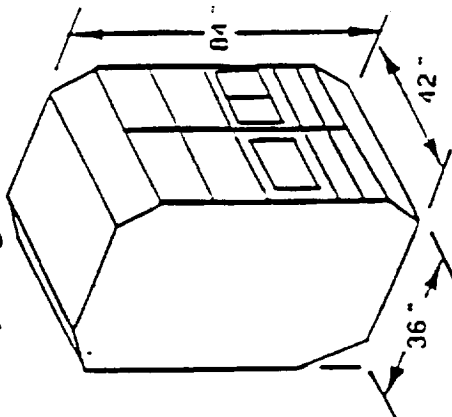
Empty Weight - 2,400 lb
Cargo Capacity - 16,000 lb

Fluids Subcarrier



Empty Weight - 1,670 lb
Cargo Capacity - 2,338 lb

Dry Cargo Subcarrier



Empty Weight - 194 lb
Cargo Capacity - 1,500 lb

Fig. 1-3 Pressurized and Unpressurized Logistics Modules

THIS PAGE HAS BEEN LEFT INTENTIONALLY BLANK

2.0 SYSTEMS LAYOUT

The Systems Layout Group divided its function into two sub-sections: Design Layout and Mass Properties.

The layout in this report represents the results of the efforts put forth to complete the vehicle's third design iteration. Since it would be very difficult to show all of the intermediate steps that led to this design, the major developments of each design area will be explained in addition to the vehicle diagrams. The layout of the final CRV configuration is a compilation of the contributions of all the design disciplines.

2.1 DESIGN LAYOUT

The Design Layout was divided into three main sections: basis drawings, component or subsystem drawings, and subsystem placement. The basis drawings are drawings of the overall external profile of the Winged CRV: body, wings, fins and tail assembly. The component drawings are more explicit drawings of the individual components, their location, physical attributes, and their relationship with the overall CRV. The subsystem weight/location table contains placement information for the various subsystems or components.

2.1.1 Basis Drawings

The original basis drawings were taken from the trade study proposed configuration figure 10-1. Several changes were made to this initial configurations based on aerodynamics, structures, and thermal protection considerations until the final configuration as shown in figure 10-2 was arrived at.

2.1.2 Component Drawings

The component drawings were assembled using a layerung option available on the CAD software utilized. The components were placed based on a compromise between two criteria:

1. The location of the application of the component.
2. The location to obtain a optimal center of gravity.

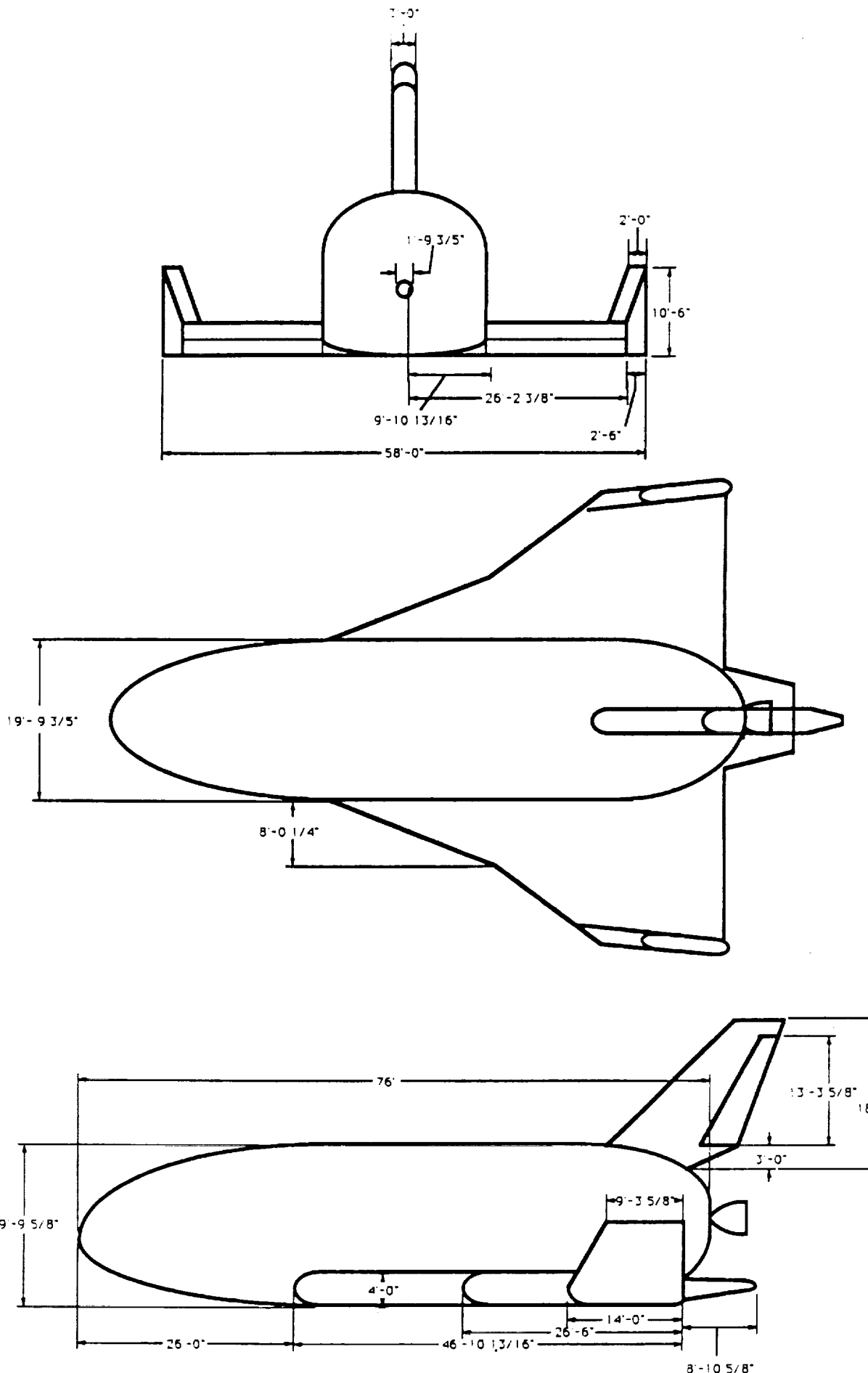


Figure 2-1 Trade Study Configuration

The OMS and RCS systems were added to the basis drawing using data obtained from the Propulsion discipline. The RCS system configuration changed to accommodate the possibility of not having an OMV. This change was to add a cold gas tank to the system (see fig. 2-5).

The avionics and power systems were added in and about the cargo bay. The fuel cells and battery packs were placed in the front of the cargo bay, under the cargo support tracks. This location was used so as to give the best accessibility for service and even more importantly, refueling. The avionics systems are mounted to the front of the docking module bay, and in avionics trays toward the aft of the main cargo bay.

In the cargo bay, SPIDS devices were added along the edges of the inner bay door. These devices are to be used in the event that the OMV is available.

A set of cargo latches were added along the cargo rails for use in securing the cargo to the cargo rails and bay. The cargo rails were placed in the cargo bay running from the front to the back., each located three feet off the center line of the vehicle. (see fig.2-6)

A docking mechanism was added to the CRV accommodate the loss of the use of the OMV. The docking module was placed just ahead of the cargo bay, in a separate compartment. This option was selected to leave room in the cargo bay for both an UNPLOG and a PLOG, as well as providing better accessibility for the Remote Manipulator System (RMS) of the space station. The separate bay was also selected so that if the Orbital Maneuvering Vehicle (OMV) were to be used, the docking module could be taken out and the bay could accommodate other equipment, such as extra Orbital Maneuvering System (OMS) or Reaction Control System (RCS) tanks to extend the capable mission time. The docking module bay will have one door which is servo driven.

The largest addition to the overall basis drawing was the structure. The placement of the structural network was dependant on the loading of the CRV as a whole, during launch and re-entry.

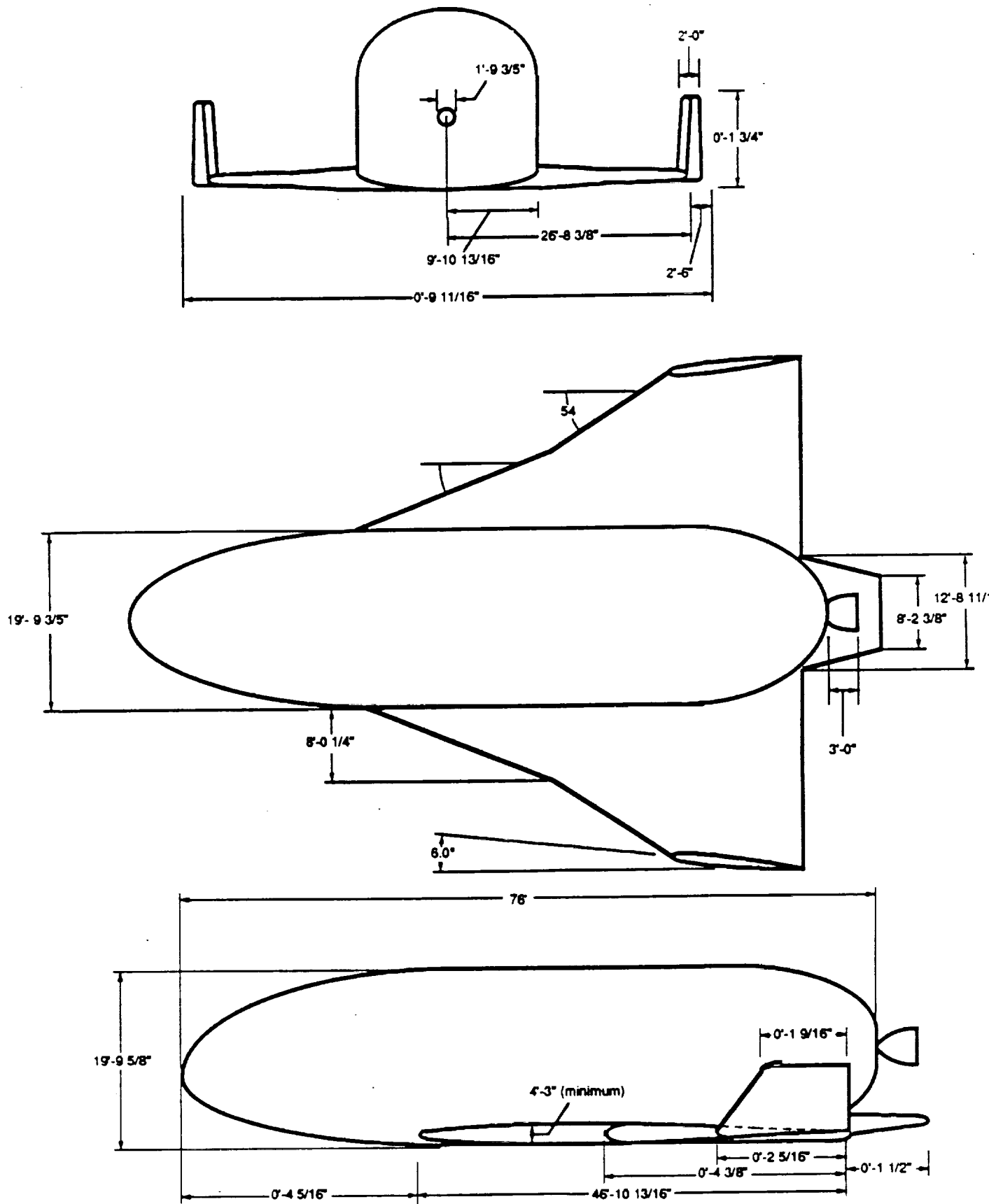


Figure 2-2 Wing Drawing

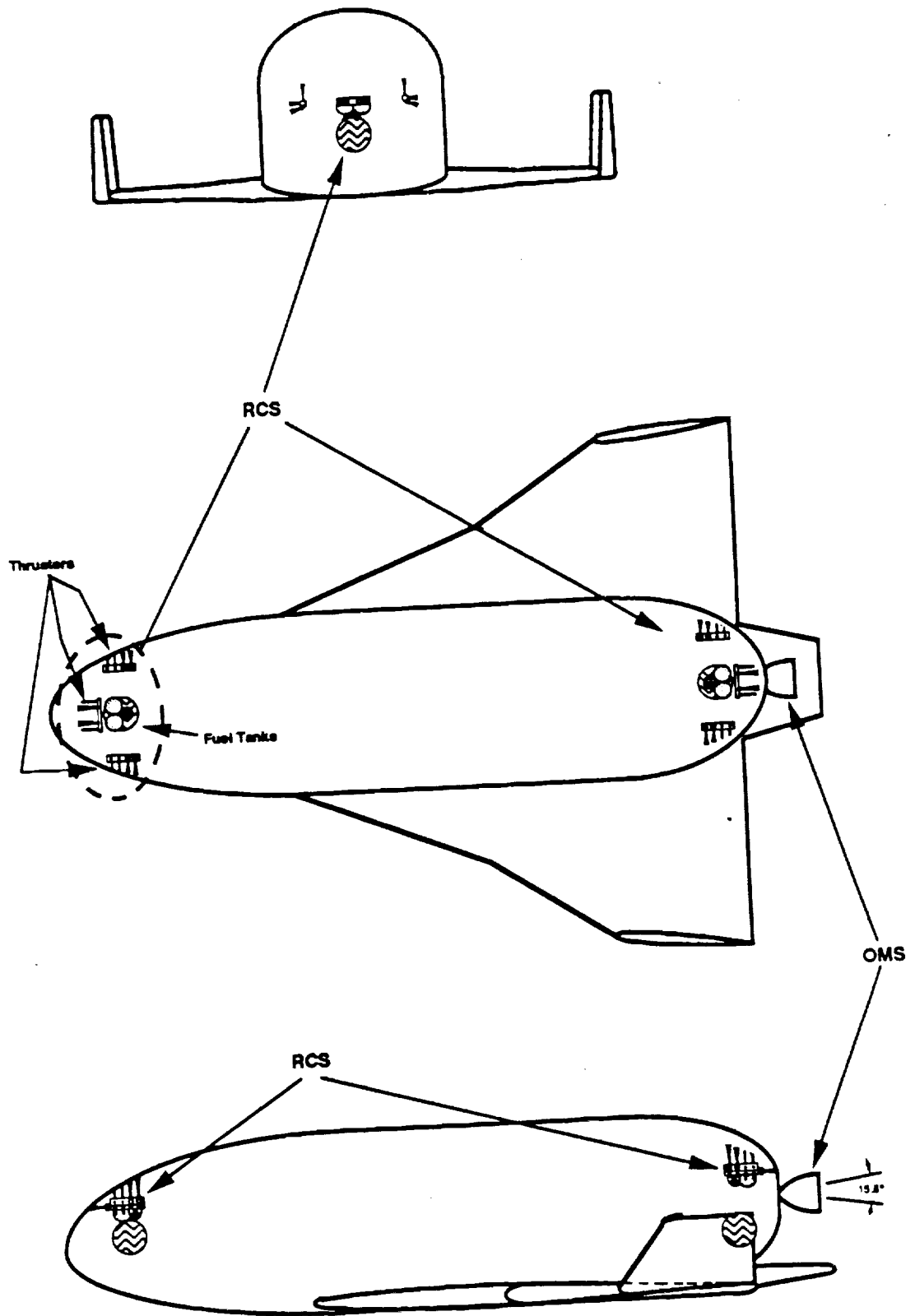


Figure 2-3 RCS/OMS

KEY

SUBSYSTEM LEGEND

-  Battery Pack
-  Fuel Cell
-  Avionics
-  System operations
-  Docking Bay Door
-  RCS
-  Cargo Latch
-  Docking Mechanism
-  SPIDS

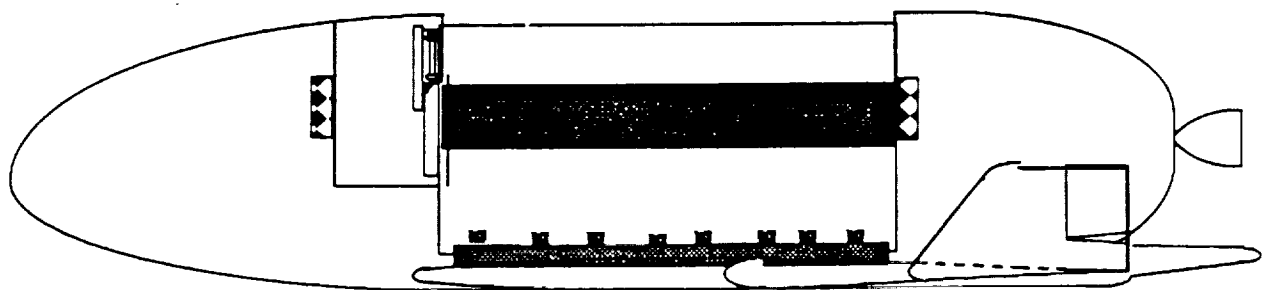
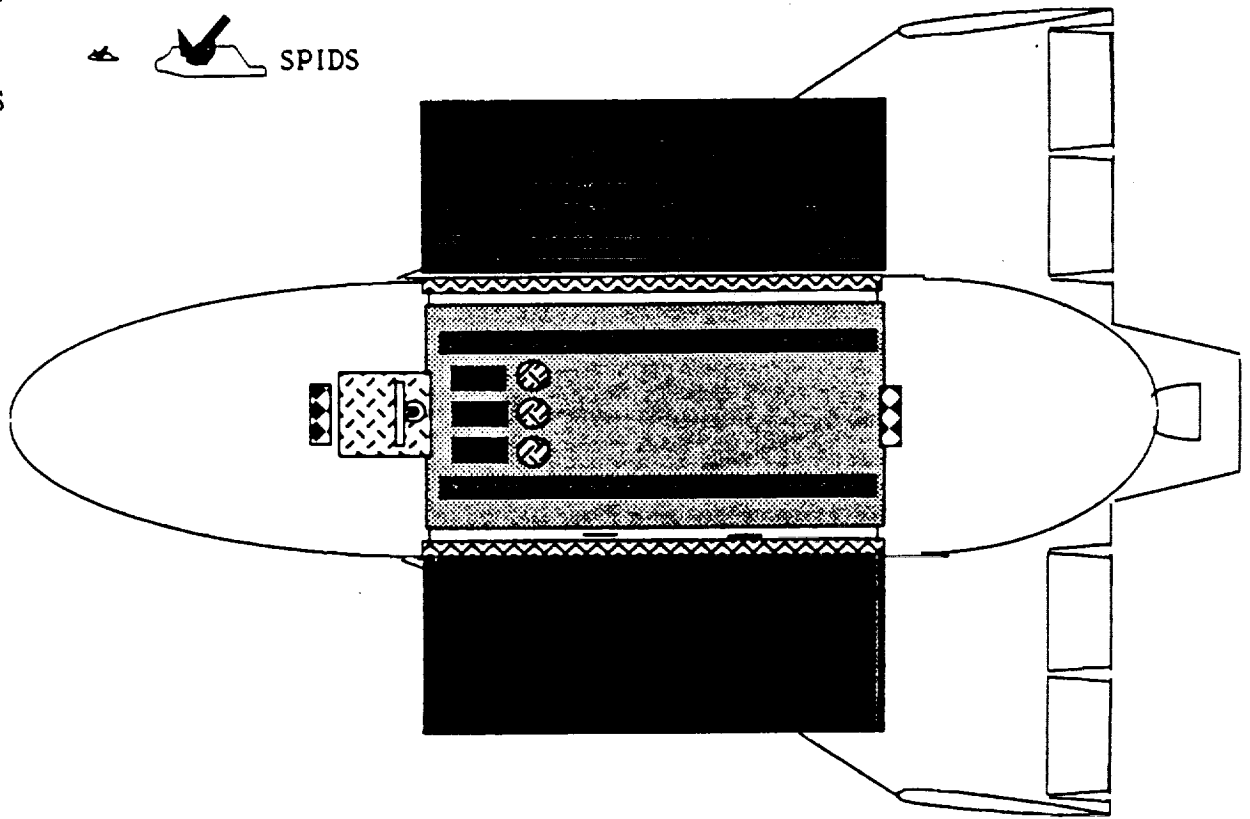
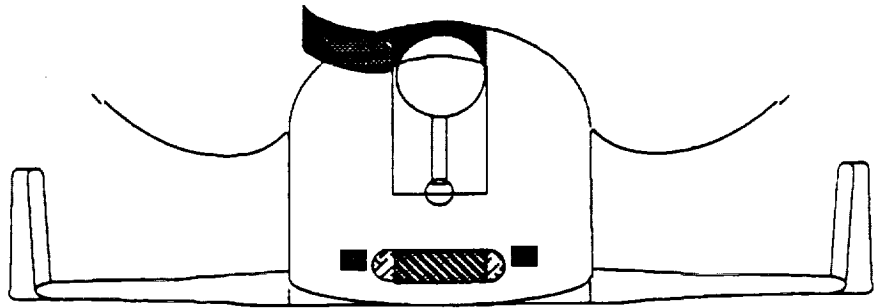


Figure 2-4 Avionics/SPDS

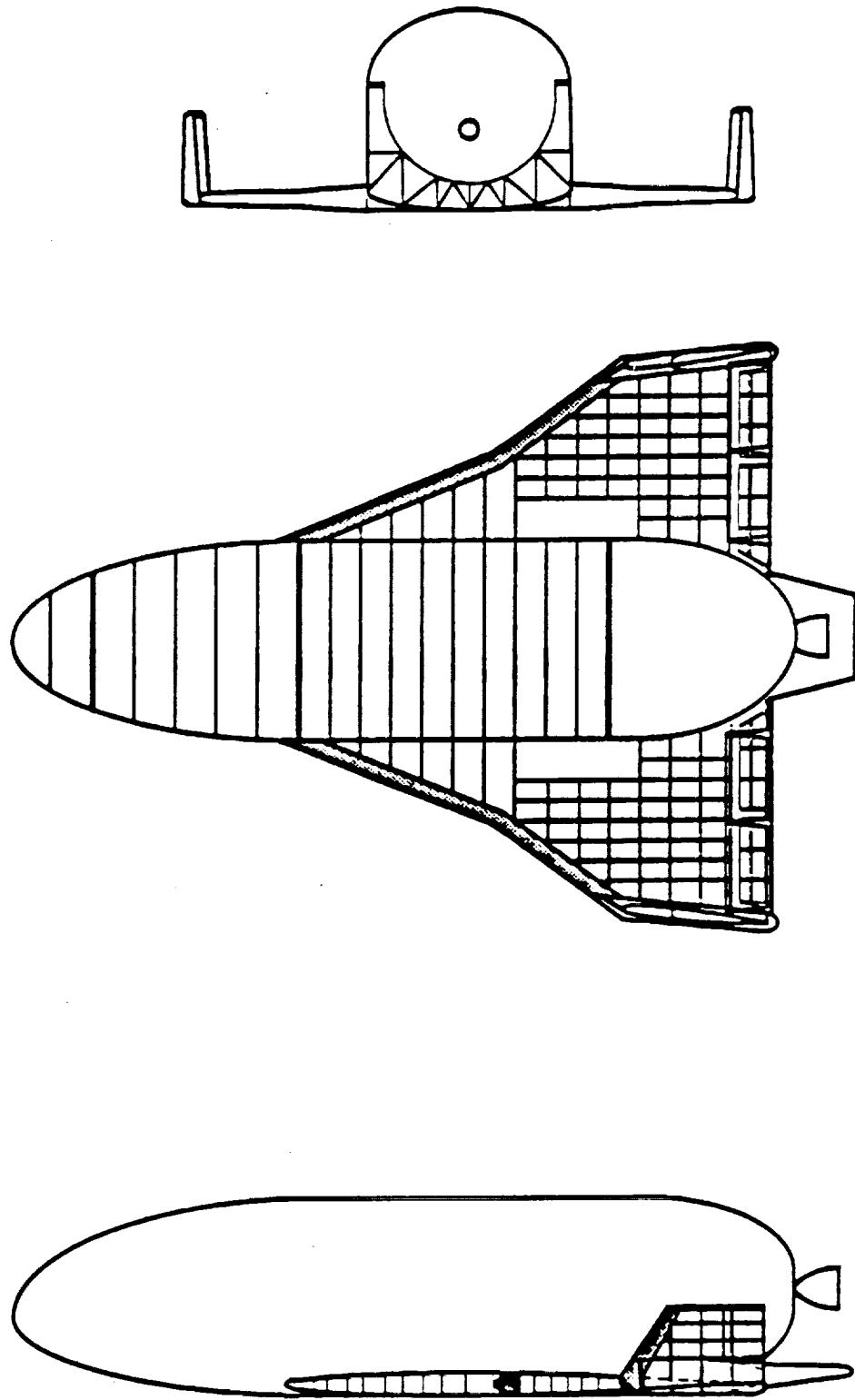


Fig. 2-5 Structural Drawing

2.2 MASS PROPERTIES

The primary purpose of the CRV is to support the logistics needs of Space Station Freedom. Included in these needs is the transport of all payload in either pressurized or unpressurized logistics modules. The primary purpose of the Pressurized Logistics Module (PLOG) will be to transport such items as food, clothing, and experiments. The primary purpose of the Unpressurized Logistics Module (UNPLOG) will be to contain fluids and dry cargo not essentially needed within the space station itself. Each of these modules have a significant effect on the CRV's weight, center of gravity location, and moments of inertia. Because of a significant cutback in booster capability from 144,000 lbs. to 113,000 lbs. the usable payload had to be scaled back considerably. In order to reduce CRV launch weight, reductions had to be made in the disciplines of Structures and Thermal Protection.

In reducing CRV payload capability, four possible payload options were investigated. The first option consisted of one PLOG as payload, while the second and third options consisted of various PLOG combinations (Using either one UNPLOG or two UNPLOGS as payload). The fourth and final option considered the use of one PLOG and one UNPLOG together as payload. This configuration has an advantage in that it would allow the maximum allowable payload to be transported to SSF, however it has two major drawbacks. The first being that each module could not be filled to capacity. The second being that with one PLOG and one UNPLOG occupying the cargo bay, their would be little, if any center of gravity envelope for the CRV. For this reason, the PLOG/UNPLOG combination wasn't explored in great detail, with emphasis primarily placed on one PLOG or one/two UNPLOGS as payload.

2.2.1 WEIGHT ANALYSIS

A preliminary weight statement based on the trade study configuration (Table 2-1) called for the CRV to have a dry weight of 63,708 lbs with payload capabilities of 73,944 lbs. This design resulted in a launch weight of 144,000 lbs. A major advantage to this system is that a cargo consisting of one PLOG and one UNPLOG each filled to capacity could be transported to SSF. When filled, the PLOG/UNPLOG combination would weight 55,590 lbs. However, with such weight, this configuration provided little or no center of gravity range and led to the vehicle being unstable in the subsonic region. This configuration would also take up nearly all of the cargo bay,

leaving little or no room for other articles that may need to be transported.

Due to a cutback in booster capability, the preliminary weight estimate of the CRV had to be refined. Reductions were hoped to take place in the Structural, Propulsion, and Thermal Protection System (TPS) disciplines. However, upon reviews with each of the specified disciplines, it was determined that there would be only very slight reductions. With the omission of the vertical tail a weight saving of 800 lbs. for the structure and 500 lbs. for the TPS was achieved. The landing gear weight, however, increased 2,200 lbs. to an overall weight of 3,200 lbs. Slight reductions also took place in the RCS/OMS propellant systems, but due to the fear of elimination of the OMV program, a cold gas system had to be added in order to accommodate operation of the CRV in the space station control zone. This resulted in an addition of 1,169 lbs. to the propulsion system. Additionally, the Avionics and Power discipline required a large increase in weight due to the use of servos, fuel cells, and batteries.

The primary purpose of the finalized weight statement was to provide as detailed analysis as possible for the CRV and its subsystem weights. Of particular importance were detailed breakdowns of the Structures, TPS, Propulsion, and Avionics and Power disciplines. These groups, which make up the majority of the CRV weight, were able to provide weights of each subsystem. Table 2-3 lists the finalized weight statement used in calculating center of gravity locations and moments of inertia.

Table 2-1 CRV PRELIMINARY WEIGHT STATEMENT

Structure:		28,000 lbs.
	A) Body:	23,200 lbs.
	B) Wing:	4,000 lbs.
	C) Tail:	800 lbs.
Thermal Protection System:		13,500 lbs
	A) Body & Wing:	13,000 lbs.
	B) Tail:	500 lbs.
Thermal Control System:		250 lbs

Table 2-1 CRV PRELIMINARY WEIGHT STATEMENT (cont.)

Propulsion Systems:	2,158 lbs.
A) OMS:	1,795 lbs.
1) Engine Dry Mass:	300 lbs.
2) Propellent System:	1,495 lbs.
B) RCS:	363 lbs.
1) Engine Dry Mass:	240 lbs.
2) Propellent System:	123 lbs.
Avionics:	7,800 lbs.
Hydraulics:	2,000 lbs.
Landing Gear:	1,000 lbs.
Growth:	9,000 lbs.
Dry Weight:	63,708 lbs.
Consumables:	6,348 lbs.
1) OMS Propellent:	5,980 lbs.
2) RCS Propellent:	368 lbs.
Maximum Payload:	73,944 lbs.
Total Launch Weight:	144,000 lbs.
Less Consumables:	6,348 lbs.
Total Landing Weight:	137,652 lbs.

Table 2-2 CRV Finalized Weight Statement

Structure:	27,850 lbs.
Body:	22,880 lbs.

Body	
Front Landing Gear Bulkhead:	1,085 lbs.
Docking Module Bulkhead:	2,100 lbs.
Cargo Bay Bulkhead:	2,340 lbs.
Forward Fuselage Support Frame:	630 lbs.
Docking Module Support Frame:	188 lbs.
Docking Module Bay Doors:	220 lbs.
Docking Module Main Platform:	250 lbs.
Forward Fuselage Skin:	1,365 lbs.
Sill Longerons:	300 lbs.
Cargo Bay:	4,542 lbs.
Aft Fuselage:	9,860 lbs.
Wing:	4,970 lbs.
Main Wings:	3,967 lbs.
Winglets:	780 lbs.
Strakes:	223 lbs.

Table 2-2 CRV Finalized Weight Statement (Cont.)

Thermal Protection System:		11,693 lbs.
Body:		2,884 lbs.
Nose Cap:		514 lbs.
Body Flap:		75 lbs.
Lower Nose Cone:		651 lbs.
Upper Nose Cone:		439 lbs.
Upper Body Flap:		25 lbs.
Body Cylinder:		1,180 lbs.
Wings:		8,809 lbs.
Winglets:		715 lbs.
Winglet Tips:		1,224 lbs.
Winglet Sides:		259 lbs.
Wing Leading Edge:		3,235 lbs.
Lower Wing Surface:		2,645 lbs.
Upper Wing Surface:		731 lbs.
Thermal Control System:		250 lbs.
Propulsion Systems:		1,353 lbs.
OMS:		423 lbs.
Engine Dry Mass:		260 lbs.
Propellent System:		163 lbs.
RCS:		461 lbs.
Engine Dry Mass:		420 lbs.
Propellent System:		41 lbs.
Cold Gas System:		469 lbs.
Engine Dry Mass:		360 lbs.
Propellent System:		109 lbs.
Avionics & Power:		12,000 lbs.
Avionics:		2,500 lbs.
SERVOS:		2,000 lbs.
Batteries:		1,000 lbs.
Fuel Cells:		2,500 lbs.
Environmental Control System:		1,100 lbs.
Control & Distribution:		2,900 lbs.
Landing Gear:		3,200 lbs.
Nose Gear:		800 lbs.
Main Gear:		2,400 lbs.

Table 2-2 CRV Finalized Weight Statement (Cont.)

Docking Module:	250 lbs.
Growth:	5,000 lbs.
Dry Weight:	61,596 lbs.
Payload:	44,416 lbs.
RCS Propellant:	241 lbs.
OMS Propellant:	4,627 lbs.
Cold Gas Propellant:	700 lbs.
Adapter:	1,420 lbs.
Total Launch Weight:	113,000 lbs.
Less Consumables:	5,568 lbs.
Less Adapter:	1,420 lbs.
Total Landing Weight:	106,012 lbs.

2.2.2 CRV CENTER OF GRAVITY LOCATIONS

The CRV center of gravity locations were calculated by treating each of the CRV subsystems as individual point masses, with the centers of gravity located a specified distance from the nose of the vehicle. The individual weight of each subsystem was then multiplied by its distance from the nose, summed, and divided by the total CRV weight to obtain the overall CRV center of gravity location. With a vehicle dry weight of 61,596 lbs. the corresponding c.g. location was 38.3 feet from the nose of the vehicle. A maximum aft c.g. location of 40.6 feet must be obtained in order to fly stable in the subsonic region. Therefore, the current CRV configuration will be dynamically stable when flying at its dry weight (i.e. no payload or propellant).

There are certain advantages to flying unstable which include larger cross range, increased maneuverability and less drag. To accomplish this, different payload configurations were examined to explore their relationships to center of gravity locations. The three basic configurations analyzed consisted of one PLOG, one UNPLOG, and two UNPLOGS as payload. Center of gravity envelopes were then developed for these calculations for the PLOG and UNPLOG combinations.

The C.G. envelope for each cargo combinations was achieved by placing the empty cargo container at the maximum forward position. Weight was then added to the container in small step until it was completely full.

With the containers held at maximum weight the propellant weights were varied. The loaded container was then moved to the farthest possible aft position and the load decreased until empty. The vehicle's C.G. location was then plotted. The resulting C.G. envelopes were based only on vehicle weight and do not reflect and restrictions that may be imposed by stability and control.

2.2.3.1 CRV C.G. Envelope with UNPLOGS as Payload

CRV TOTAL WEIGHT VS. C.G. LOCATION
(UNPLOG)

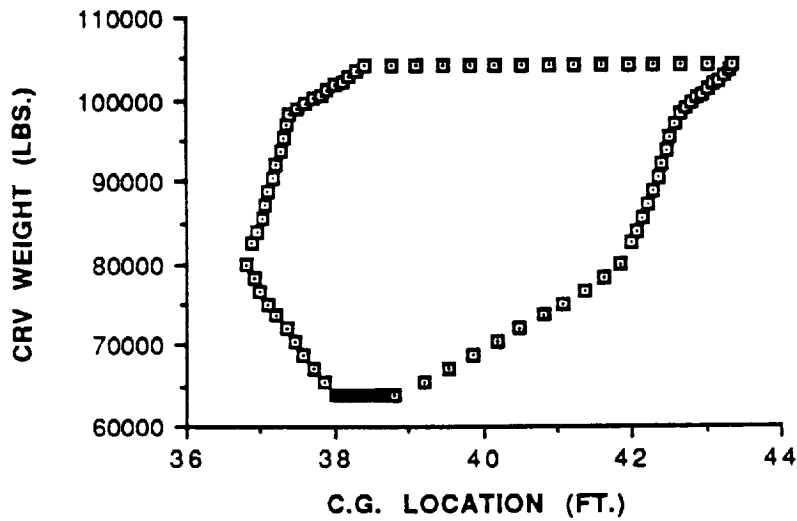


Figure 2-6 C.G. Envelope for UNPLOG(ft.)

CRV TOTAL WEIGHT VS. C.G. LOCATION
(UNPLOG)

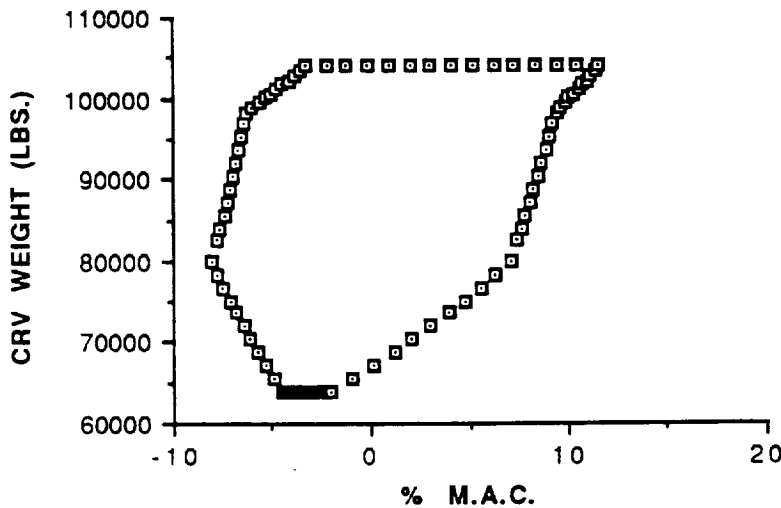


Figure 2-7 C.G. Envelope for UNPLOG(%M.A.C.)

2.2.3.2 CRV C.G. Envelope with PLOG as Cargo

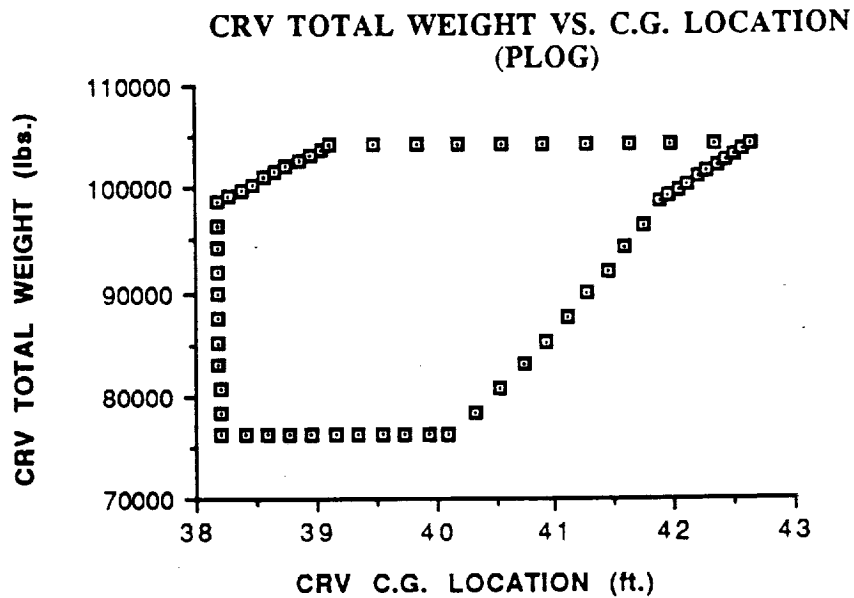


Figure 2-8 C.G Envelope for PLOG(ft.)

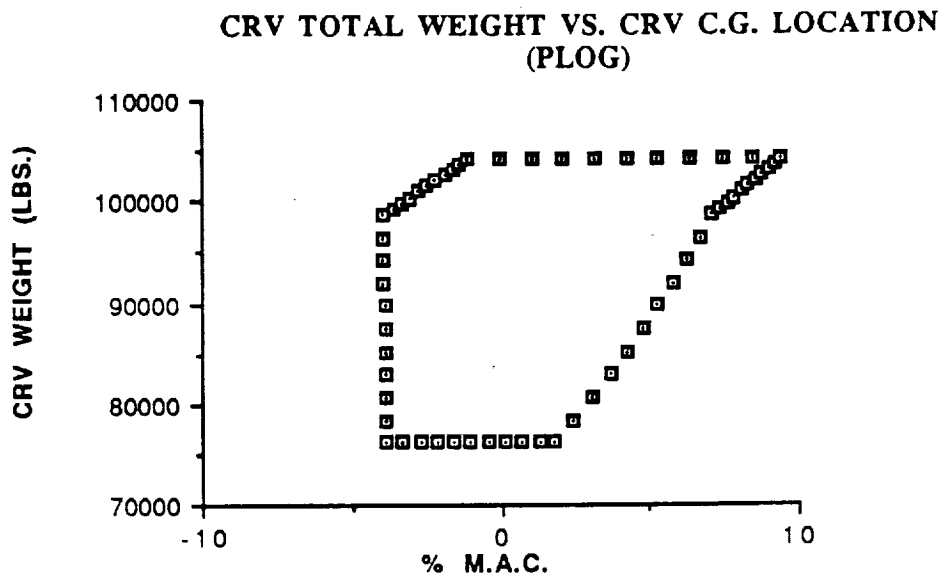


Figure 2-9 C.G Envelope for PLOG(%M.A.C.)

2.2.4 Moments of Inertia

Preliminary CRV moments of inertia were obtained from equations derived in Reference 2.1. The equations were originally derived for the Space Shuttle, and because of the similarity of the CRV, were

assumed to be applicable. Moments of inertia were calculated for the roll, pitch, and yaw axes from one general equation. This equation consisted of the vehicle gross weight (W) and the radius of gyration (K) (which was dependent on the axes of particular interest). The resulting moments were obtained by dividing the vehicle gross weight by 32.2 ft/sec^2 and multiplying by the square of the corresponding radius of gyration.

The radius of gyration, in turn, is dependent on the span (b) and length (L) of the vehicle, and also on whether the vehicle is in launch or landing mode. The roll radius of gyration is proportional to the wing span, the pitch proportional to the length, and the yaw proportional to both span and length.

The amount of payload will have a dramatic effect in calculating the various moments. Four different payload possibilities were considered when calculating the moment of inertia. These consisted of: one PLOG, one UNPLOG, two UNPLOGS, and one UNPLOG. In each configuration moments of inertia would vary depending on weight and whether the CRV is in launch or landing mode. This is due to changes in cargo weight, and a reduction in propellants on board due to use during the mission. Figures 2-5 and 2-6 show all possible moments of inertia for launch and landing configurations. Table 2-5 shows roll, pitch, and yaw moments for each of the different configurations at maximum weight.

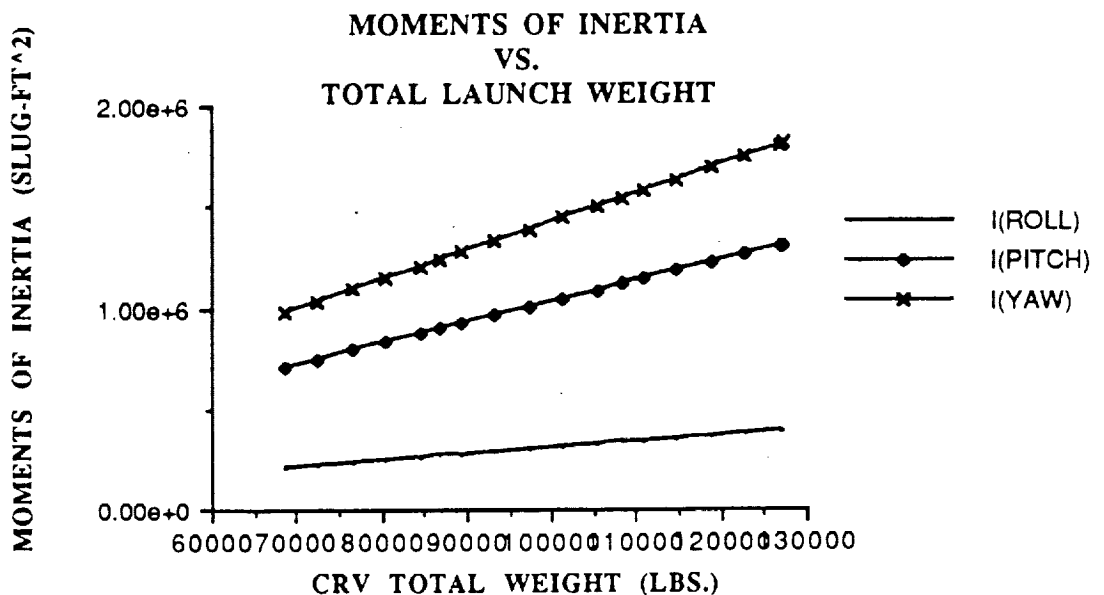


Figure 2-10 Moment Of Inertia vs. Total Launch Weight

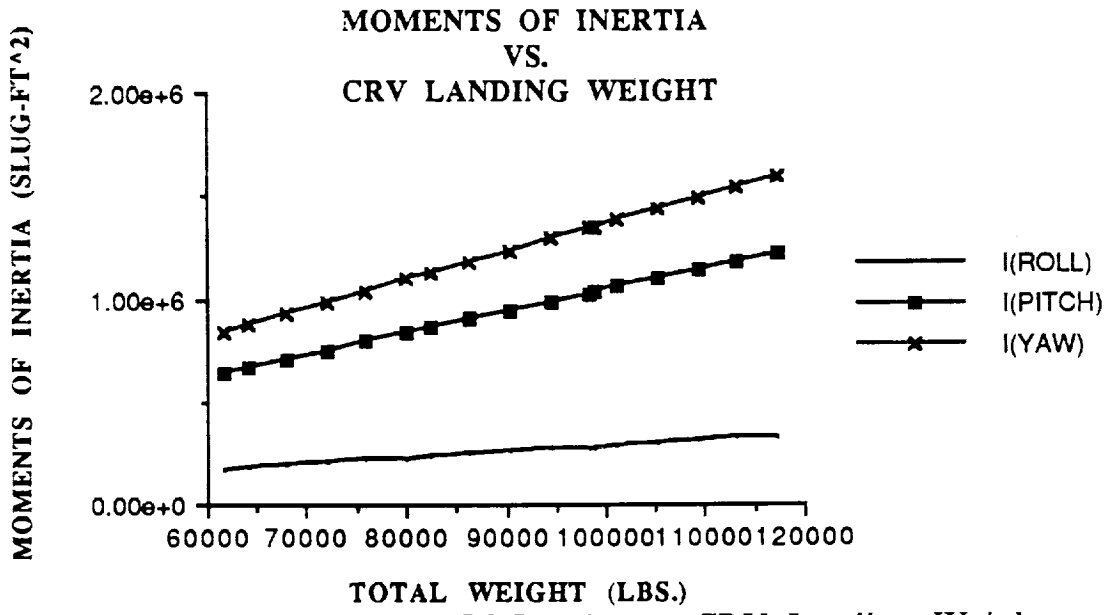


Figure 2-11 Moment Of Inertia vs. CRV Landing Weight

3.0 MISSION OPERATIONS

Mission Operations is primarily concerned with procedures near the space station dealing with proximity vehicle control and cargo transfer. It also includes ground operations and cargo bay design. The nominal mission will be use the Orbital Maneuvering Vehicle (OMV) to transfer cargo from the CRV to the space station. The alternate mission will deal with the possibility that the OMV will not be in service and the CRV will have to hard dock to the space station in order to transfer the cargo. Both missions have been examined in detail and will be discussed in the following sections.

3.1 ASSUMPTIONS, REQUIREMENTS AND DESCRIPTION OF SSF

3.1.1 OMV Description

The Orbital Maneuvering Vehicle (OMV) will be a remotely controlled payload retrieval vehicle.

It is a variable range vehicle that consists of two separate units-the Short range vehicle (SRV) and the Propulsion Module (PM). The SRV is the core of the OMV and will be joined with the PM for all payload transfers.(Ref. 3.3)

3.1.2 Assumptions

The nominal mission assumes that the OMV will be in use and will be capable of transferring the cargo. Ground operations assumes that the facilities in use now will not be modified. If the space shuttle missions do not increase beyond five missions per year then the present facilities will be enough to handle both the space shuttle and CRV processing.

For orbital mechanics analysis, it was assumed that there are no perturbing forces from an ideal Newtonian centralized force field. As a result, earth oblateness, moon effects, and solar/atmospheric drag are neglected. Additionally, all orbital changes are assumed to take place via an instantaneous change in velocity. In other words, the time required for a maneuver burn is considered to be negligible. Mission analysis without these assumptions may be performed at a later date. For the purposes of this design phase, however, these assumptions give results that are sufficient for an accurate approximation of the parameters involved.

The basic tradeoff involved in mission analysis is fuel used versus time required. Since mass of fuel used is of primary importance in the overall efficiency of the CRV, fuel use is minimized whenever possible at the expense of mission time.

3.1.3 Requirements

3.1.3.1 Nominal Mission

The CRV will be controlled by the ground crew outside the Command and Control Zone. Cargo transfer will be accomplished by OMV.

3.1.3.2 Alternate Mission

CRV must be equipped with rendezvous and navigation hardware/software.

CRV will be equipped with visual ranging cues (running lights, markings, targets of known dimension) unless the CRV vehicle structure is sufficient for ranging techniques.

The CRV will be attached to the space station during cargo transfers. During cargo transfer the SSF crew will be able to monitor the CRV for safety considerations.

- CRV must possess command/control capability
- Must have some provisions for electrical power and signal interfaces with SSF (remotely operated umbilicals)
- All mechanisms to be operated as part of the CRV berthing/docking, payload exchange must be designed to be fault tolerant, designed for EVA accessibility, manual EVA backup.
- For safety critical items, such as mechanisms holding the logistics module to the CRV during transfer and docking, a requirement for 3 independent electrical inhibits has been imposed to prevent inadvertent operation.

3.1.2.3 Space Station Freedom (SSF) Requirements

The final approach to the space station shall be from the plus V-bar (along the positive velocity vector) position.

Only one free flyer at a time will be allowed within the Command and Control Zone (CCZ). If the CRV is docking it will be the only free flyer in the CCZ

An arriving logistics module will be attached and checked out before the departing logistics module leaves.

SSF shall have hazard critical systems monitoring/command capability available for the unmanned CRV.

The SSF Mobile Servicing System will be utilized in the transport of payloads, berthing/deberthing of the CRV, capture of the CRV, positioning, maneuvering and release of the CRV.

The CRV must travel from the 50 x 100 n.mi orbit from launch to a rendezvous with the SSF at a 220 x 220 n.mi orbit, and 28.5 degree inclination. It must also return to the atmosphere from this orbit in a trajectory suited for re-entry.

3.1.3 Space Station Freedom

3.1.4.1 Description of SSF

SSF would have three docking ports: the primary, secondary and the contingency (see figure 3-1). The primary and secondary would be located on the plus V bar side, while the contingency will be at the opposite end. The primary docking port would be located on node 4, and the secondary on node 3. Node 4 would be located forward and on the port side of the space station. This node contains subsystems, a storage facility, and the upper cupola. The cupola to observe docking would be on the bottom of node 3. Node 3 would be located forward and on the starboard side. It would contain subsystems, a secondary docking port, and the primary control console. The docking ports would be connected to the habitation modules. These in turn would be attached to nodes 1 and 2. Airlocks would be connected to both nodes 1 and 2, and also at locations for the pressurized logistics module. Node 1 would be located aft and on the starboard side. It would contain subsystems, and a stowage facility. Node 2 would be located to the aft and on the port side. This node would contain subsystems, and a secondary control console. The truss would connect to the top of the habitation modules. SSRMS would be located on the face of the truss. Solar panels would be located at the ends of the truss.

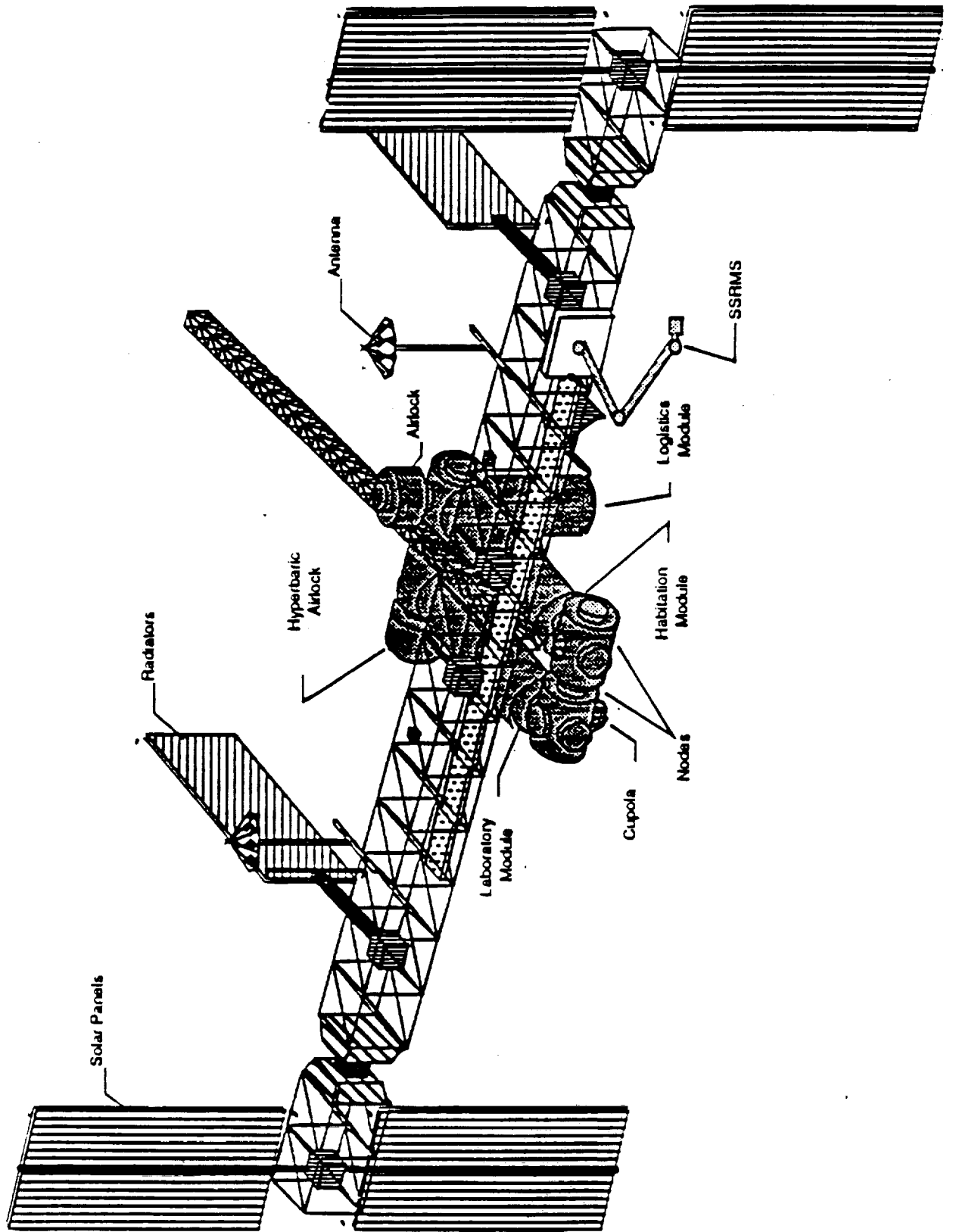


Figure 3-1 space station freedom

3.1.3.2 Operations

The vehicle operations would include the standard SSF operations procedures along with ground support. There are three levels of operations. The first is strategic, which is the planning stage. At this stage plans are drawn to achieve future goals. Tactical is the second. This is where the policies generated by the strategic level are implemented. The third level is the real-time execution. This will be based on any existing guidelines and constraints. The ground operations will accomplish long-term, tactical and weekly planning. The space station crew will accomplish the day to day execution of the schedule.

3.1.3.5 Evolution

The total mass in orbit will increase approximately 833 % from 1998 to 2006. The SSF must receive approximately 115,000 pounds of cargo per year. Of this cargo, 76% would be returnable and the other 24% would be trash. The SSF will need fluids for continued growth and for use in the experiments to be conducted on the station. In order for growth to occur there is a need for 12 flights per year by the year 2004. During the growth of the station the U.S. will be responsible for carrying 42% of the cargo to the SSF. The CRV must have the ability to meet SSF cargo requirements. The station will have the capability of 275 KW of power, 24 crew members, and 5 or more modules. Cargo transfers must be of the order of 200 metric tons per year, which can be provided by 9 enhanced CRV flights per year.

3.2 GROUND OPERATIONS

Ground operations includes the payload processing, pre-launch of the CRV, launch, and post flight operations. It also covers the facilities used during the operation and descriptions of them. The primary landing site was set to be Kennedy Space Center with the alternate site at Edwards Air Force Base.

3.2.1 Logistics Module Description

The cargo will typically be a single pressurized logistics module (PLOG) and possibly one unpressurized logistics module (UNPLOG). The PLOG is essentially a cylindrical vessel with a length of 20.15 feet and a diameter of 14.58 feet. It will contain goods requiring

pressurization, such as food and certain experimental setups. The UNPLOG will be a basic carrier, fluids subcarrier or dry cargo subcarrier and is dimensioned to fit within the PLOG if necessary. The UNPLOG will contain those goods not requiring pressurization.(Ref. 3.5)

3.2.2 Payload Processing

Payload delivered by the CRV will use either the unpressurized logistics module (UPLOG) or the pressurized logistics module (PLOG). The CRV is designed to carry both the UPLOG and the PLOG in any one flight. If both logistics modules are to be used, neither can be fully loaded do to the payload capacity of the CRV. Payload processing will occur either at the Orbiter Processing Facility (OPF) or at the Vertical Assembly Building (VAB). The only payload that would require the use of the VAB would be specialized payload that needs to be loaded in the vertical position.

Payload safing is also part of payload processing. NASA Technical requires that all payloads must meet with failure tolerance limits. The payload must be able to tolerate a minimum numbers of credible failures and/or operator errors. The hazard level of the payload shall determine the level of failure tolerance. The payload must be designed to maintain the fault tolerance without ground support.

3.2.2 Post Flight/Prelaunch of the CRV

Upon completion of a CRV's mission, the vehicle will return to Kennedy Space Center. During landing, the CRV will be aided by a Tactical Air Navigation (TACAN) Station, which is located along the center of the runway. The CRV can receive a signal from TACAN to guide it in for a landing. At Kennedy the CRV will touch down at the Shuttle Landing Facility (SLF). The runway is 15,000 feet long, which is adequate for the CRV. The CRV was designed to land on a conventional runway of 10,000 feet, so the CRV has 5,000 extra feet that it could utilize if necessary. The runway was designed to provide a rapid drain-off for rain, as well as, a skid resistant surface. At the southeast end of the runway is a ramp where the Mate/Demate Device is located. This is used to attach or remove the CRV from a 747 carrier aircraft. The ramp also provides movable platforms which can be used to access different components of the CRV. After landing the CRV will be safed and transported to the Orbiter Processing Facility (OPF).

At the OPF the cargo would be unloaded. Since the OPF consists of two identical high bays it is capable of handling both a CRV and a space shuttle at the same time. Each of the high bays is equipped with two 27 metric ton bridge cranes used for supporting payload processing. There is also a low bay which houses electronic, mechanical and electrical support systems.

After the payload is unloaded, CRV maintenance begins. Engine maintenance follows, along with system verification. Any modification or overhauls that need to be accomplished will be done at the Orbiter Modification and Refurbishment Facility. At this point in the ground operations the CRV will be towed to the Vehicle Assembly Building (VAB). At the VAB, integration and stacking occurs and will be done in high bay number one or three. This is the facility where a possible conflict with the space shuttle do mission schedule conflicts could occur. Since SRB stacking is considered hazardous, operations in the other bays will be suspended during this time. The CRV will then be integrated with its launch vehicle. Integration and operation tests would be conducted before the CRV moves to the next phase of processing.

3.2.3 Launch

When the integration is complete, the CRV would be ready to be moved to the launch pad. The Crawler-Transporter provides the necessary transportation by moving under the Mobile Launcher Platform that holds the assembled CRV system. The Crawler-Transporter has a maximum speed of 2 miles per hour unloaded. Loaded with the space shuttle the maximum speed is 1 mile per hour. The distance to launch pad 39A is 3.5 miles, while launch pad 39B is 4.25 miles away. Transportation of the CRV will take approximately 4-5 hours.

At the launch pad, Launch Control Center will take over. The Launch Control Center conducts NASA and military launches by the use of four firing rooms. Each room is equipped with a Launch Processing System which will be capable of monitoring CRV assembly, checkout and launch operations. It consists of two major parts, the Monitor Subsystem and the Central Data Subsystem. The Central Data Subsystem stores test procedures, vehicle processing data, and pre/post test analysis. The Monitor Subsystem actually processes and launches the CRV. Launch can take place at either launch pad

39A or 39B. Since the Shuttle already launches from these pads only minor adjustments would need to be made.

3.2.4 Ground Support Complexes for the CRV

The basic guidelines for vehicle and operations management is that any vehicle within the SSF Command and Control Zone (CCZ) will nominally be controlled by the SSF crew from the command and control consoles (located in cupolas). Any vehicle outside the CCZ will nominally be controlled (via ground uplinks) from one or several ground support centers. The main ground support centers are the Mission Control Center and the Space Station Support Center (SSSC). The MCC will have primary control of CRV activities including mission planning, execution, and monitoring of CRV telemetry and trajectories. The SSSC will have primary control of ground support operations for the SSF, including SSF systems, data monitoring and SSF/vehicle interactions. In addition, several sub-support groups play a significant role in operations and may have vehicle specific primary control or just provide additional support. They will, however, operate in close coordination with the SSSC and MCC. These groups are described in more detail in the following sections.

3.2.4.1 Ground Support Complex (GSC)

This is the collective ground support resources required to support the space station.

3.2.4.2 Space Station Support Center (SSSC)

The Space Station Support Center (SSSC) provides support for SSF and is located at Johnson Space Center (JSC). SSSC provides the following functions as part of its support role.

1. It provides all ground based functions necessary to insure that the space station meets all the operational objectives.
3. The space station data is monitored.
3. SSSC interfaces with different Operation Support Centers (OSC) to analyze systems performance.
4. The strategy for systems configuration is developed and analyzed.
5. SSSC is responsible for the integration of SSF and user systems operations at a tactical level, done weekly and monthly.

6. The launch countdown of the CRV is monitored at Johnson Space Center.
7. If the CRV docks to the space station, control of the CRV between the space station crew and the ground crew will be defined by SSSC. The actual transfer of control will also be handled by JSC.
8. After the CRV docks the SSSC will provide direct support to in-bay payload checkout activities and payload transfer to the space station.

3.2.4.3 Operations Support Center (OSC)

The operations support center is located at various places throughout the U.S., but most notably at Goddard Space Flight Center (GSFC). The facility has the following responsibilities.

1. It will provide support personnel to SSSC to serve as a liaison between them.
2. The attached payloads to the space station and SSF servicing bay will be provided with space systems and user support.
3. The Operations Support Center will perform the monitoring of the attached payloads, support systems and activities of the servicing bay.
4. The center will provide support operations for the payloads located on the external trusswork, as well as, the systems on the servicing bay.

3.2.4.4 Mission Control Center

This center handles communications, data processing, and display equipment which is interfaced in various flight control rooms used to conduct operations.

1. Space station logistics operations will be directly involved with MCC.
2. The center will be involved in planning, training and execution of CRV/SSF missions.
3. All CRV activities involving the space station will be monitored from MCC.
4. MCC will be in charge of ascent and rendezvous support of the CRV with SSSC monitoring.

5. The center will also be involved in telemetry monitoring, trajectory determination, and command up-link.

3.2.4.5 Orbital Maneuvering Vehicle Control Center (OMVCC)

1. The OMVCC provides planning, coordination, and support during SSF related OMV operations.
2. The center serves as an active operations interface between the operation centers of the target vehicle and SSSC.
3. The primary control for OMV operations outside the command and control zone lies with OMVCC.
4. The center will continue to monitor the OMV systems in control zones one and two, and is able to take over in an emergency situation.(Ref. 3.2)

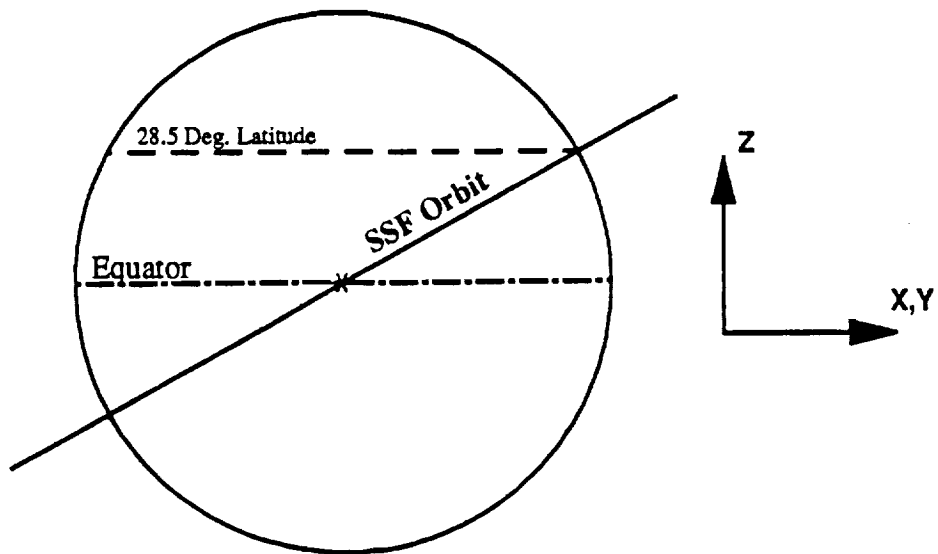
3.3 ASCENT TO RENDEZVOUS WITH THE SSF

3.3.1 Launch Restrictions

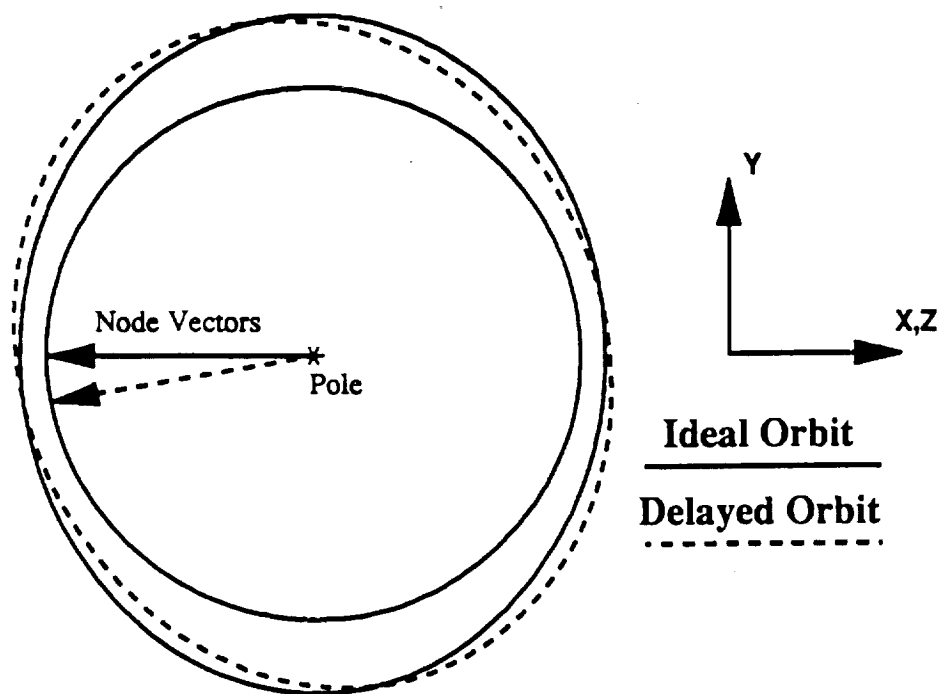
The SSF orbits in a plane angled at 28.5 degrees to the equator, and the CRV will be launched from a point at 28.5 degrees, N. latitude. As shown in Figure 3-2a, the launching point will only intersect with the orbital plane once per day. The phase angle correction time between the CRV and SSF would be at a minimum once every 4 days. The launching of the CRV must coordinate with these times so that it would place the 110x110 n.mi. phasing orbit in the same plane as the SSF. A delay in launching would result in a difference between the angle of nodes (the line of the intersection of the orbital and equatorial plane) of the CRV and the SSF orbits (Figure 3.-3b). This would necessitate a plane change maneuver, which is costly in fuel. It is important to keep this effect to a minimum.

3.3.2 Separation from Launch, Insertion into 110 X 110 Nautical Mile Circular Orbit

After the launch vehicle has completed its burn, both it and the CRV will be in a 50x100 n.mi. elliptical orbit. Explosive bolts will be used to separate the CRV from the launch vehicle. At the apogee (highest point) of this orbit the CRV would perform a burn, accelerating away from the launch vehicle, and positioning itself in a 100x110 n.mi. Hohmann transfer orbit.



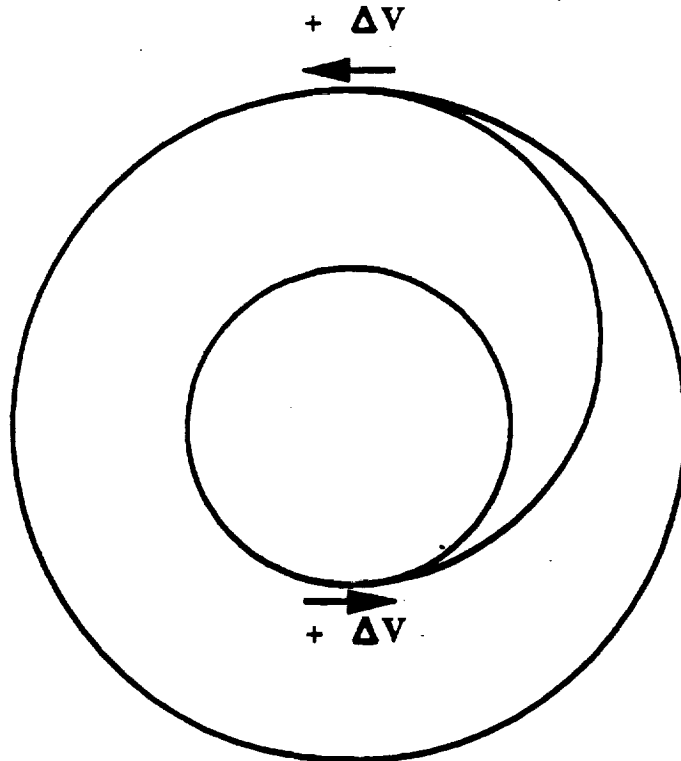
a) Requirement for Intersecting SSF Orbital Plane



b) Effects of Delayed Launch

Figure 3-2 Phasing Orbit

All orbital transfers will be made using the Hohmann transfer method (Figure 3-3). This method uses the minimum energy required for a transfer between two co-planar circular orbits. Two burn times are required: one to exit the circular orbit and one to enter into the new one. A Hohmann transfer entails the highest transfer time, but this is on the order of 0.75 hours and is acceptable for mission purposes.



Hohmann Transfer

Figure 3-3 Hohman Transfer

When the CRV reaches a 100 n.mi. altitude in its transfer orbit, it will be circularized into a 110 x 110 nmi orbit. At this point any error in the phase angle relation for rendezvous would be corrected by waiting in this lower orbit. The CRV gains on the SSF by 10.9 degrees per hour, as shown in Figure 3-4.

3.3.3 Ascention for SSF Rendezvous

This section of the mission is illustrated in Figure 3-5 and 3-6. Once the phase angle is correct, the CRV burns into a 110x210 transfer orbit and inserts into a 210 x 210 nmi. orbit at a phase angle of approximately 5 degree to the SSF. While the phase angle is reduced (Fig. 3-7), fine tuning of the CRV orbit will be performed in preparation for SSF rendezvous. This phase takes approximately 5 hours. The CRV will then perform another Hohmann transfer to the 220x220 nmi SSF orbit for rendezvous. Its final position is 20 to 22 nmi behind and planar to the SSF.

3.4 COMMAND AND CONTROL ZONE OPERATIONS

Operations within the SSF Command and Control Zone (CCZ) would consist of three basic procedures: payload transfer between the CRV and SSF, payload exchange at the CRV, and payload exchange at the SSF.

3.4.1 Payload Transfer

With the CRV in a standoff position, 20-22 nmi. behind the SSF, an Orbital Maneuvering Vehicle (OMV) will be utilized to perform all payload transfers between the CRV and the SSF. In doing so, the OMV would traverse a dual roundtrip path so that SSF requirements will be met. The unloaded OMV, aided by the Space Station Remote Manipulator Servicer (SSRMS), would depart the SSF approximately one hour before the CRV would arrive at its predetermined "parking orbit". It would then fly back and rendezvous with the CRV. Upon removal of the new Logistics Module (LM) from the CRV, the OMV and payload would depart the CRV and fly back to the SSF. The OMV would berth the payload onto an LM docking node or external structure, capture a spent LM from the SSF, and return to the CRV. The OMV would then deposit the spent LM in the CRV and return to the SSF. In the course of each leg of the payload transfer process, the OMV will perform a series of three burns denoted as TI, SB, TF. Enroute to the CRV the OMV would perform an initial thrust (TI) using cold gas (GN₂) to propel it to a safe distance from the SSF (approximately 8 nmi. outside the contamination envelope). The secondary burn (SB) would be initiated to propel the OMV towards the CRV using Hydrazine as fuel. Finally, the OMV would perform a terminal braking maneuver (TF). This will slow the OMV for rendezvous and payload exchange. Once again cold gas would be

Mission Profile - Ascent for Rendezvous

Altitude vs. Time
Numerically Generated

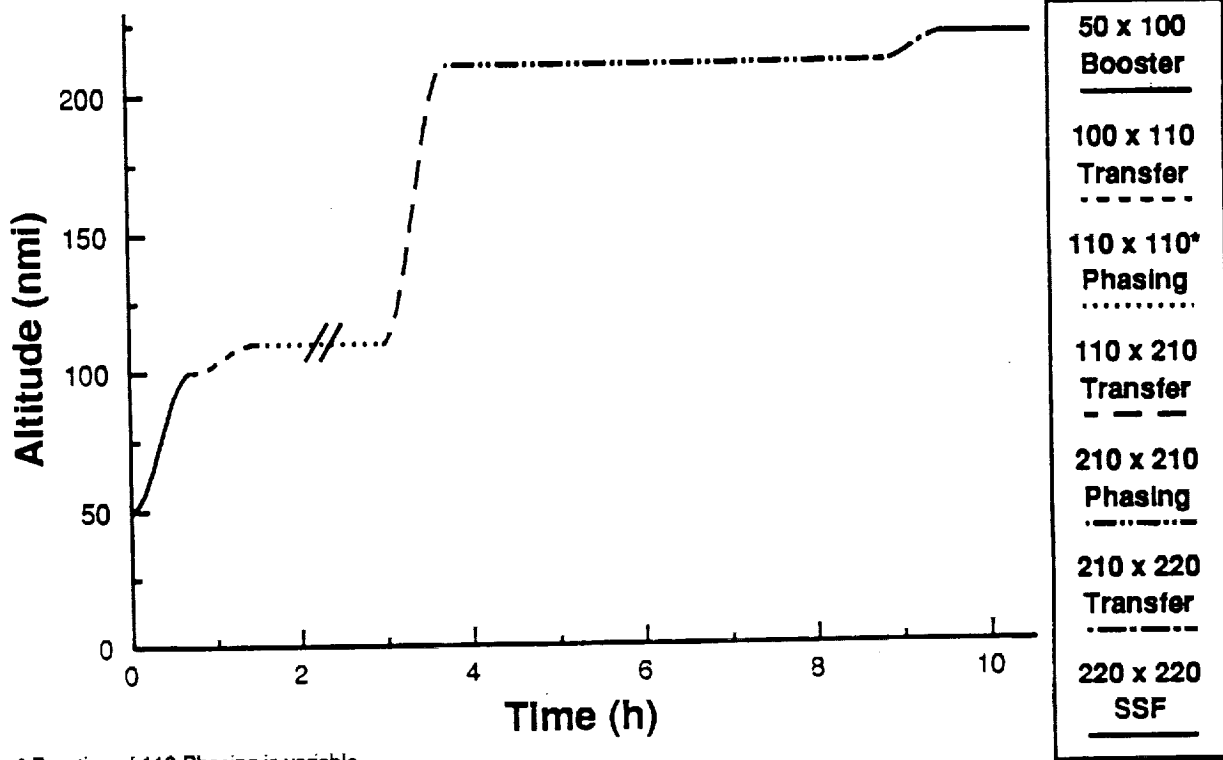


Figure 3-4, Mission Profile Ascent for Rendezvous
Mission Profile - Ascent for Rendezvous

Exploded View
Numerically Generated

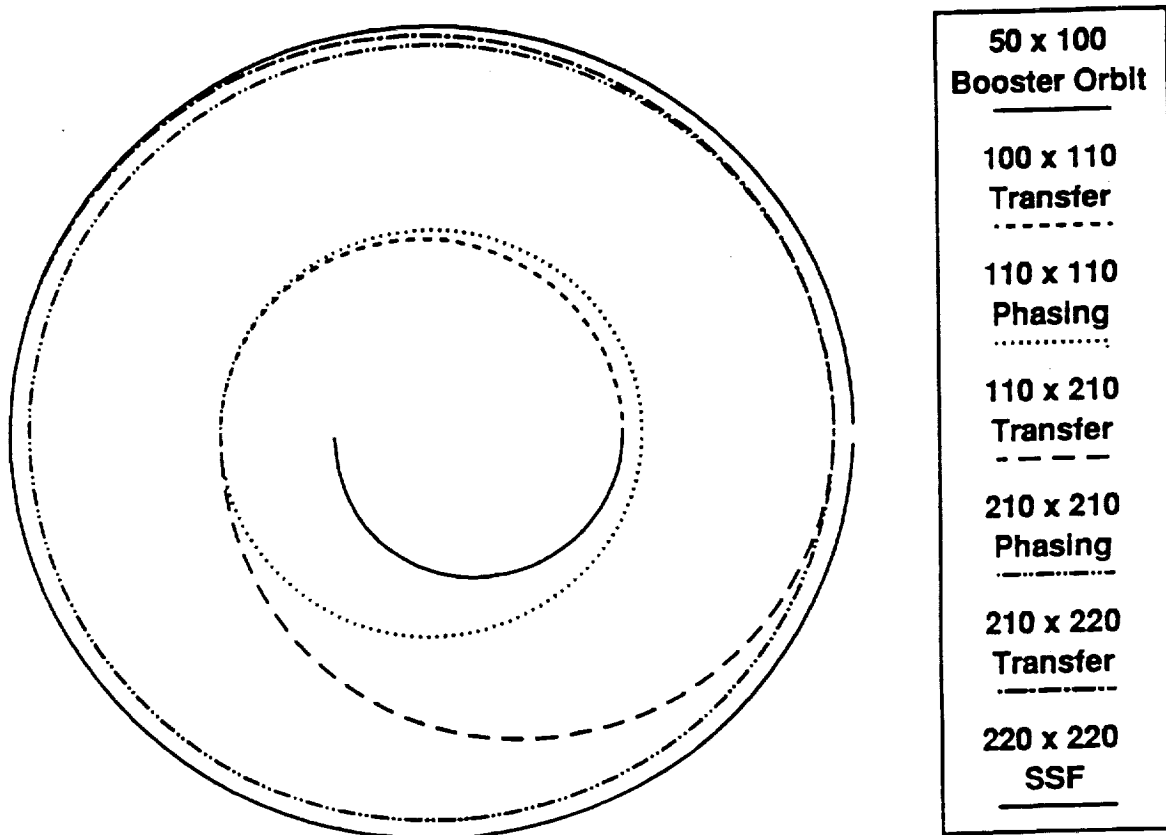


Figure 3-5, Mission Profile Ascent for Rendezvous, Alt vs. Time

Phase Angle Correction Time

Between SSF and CRV at 110 n.mi.

Correction = 10.89983 Deg/h

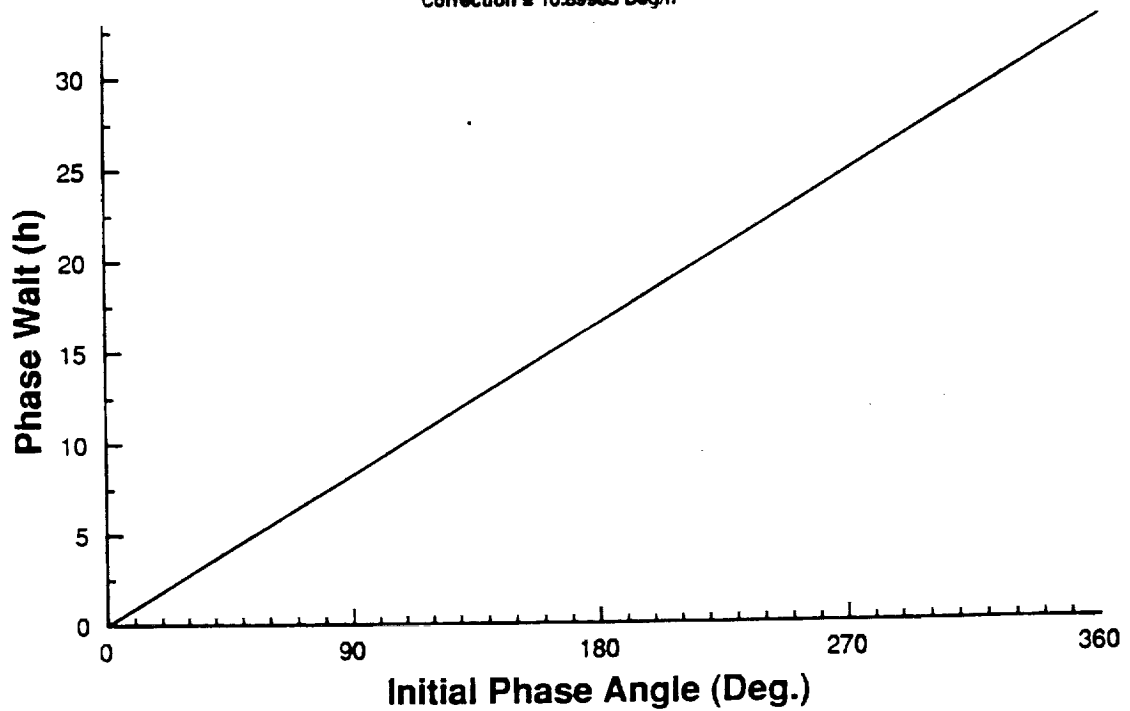


Figure 3-6, Phase Angle Correction Time at 110 Nmi.

Phase Angle Correction Time

Between SSF and CRV at 210 n.mi.

Correction = 0.957006 Deg/h

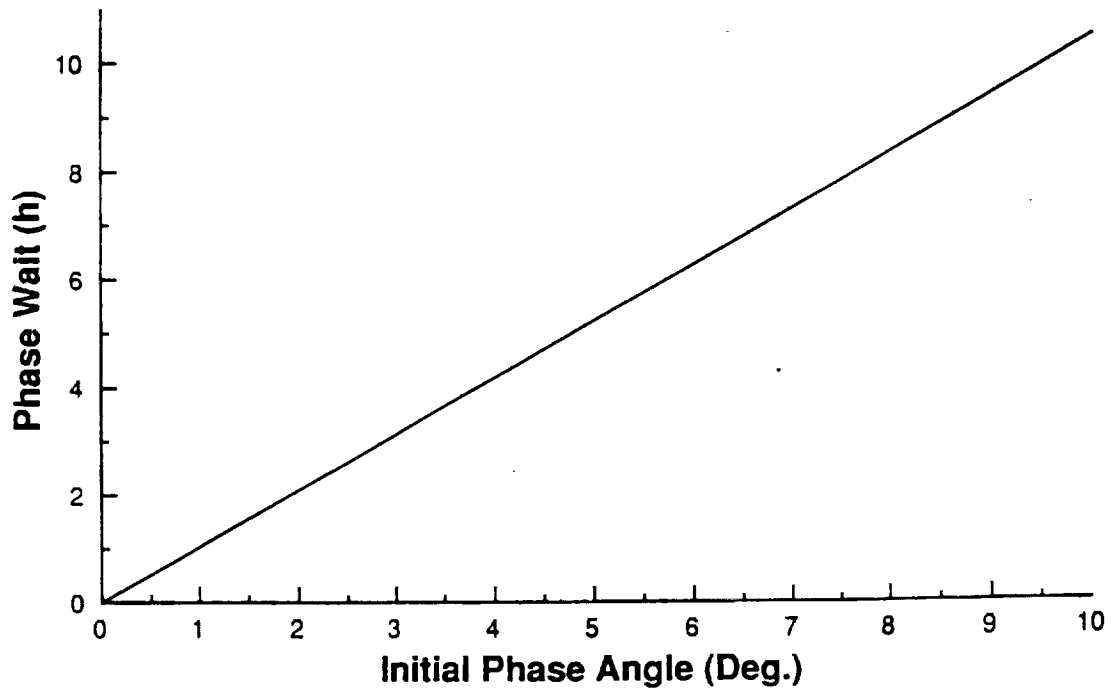


Figure 3-7 Phase Angle Correction Time at 210 Nmi.

used. Enroute to the SSF, the OMV will perform an initial thrust (TI) using cold gas and switch to Hydrazine once at a safe distance from the CRV. In this case, the TI burn would be used to propel the OMV towards the SSF and the Secondary Burn (SB) would be used to position the OMV on the plus V-bar of the SSF. The OMV would perform a final braking maneuver (TF), using cold gas, to complete rendezvous and payload exchange.

Table 3-1 Mission Profile

Event	(OMV) MET	(CRV) MET
Pre-mission SSF Activities		
(CRV enroute to parking orbit, 220 nmi circular)		-----
SSF configures for mission, "shuts down", (except SSRMS)	-:30	-----
SSRMS grapples OMV (attached to SSF), systems checked	-:20	-----
SSRMS deberths OMV, maneuvers it to plus V-bar side of SSF	0	-----
Mission Outline:		
SSRMS releases OMV, OMV performs proximity operations	-----	
OMV performs initial burn (TI), enroute to CRV	:30	
CRV arrives at "parking orbit"	1:00	-----
OMV performs second burn (SB), once outside the SSF contamination envelope	1:15	:15
SSF configures for normal operations	1:20	:20
CRV bay doors open	1:50	:50
OMV performs terminal burn (TF) (braking maneuver)	1:55	:55
OMV arrives at CRV, docks on LM (LM is attached to CRV SPDS unit), confirm interface	2:25	1:25
OMV/NEW LM depart CRV, perform TI burn	2:40	1:40
OMV/NEW LM perform SB burn	3:55	2:55
SSF configures for OMV arrival	4:05	3:05
OMV/NEW LM perform TF burn (braking maneuver)	4:35	3:35
OMV/New LM rendezvous with SSF, perform prox. ops.	5:05	4:05

Mission Outline:	(OMV) MET	(CRV) MET
OMV docks NEW LM on vacant LM node (pressurized LM only), on secure SSF platform (unpressurized LM)	5:35	4:35
OMV captures Spent LM from SSF, OMV/Spent LM depart SSF, perform prox. ops	5:50	4:50
OMV/Spent LM perform TI burn	6:20	5:20
OMV/Spent LM perform SB burn	7:05	6:05
SSF configures for normal operations	7:10	6:10
OMV/Spent LM perform TF burn	7:45	6:45
OMV/Spent LM dock on CRV	8:15	7:15
OMV releases LM, performs TI burn	8:30	7:30
LM secured in CRV bay, bay doors close	9:00	8:00
CRV ready to move to departure zone	9:30	8:30
OMV performs SB burn	9:45	
SSF configures for arrival	9:55	
OMV performs TF burn	10:25	
OMV rendezvous with SSRMS	10:55	
SSRMS grapples OMV	11:25	
OMV systems shutdown, OMV berthed	11:30	

*Fuel Burning Times

3.4.2 Payload Exchange

Payload, in the form of pressurized and unpressurized logistics modules (LM), will be exchanged at two different locations within the entire transfer process between the CRV and the SSF. An OMV would remove a new LM from the CRV and replace it with a spent LM, and then perform the exact opposite procedure at the SSF. Each removal and replacement would require direct contact with the SSF, thus, the target vehicle must be able to interact with the OMV in such a way as to minimize procedural complications and payload changeout times.

3.4.2.1 CRV Payload Exchange

3.4.2.1.1 Doors

The doors must open to an angle greater than 85 degrees, measured from the vertical axis at the door joint, in order for the payload retention and deployment systems to operate.

3.4.2.1.2 Payload Disconnect Mechanism (PDM)

The PDM would come from the Remotely Operated Electrical Umbilical (ROEU) kit. The actuation is fail-safe and the motors have additional redundancy. This disconnection device operates upon an actuation force of 400 pounds (See Figure 3-8).

3.4.2.1.3 Stabilized Payload Deployment System (SPDS)

The payload deployment system would be a two fault tolerant system. The SPDS would be able to function safely with up to two system failures, but would cease to function upon the third failure within the system. It has the ability to interface with existing systems. Two pedestals are required to rotate the logistics module out the the cargo bay. The transfer operation to the OMV would take approximately 22 minutes. The SPDS is a system designed to rotate the logistics module out of the payload bay and used to rotate the returning logistics module into the cargo bay. SPDS can operate on either side of the payload bay. An interface plate would attach both the logistics module to the SPDS system. During release the interface plate would separate into two halves, one would remain attached to the logistics module and the other to the SPDS. The operational sequence would start with the keel latch release. The logistics module would then translate up two inches and the adjacent retention latches released. Next, the Yo drive system would be used to translate the cargo outboard three inches. When this is done the farside longeron latches would be disengaged. The payload would then be rotated out of the payload bay. At this time the final CRV maneuvering would be performed and the oscillations damped out. The OMV would then hook up to the logistics module and the interface plate would be released. The advantage of the SPDS is that it would have a high failure tolerance. The time SPDS needs to fully rotate and release the logistics module can be broken down as follows:

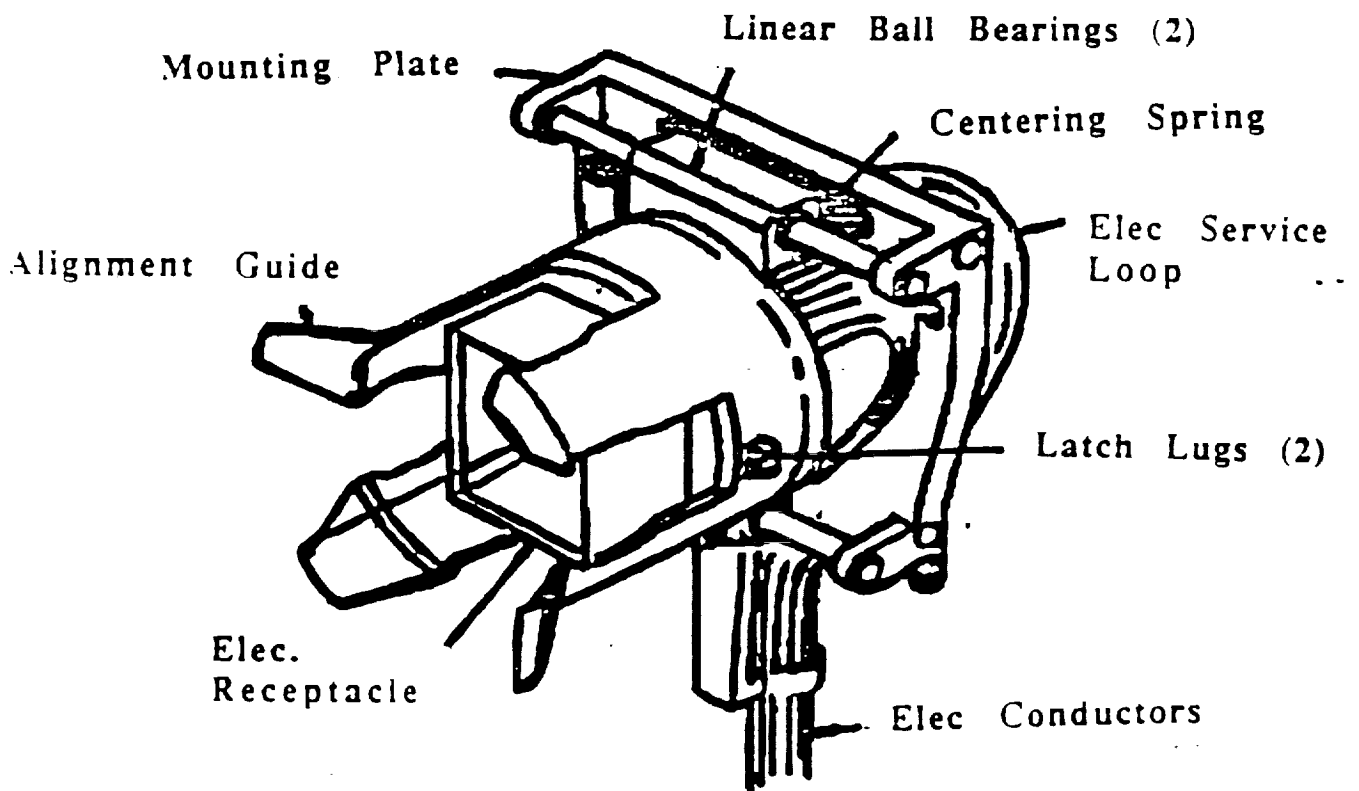


Figure 3-8 Payload Disconnect Mechanism

Table 3-2 SPDS Rotation Time

	(Min:Sec)
•Keel latch release	:26
•Adjacent longeron latch release	:21
•Yo drive outboard	:48
•Farside longeron latch releas	:21
•Payload rotation (deploy)	5:04
•Payload rotational damping	2:00
•FCS maneuver to final attitude	9:00
•FCS attitude hold	2:00
•FCS free drift	2:00
•Payload separation	----

TOTAL TIME REQUIRED 22 min

3.4.2.1.4 OMV Docks to the Logistics Module

Docking to the logistics module would be accomplished with a simple ring which would be attached to the cargo modules. The docking port would be attached to the bottom of the logistics module. The OMV would then approach with its guidance system and dock to the module.

3.4.2.2 SSF Payload Exchange

3.4.2.2.1 General

Payload exchange at the SSF would occur when the OMV returns from the CRV with a new Logistics Module (LM) for the SSF. The OMV would approach the SSF from a point approximately 1000-3000 feet ahead of the SSF on the plus V-bar, placed there by the (SB) burn. The OMV would then maneuver towards the payload docking point, typically a pressurized LM docking node, and berth the new LM. The OMV then proceeds to the alternate LM node, removes the spent LM and flies back to the CRV.

3.4.2.2.2 Interface Mechanisms

The OMV would be equipped with a Three Point Docking Mechanism (TPDM) for docking to the LM. The OMV would also be equipped with a Remote Grapple Docking Mechanism (RGDM) for grappling by the SSRMS during OMV deberting from the SSF and for contingency operations.

3.4.2.2.3 Operations Management

The OMV would be remotely controlled by an SSF crewmember from the primary station control console located in the lower cupola of node 3 (See figure 2.1). The command and control workstation would have high resolution displays driven by analog video signals and OMV on-board computer graphics. The source of the graphics would be several OMV-based video cameras, at least two Pan-Tilt-Zoom cameras to view around the payload (max. diameter of 15 feet). Additionally one stabilized camera would be mounted within the perimeter of the TPDM. These cameras, along with radar tracking and direct viewing, would provide the SSF crew-member with several vantage points while manipulating the OMV around the SSF via a hand controller (joystick). SSF-based and OMV mounted lights would provide illumination for all payload exchange maneuvers.

3.5 DESCENT AND DE-ORBIT

3.5.1 Reposition to Departure Zone

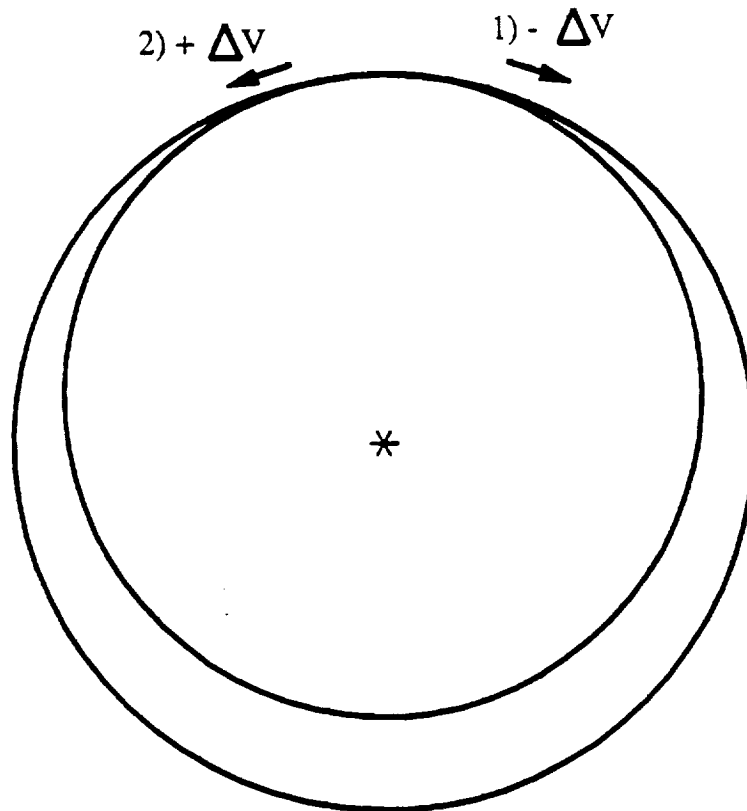
Before leaving SSF proximity, the CRV is required to maneuver to the departure zone. This would be accomplished using a full Hohmann repositioning orbit (Fig. 3-9). This maneuver would require relatively little change in velocity and is illustrated from the SSF perspective in Figure 3-10. At the end of repositioning the CRV would be from 20 to 22 nmi ahead of the SSF and in the departure zone.

3.5.2 Transfer to De-orbit Position and Phase Delay

Figures 3-11 and 3-12 show the mission profile from the departure zone point to descent into the atmosphere. The CRV would perform a Hohmann transfer to the 210 x 210 nmi circular orbit in preparation for de-orbit. The CRV would then wait in this orbit for the correct phase angle relation between itself and the landing site. Figure 3-13 shows a typical ground track of the CRV in this position over one day. As illustrated, the CRV pass near any particular point only once per day with the nearest point varying from 0 to 11 longitudinal degrees away. This effect would reach a minimum once every 4 days.

3.5.3 De-orbit

When the proper relation between the landing site and the CRV has been achieved, the CRV would perform its de-orbit burn. This burn would essentially be another Hohmann transfer, intersecting the 400,000 ft. atmospheric mark at a flight path angle of 1.5 degrees.



Reposition Orbit

fig. 3-9 Reposition Orbit

The delta-V required would be slightly higher for a tangential intersection (0 degree flight path angle). This was the value used for tabulation purposes. Once the CRV enters the atmosphere, Re-entry Dynamics determines its trajectory.

CRV Proximity Operations Profiles

From SSF Perspective
Numerically Generated

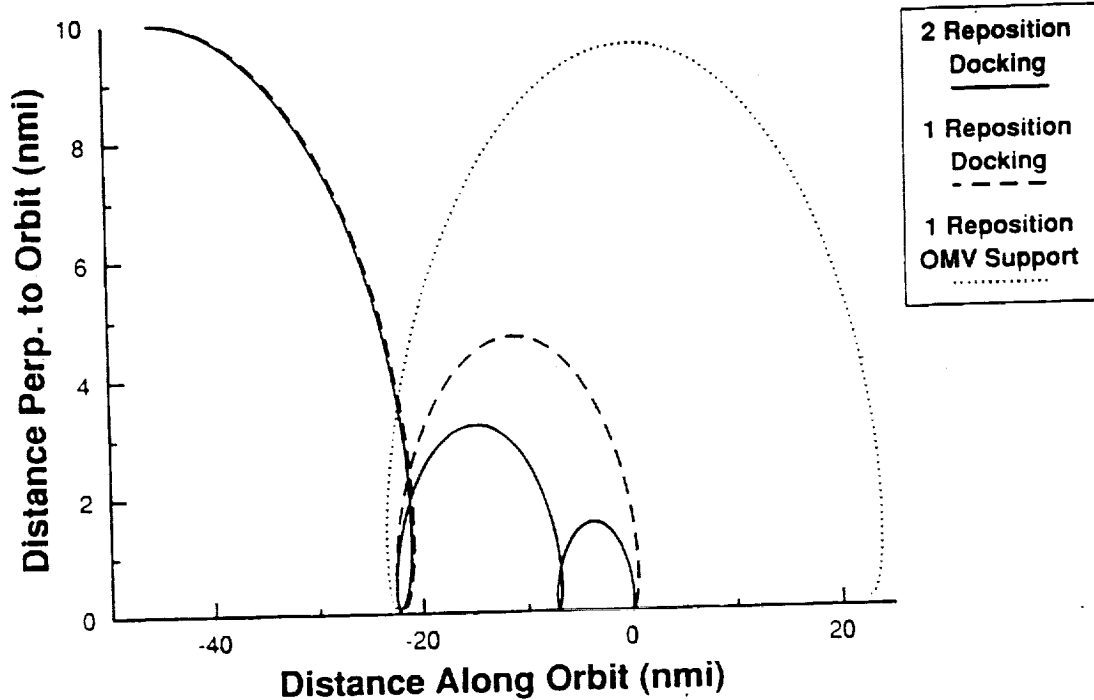


Figure 3-10, CRV Proximity Operations

Mission Profile - Descent to Re-entry

Exploded View
Numerically Generated

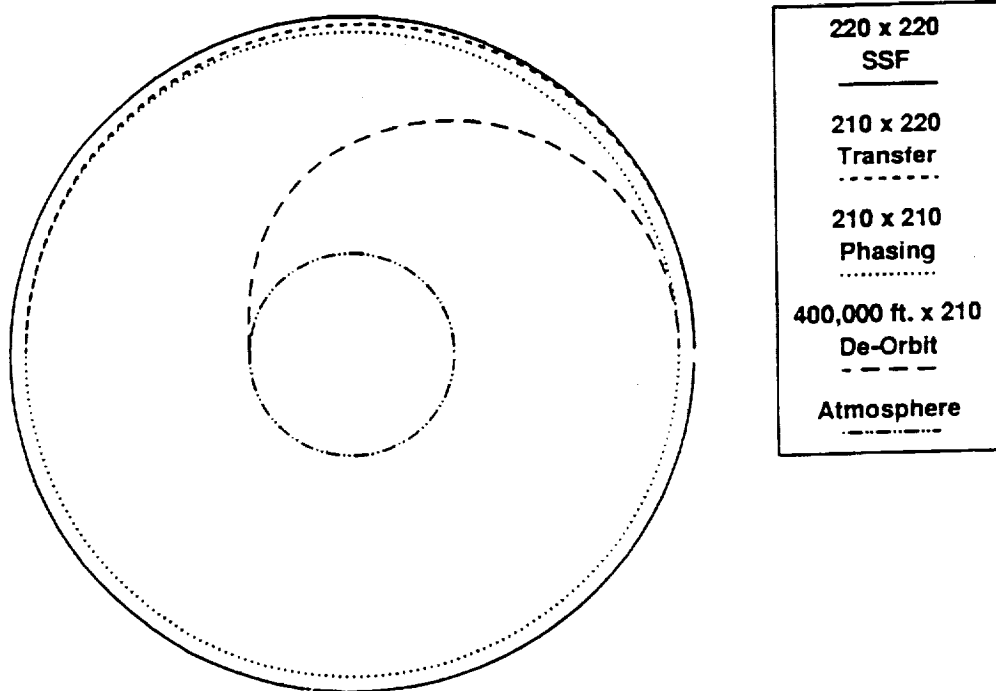
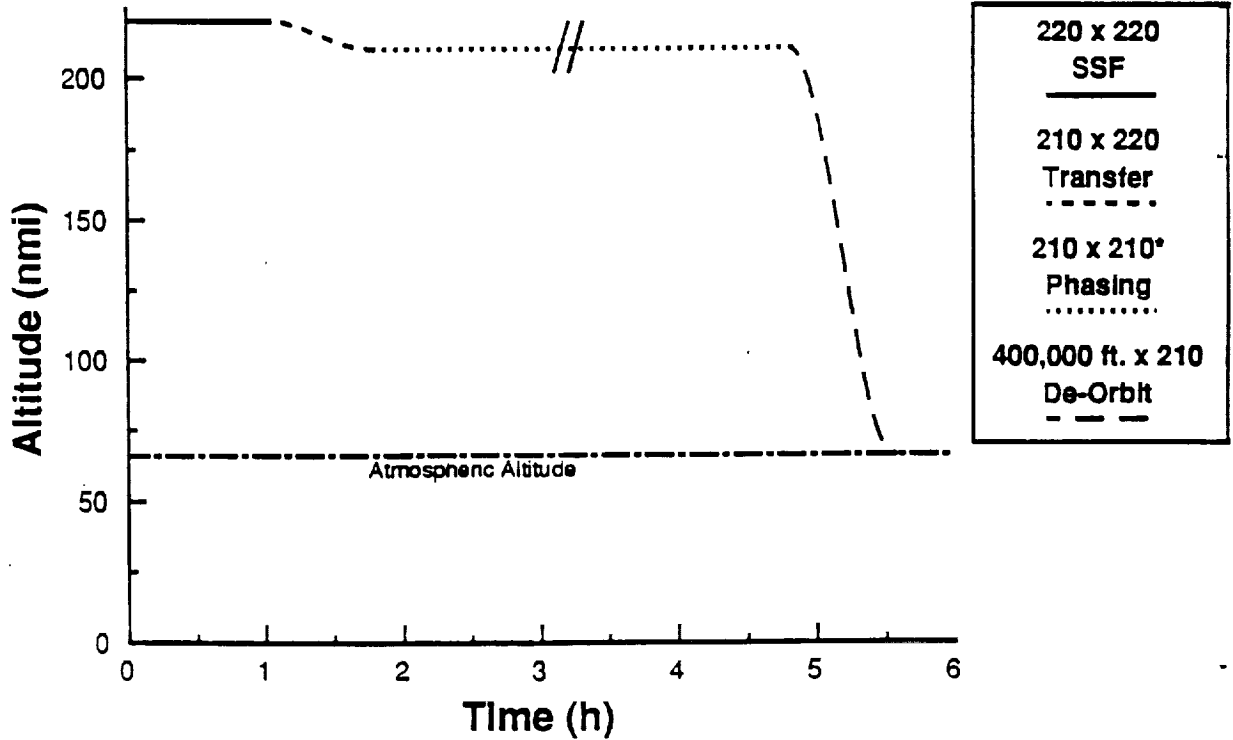


Figure 3-11, Mission Profile Descent to Re-Entry

Mission Profile - Descent to Re-entry

Altitude vs. Time
Numerically Generated



* Duration of 210 Phasing is Variable

Figure 3-12 Mission Profile Descent to Re-Entry

Ground Track

210 n.mi. Orbit , 28.5 Deg. Inclination
Timespan = 1 Day

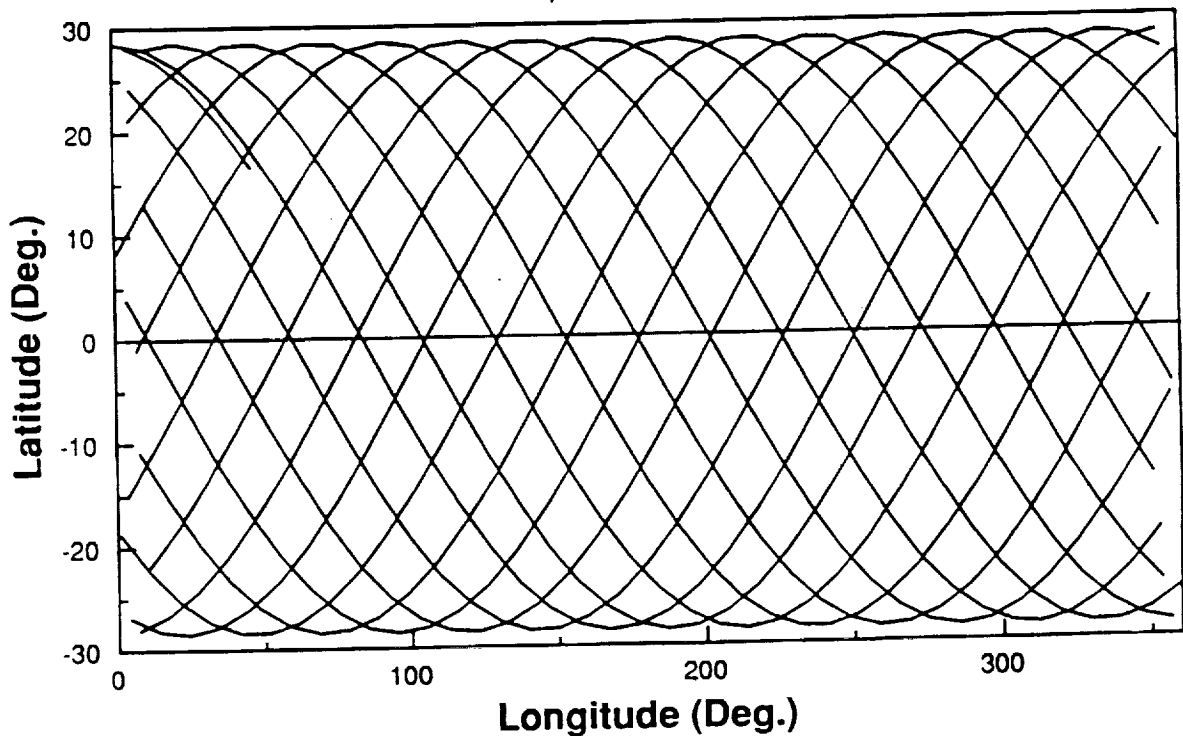


Figure 3-13 Ground Track

3.6 ALTERNATE MISSION PLAN (CRV HARD-DOCK)

This mission plan provides an alternative in the event that an OMV would not be available for use for payload transfer. In this case, the CRV would hard-dock to the SSF.

Instead of reiterating the overlapping sequences, the focus of this section is placed on those aspects that are significantly different. For further details, refer to the primary mission plan.

3.6.1 Space Station Preparations

The space station would need to prepare in advance for the CRV's arrival. All of the stowable antennas and booms in the flight path would have to be retracted. Radiators, solar collectors, and payloads would need to be re-orientated or covered to protect against RCS plume exhaust. During the rendezvous a "power-down" mode of the SSF would be performed. Any MSC/RMS operations would have to be halted until the CRV was docked.

3.6.2 Proximity Operations For Docking

If the OMV is not available, the CRV must move from the rendezvous zone to within 0.5 nmi of the SSF, where docking procedures would begin. To accomplish, this reposition orbits would be necessary. Figure 2-14 illustrates two scenarios for this procedure from an SSF perspective. The greater the number of repositions the smaller the total velocity change that would be required with the time necessary to complete the move increasing linearly (about 1.5 hours per reposition). The two reposition scenario was the one selected for use in docking rendezvous because the time required was not excessively long and it would allow corrections to be performed between the two repositioning orbits. First a 15 nmi reposition was performed, followed by a more accurate 5-7 nmi reposition. The CRV would not recover its circular orbit in between the two repetitions. This would reduce the amount of fuel used inside the CCZ but would also lessen the amount of time available for error corrections.

For departure from the SSF after docking, a similar method would be used. Two repositioning orbits (to reduce fuel use inside the CCZ) would position the CRV in the departure zone where descent and de-orbit maneuvers could be performed.

3.6.3 Berthing/Docking

In this scenario, the CRV would complete a maneuver along the plus V-bar which would place the CRV within reach of the Space Station Remote Manipulator Servicer (SSRMS). Arriving at a point approximately 3000 feet forward of the SSF (+ V-bar), in a tail down orientation (along the Nadir vector), the CRV cargo bay doors would open and expose the payload. Concurrently, the docking module bay compartment door would open to expose the retracted interface arm and TPDM. The SSRMS would then grapple directly onto the LM in the CRV bay and pull the CRV in to berth (upon extension of the mechanized docking arm) on the primary docking node (the forwardmost node on the port side of the module cluster).

Upon completion of this maneuver and reconfirmation of the payload interface the CRV would power down and the SSRMS would off-load the fresh LM and transport it to the vacant LM node (lower, aft node in +Z direction). The SSRMS would then unberth the spent LM from its node and transport it to the CRV bay.

This LM changeout process would take approximately 2.5 to 3 hours but, the CRV would remain at the SSF for a minimum duration of 6 hours until the next launch window open. At the designated time, the CRV would power up and the SSRMS would deberth the CRV. The SSRMS would grapple onto the LM in the CRV bay and the CRV docking mechanized arm would detach from the docking node and retract into its bay. Upon release, the CRV cold gas thrusters would fire and the bay doors would be closed. The CRV would then proceed to the departure zone. Throughout the entire docked period the SSF would monitor all CRV systems and subsystems and relay information to ground control support groups.

3.6.3.1 Payload Manipulation

The SSRMS would be used in all payload changeout procedures. It is a 17 foot long, multi-jointed remotely controlled, mechanical arm with a work envelope of 46.67 feet. It would be capable of controlling a 45,000 pound payload, as well as, docking a 250,000 lb. vehicle. The arm would be affixed with 4 video cameras (2 fixed, 2 with pan and tilt) and a light with each camera. Using the cameras, the SSRMS would be able to automatically track a moving target utilizing an Artificial Vision Function Tracking Mode (AVF). The SSRMS would be controlled by a SSF crewmember located in the

command and control console of the cupola in the secondary docking node. The crewmember would use the video cameras, radar acquisition, and direct visualization would also manipulate the SSRMS with a hand controller. The crewmember would also be capable of switching visual vantage points by utilizing the various camera setups at the SSF and the cameras mounted within the CRV bay.

3.7 ERROR IN PHASE ANGLE

Should the CRV gain a negative phase angle relation to the SSF (i.e. the CRV is ahead of the SSF in its orbit) correction would be necessary. The most likely cause of such an event would be a failure to insert into a circular orbit (110,210, or 220 nmi.) from the transfer orbit. This would necessitate waiting a full orbit for the next opportunity to re-insert. A failure to insert into the 210 x 210 nmi orbit from the 110 x 210 nmi transfer orbit, whether due to engine or guidance failure, would result in a phase angle error of 5.84 degrees. This particular situation will be examined as an example of possible correction procedures.

In the case of an insertion error there are two possible responses. One option is to let the CRV wait in its transfer orbit (if it remains out of the atmosphere) until the phase angle returns to its desired value. The time required for this, however, may be unacceptable. For instance, the 5.84 degree error resulting from a missed 210 x 210 nmi. insertion must wait in the 110 x 210 nmi. transfer orbit for approximately 60.6 hours (2.5 days). Another method of correction would be to transfer to the 220x220 nmi circular SSF orbit and perform a repositioning maneuver. As before, the change in velocity required for such a maneuver would be dependant upon the number of orbits used to reposition and, thus, the time these orbits take. Figure 3-14 shows the relation between time and delta-V required for a correction of phase angle error for the example. For this example problem it would be more efficient to perform a low delta-V, long time reposition correction rather than correct from the 110 x 210 nmi transfer orbit.

In general, the delta-V needed to perform the correction in a certain time would be dependant upon the magnitude of the error in phase angle. Figure 3-15 shows the relationship between delta-V and phase angle error for a two-orbit reposition from a 220x220 orbit in a time of about 3 hours. The method used for correction of a phase

Time Required vs. D-V
 For Repairing Orbit after Missed 110-210 Insertion
 Correction Made from 220 orbit

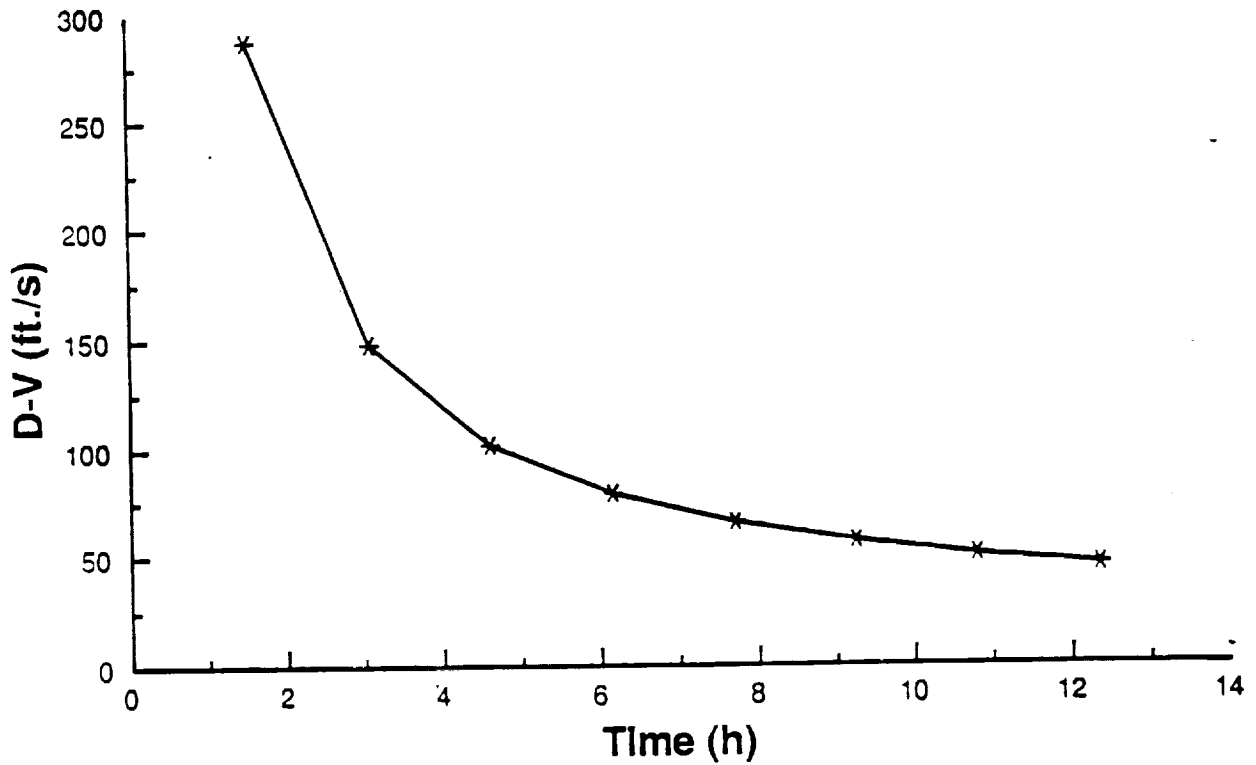


Figure 3-14 Time Required vs. Delta V
Correction Angle vs. D-V
 For Error In 220 Insertion
 Time Required = 3 hours

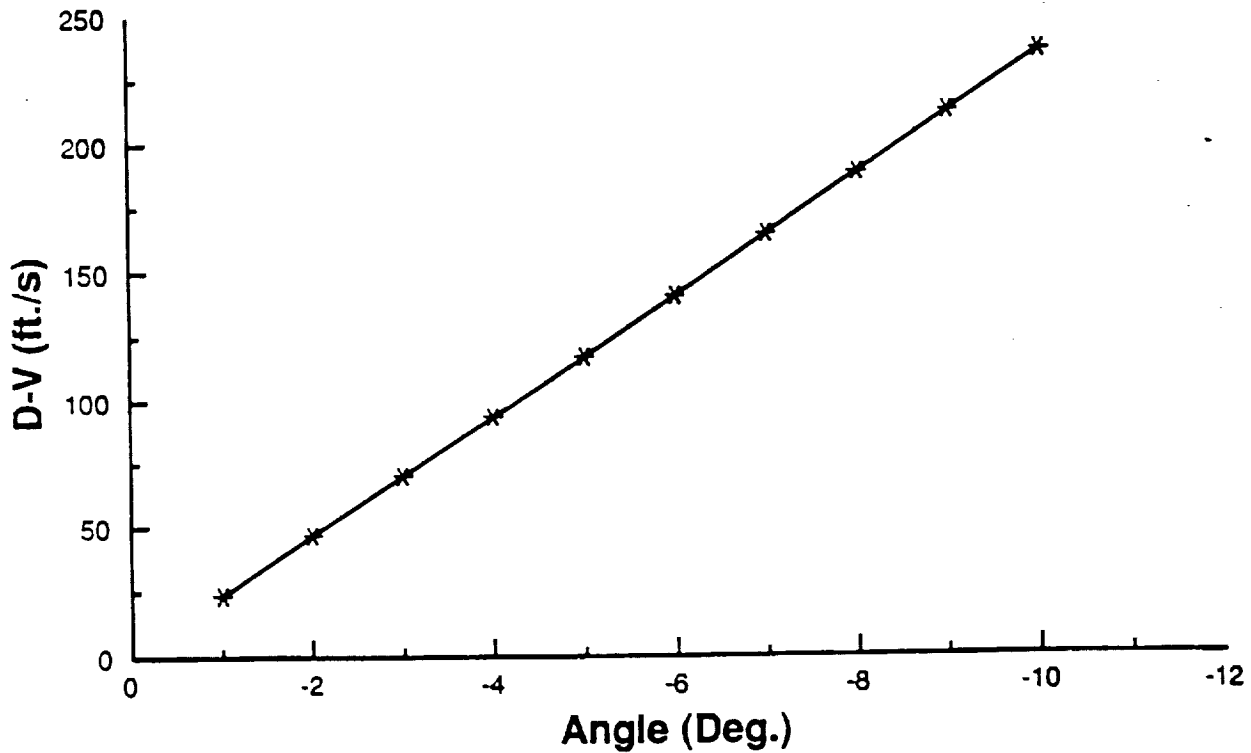


Figure 3-15 Correction Angle vs. Delta V

angle error would have to be determined on a case by case basis, depending on the time vs. the energy required.

3.8 MAN RATING THE CRV

The definition of man rating is to design piloted vehicle systems to safely accommodate people and to use their capabilities to ensure a successful mission. Since the CRV would not be used as an Assured Crew Return Vehicle (ACRV), it does not need to be man-rated. Redundancy, however, must be incorporated into the system to ensure that a single failure of a CRV system will not result in an abort or launch delay.

3.9 CONCLUSION

The CRV will be capable of performing the required mission utilizing one of two possible mission plans-denoted nominal (primary) and alternate (secondary).

In the nominal plan, the CRV would leave a 110 nmi. injection orbit, enroute to a stabilized "parking orbit" at the rear edge of the SSF CCZ. An OMV would be dispatched from the SSF and perform two roundtrips in the process of transferring and exchanging the logistics modules (LM). LM pickup and dropoff at the CRV would take approximately 30 minutes each and would be simplified by the inclusion of a Stabilized Payload Deployment System (SPDS). LM exchange at the SSF would nominally be performed solely by the OMV (approx. exchange time 1 hour) and contingently by the OMV with the aid of the SSRMS (approx. exchange time 2-3 hours). The overall nominal mission would be completed in (18.8 hours).

In the alternate mission plan, the CRV would leave the injection orbit and proceed directly to the SSF and dock with the help of the SSRMS. The SSRMS Would berth and deberth the CRV and perform all LM exchange maneuvers. The CRV would be required to stay docked to the SSF for at least 6 hours, until a launch window opens. As a result, the alternate mission plan would take considerably longer to perform.

In either mission plan, the flight would be directed by several ground control centers and the SSF crew. Any vehicle inside the CCZ would be controlled by the SSF crew and any vehicle outside the CCZ would be controlled by ground crews.

THIS PAGE HAS BEEN LEFT INTENTIONALLY BLANK

4.0 RE-ENTRY GUIDANCE AND DYNAMICS

The information gathered in this report comes mainly from the computer simulation IMP and comparisons to shuttle data. This report will concentrate on the re-entry phase of flight from an orbit of 220 nmi.

4.1 FLIGHT PROFILES CONSIDERED

The analysis was begun by assuming unconstrained heating rates and a landing weight of 134,000 pounds. At a bank angle of 48 degrees and no heat constrains the downrange was found to be 5291 nmi and the crossrange was found to be 1370 nmi. Adjusting the final weight to be 100,000 pounds and adding a heat constraint of 70 BTU/FT²- sec, a maximum L/D of 1.49, a downrange of 5291 nmi, and a crossrange of 1351 nmi was calculated (See Fig 4-1). From the IMP program two other profiles were also measured, Altitude vs. ime and Mach vs. Time (see Figures 4-2,4-3). The FOOTPRINT program written by Andrew Johnson (University of Minnesota Aerospace student) was also used in the analysis.

The first analysis used the IMP program to simulate re-entry an angle of attack of 45 degrees. Later it was found that maximum L/D occurred at an angle of 25 degrees. As a result, the program was modified using this value (Figure 4-4). The angle of attack was changed to 20 degrees prior to landing to give a max L/D of 6 in order to perform the flare maneuver.

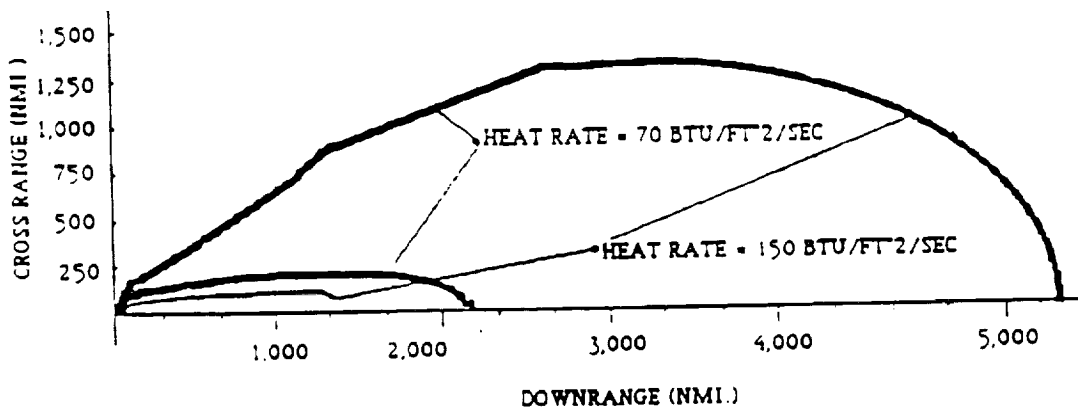


Figure 4-1 Footprint

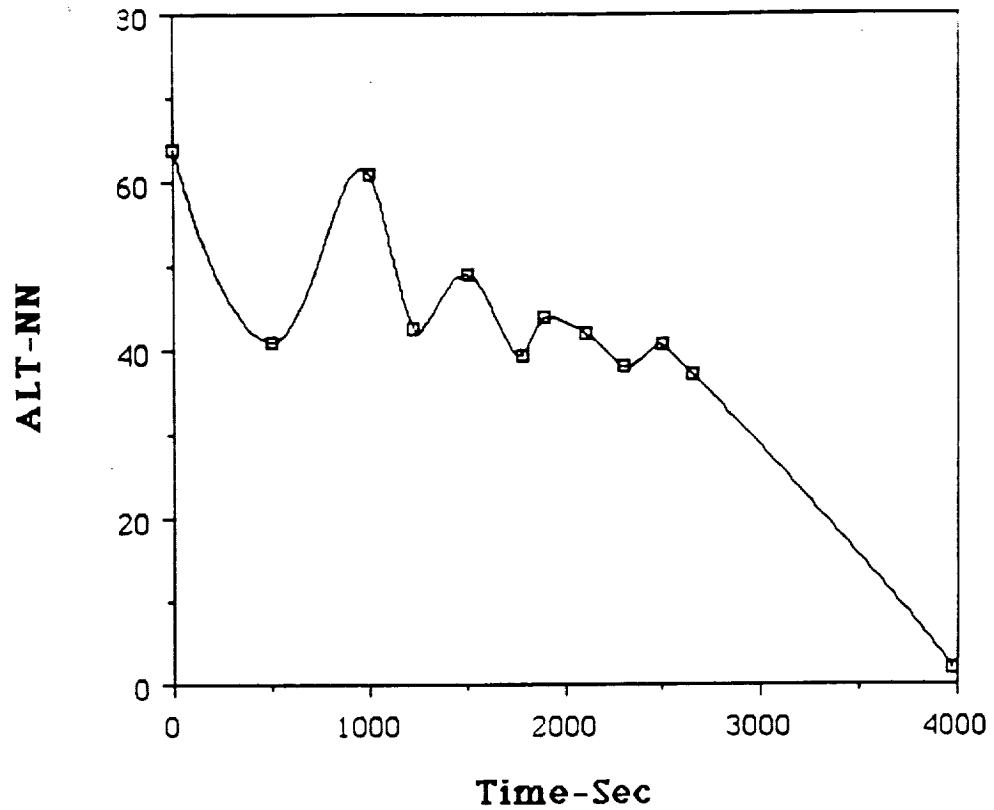


Figure 4-2 Altitude vs Time

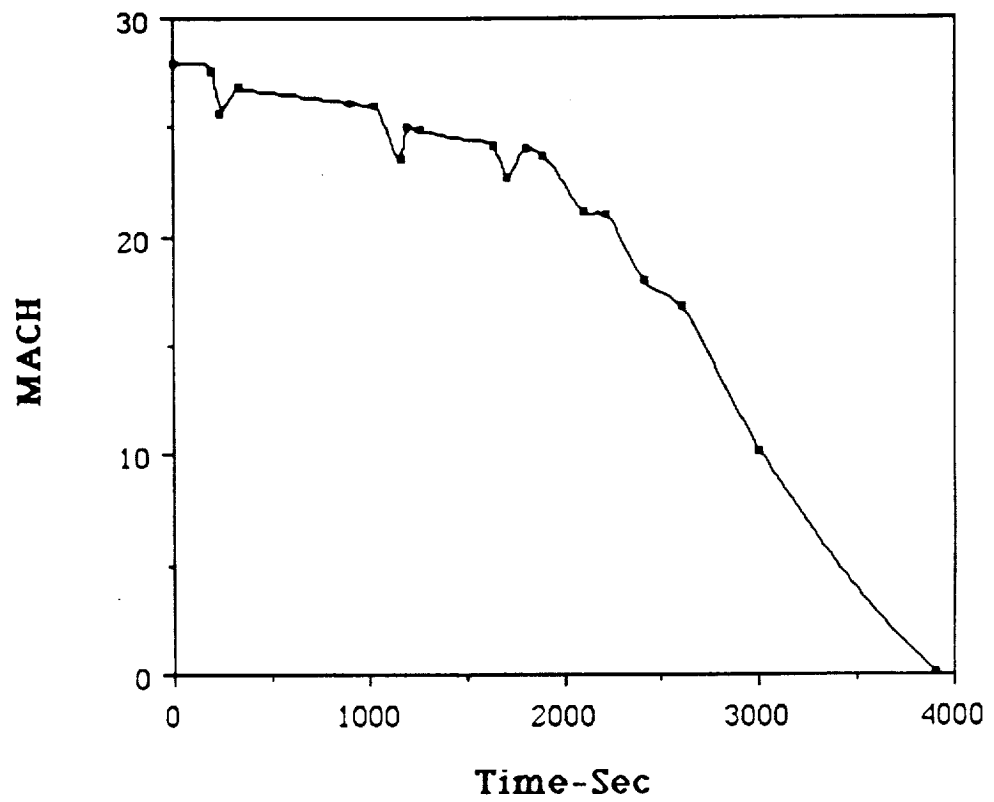


Figure 4-3 Mach vs Time

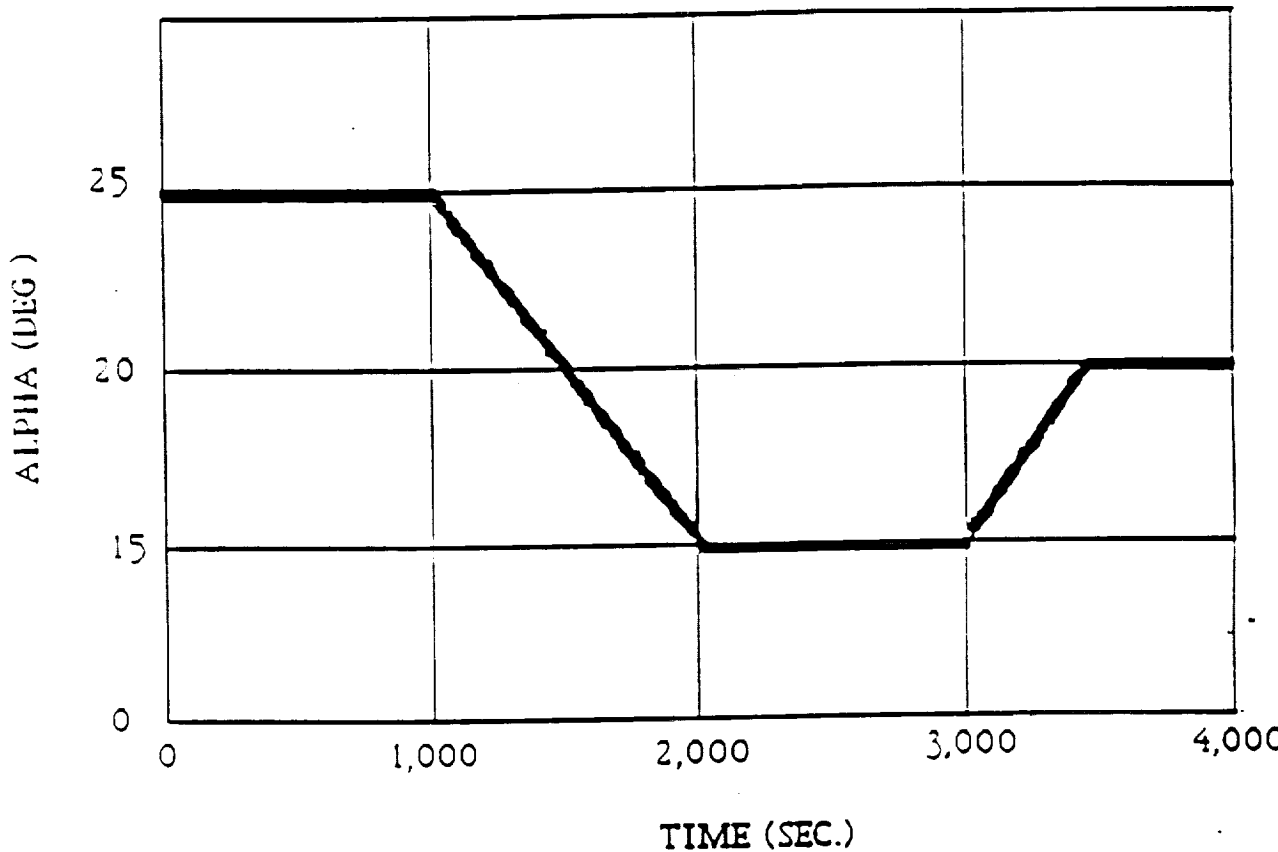


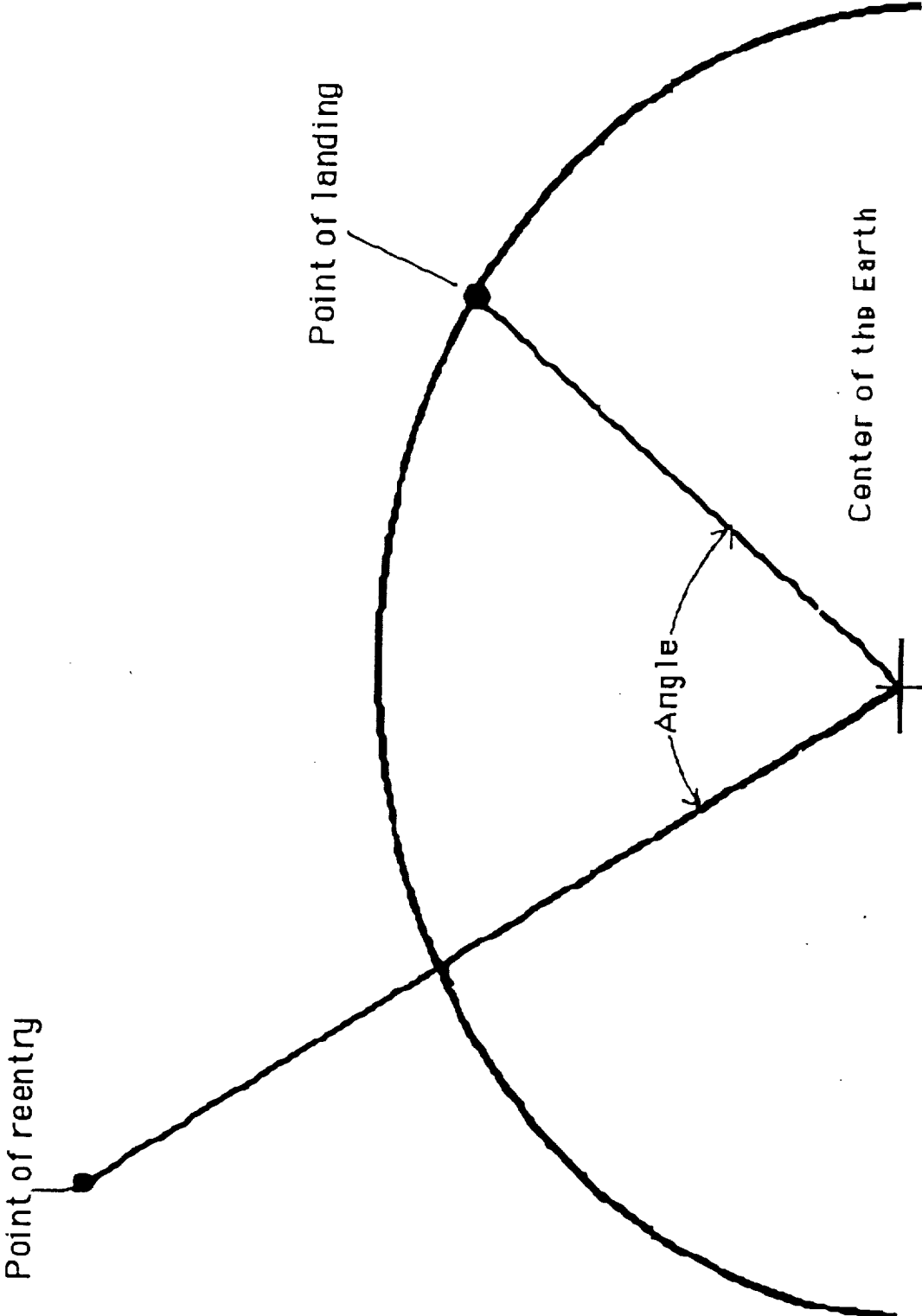
Figure 4-4 Angle of attack for IMP simulations

Several runs were made varying the angle measured from the center of the Earth between the re-entry point and the landing site (Fig 4-3). It was found that by increasing this angle the impact latitude and longitude calculated by IMP came closer to the desired landing site of KSC (Fig 4-6 and Fig 4-7). This simulation was done with a desired landing window of ± 500 nmi latitude and ± 700 nmi longitude.

Using the IMP program, different flight path angles were run during re-entry and the optimum was found to be -1.5 degrees. Originally the re-entry weight was estimated to be 134,000 pounds and the angle of attack of 45 degrees. When the weight was lowered to 100,000 pounds the optimum re-entry angle of attack was of 25 degrees with a maximum L/D of 1.49 (from HABP), the maximum cross-range was found.

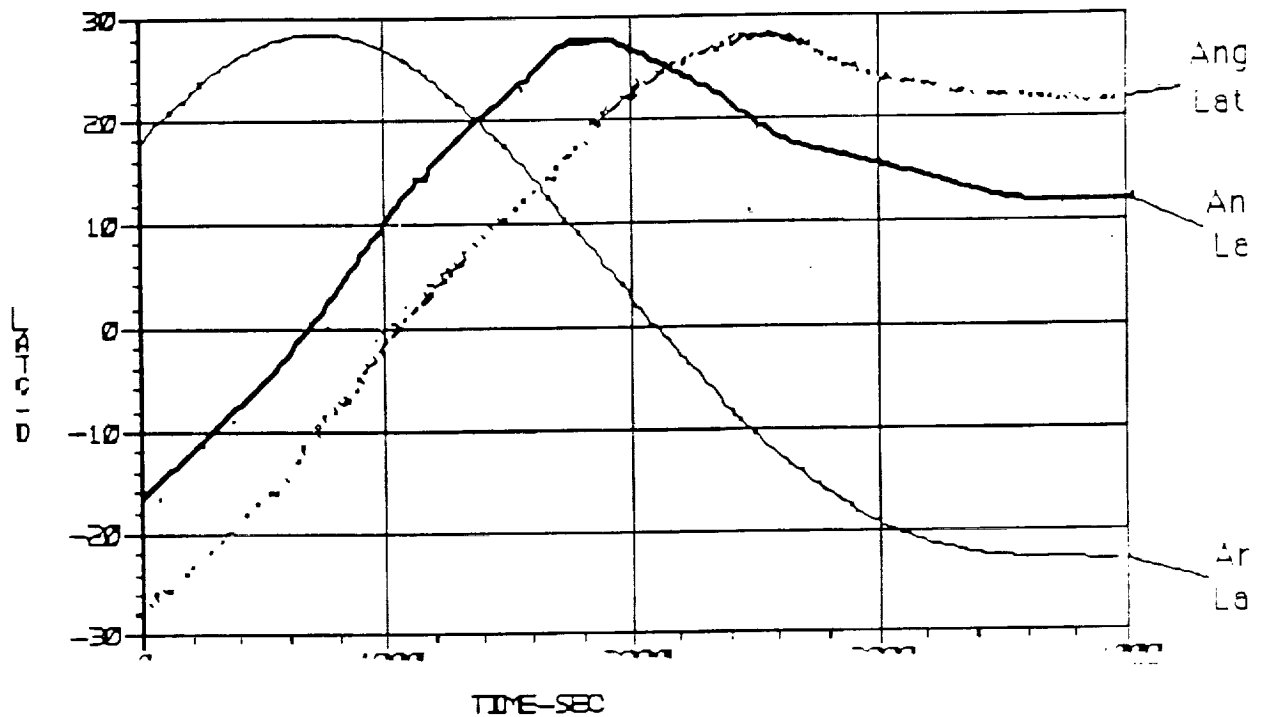
After leaving the space station the CRV would perform a 180 turn (yaw) in order to turn tail first. The de-orbit maneuver would then begin. A pitch maneuver would turn the CRV to a nose up position for re-entry. The CRV would then re-enter using an angle of attack

Figure 4-5 Angle From Re-Entry Point To Landing Site.



of 25 degrees with a flight path angle of -1.5 degrees. The atmospheric re-entry would begin at approximately 400,000 ft.

The re-entry velocity would be Mach 26 and a large portion of the CRV's energy would be dissipated by atmospheric drag. According to the TPS group the maximum heat value would be 3000 °F. This was the limiting variable for crossrange. During re-entry the CRV would enter a black-out zone for 12 minutes during which the CRV would have to totally rely on on-board computers. Ground control would not be possible because of interference. Banking maneuvers would be executed at an optimal angle of 47.8 degrees, which is when maximum heating would occur.



Angle= estimated reentry position to landing site angle from the center of the Earth.

Fig 4-6 Latitude calculated using IMP

The CRV would rely on the RCS system for stability control throughout most of the flight profile in the upper atmosphere and then phased out in stages during descent. Based on shuttle data, the phase out would occur as follows: when the dynamic pressure reaches 10 psi the aft roll jets would be turned off and the ailerons activated; at a dynamic pressure of 20 psi the aft pitch jets would be turned off and the elevators would become active; at Mach 3.5 the

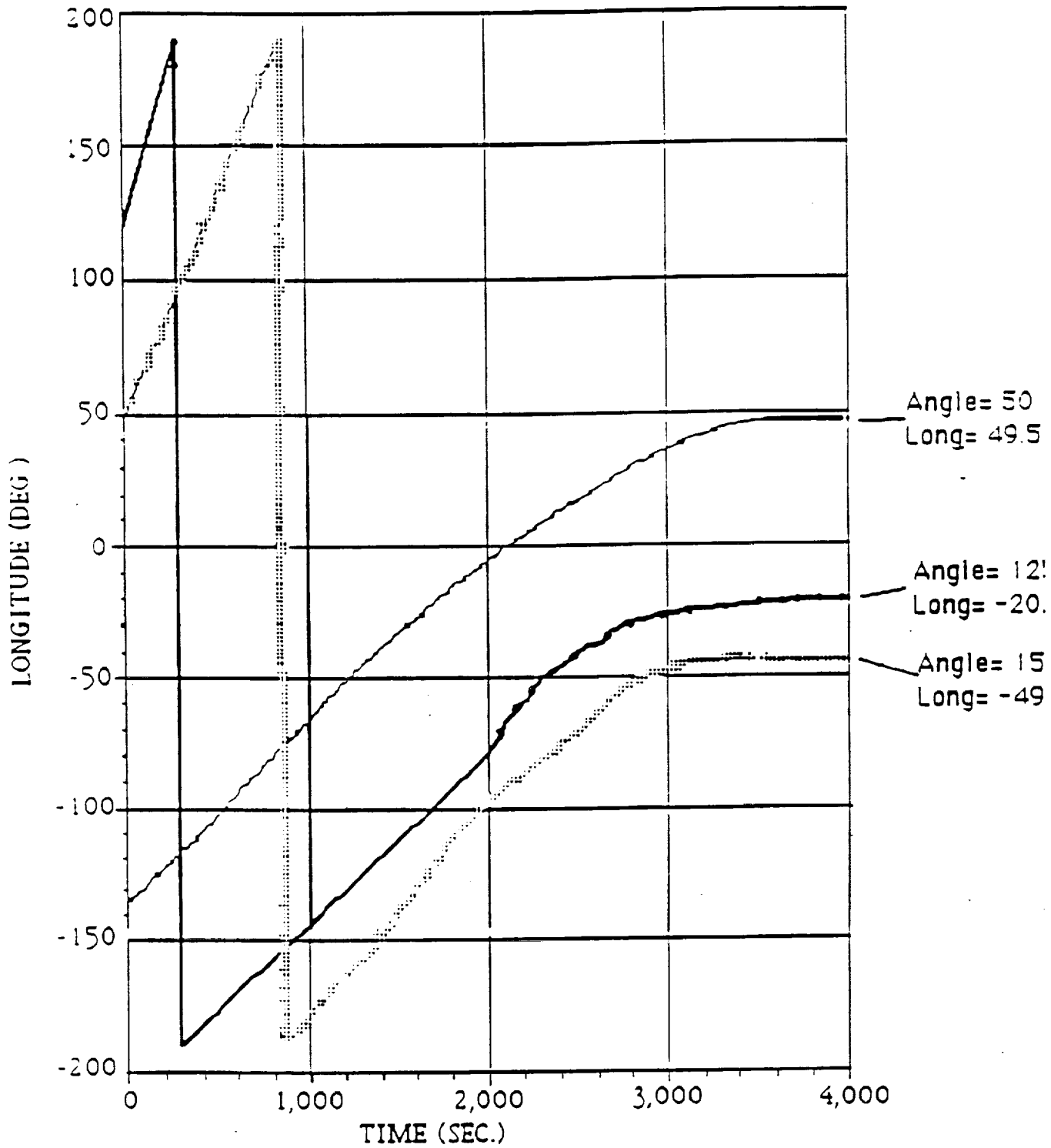


Figure 4-7 Longitude Calculated Using IMP

winglets would become effective. It should be noted that, depending on the size of the control surfaces and strength of actuators (servos), these values would change for the CRV.

4.2 Atmospheric Guidance and Navigation

Atmospheric entry would begin at approximately 400,000 feet (see Fig 4-8). As the vehicle descends atmospheric drag would dissipate its energy and generate a great deal of heat, with portions of the CRV reaching up to 3000 degrees Fahrenheit. This heat ionizes the air surrounding the vehicle and blocks communication with the ground. This lasts about 12 minutes.

At approximately 180,000 feet (following black-out) the vehicle would intercept the TACAN at KSC which would give both range and bearing measurements. This information would be updated every 37 seconds. The on-board system would compute the angle between lines from the CRV to magnetic north and to the ground station, thus, providing the bearing to the station. The system aboard the spacecraft would act as a DME and give distance information to the TACAN station.

During the flight, S-turns could be done as high as 180,000 feet to help decelerate the CRV and control its rate of descent (Fig 4-9). The number of S-turns to be performed would depend on the landing site and the required cross-range. The CRV would make S-turns with bank angles of as much as 60 degrees. Additionally, if the pitch control surface is used to keep the descent rate constant, the angle of attack will increase, which would increase drag on the CRV. Starting from 180,000 feet, the CRV would use the TACAN to provide guidance while performing S-turns to provide a controlled descent profile to the landing site.

When the vehicle reaches about 85,000 feet and is approximately 60 miles from the landing site the terminal-area energy management systems (TAEM) begin. They will update the state vector to give the optimal trajectory to the landing site. These TAEM would provide a vector for the vehicle to fly to the first waypoint (latitude, longitude), which is located on one of the two heading alignment cylinders (two big imaginary circles 7.5 miles from the runway). TAEM would line the vehicle up with one of these cylinders, follow its curve, and ultimately line the CRV up with the runway.

DEORBIT BURN
1 HR BEFORE LANDING
220 NMI.
MACH 26



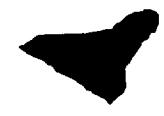
BLACKOUT
30 MINUTES BEFORE LANDING
300,000 FEET 23,900 FT/SEC



MAXIMUM HEATING (3000°F)
20 MINUTES BEFORE LANDING
230,000 FT 19350 FT/SEC.



EXIT BLACKOUT
12 MINUTES BEFORE LANDING
180,000 FT 13,500 FT/SEC



BEGIN ENERGY MANAGEMENT SYSTEMS
5 MINUTES TO TOUCHDOWN
80,000 FT 1,900 FT/SEC



INITIATE AUTOLAND SYSTEMS
1.5 MINUTES TO TOUCHDOWN
14,000 FT 650 FT/SEC.



AUTOLAND INTERFACE WITH MICROWAVE LANDING SYSTEMS
ADJUSTING SPEED BRAKE TO KEEP ON GLIDE SLOPE
7.5 MILES TO RUNWAY

24 DEGREE GLIDE SLOPE



INITIATE PREFLARE (INCREASING ANGLE OF ATTACK)
30 SECONDS TO TOUCHDOWN
2 MILE FINAL APPROACH
2,000 FT 580 FT/SEC



COMPLETE FLARE
1.5 SECONDS TO TOUCHDOWN
1/2 MILE FINAL APPROACH 450 FT/SEC / 115 FEET ABOVE GROUND
135 FT 450 FT/SEC

1.8 DEGREE GLIDE SLOPE



LANDING GEAR DOWN
10 SECONDS TO TOUCHDOWN
1/5 MILE FINAL APPROACH
100 FT 400 FT/SEC.



TOUCH DOWN
320 FT/SEC

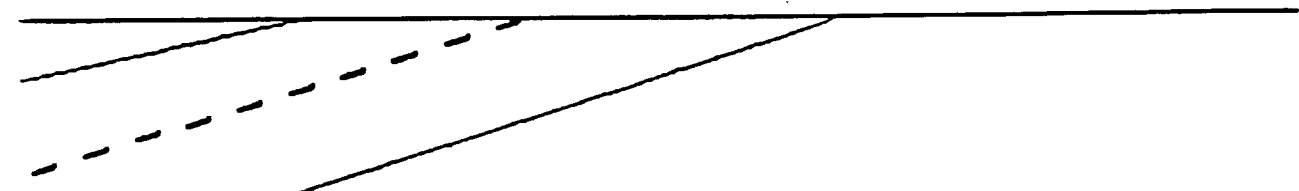


Figure 4-8 Atmospheric Re-Entry

ORIGINAL PAGE IS
OF POOR QUALITY

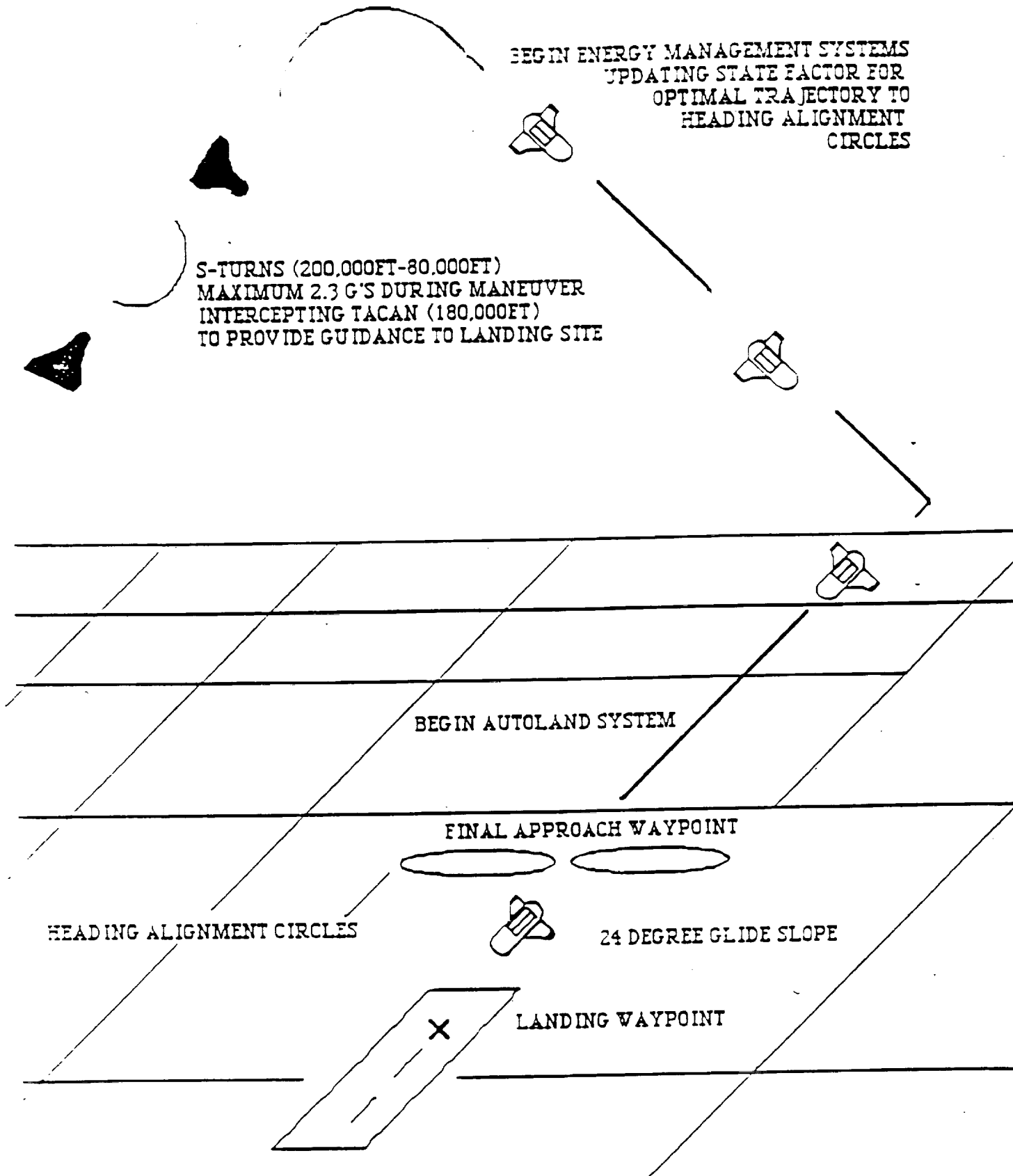


Figure 4-9 S-Turns Manuevers

At this point, the autoland interface would commence. The vehicle would be about 14,000 feet above the ground, travelling at 650 feet per second, and would intercept the Microwave Landing System (MLS). This system provides angle of elevation, angle of azimuth, and range. The beam scans about 15 degrees to the left or right of the runway centerline and about 35 degrees of vertical range. As the CRV deviates from the 'ideal' flight path projected from the ground, the autoland system would correct using the control surfaces and the speed brakes as necessary. The glide slope was calculated using the formula:

$$\text{Average Angle(Descent)} = -\text{Drag/Weight}$$

which gave an angle of about 24 degrees for use on the MLS (Fig 4-10). The vehicle would fly this glide slope down to approximately 135 feet above the ground where it would then transition to a descent angle of 1.8 degrees (1.5 for Shuttle). This would be accomplished by carrying excess airspeed during the final approach so that when it maneuvers to a shallower angle, the rate of descent would still be within landing parameters. The final landing lift to drag ratio would be around 6, and is within the requirements necessary for a flare maneuver.

Precise altitude information is provided by radar altimeters. The difference in time for an emitted pulse to return provides with data to measure the height above the ground. This is critical during touchdown because it provides precise data for the sink rate and the height of the rear wheels above the runway. This is important in order to achieve a smooth landing and so the 4g. limit is not exceeded at touchdown.

All of the required ground based equipment would provided at the primary and secondary landing sites (Edwards, Hawaii, Guam, Dakar).

4.3 PREDICTION OF G-LOADING ON VEHICLE

Using the program IMP the g-loading of the vehicle came to a maximum of 1.1 g's during reentry. As the vehicle goes through transition from zero gravity to the earths atmosphere (1g), the loading on the vehicle will increase. The greatest change in g's occurs when the vehicle comes in contact with the earth's atmosphere. The loading during this phase can exceed 8 g's for a ballistic reentry.

Figure 4-11 shows the acceleration in g's for the S-turn or roll reversal maneuvers. Similar to the shuttle, the CRV would execute these S-turns in the form of sixty degree banking turns which would increase the g-loading by a factor of 2 times to that of the straight and level reentry.

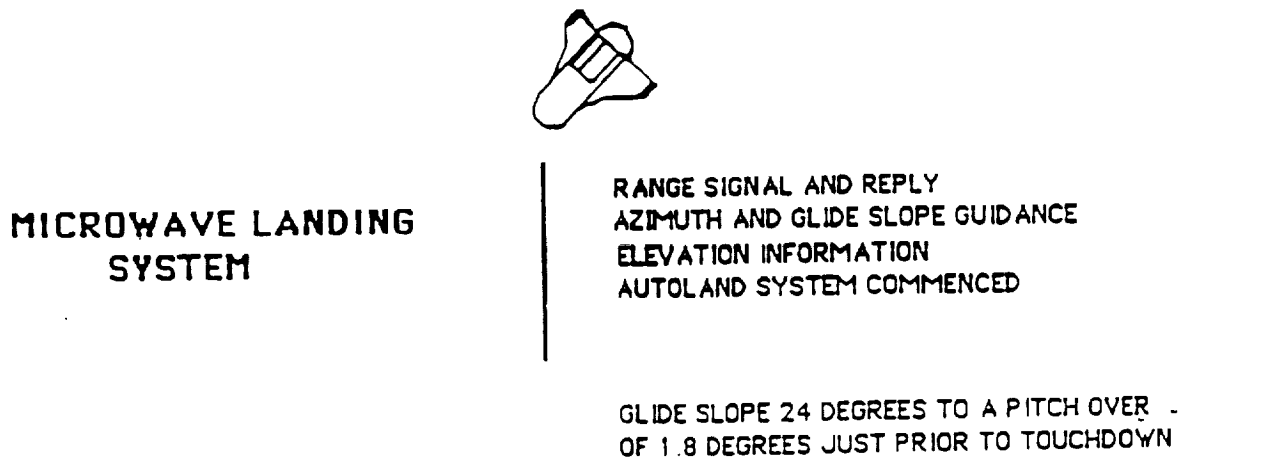


Fig. 4-10 Autoland Sequence

Empirical formulas were also used to estimate the g-loading. The maximum loading was found to be approximately 1.4 g's.

$$\text{S-turn g-loading} \quad \text{Load Factor} = \frac{\text{Weight} \cdot (\text{Velocity}^2)}{g \cdot \text{Radius}(\text{turn}) \cdot \cos(\text{bank})}$$

$$/a/ = \text{acceleration} = \frac{g (1 - \text{Vbar}^2)}{L/D} \quad \text{Vbar} = \frac{\text{Reentry velocity}}{\text{sqrt}(g \cdot \text{radius}(\text{earth}))}$$

4.4 RANGE CALCULATIONS

The range calculations were performed using formulas (Ref. 4.1, pp. 22-29). The footprints were plotted using a computer program written by Andrew Johnson, a student at the University of Minnesota. This footprint was constrained by not allowing the heating rate to exceed 70 btu/ft²-sec.

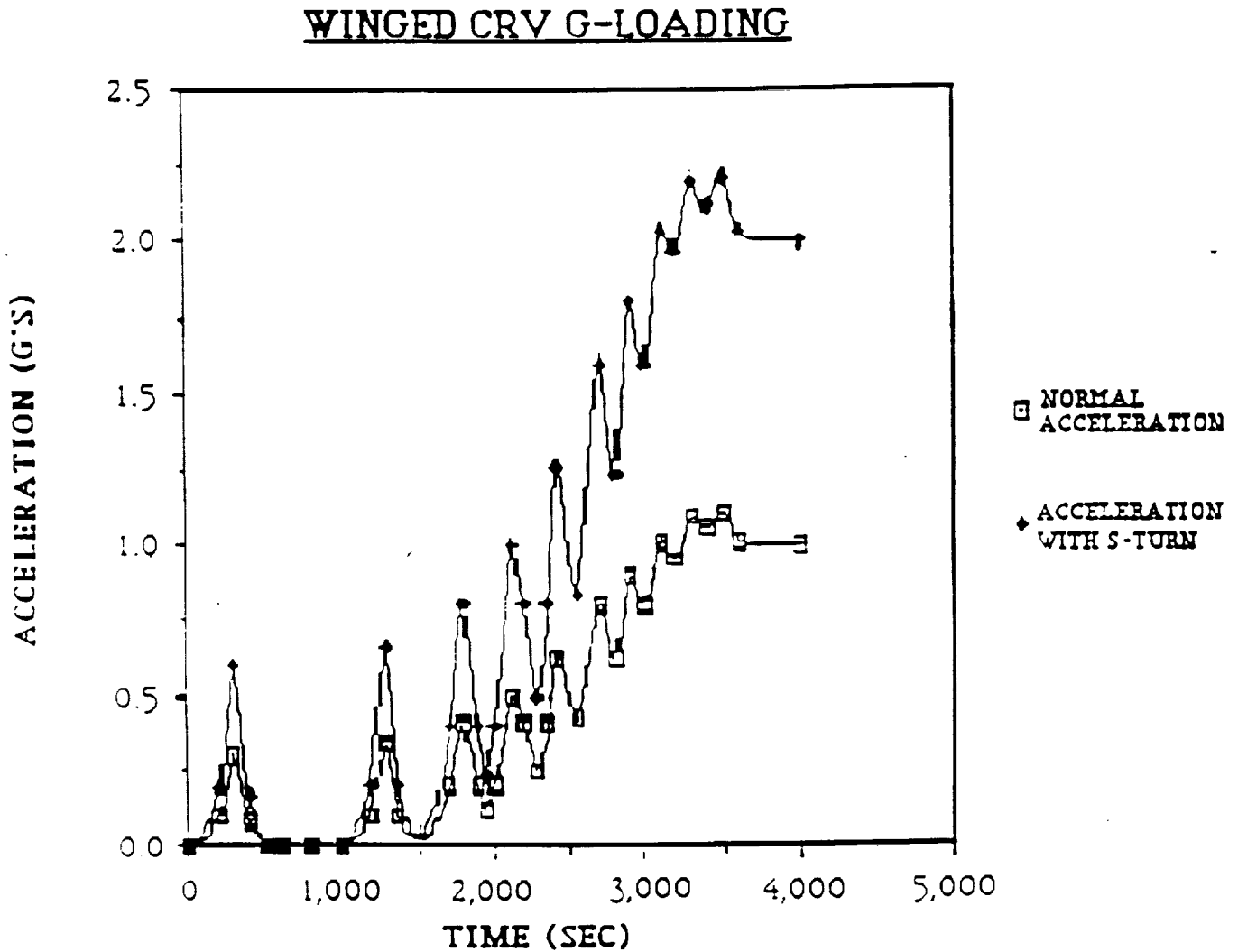


Fig. 4-11 Change in g-loading during banking
If an emergency were to occur the range would be adequate to reach landing sites that required less than 3400 nautical miles of downrange (Fig. 4-1).

5.0 AERODYNAMICS

5.1 GENERAL AERODYNAMIC CONSIDERATIONS

5.1.1 Hypersonic and Supersonic Wing Characteristics

The optimum wing shape for a hypervelocity vehicle involves a highly swept leading edge. This is because large sweep reduces drag and aerodynamic heating. The drag is due primarily to wave drag (Ref 5.5, p.23). The heat load on the wing is greatest at the leading edge and on points of protrusion on the wings lower surface. Sweeping the wing reduces the heat load by decreasing the stagnation effects along the wing. Aerodynamic heating is also a function of L/D and wing loading. The heat load increases as L/D decreases or as wing loading increases (Ref 5.5, p.13). Another advantage of wing sweep is that it allows the use of a larger leading edge radius (Ref 5.5, p.23).

A characteristic of highly swept wings is that increasing the angle of attack geometrically unsweeps the leading edge (Ref 5.5, p.16). The effective leading edge sweep is given by the equation:

$$\text{i.e. sweep} = \text{SIN}^{-1} * [\text{SIN}(\text{sweep}) * \text{COS}(\alpha)]$$

This results in highly swept wings gaining their best L/D values at high angles of attack.

A major disadvantage of highly swept wings is that high pitch inertias are produced (Ref 5.5, p.23). This is a problem because large pitch inertias may be difficult for the control system to overcome. A second disadvantage of swept wings is that it results in a degradation of subsonic performance. This is especially critical during approach and landing. As a result, the advantages of high speed performance must be balanced against the need for low speed stability and control.

The hypersonic L/D of a wing is a function of the planform area. This is because the pressure forces on the upper surface of the wing can be neglected when compared to the dynamic pressure forces on the windward side (Ref 5.5, p.23). This effect becomes more dominate as Mach number increases. As a result of this high speed phenomena the best hypervelocity L/D values are achieved using large planform

areas and low aspect ratios (Ref 5.5, p.26). Low aspect ratio helps reduce wave drag and aerodynamic heating of the wing.

The aerodynamic center and center of pressure of a hypersonic wing while in the hypersonic regime are at approximately the same position, 50% of the mean chord. During subsonic flight, however, the aerodynamic center is at approximately the 25% mean chord point while the center of pressure is between 40-45% of the mean chord (Ref 5.5, p.23). These changes will alter the stability and control requirements of the vehicle as it transitions from one speed regime to another.

The best wing configuration for a hypervelocity vehicle would employ a low wing. This is because a low wing would supply a uniform surface which could also act as a heat shield and protect the fuselage and payload from excessive heat buildup. A low wing also allows for a continuous carry-through wing structure (Ref 5.5, p.26). This is important from the view point of structural strength and efficiency of material use. An additional advantage of a low wing is that it allows the landing gear to be stored within its structure instead of within the fuselage. This is useful because it provides a more stable base for landing (because the distance between the main gear can be made larger). Storing the gear in the wings also eliminates the need to raise the payload bay above the wheel wells (which would waste space and increase parasite and profile drag) as would be necessary with fuselage stored gear. A final benefit of a low wing is that during landing it will experience a reduction in induced drag due to ground effect.

A delta shaped wing is recognized as having the best hypersonic performance. This is because it employs large sweep angles and gives a large planform area with a relatively short span. This results in good hypersonic L/D values and heating characteristics. Disadvantages of delta wings are high pitch inertias and poor slow speed performance. A further disadvantage is that a delta wing achieves its best performance at high angles of attack (30-40 deg.), which limits its usefulness because it may blanket the control surfaces and could cause loss of directional stability (Ref 5.5, p.18). The high angles of attack required to attain C_{lmax} are also too large for realistic operations.

5.1.2 Subsonic Characteristics of Hypervelocity Wings

In the subsonic region it is desired to have a wing configuration which will provide good stability and control during the approach and landing phase. It is also desirable to have a low stall speed so that the landing speeds will be low and the vehicle can be stopped easily within a reasonable distance with a minimum g-loading due to deceleration. In order to achieve good low speed performance the hypersonic wing will have to generate as much subsonic lift as possible. This lift is a function of the area and C_{lmax} (Ref 5.5, p.18). To attain the shortest landing distances it is desirable to have a high C_{lmax} and low wing loading (W/S). For a runway landing a $C_{lmax} = 1.0$ is a good approximation (Ref 5.5, p.18).

Subsonic flight considerations are limited mostly to the approach and landing phase because the vehicle will not experience subsonic flight over extended distances. This is because the hypervelocity craft will be energy rich when it re-enters and descends through the atmosphere. This energy is best used by keeping the vehicle in the hypersonic and supersonic regimes right up until the vehicle is in the proximity of the landing site. This is due to cross-range and down-range considerations.

Subsonic L/D performance is best achieved by increasing lift than by attempting to reduce drag (Ref 5.5, p.13). Subsonic L/D is very span dependant and can be significantly improved by increasing the span. Large spans, however, cause a reduction in hypersonic performance due to wave drag and excessive heating. Additionally, subsonic L/D also improves when the wing sweep is small.

A delta wing performs poorly at low speeds because it has a large planform area in relation to its span. The large planform area and small span (low AR) results in low L/D because of the large amounts of drag generated. The L/D is further reduced because the C_{lmax} for a delta wing is achieved at much too large of an angle of attack for flare (30-40 deg compared to the desired flare angle of 15-20 deg.) (Ref 5.5, p.18).

A good compromise between hypervelocity requirements and subsonic performance is achieved by a dual trapezoid wing. This type of wing shape consists of a highly swept root section (for high speed performance) and a less swept outboard section (for the desired low speed span effects).

5.1.3 Leading Edge Radius

The size of the leading edge (l.e.) radius effects the aerodynamic heating of the leading edge (l.e.), the wing lift, and wing drag. For subsonic speeds a smaller l.e. radius will create flow separation sooner, and generally decreases the coefficient of lift. For supersonic speeds a large l.e. radius creates a larger drag. A smaller l.e. radius effects aerodynamic heating by creating a higher stagnation temperature at the leading edge. The minimum l.e. radius for the shuttle is approximately equal to 0.35 feet.

5.1.4 Wing Camber

The best wing type for hypervelocity vehicles is a bi-convex wing with no camber. The reason camber is not used is that at supersonic speeds the wave drag penalty associated with camber would be too great. This increase in drag would increase the thrust requirement at take-off and reduce the L/D ratio for super and hypersonic speeds during re-entry. The subsonic L/D ratio would not be greatly effected since a cambered airfoil also increases the coefficient of lift, which would compensate for the increase in the drag coefficient.

5.1.5 Directional Stability

During re-entry directional stability is provided in part by the RCS. As the vehicle decreases in altitude the atmosphere will become more dense and directional stability will become more dependant on the use of vertical surfaces, such as a vertical tail, wing tip fins, or ventral fins. These surfaces will then be the primary source of lateral-directional stability with the RCS functioning as a secondary source of stability and control (Ref 5.9, p.21).

5.1.5.1 Vertical Tail

Directional control of a hypervelocity vehicle can be achieved through the use of a vertical tail. The vertical tail would be mounted on the aft section of the craft along the center line. The height of the tail would depend largely on the vehicle length and the wing size and shape. This is because during re-entry the angle of attack is very high (optimum when AOA=45 deg.) due to heating and stability considerations. At high angles of attack the body and wing tend to blanket the tail from the free stream flow (Ref 5.5, pp. 31, 32, 35). In order to retain directional stability some amount of the tail must

be exposed above the blanketed region. This requires that the tail be reasonably large. The size of the tail would be limited by its weight; which effects the location of the vehicle center of gravity (Ref 5.5, p. 35).

5.1.5.2 Wingtip Fins

An alternative to a large centerline tail is the use of wingtip fins. Wingtip fins are capable of providing lateral-directional stability and control in both the hypersonic and subsonic regions (Ref 5.9, p.3-21). Fins actually improve the hypersonic stability compared to a single vertical tail and reduce the dependance on the RCS for control throughout the entire re-entry envelope (Ref 5.9, p.3-21).

For optimum stability symmetrically shaped fins should employ "toe-in" (Ref 5.5, p.32). During hypersonic flight the "toe-in" would increase drag on the fins. This would tend to "weather vane" the vehicle into the relative wind. If the vehicle shifts laterally to one side the drag will increase on that side due to the increased exposure of the surface area. The lift generated by the "toe-in" will also tend to act as a restoring stability force.

In the subsonic region the "toe-in" will be oriented so that it is at an angle of attack to the relative wind. Since the drag will be less of a factor at these speeds it is the lift due to this incidence angle which creates the restoring forces for stability. The yaw moment equation is:

$$C_y = 2\sin^2 B$$

An alternate to "toe-in" of a symmetric fin would be to use a wedged shaped fin. A wedge shaped fin accomplishes the same result as "toe-in" (Ref 5.5, p.32). Both techniques result in increased lateral stability.

In addition to greater stability wingtip fins allow the wing to produce more lift than a wing of comparable size and span without winglets. This is because the winglets decrease induced drag due to a reduction in spanwise flow and wingtip vortices (Ref 5.5, p.32). The net result is an effective increase in the wings aspect ratio.

Disadvantages of wingtip fins used in conjunction with a highly swept delta wing are that at high angles of attack large vortices are shed from the wings leading edge. These vortices could blanket the

fins (Ref 5.5, p.33). An additional disadvantage -compared to the vertical tail- is that the fins produce more drag. As a result the L/D performance of a finned vehicle would be less than for the single tailed vehicle.

5.1.5.3 Ventral Fins

Ventral fins could be added to the bottom side of a hypervelocity vehicle to improve its hypersonic stability. The ventral fin could be mounted either along the aft centerline of the craft (ie. like X-15) or be included as lower extensions of the wingtip fins.

A major advantage of the use of ventral fins is that they will not be blanketed from the free stream flow and, as a result, could be made relatively small and still provide lateral stability. The disadvantages are that large stagnation temperatures would develop along the ventrals leading edge and where they join the body or wing. To adequately thermally protect these surfaces would result in the added weight of approximately 10 lbs per square foot (quoted by thermal protection discipline). Depending on the size and mission of the hypervelocity vehicle, increasing the height of the upper tail or wingtip fins may be justified based on weight considerations.

5.1.6 Variable Geometry Wings

Variable wings enhance a vehicles operational flexibility by improving overall aerodynamic behavior in all flight regions. In the hypersonic regime the wings could be oriented in such a way that the high speed characteristics would be optimized. This would maintain acceptable stability, control, and L/D. When the vehicle becomes subsonic the wings could be deployed to improve the slow speed handling qualities and generate increased lift in preparation for the landing. To achieve this type of subsonic performance the wing would have to increase the crafts wing span and employ only small angles of leading edge sweep.

For the deployed wings to be effective they could not be deployed until the atmosphere becomes dense enough to be able to provide lift based on pressure differences on the upper and lower surfaces of the wing (ie. altitude < 30,000 ft). Additionally, the wings should not be deployed until the craft is well within the subsonic region (ie. $Ma < 0.8$) due to heating, drag, and structural considerations.

It is important that the wing deploy at the same time and same speed. A failure to do so could result in a differential in the lift and drag on opposite sides of the craft which could lead to instability or even loss of control.

In configurations where the wing slides forward or aft (ie. jack-knife or scissors) the vehicle will want to pitch up when the wings are deployed (Ref 5.8, p.12). The wing deployment will also tend to induce flight path oscillations. During deployment the objective would be to maintain either a constant flight path angle or transition to a new flight path angle (Ref 5.8, p.13).

Disadvantages of variable wings are that they require complex systems to operate them, which may reduce their reliability. Considerations regarding the vehicles ability to land safely must be made in the event that the wings fail in the undeployed or intermediate positions. Due to the drive system, there is the added difficulties of designing a strong wing substructure. In the final analysis these factors will produce added costs and increased weight. The increase in the vehicles performance due to a variable wing would have to be large enough to justify the vehicles increased weight and complexity.

5.2 HABP GEOMETRY INPUT

The Mark IV Supersonic/Hypersonic Arbitrary Body Program (HABP) also known as the Gentry program was used to evaluate the winged CRV's aerodynamic characteristics in the hypersonic and supersonic regions. The HABP program is a system that is capable of calculating the aerodynamic characteristics of arbitrary 3-D shapes in both the hypersonic and supersonic regions. The program uses local-slope pressure calculations for hypersonic speeds and embedded flow fields for supersonic speeds. If the body geometry data, Mach number, altitude, reference measurements, and aerodynamic evaluation commands were inputted into HABP, then the aerodynamic characteristic coefficients (C_D , C_L , L/D , C_{LL} , C_{LN} , C_M) of the inputted geometry were available as output. These aerodynamic characteristics were then used to evaluate the configuration.

5.2.1 HABP Coordinate Axis Definition

All geometry inputs were done with a coordinate axis defined by HABP. These axes are defined as in Figure 5.1.

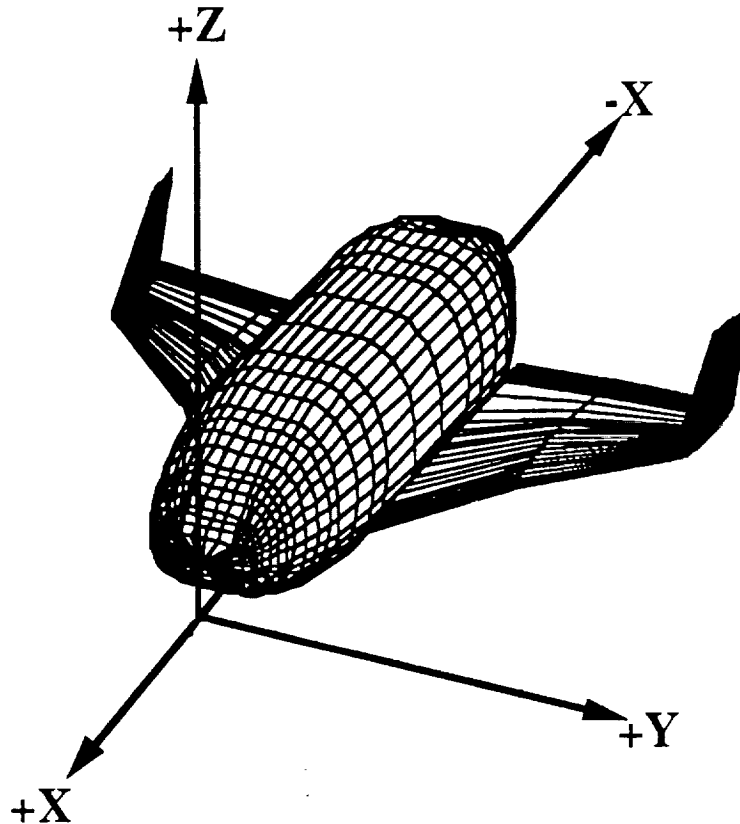


Figure 5-1
HABP Coordinate Axes - Isometric View

5.2.2 Geometry Creation

The input data for the HABP program defines a series of surface elements upon which calculations can be performed. Each surface element consists of four related points which form the corners of a quadrilateral. Calculating and entering each of these points manually would be extremely tedious and so a specially prepared version of the 20/20 spreadsheet on the Marshall Space Flight Center VAX was used to create the points defining the fuselage. The 20/20 spreadsheet required a minimal number of parameters to define the entire fuselage. The spreadsheet calculated the required points on the fuselage surface and placed them in a data file which was properly formatted for use with HABP. After several comment lines

were removed from the fuselage data file, it was merged into the main HABP input data file.

Several methods were available to input the remaining surfaces of the CRV. HABP provides an option by which common aircraft structures can be created in a slightly simplified manner. This method is called the aircraft geometry option. Some of the surface types which can be created with this option are: wings, fins, horizontal tails (or canards), and general airfoils. The general airfoil method was chosen for the construction of all surfaces other than the fuselage because it was the most flexible. The wing method did not have the capability to include dihedral. The fin method could not handle complex wing geometries, such as when toe-in was required, so this method was ruled out. Using the general airfoil method for all of the surfaces allowed certain data to be shared between different surfaces and a standard data format to be used.

5.2.3 Control Surfaces

Control surfaces were added to several configurations (See Figure 5-20). These included a rudder, inboard and outboard elevons, and on the final version a body flap. A version with a split rudders deflected 44 degrees in each direction was also created to measure its effect on hypersonic stability (Fig. 5-20).

To speed the process of rotating the points which define the control surfaces, an Excel spreadsheet was created to handle this task. The spreadsheet required the following inputs: the coordinates of the hinge line, the angle of rotation (in degrees), and the airfoil surface coordinates which define the control surface. The spreadsheet then calculated the the coordinates for the rotated airfoil and placed them in a table beside the original values. The spreadsheet is limited to 2-D rotations although it could easily be modified to work in 3-D if the need should arise in the future. The control surfaces were modeled as in Fig. 5-2.



Figure 5-2

CRV Control Surface - Neutral Position

Other methods of modeling control surfaces are possible but have distinct disadvantages.

- A. Wedge Shape Control Surface: Least difficult to calculate, but may expose sharp edges to the airflow when deflected causing unrealistic shock waves to be predicted (Fig. 5-3).



Figure 5-3

Wedge-Type Control Surface

- B. Two - Airfoils : The total airfoil is not smooth and does not resemble the 64-012 airfoil. Neither airfoil by itself is similar to a 64-012 (much thicker) making the individual airfoils difficult to calculate (Fig. 5-4).



Figure 5-4

Two-Airfoil Control Surface

- C. Bent - Airfoil : (Fig. 5-5) This method could prove to be very realistic, but was not attempted because of time constraints. This could be calculated by combining parts of the Excel spreadsheets already created to rotate an airfoil and recalculate the new thickness distributions.



Figure 5-5
Bent Airfoil Control Surface

It should be noted that because of a limited number of available HABP runs, configurations with control surface deflections were never run.

5.3 ANALYSIS METHODOLOGY

The HABP program was initially written solely for hypervelocity analysis of vehicles, but was later modified to also evaluate supersonic aerodynamic characteristics. The supersonic analysis is performed using embedded flow fields. The program flow field choices, as such, are somewhat limited. Since the supersonic analysis options were part of a revision of the hypersonic program, the aerodynamic data is somewhat less accurate than that for hypersonic speeds. The program data is more accurate at higher supersonic speeds than at lower supersonic speeds and should be kept in mind when evaluating the resulting aerodynamic characteristics. The supersonic region is defined to be between Mach 1.0 and Mach 5.0.

The inviscid pressure calculation methods can be divided into 3 types: 1) analysis techniques for pointed slender configurations, 2) analysis methods for blunt shapes, and 3) force predictions in the free molecular regime (Ref. 5.6, p. 164). The CRV in general can be considered a blunt body which will result in a detached bow shock

wave. In analyzing individual components, however, a pointed slender body approach may be more applicable.

The Modified Newtonian+Prandtl-Meyer Method is used to improve the accuracy of Newtonian calculations on blunt leading edges in the region of small impact angles. This is because the Newton Method decreases in accuracy downstream of the stagnation point. This method requires that the Mach number be smaller than 3.0 due to the matching techniques used for the pressure slopes. Additionally, incorrect pressures will be calculated if the slope approaches zero. For sharp corners in supersonic flow this method does not allow for the recompression which occurs downstream. The Modified Newtonian+Prandtl-Meyer Method is best used only in the region of the nose of a blunt body (Ref. 5.6, p.185).

The tangent cone method agrees well with exact results for Mach numbers greater than 2.0 with a maximum error of less than 1%. This method is also accurate at high angles of attack in contrast to the tangent wedge method which is good only for small angles of attack. The tangent cone method is especially good for highly swept delta wings (i.e. 80 deg.). A combination of two approximate techniques are used- one for the low supersonic range and one for the high supersonic range. Transfer functions are used to give uniformly valid solutions over the entire speed range (Ref. 5.6, p.186).

The shock expansion method calculates pressures by proceeding in strips of elements along the length of the vehicle. This method gives reasonable results for highly swept delta wings at moderate angles of attack in supersonic flight with conditions of a detached leading edge shock (Ref. 5.6, p.187).

A limitation in taking the CRV as one component was that only two theories could be used to generate pressure data: one to calculate impact forces and the second for shadow force calculations. For the hypersonic regime the Modified Newtonian method was used to calculate the impact forces and the Newtonian method was used to calculate the shadow forces.

Some reasons should be mentioned why the other theories to evaluate forces in HABP were not as accurate when applied over a configuration with both "blunt" and "sharp" shapes (as the modified and straight Newtonian methods) at hypersonic speeds. In the

Tangent wedge, Tangent cone, Tangent wedge empirical, and Inclined cone methods attached shock waves are assumed. For "blunt" bodies this assumption is not valid because a detached shock wave is present. The Van Dyke Unified Method is useful for thin profile shapes and does not apply to CRV because of its large blunt areas. The Shock-expansion Method uses the Prandtl-Meyer Expansion theory to calculate forces, but the Prandtl-Meyer Expansion method results in too high of pressure predictions for a surface that has a gradual curvature change to zero slope.

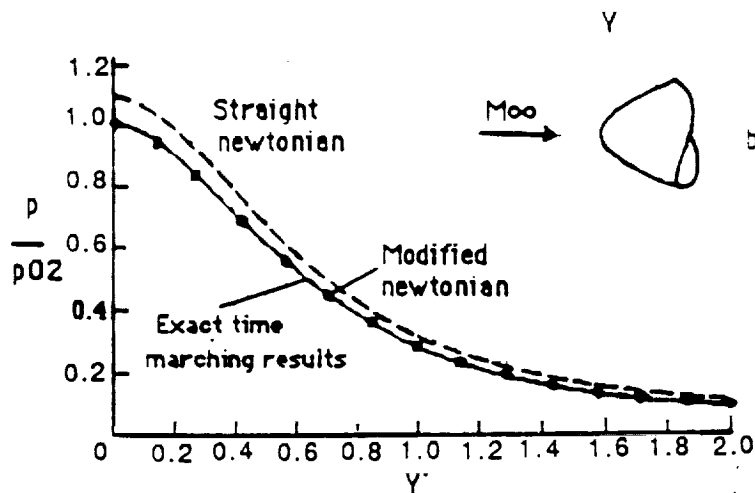


Figure 5-6: Surface pressure distribution over a paraboloid at $M_{\infty}=8.0$

The modified Newtonian method produces results with zero error when compared to exact results of a blunt body at hypersonic speeds as shown in the figures of the geometry section (Sec. 5.2). The greatest error incurred using this method was over the application of the "sharp" shapes (i.e. wings, and vertical fins). This error can be approximated by figures 5-6 and 5-7. Figure 5-7 shows the relative error between two-dimensional "sharp" shapes and the Newtonian theory's results. The percentage difference can be as high as 19 percent for Mach numbers greater than 10 (Ref 5.6). The percentage difference between the Modified Newtonian method and the exact results for a "sharp" two dimensional shape can be as great as 22 percent. This should be kept in mind when examining the results.

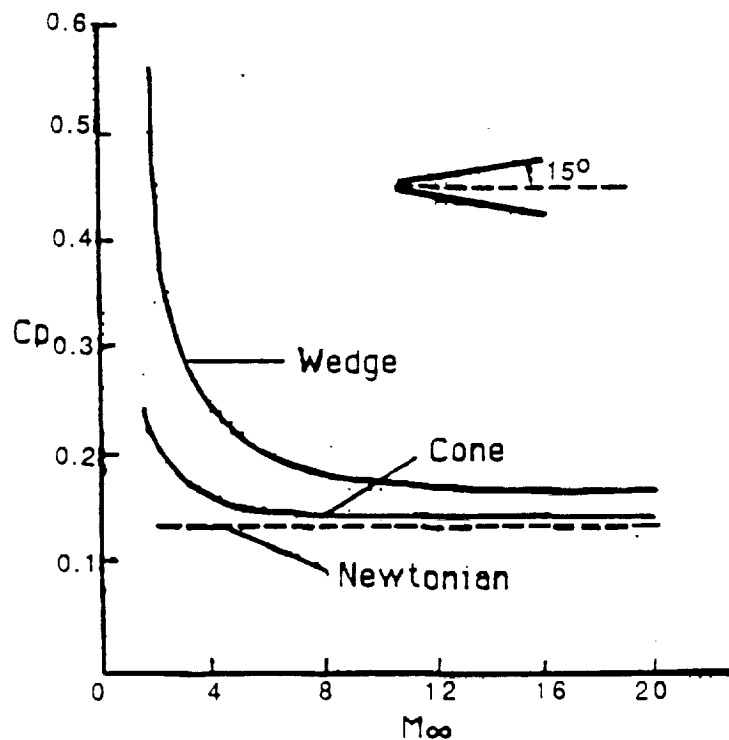


Figure 5-7, Comparison Between Newtonian and Exact Result

In the shadow regions as shown in figure 5-8 the Newtonian theory assumes $C_{pmax} = 0$.

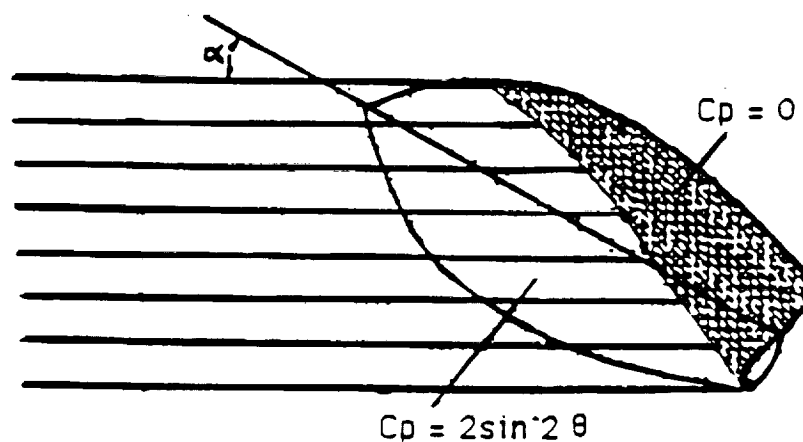


Figure 5-8, Shadow Region on the Leeward Side of a Body, Based on Newtonian Theory.

Initially it was planned that each of the CRV components (i.e., nose, i.e. of wings and fins, etc.) would be assigned pressure calculation methods that would best fit their analysis requirements. This, however, required that the input geometry be defined as components. The geometry of our CRV was input as a whole vehicle using a different input technique so a component analysis could not be applied. Instead, only one pressure option was chosen to evaluate the entire vehicle. A disadvantage of this is that shielding effects, interference effects, and component build-up data could not be obtained. As a result this approach does not provide as accurate of an analysis as the component approach, but should still give reasonable results. A benefit of this simplified pressure option is that it allows the option cards to be modified quickly so that several different vehicle configurations can be evaluated in a minimum amount of time. The simplified option approach will also result in less computer run time, which aids in keeping costs to a minimum. Using HARP in this manner allowed the evaluation of several configurations with a higher degree of accuracy than could be achieved with the program AIREZ and still allowed modifications to be made relatively easily.

5.4 SUBSONIC AERODYNAMICS

This study of subsonic aerodynamics was initiated as a precursor to using wind tunnel testing methods. Initially, the computer program AIREZ was utilized to estimate characteristics of all flight regimes, from subsonic up to hypersonic. AIREZ is a program written in BASIC which uses simple shock-expansion equations for its calculations and then adjusts them using empirical data. A vortex-lattice computational method called ULTIMATE was employed to reveal flight qualities that AIREZ was not capable of performing. Also studied was the possibility of employing canard surfaces for longitudinal control.

5.4.1 The Vortex Lattice Method

An investigation of subsonic aerodynamics was aided by a finite element analysis called the vortex-lattice method. This numerical method involves breaking a wing up into small, two dimensional panels and assigning each panel a "lifting line" vortex. The strength on each panel is such that the sum of the vortices on all the panels satisfies flow tangency at the $3/4$ chord point on every panel.

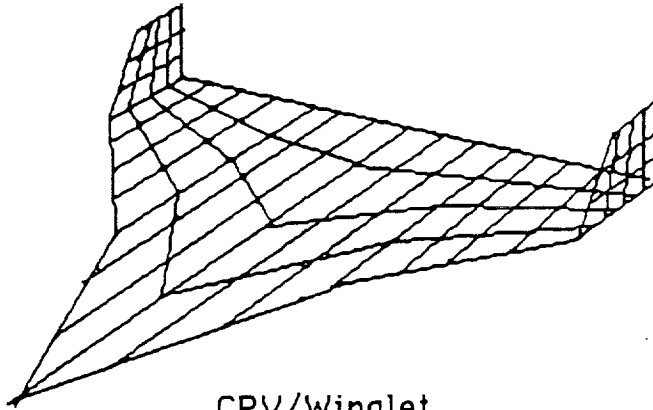
Professor Jack Moran, of the University of Minnesota, has written two computer programs that work using the vortex-lattice method. One program, Vorlat, performs as described above. The second program, ULTIMATE, can handle more than one lifting surface, as well as winglets. The ULTIMATE program was used to model the CRV's subsonic performance. ULTIMATE models a wing according to thin airfoil theory, and according to professor Moran, should model the wings of the CRV quite well. Since this was a thin airfoil approximation, however, there really was no way to model the flow around a thick body with this program.

One advantage of this method was that it could deal with the vortex coupling between the canard and the main wing, to be discussed in more detail later. This was a big concern, since there was some fear that the canard might interfere destructively with the main wing. A drawback to this approach was that it could not take into account the flowfield generated by the body. It was expected that the nose would make a generous contribution to the total lift, so an educated guess of exactly how much was made. Since this vehicle was so similar to the space shuttle, the shuttle's wings could be modeled on ULTIMATE and the two compared. This comparison should give a fairly good estimate of the CRV's real performance. Three basic wing configurations were tested using ULTIMATE. One was the final CRV configuration, another was the same configuration with canard surfaces, and the last were the shuttle's wings. The canard layout was modeled but not analyzed, since that configuration was dropped. Models as represented by the program ULTIMATE are shown in Fig. 5-9.

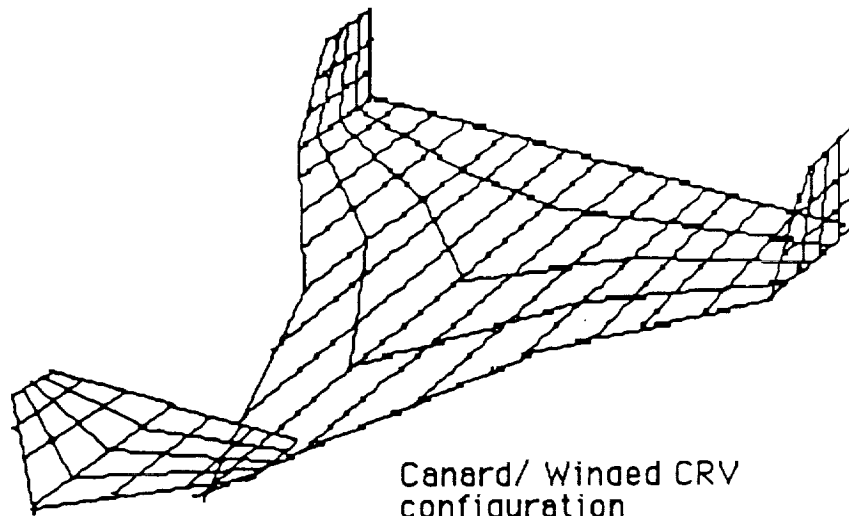
5.4.2 Program ULTIMATE Analysis

Variables used in this section

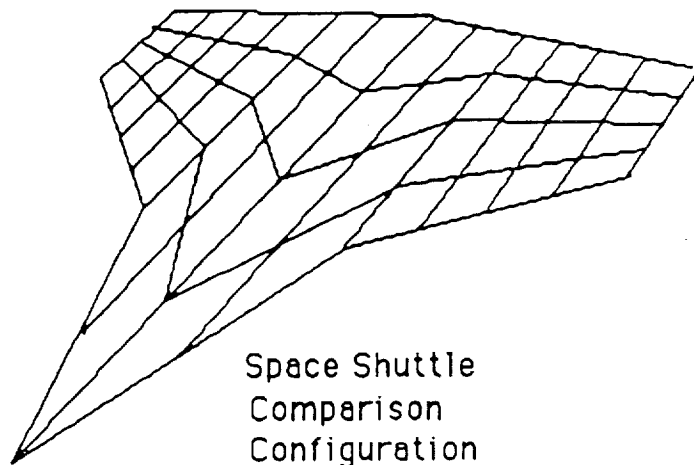
- A - wing planform area
- Alpha - angle of attack
- AR - aspect ratio
- B - wing span
- Cd - drag coefficient
- Cdi - induced drag coefficient
- Cdo - form drag coefficient



CRV/Winglet
configuration



Canard/ Winged CRV
configuration



Space Shuttle
Comparison
Configuration

Figure 5-9, ULTIMATE Models

- Cl - lift coefficient
- Cm - moment coefficient
- H - distance in x from center of lift to center of mass
- L/D - lift to drag ratio
- Z - distance in z from center of lift to center of mass

A run was made on the program ULTIMATE for the wing surfaces of the CRV for angles of attack ranging from 0 - 35 degrees. The results found are illustrated in table 5-1

Table 5-1 ULTIMATE Output

<u>Alpha</u>	<u>Cl</u>	<u>Cd</u>	<u>π AR CD/CL²</u>
0	.03334	.00306	4.78538
5	.20173	.01592	.67923
10	.37140	.04941	.62189
15	.53848	.10228	.61242
20	.70170	.17298	.60998
25	.85981	.25944	.60933
30	1.01161	.35908	.60923
35	1.15594	.46894	.60933

The induced drag was calculated using

$$C_{di} = (C_l^2) / (\pi \text{ AR } e)$$

and could be derived from the π AR CD/CL² term by dividing through by Cd. The aspect ratio, B²/A, used by the program accounted for all the area of the wing, including the vertical winglets. The planform area should be changed from 627 square feet to 534.6 square feet, changing the aspect ratio from 0.6003 to 0.7040, making it necessary to correct by a factor of 1.173. This yielded an induced drag coefficient as illustrated in figure 5-9. For an initial flight characteristics evaluation, C_{do} was set at .03, slightly higher than that given for any aircraft in reference 6, and L/D estimates derived are shown in figure 5-11.

$$C_d = C_{do} + C_{di}$$

$$L/D = C_l / C_d$$

These values underestimate the actual L/D's, since the program AIREZ estimates a max L/D of 5.88.

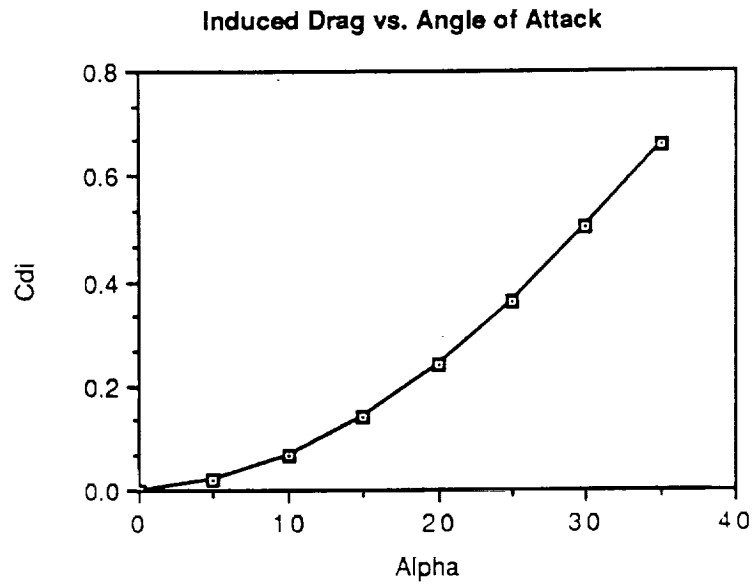


Figure 5-10

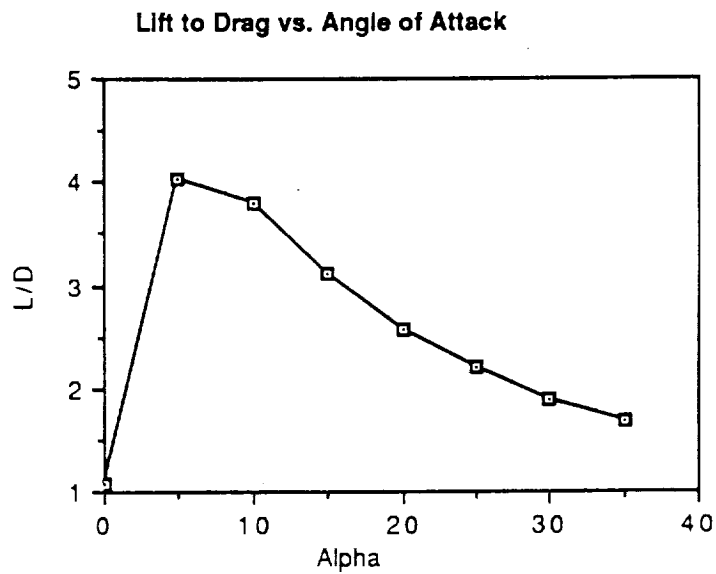


Figure 5-11

5.4.3 Adjustment Factor Determination

ULTIMATE, as has been said before, yields results only for the wings of a vehicle, not the body. Since an appreciable portion of the lift and drag comes from the body, a comparison of space shuttle ULTIMATE test results and real data could be used to correlate the CRV performance figures to more realistic ones. This program will underestimate the actual lift, so that could also be corrected. Additionally, form drag exists, and since this vehicle is similar to the shuttle in general layout and wing thicknesses, C_{do} could be taken right off the shuttle data. The size of these errors would be estimated by comparing ULTIMATE shuttle data with that found in the wind tunnel, and applying those differences to the CRV. One of the assumptions made when choosing this methodology is that it would be possible to acquire space shuttle data to compare with, but this assumption proved to be wrong. It was still of interest to compare the program data, however, in order to determine if the vehicle was viable. Modeling both and looking at lift and induced drag, as shown in figures 5-12 and 5-13, it can be seen that each vehicle performs similarly for induced drag, while the CRV has a better CL for all angles of attack than does the shuttle.

5.4.4 Winglet Effect

In lifting flight, air spills over from the bottom surface of a wing to the top surfaces, shedding vortices into the flow and creating drag. One method of reducing wingtip vortices is to add winglets to the wings. If these winglets are toed in, they create their own vortices that spin in the opposite direction than those naturally shed from the wingtips, thereby reducing the total induced drag. The disadvantage of adding winglets is that since they are a vertical surface, they add none of their own lift, and better wing efficiencies can be obtained simply by increasing the span.

The final CRV design employs winglets, as opposed to using a rear body mounted tail like the shuttle, for reduced control blanketing at high angle of attack (Fig. 5-39). Since this vertical surface is already useful as a control surface, it is desirable to employ them as lift enhancing devices as well by toeing them in.

To optimize the toe-in angle for lift to drag, the program ULTIMATE was run at an angle of attack of 5 degrees seven times for angles of 0,2,3,4,5,6,7 degrees toe-in. Lift to drag ratios were found for each placement setting and are illustrated in figure 5-14.

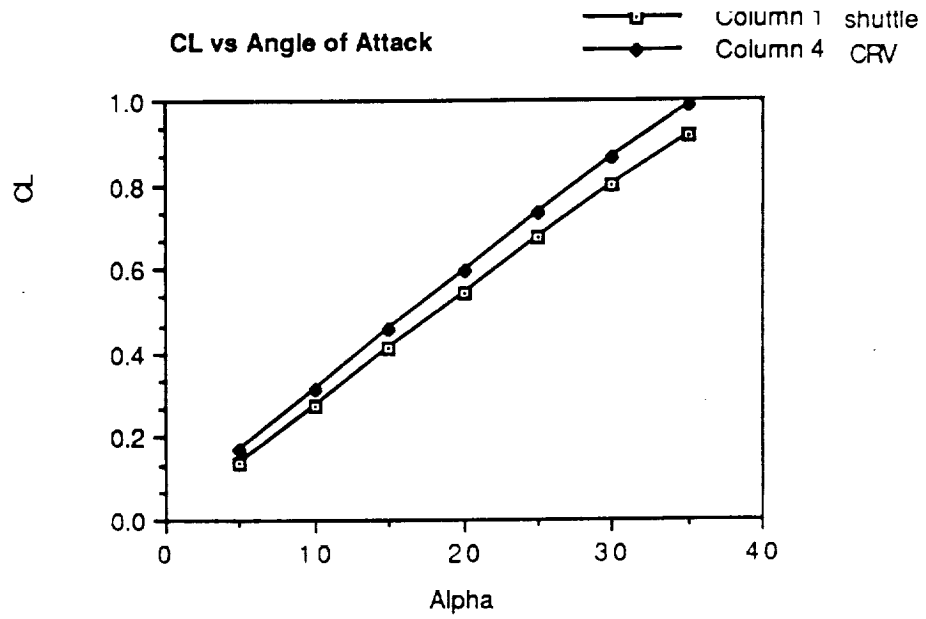


Figure 5-12

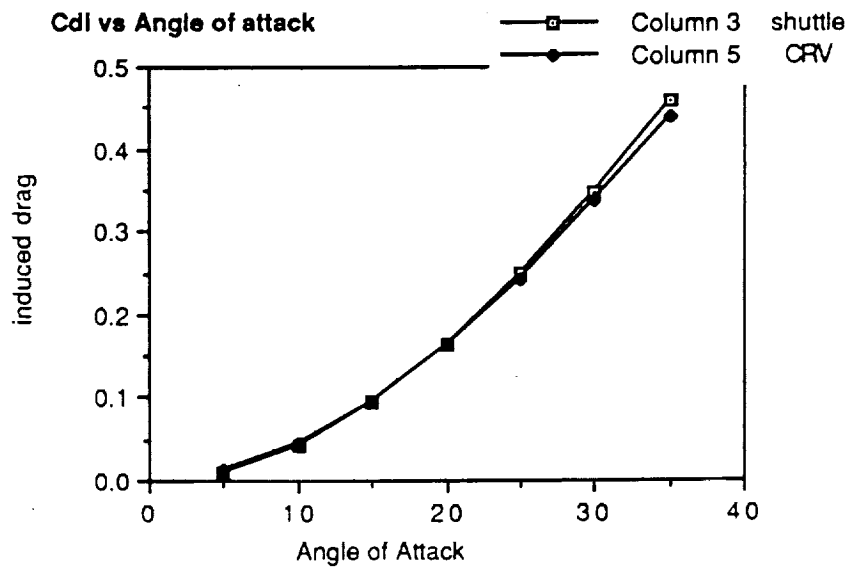


Figure 5-13

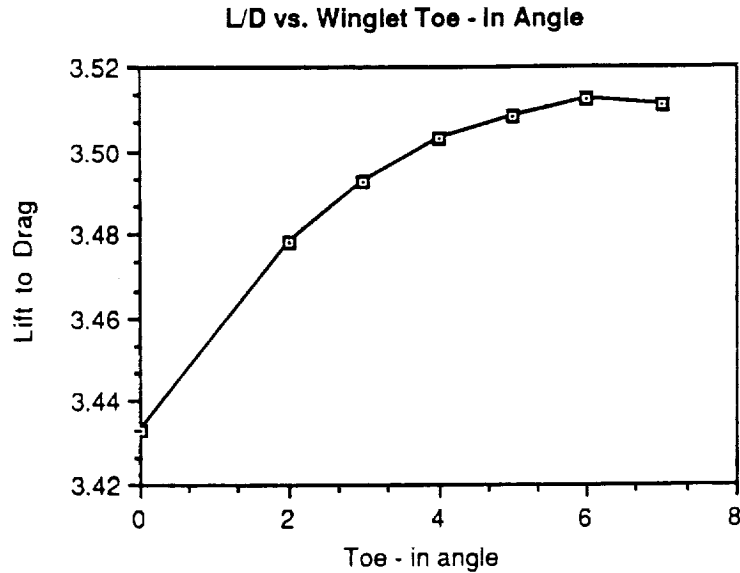


Figure 5-14

These lift to drag ratios were not adjusted for realism, but were intended only to show that induced drag is lowest, and therefore lift to drag maximized, at a toe-in angle of around six degrees.

5.5 CANARDS

Upper control surfaces can become blanketed at high angles of attack by flow separation from the wing leading edge. Since a canard surface is in the free stream flow (or nearly so) , this blanketing would not occur, maintaining longitudinal controllability at all times.

The main complexity of the canards is due to flow field coupling between the canard and the main lifting wing. The canards shed vortices that flow over the main wing, which can interfere either positively or negatively on the main wing's flow. In reference 5.2 a model was flown at subsonic speeds in a wind tunnel. The two geometries involved a coplanar canard and a canard which was offset above the plane of the wing. At an angle of attack of 20 degrees, the coplanar canard prevented stall better than did the offset canard. No periodic disturbances were found from either configuration. The coplanar canard, however, produced unfavorable interference on the wing midsection and favorable interference near the tips. This was reversed for the offset canards. This test only dealt with subsonic flow, but several high speed canard aircraft have flown. Examples

are the North American XB-70A Valkyrie or the more modern Saab Viggen.

Placing the canard in the free stream would mean that the surface would get very hot. The heating could be reduced by increasing the leading edge sweep of the canard. Upon a preliminary investigation, the thermal protection discipline decided that it would be possible to protect a canard from overheating, but only at great cost in weight. As a result, the use of canards was abandoned.

The bulk of this subsonic study came from the vortex lattice program ULTIMATE, which although it did not give accurate performance predictions, did make qualitative comparisons between the winged CRV and the space shuttle possible. This comparison predicted that the CRV's wings would provide a higher subsonic lift to drag than do the shuttle's. The AIREZ program failed to show that winglet toe-in angle had any effect on subsonic lift to drag performance, whereas ULTIMATE made a reasonable estimate that a six degree toe in would be optimum for lift to drag.

A much better prediction of subsonic performance will be gained using wind tunnel models to evaluate lifts, drags, and moments. Additionally, water tunnel testing will aid in looking at the vortex flows generated by the CRV.

5.6 BASELINE CONFIGURATIONS

The aerodynamics of the CRV are determined by a combination of physical constraints and design requirements. Due to the large number of variables which can effect the shape and performance of the vehicle a common baseline was established in order to facilitate comparisons between the configurations being evaluated.

The size and shape of the vehicle was initially set to the same dimensions as that of the Trade Study analysis (Fig. 5-15). The vehicle length was set at 76 ft, which included a 27 ft nose cone, 30 ft fuselage, and an 18 ft tail cone. The nose employed a droop of -2 ft measured from the vehicle's geometric centerline. The wing planform was dual trapezoid shaped with a sweep of 54 deg. (outboard wing section). The wing span was set at 58 ft and the airfoil shape was a bi-convex NACA 64-012 employing a leading edge radius of 0.35 ft.

Like the trade study CRV proposal the baseline configuration employed both a vertical tail and wingtip fins. Each of these components were of the same airfoil type as the wing. The initial reasoning for such a configuration was that the wingtip fins could be variable which would result in the achievement of two high priority characteristics: 1) reduced moments due to lift during launch and forces due to windage while on the pad; 2) increased subsonic L/D performance when the winglets were deployed for approach and landing. Both of these characteristics are functions of span. The larger the span the larger the moment forces and the larger the hypersonic wave drag -both of which are undesirable. A large span (with less sweep), however, is desirable in order to achieve a low landing speed and maintain good controllability during approach and landing. A primary objective during the trade study was to obtain a subsonic L/D of about 8.0. The variable winglet option was found to be the best method to achieve this goal and still satisfy the requirements for a short span size during launch.

Small changes were made in the trailing edges of the wing planform, the trailing edge of the wingtip fins, and the vertical tail size from that of the trade study configuration (Fig. 5-16). The trailing edge of the wing was redefined to be straight the whole distance from the fuselage out to the winglets instead of including reverse taper on the outboard section as in the trade study version. The trailing edge of the wingtip fin was modified from having sweepback to being straight from the tip to the base where it joined the wing. The vertical tail chord was shortened to reduce its surface area and make it more proportionate with the rest of the vehicle. These were small changes and were meant only to consolidate the vehicle in an effort to facilitate aerodynamic analysis using the HABP program.

The trade study CRV proposal included the option of variable canards. This option was completely replaced with the option of fixed canards (Fig.5-17). The canards were initially omitted from all aerodynamic analysis and were reserved in the event of a need for more control. The canards were to use a movable trailing edge "elevator" instead of an all movable "stabilitor" approach.

The size of the fuselage was based on the hard requirements established by the dimensions of the pressurized and unpressurized Logistics Modules. The trade study CRV used a shortened "Shuttle" type of fuselage which was uniformly rounded at the top and bottom and had flat sides. The baseline HABP body shape was set having

the sides of the fuselage being less flat and having the addition of a flat section at the top and bottom of the body (Fig. 5-18). This was because the ellipse option of the HABP program was used to generate the fuselage. The HABP body shape was used because it was easy to define and was meant only as a model to predict the vehicles performance. The actual CRV would employ flat sides. The effect of this approximation was not determined because the vehicle could not be separated into its component parts and analyzed using the interference and blanketing options of HABP. A detailed wind tunnel analysis would be required to explore the differences produced by each body shape.

Initially, it was thought that the OMS engine could be housed inside the tail cone in order to achieve desirable aerodynamic effects in the subsonic flight region. It was determined by the propulsion group, however, that the engine would not receive the proper cooling and/or that the tail cone thermal protection would not be able to handle the engines heat output. No data was found that covered the use of a tail cone and OMS engine combination. As a result, the engine was decided to be mounted outside of the cone. A body flap similar to the existing shuttle's was added to protect the engine during re-entry. The body flap was made to have a variable angle and has the added benefit that it can be used to change the amount of loading experienced by the flight controls. Due to the complexity of this shape it was not incorporated into the HABP analysis of the different CRV configurations. The increased planform area of the actual vehicle due to the body flap over that of the HABP geometry inputs, however, should serve to increase the vehicles hypersonic L/D performance.

The number of HABP runs was limited to 14 due to the cost of the required computer time and the limited analysis budget. As a result, many concerns about the effects of fine details in the vehicles aerodynamics were not explored. It was necessary to get general aerodynamic data at several Mach numbers for each configuration type, and since HABP could only evaluate one Mach number per run, the majority of the allotted trials were used to this end. The remaining trials were used at select Mach numbers to analyze effects due to strake and wingtip fin toe-in.

The flight conditions for the HABP analysis were set to evaluate the vehicle at 0, 5, 10, 15, 25, 35, and 45 deg. at $Ma=20.0$ and $Ma=10.0$; and were set at 0, 10, 15, 20, 25, 30, 35, and 40 deg. at $Ma=5.0$ and

Ma=2.0. Additionally, the vehicle was analyzed at the yaw angles of 0, 5, and 10 deg. for each of the above angles of attack in order to provide the stability group with needed information. The HABP program has a limit of 20 different angle of attacks it can evaluate per run, so the values were chosen so that the most detail would be concentrated in the area of the maximum L/D (25 - 45 deg. for Mach 20 and Mach 10; 15 - 35 deg. for Mach 5 and Mach 2).

The flight conditions card for the HABP program requires both the Mach number and altitude to be input. Based on data received from the re-entry group the baseline flight conditions were set as: Alt.=226,500 ft at Ma= 20; Alt.=165,900 ft at Ma=10; Alt.=126,000 ft at Ma=5; and Alt.=84,800 ft at Ma=2.

According to the thermal protection group the TPS tiles would retain heat during re-entry. This causes the tiles to expand and changes the shape of the airfoil. Depending on the type of tiles used and their location the degree of deformation will vary. Thus, different sections of the wing may expand different amounts and drastically change the airfoil shape. This effect is complicated by the fact that the tiles will tend to retain the absorbed heat throughout the entire re-entry flight. These changes should be accounted for when designing the wing so that the airfoil will assume the desired shape in the subsonic regime where the wing shape will be most critical and the absorbed heat will be the greatest. This topic requires detailed analysis and was not addressed during the analysis of the CRV configurations.

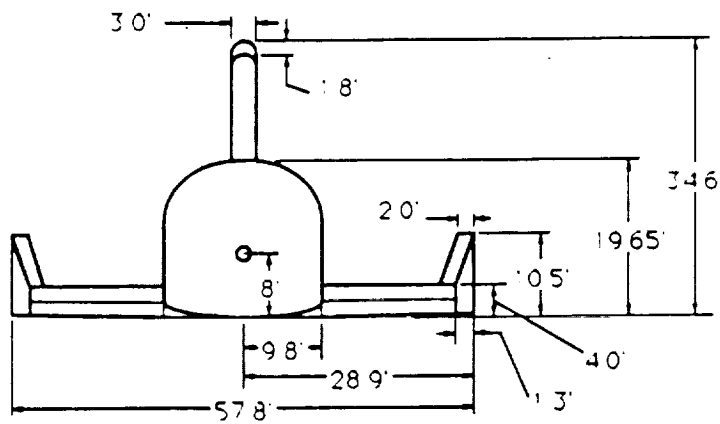
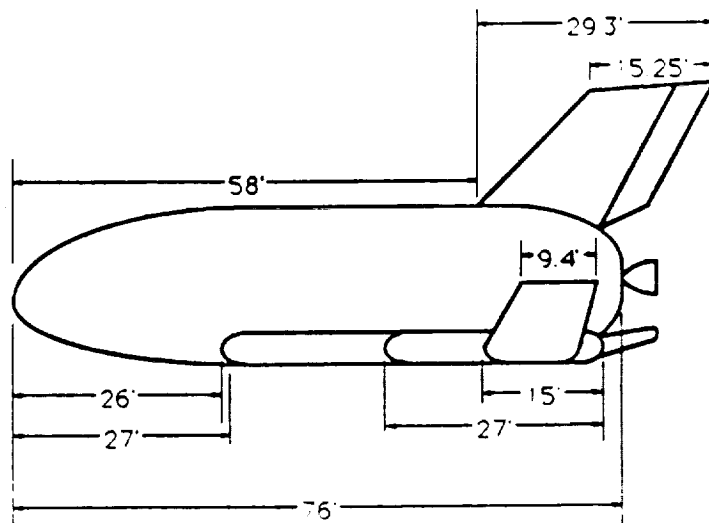
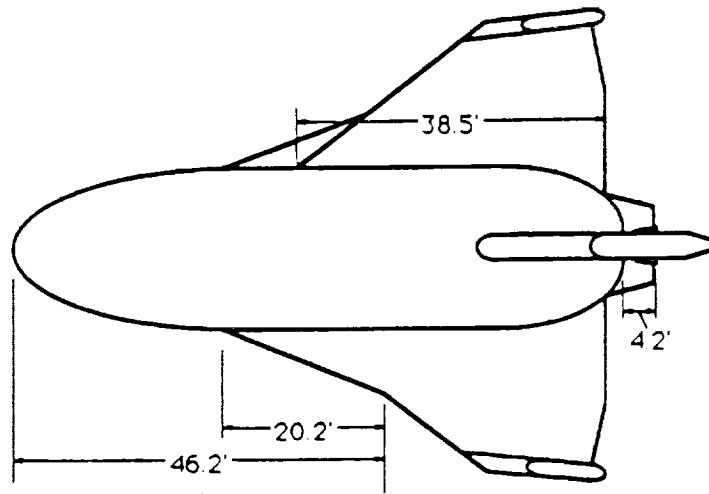


Figure. 5-15 Trade Study Configuration

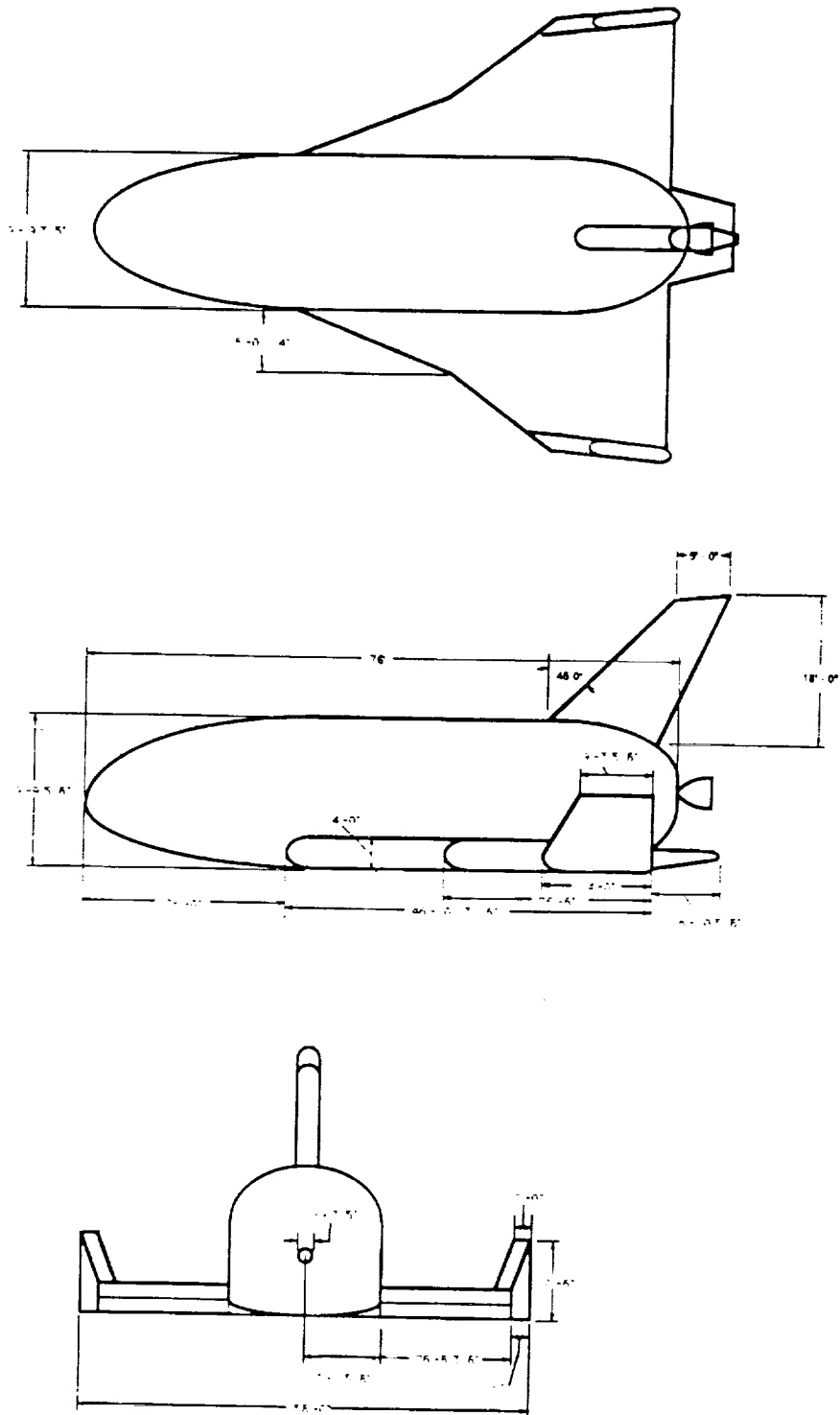
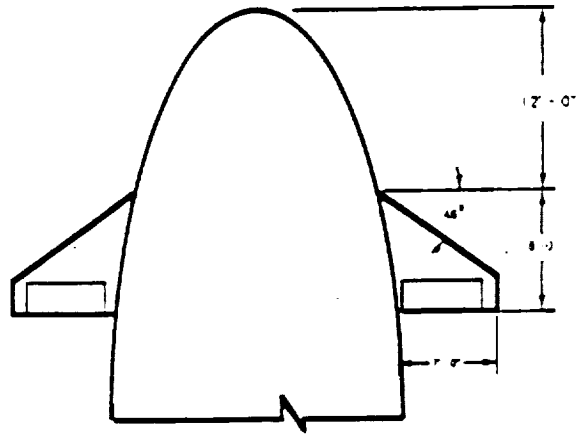
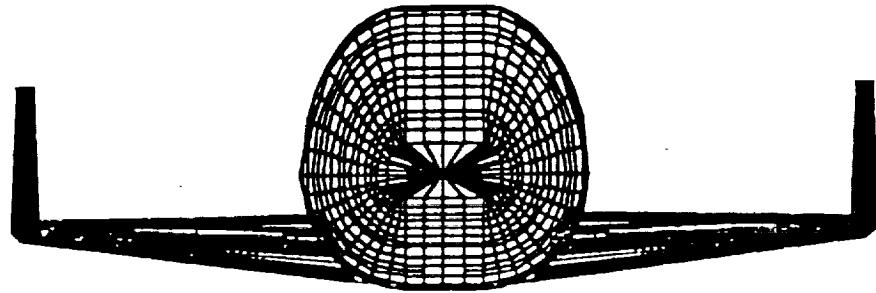


Figure. 5-16 Baseline Configuration

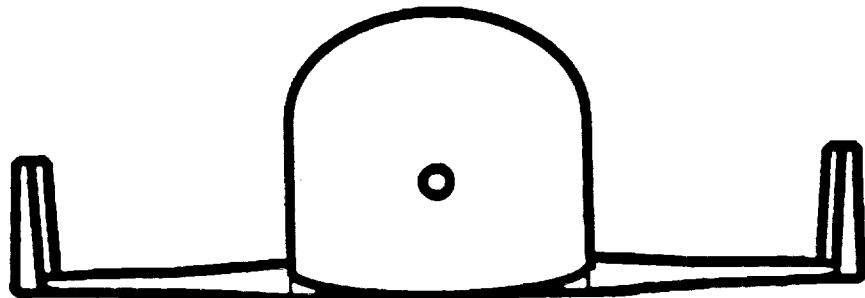


Fixed Canard Option

Figure. 5-17 Fixed Canard Option



HABP Body



Trade Study Body

Figure. 5-18 Trade Study vs. HABP Body Shape

5.7 CONFIGURATIONS CONSIDERED

There were three general configurations derived from the baseline configuration which were considered: 1) a CRV using both a vertical tail and variable winglets, 2) a CRV which used a vertical tail and no winglets, and 3) a CRV using fixed wingtip fins with no vertical tail.

5.7.1 Configuration #1 -Vertical Tail With Variable Winglets (Fig. 5-21)

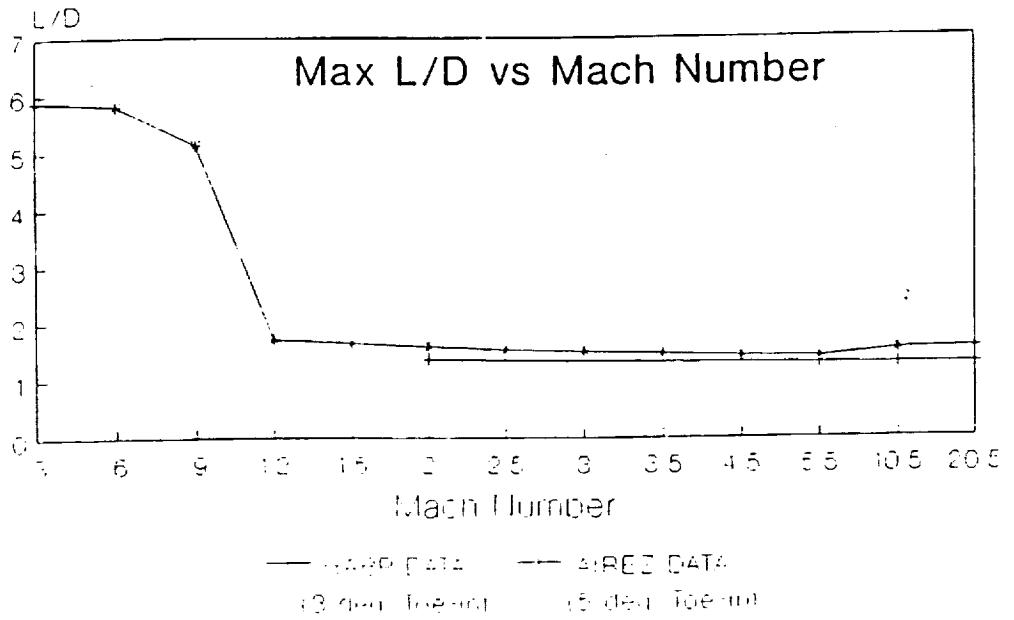
The aerodynamic analysis of the CRV for this term was concentrated on gaining detailed data in the hypersonic and supersonic region using the program HABP. The concept for the variable winglet design was based on the deployment of the winglets at subsonic speeds to increase the vehicles L/D during approach and landing. Since the aerodynamic analysis was limited to Mach numbers ranging from 2.0 to 20.0 the wingtip fins were always evaluated in the upright position.

This configuration was run using HABP and a maximum L/D ranging from 1.28 at Mach 20.0 to 1.36 at Mach 2.0 was achieved. These L/D values were significantly less than those predicted by the AIREZ program of 1.56 at Mach 20.0 to 1.59 at Mach 2.0 (Table 5-2). This difference in L/D meant that a slight span increase would be needed to attain the L/D values established as requirements in the trade study. Increasing the span would increase the wave drag in the hypersonic and supersonic regions, but the lift due to the area increase was thought to be able to offset this deficiency. This is because hypersonic L/D is a function of planform area while subsonic L/D is a function of span.

An analysis was made of the vehicle at three yaw angles to evaluate the effect on the L/D and to provide the stability group with moment data. The maximum L/D values at 5 deg. of yaw was reasonably close to that at 0 deg. yaw. A yaw of 10 deg., however, resulted in a significant decrease in L/D performance at all Mach numbers (Fig. 5-20). Greater amounts of yaw will most likely have an even more profound effect on the L/D values. From figure 5-20 it can be seen that the slope of the curves decrease in the lower Mach region with increasing yaw. At low Mach numbers (i.e. < 2.0) the L/D of the CRV will begin to rapidly increase reaching a global maximum in the low subsonic region (Fig. 5-17). Figure 5-20 shows that yaw angles greater than 5 deg. tend to limit this desirable L/D rise. Proper use

Wingtip Fins & Vert. Tail

(0 deg. Yaw; Strake)



Figures 5-19, Baseline Configuration Comparison AIREZ vs. HABP

Wingtip Fins and Vert. Tail

(Strake; 0 deg. Toe-in)

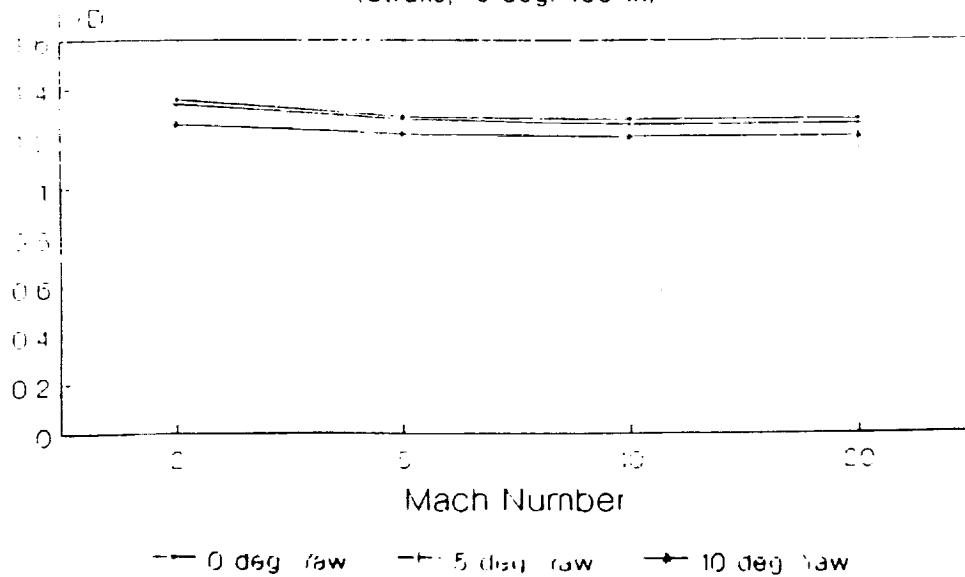


Figure 5-20, Max L/D vs. Mach - Baseline Configuration

ORIGINAL PAGE IS
OF POOR QUALITY

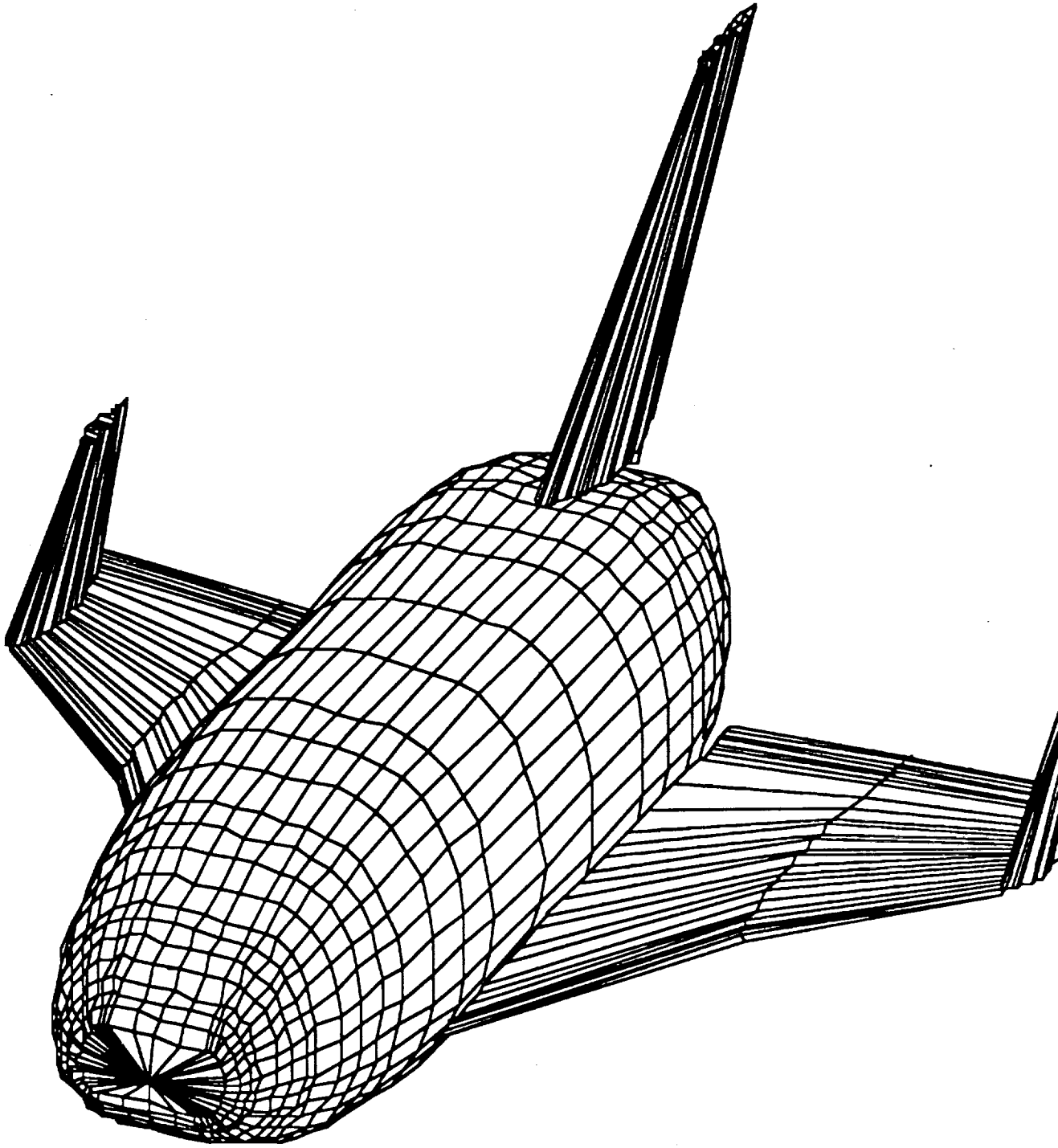


Figure 5-21, Vertical Tail With Variable Winglets Configuration

of yaw, though, could be used to decrease cross range and lose excess altitude when landing at locations near the orbital flight path.

Problems with this configuration were expressed by the thermal protection group regarding the large percentage of TPS weight required to protect the wingtip fins and the leading edge of the strake. (14% for fins, 3% vertical tail, and 12% for strake). During this initial evaluation phase the fixed canards were not included in the aerodynamic analysis, but were reserved as an option. The thermal group stated that the weight to protect the canards would be about 14% of the total TPS weight. Since the use of the canards and the wingtip fins would consist of a large fraction of the total TPS weight it was decided that both of the components could not be used in conjunction with each other. As a result the optional use of canards with this configuration was dropped.

Another concern of the thermal protection group was the large weight required to protect the leading edge of the wing strake. A significant amount of the TPS weight is associated with protecting the leading edge of surfaces and the TPS group desired a reduction in the strake size in order to save weight. Hypersonic L/D, however, is very dependant on planform area and a strake reduction would mean a reduction in the CRV's maximum L/D values. This topic of strake area reduction was decided to be addressed after the final configuration had been chosen so that HABP runs would not be wasted on evaluating this condition for each of the three vehicle types. Refer to the winglet configuration section for a complete discussion of this matter (Sec. 5.7.3).

A potential problem with a variable winglet configuration could be heating of the joint area between the winglet and main wing during re-entry. Since the winglets would remain in the up position until near the landing phase the joint areas could be treated as the wheel doors on the Shuttle. The joint could be sealed and its integrity tested prior to launch. As long as the wings were not disturbed before re-entry, heating should not be a problem. Other possible solutions would be to use a fixed shielding over the bottom joint area or an active cooling system in the joint itself.

A decision not to pursue the wingtip fin and vertical tail configuration was made when the Re-entry Dynamics group stated that the CRV did not need the subsonic L/D of 8.0 as was established in the trade study. A subsonic L/D of about 6.0 was determined to

be sufficient by the re-entry group. This new requirement meant that the use of variable winglets to increase the subsonic span were no longer needed. As a result this configuration was abandoned and further aerodynamic analysis was concentrated on the evaluation of the wingtip fin only configuration and the vertical tail only configuration.

5.7.2 Configuration #2 -Vertical Tail Only (Fig. 5-22)

This configuration is based on a "Shuttle" type of arrangement. A benefit of this is that much data has been gathered on the performance of this type of layout and the design has been proven to be reliable.

A benefit of a vertical tail configuration over the winglet design is that the tail can be made to have less weight than the wingtip fins. This is because the tail is not as exposed to the flow as much as the winglets, and as a result require less TPS. This benefit, however, is also a deficiency because the tail tends to be blanketed at high angles of attack such as during re-entry. This requires that the tail be made very tall in order to generate acceptable amounts of lateral stability.

A thorough analysis of this configuration was not completed because midway through the term it was determined that the vertical tail restricted the flexibility of docking orientation with the space station. This led to the acceptance of the wingtip fin configuration before a complete aerodynamic comparison could be made. The data which had been attained, however, showed that the winglet only and vertical tail only configurations both performed almost identically over the $Ma=2.0$ to $Ma=20.0$ range (Fig 5-23; Fig. 5-24).

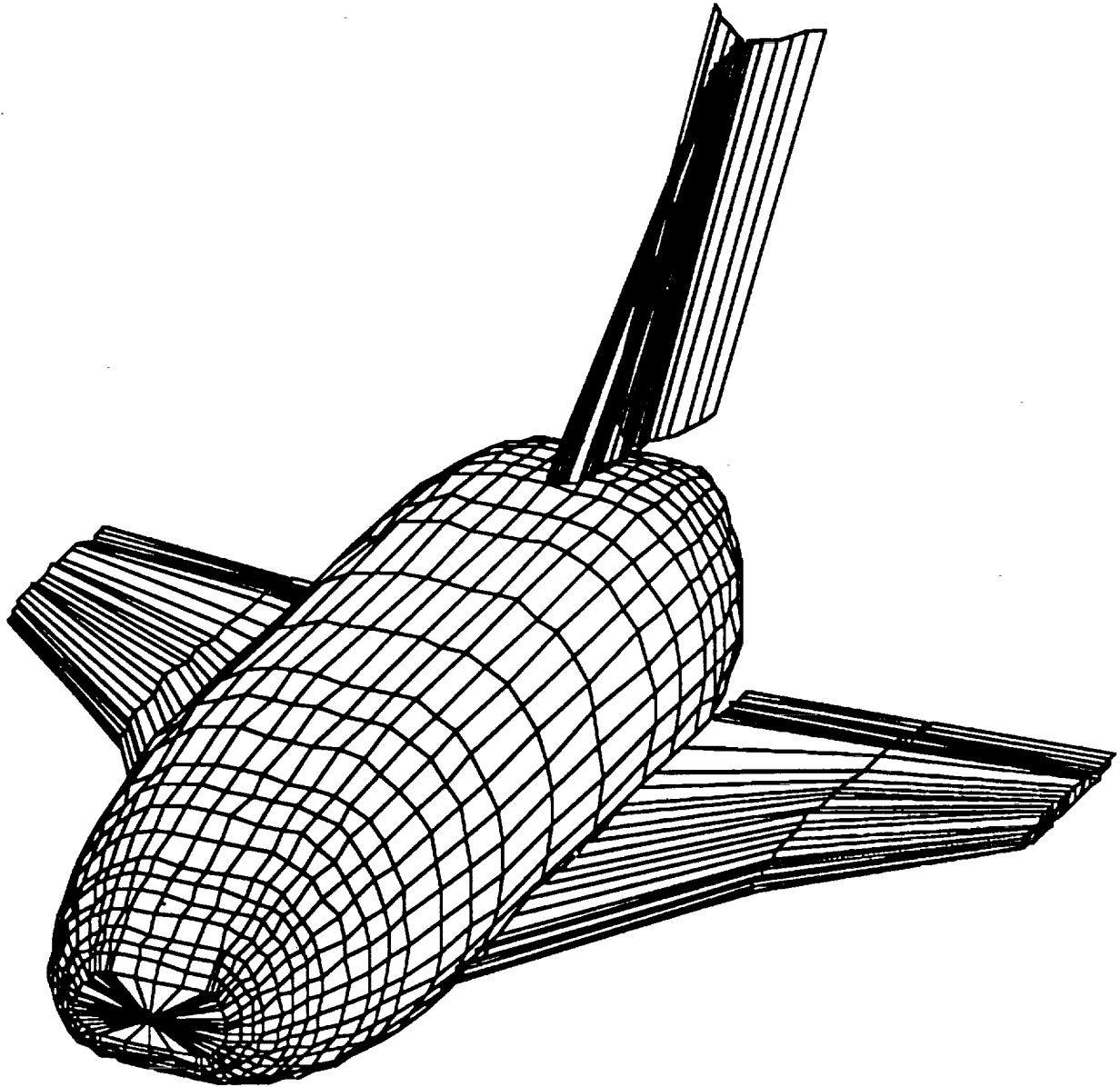


Figure 5-22, Vertical Tail Only Configuration (With Split Rudder)

Max L/D vs Mach Number

(0 deg. Yaw; Strake)

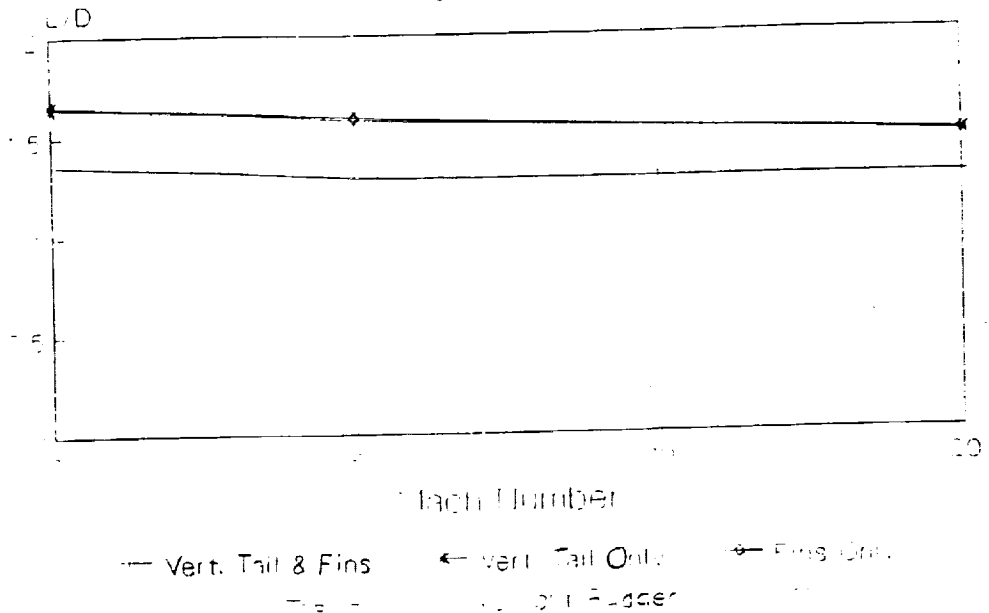


Figure 5-23, Configuration Comparison

Max L/D vs Mach Number

(0 deg. Yaw; Strake; 0 deg. Toe-in)

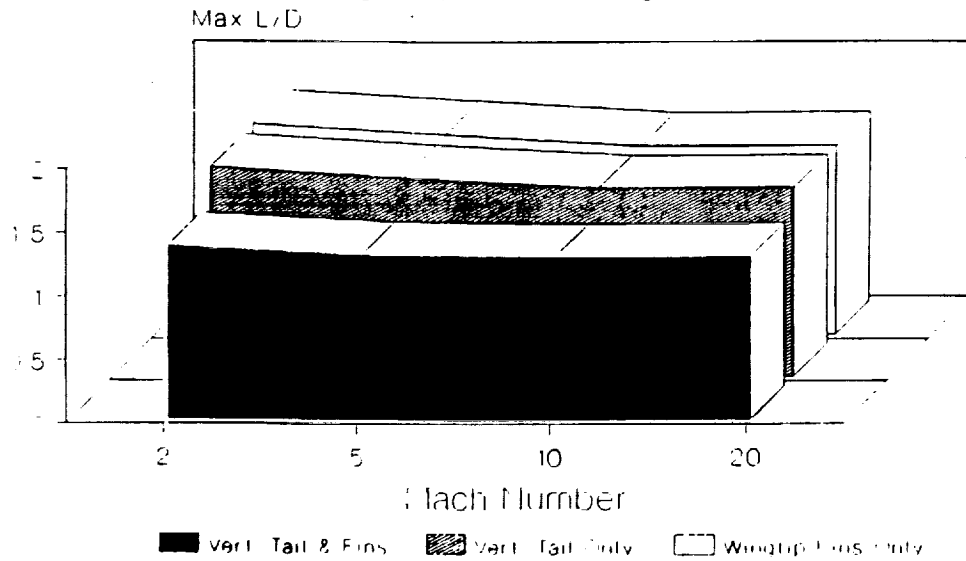


Figure 5-24, Configuration Comparison, 3-D

5.7.3 Configuration #3-Wingtip Fins Only (Fig.5-32 to 5-39)

This configuration consisted of the baseline configuration with the vertical tail removed. Due to the large amount of TPS weight required for a layout employing both the winglets and fixed canards, the use of canards in this configuration was not considered to be an option worth evaluation.

This vehicle type was run on HABP and the maximum L/D values ranged from 1.49 at $Ma=20$ to 1.66 at $Ma=2.0$. From figure 5-26 it can be seen that yaw angles greater than 5 deg. significantly decrease the L/D performance. This is especially apparent at the lower Mach numbers. Unlike the vertical tail/winglet configuration the yaw at 5 deg. and 0 deg. tend to converge and result in only small differences in the relative L/D (Fig. 5-20). Compared with the data for the vertical tail/winglet configuration (Fig. 5-26) it can also be seen that the slopes of the plots are greater for the $Ma=2.0$ to the $Ma=20.0$ range. This indicates that the L/D performance for the winglet configuration increases at a faster rate with decreasing velocity than the baseline configuration.

The L/D vs. angle of attack is plotted in figure 5-27. This shows that the maximum L/D at $Ma=20.0$ is reached at about 25 deg., while the maximum L/D at $Ma=5.0$ and $Ma=2.0$ occurs at approximately 20 degrees. It can also be seen that at lower Mach numbers the L/D drop-off at small angles of attack is delayed longer. As a result, the angle of attack at $Ma=2.0$ can be decreased down to about 15 deg. with only a small L/D penalty. This will allow some flexibility of the CRV's pitch in the later stages of its return flight.

The benefit of the use of winglets is that they give an effective increase in the span size due to a decrease in the induced drag at low Mach values. Wingtip fins also have the advantage of providing better stability than a vertical tail. This is because the fins are less susceptible to blanketing at high angles of attack during re-entry. The added stability due to the winglets should also aid in reducing the need to use the RCS during re-entry for stability. A final benefit from the use of this configuration is from the standpoint of docking with the space station. Not having a vertical tail allows the CRV to dock in more than one orientation which increases its overall versatility.

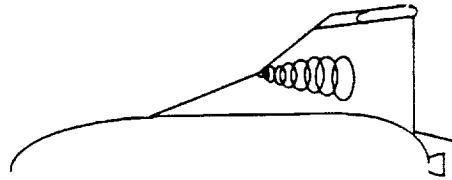
There were no changes in the baseline dimensions of the CRV over the term so these variables were treated as constants and the analysis of this configurations performance was concentrated on optimizing the toe-in angle and strake area. Some amount of fin toe-in is desirable for hypersonic lateral stability. Using the program Ultimate it was found that the optimum toe-in with respect to subsonic L/D performance was about 6 degrees. Due to budget limits on the use of HABP a complete analysis of the toe-in angles was not performed. It was found, however, that the amount of toe-in at $Ma=20.0$ (0 deg. vs 6 deg.) gave the same L/D results. Since 6 deg. was the optimum toe-in angle in the subsonic region this value was chosen for use on the final vehicle. It is assumed that the supersonic performance will be acceptable with this toe-in angle, but an analysis should be completed in this region for confirmation.

An alternative to fin toe-in was thought to be the use of split rudders on the fins for use in the hypersonic regime. The toe-in angle for the fins in this set up would be zero degrees. It was thought that no use of toe-in would help reduce subsonic drag and result in an increase in the overall L/D performance. Analysis using the Ultimate program proved this idea to be incorrect, so no HABP analysis was executed.

The thermal protection group had expressed a desire to decrease the amount of wing strake in order to save weight. This is because the strake has a long leading edge and this area accounts for a large percentage of the wings TPS weight. From an aerodynamic view a decrease in strake area is undesirable.

To evaluate the effects of strake on the winglet configuration a comparison was made at Mach 20, 5, and 2 between a vehicle which incorporated the baseline amount of strake and a vehicle with the strake completely removed. In the later case the wing chord was increased so as to make up for the lost area due to the strake. In this manner the reference wing area was kept constant which meant that any differences in L/D were caused by the different sweep angles of the inboard wing section (Fig. 5-38 & 5-33). Using the HABP program it was found that the elimination of the strake resulted in a significant reduction in the maximum L/D that the CRV could achieve, even with the wing reference area held constant (Fig. 5-27, Fig. 5-28). This indicates that the L/D is being positively effected by the larger sweep angle created by the strake on the inboard wing section. Based on this analysis it was concluded that the strake

should be kept. The TPS weight penalty was more than made up for in the increased L/D performance that the strake produced.



Strake Vortices

Fig. 5-25

Large sweep angles have the effect of reducing wave drag because the leading edge stagnation pressure is reduced. The strake section also has the beneficial effect of causing vortex shedding across the wings upper surface at the juncture between the inboard and outboard wing. This causes "vortex lift" because the vortices create a decrease in pressure in this region (Fig. 5-25). The contribution of vortex lift, however, decreases with increasing Mach number. As a result, vortex lift effects are limited mostly to the supersonic region.

A final comparison of the AIREZ data and the HABP data was made for this winglet configuration (Fig. 5-30, Fig. 5-31). These data sets compare much more favorably than they did for the baseline configuration comparison. This is because the AIREZ program was not set up to accept a variable winglet design and approximations had to be made in the geometry input. The AIREZ program was capable of accepting a winglet only design type so the analysis methods for this configuration match more closely as a result. AIREZ predicts a L/D "depression" between $Ma=2.0$ and $Ma=10.0$, but HABP does not indicate such an occurrence. HABP performs more detailed calculations so it is most likely the more accurate prediction of the two methods. Since AIREZ uses simple shock-expansion equations for its calculations and then adjusts them using empirical data the "depression" was assumed to be due to the limitations of that program rather than representing the actual CRV's performance.

5.8 SUMMARY

Based on the determination that a subsonic L/D of 6 would be adequate for approach and landing (instead of 8) the variable winglet option was eliminated. Thus, the use of both fins and a vertical tail was redundant. The performance of the winglet only and vertical tail only configurations in the hypersonic and supersonic regions were found to be comparable. Theoretically, however, the use of fins should increase the L/D favorably in the subsonic region due to a reduction in induced drag. Fins also are less susceptible to blanketing during re-entry. Finally, the use of fins allow flexibility in docking with the space station. As a result of these benefits the winglet only configuration was chosen to be the final form for the CRV.

Wingtip Fin Configuration

(Strake: 0 deg. Toe-in)

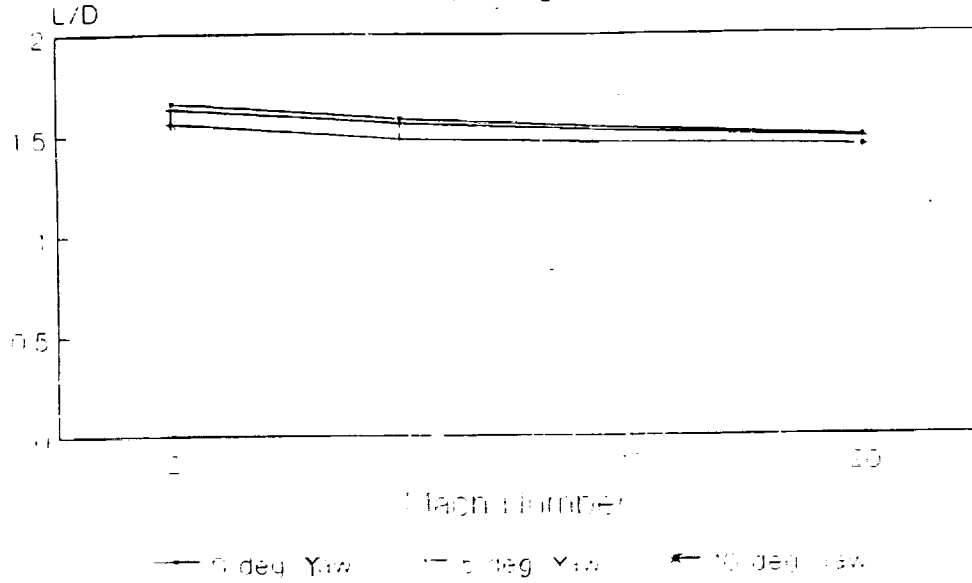


Figure 5-26, Maximum L/D vs. Mach Wingtip Fin Configuration

Wingtip Fin Configuration

(0 deg. Yaw; Strake: 0 deg. Toe-in)

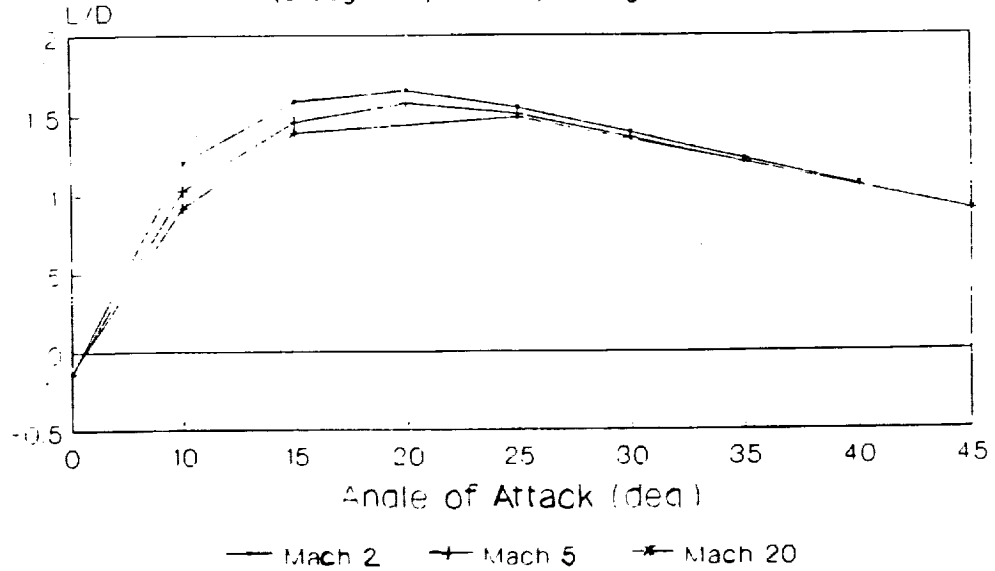


Figure 5-27, L/D vs. Angle of Attack Wingtip Fin Configuration

Wingtip Fin Configuration

(0 deg. Yaw; 0 deg. Toe-in; Const. Wing Ref. Area)

Max L/D

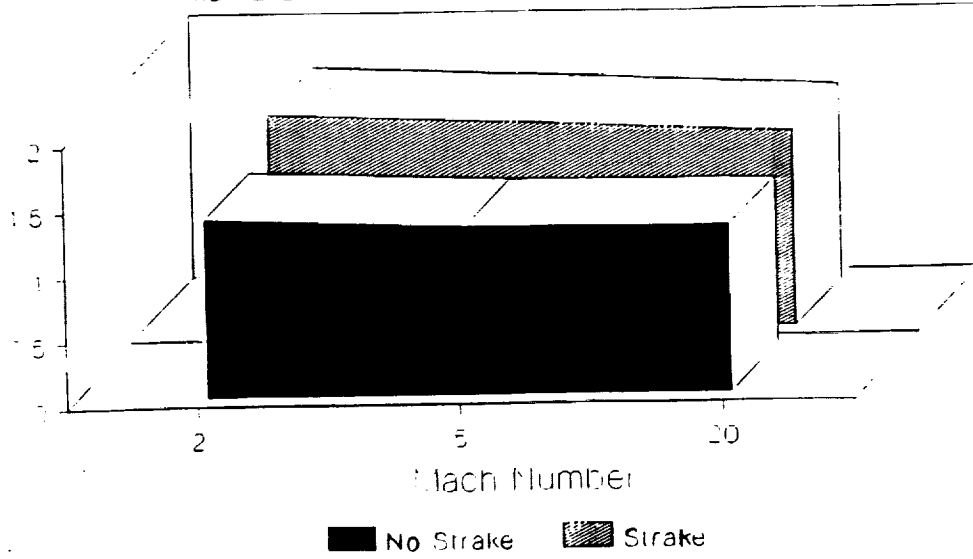


Figure 5-28, Strake Comparison Wingtip Fin Configuration

Wingtip Fin Configuration

(0 deg. Yaw; 0 deg. Toe-in; Const. Wing Ref. Area)

Max L/D

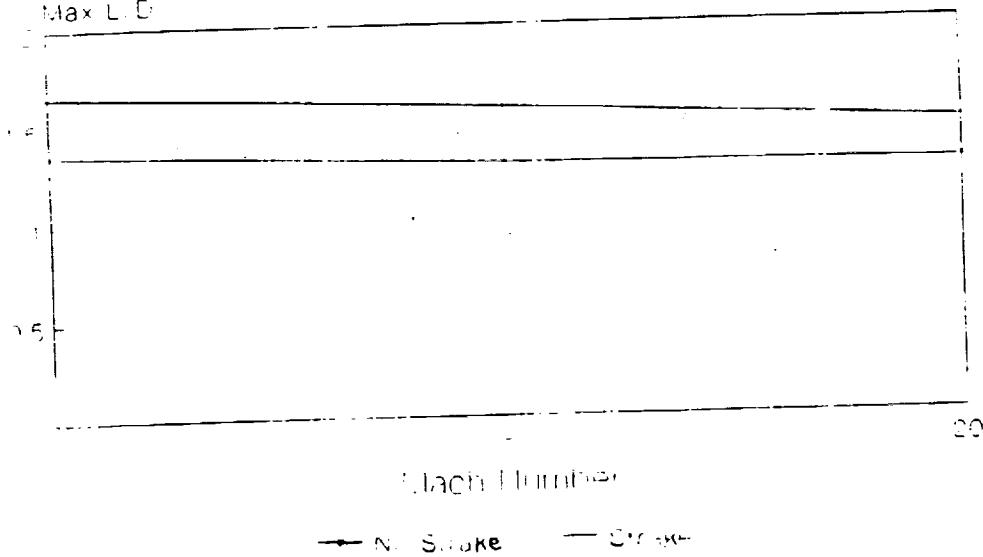


Figure 5-29, Strake Comparison Wingtip Fin Comparison, 3-D

Wingtip Fin Configuration

(0 deg. Yaw; Strake)

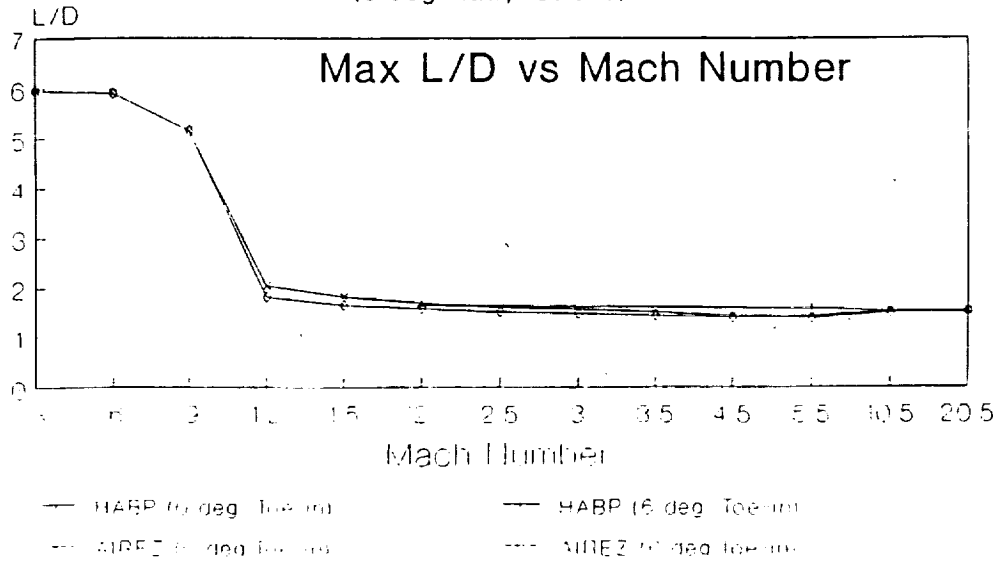


Figure 5-30, AIREZ vs. HABP Comparison Wingtip Fin Configuration

Wingtip Fin Configuration

(0 deg. Yaw; Strake)

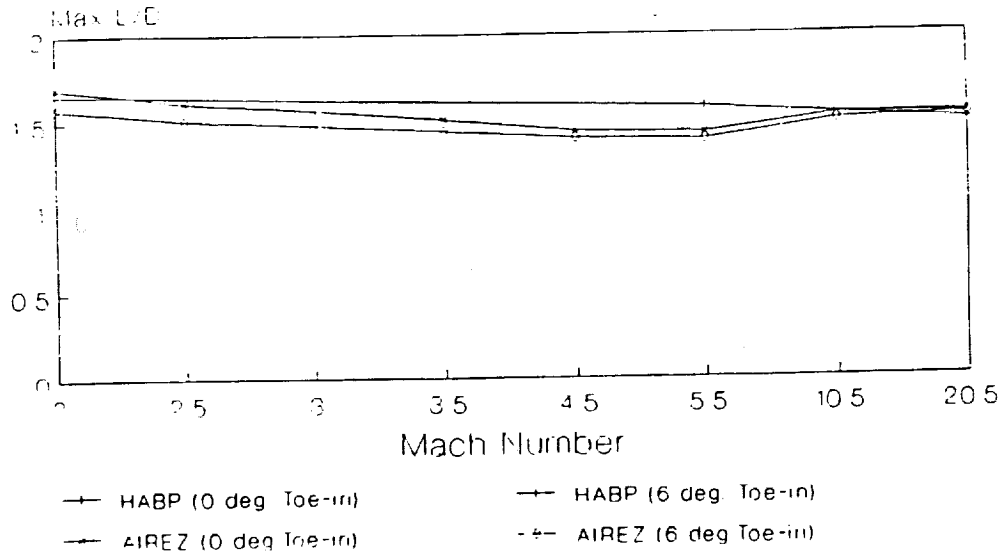


Figure 5-31, AIREZ vs. HABP Comparison Wingtip Fin Comparison

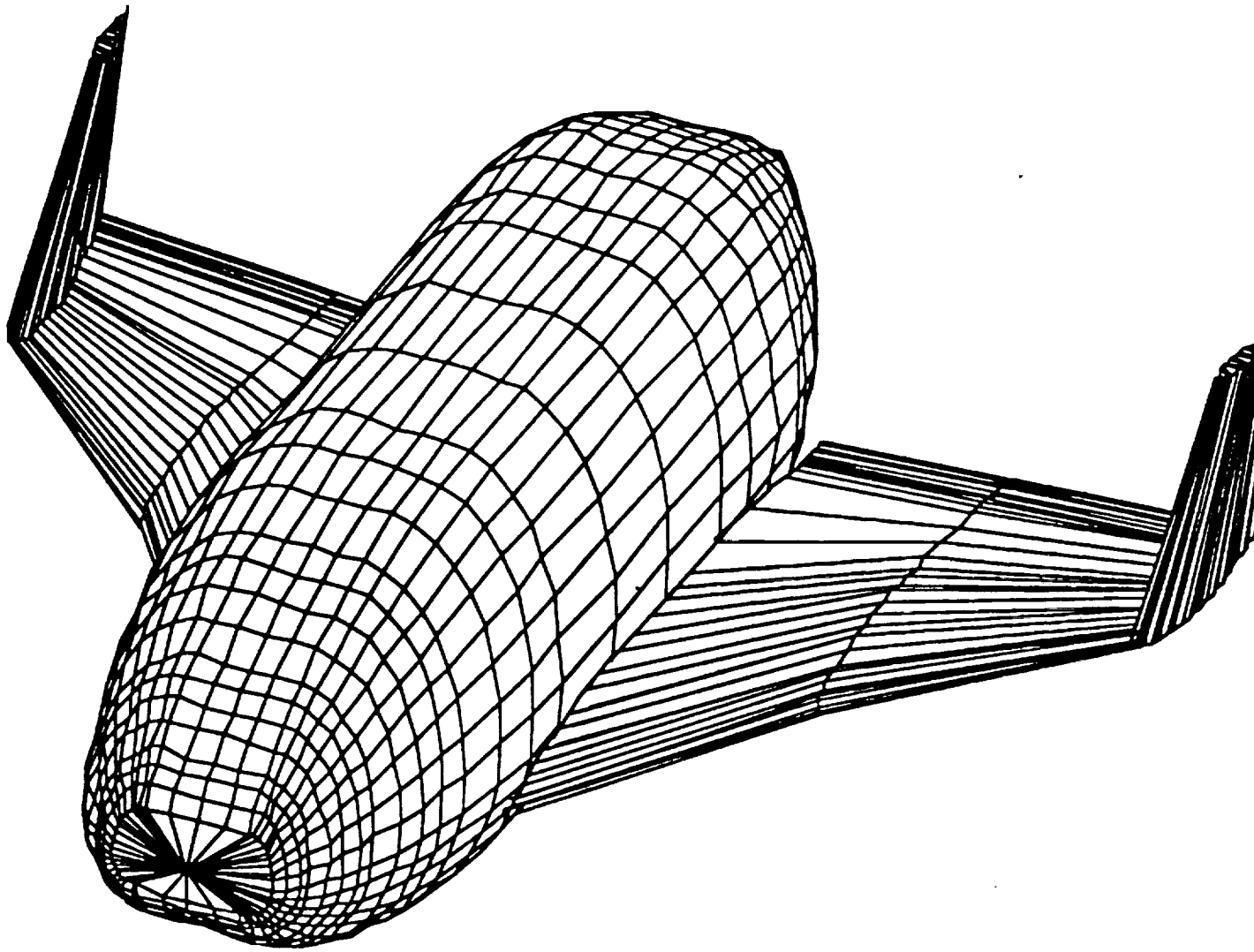


Figure 5-32 Final Configuration-Perspective View

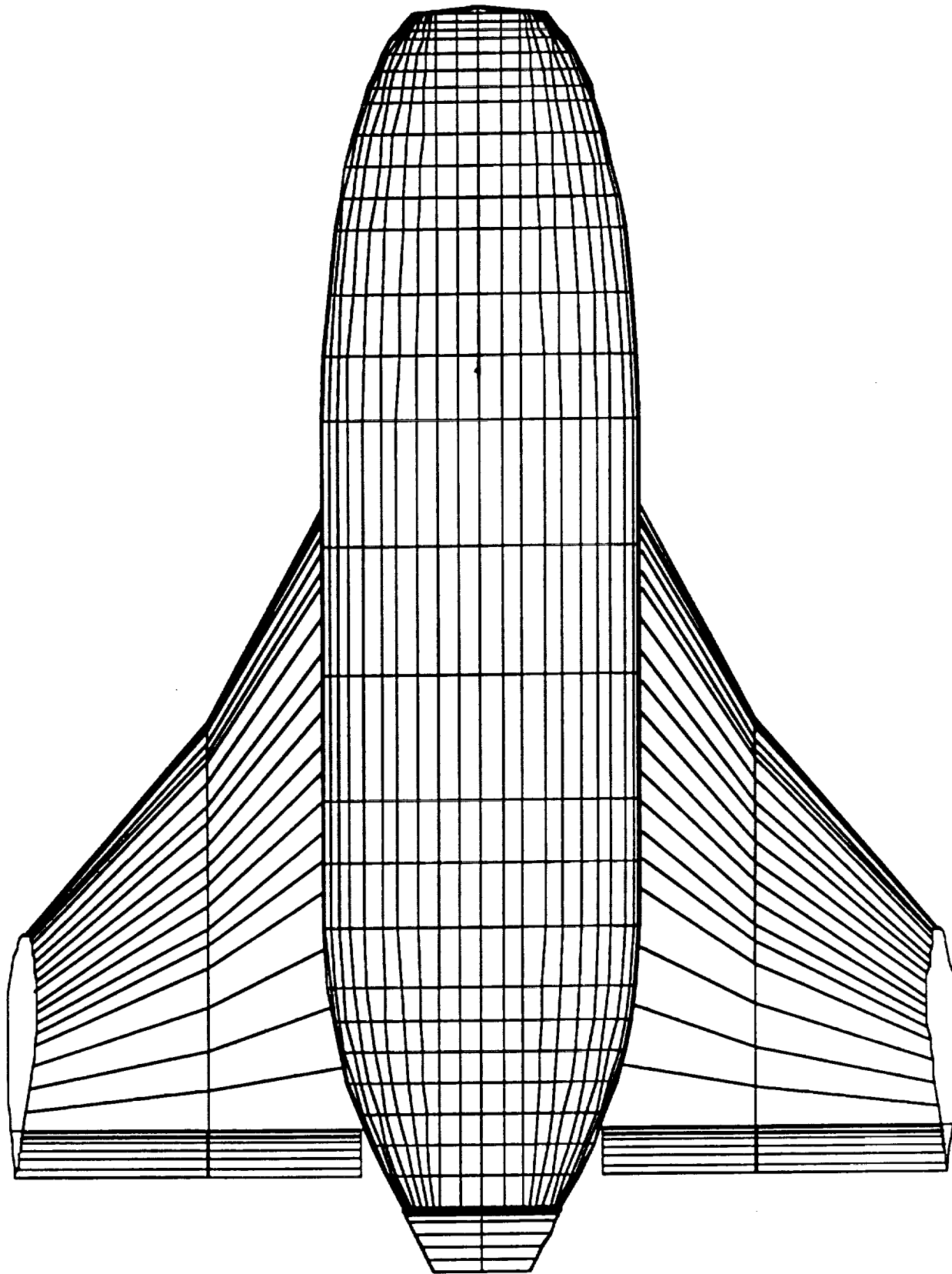


Figure 5-33 Final Configuration -Top View



Figure 5-34 Final Configuration -Side View

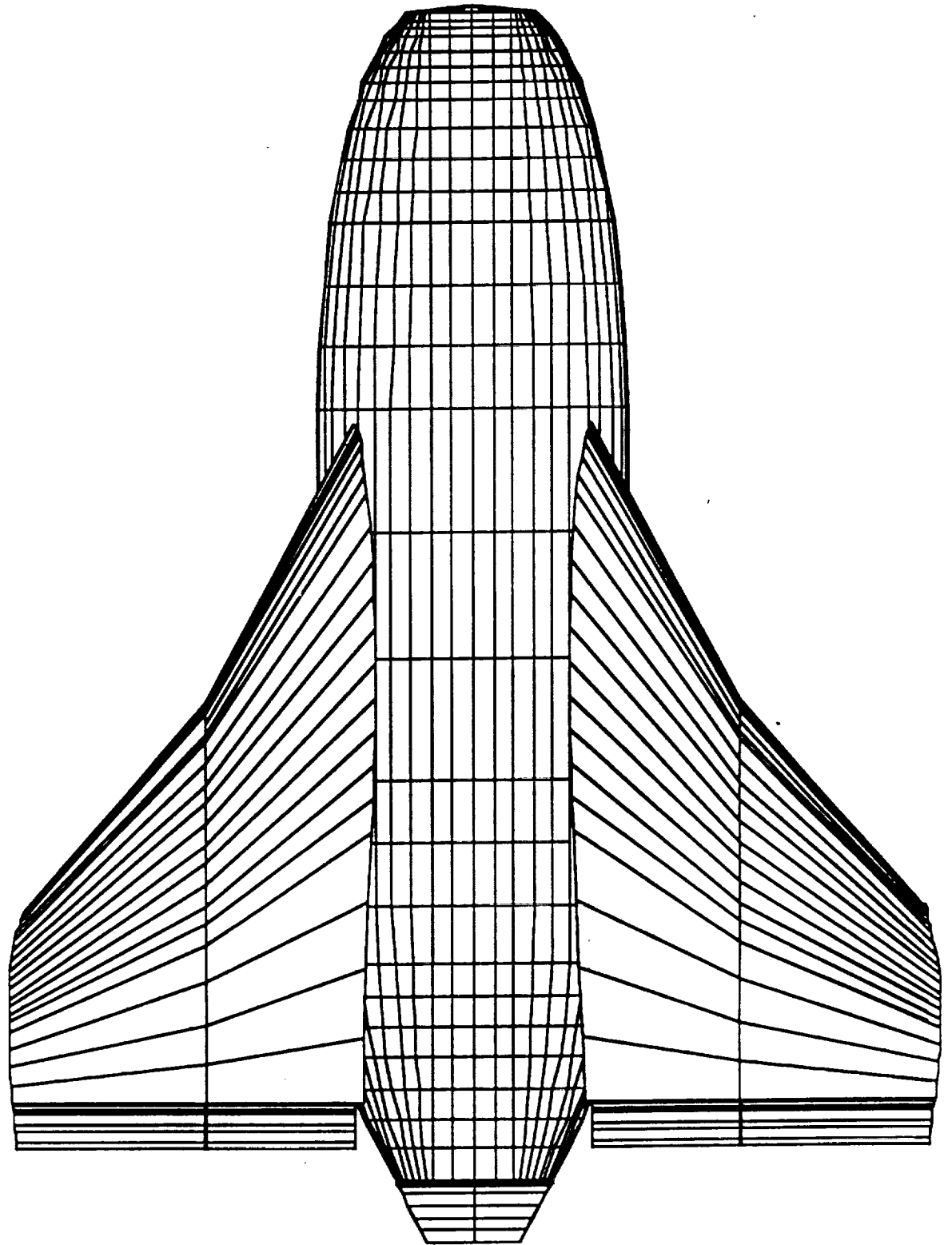


Figure 5-35 Final Configuration -Bottom View

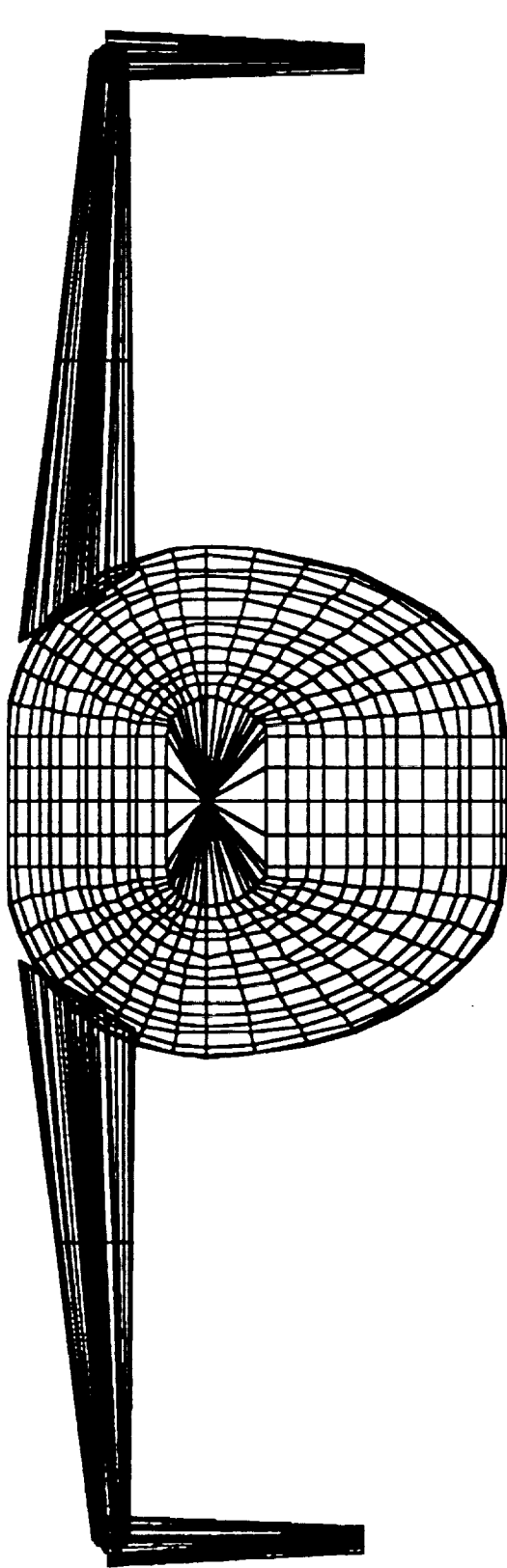


Figure 5-36 Front View

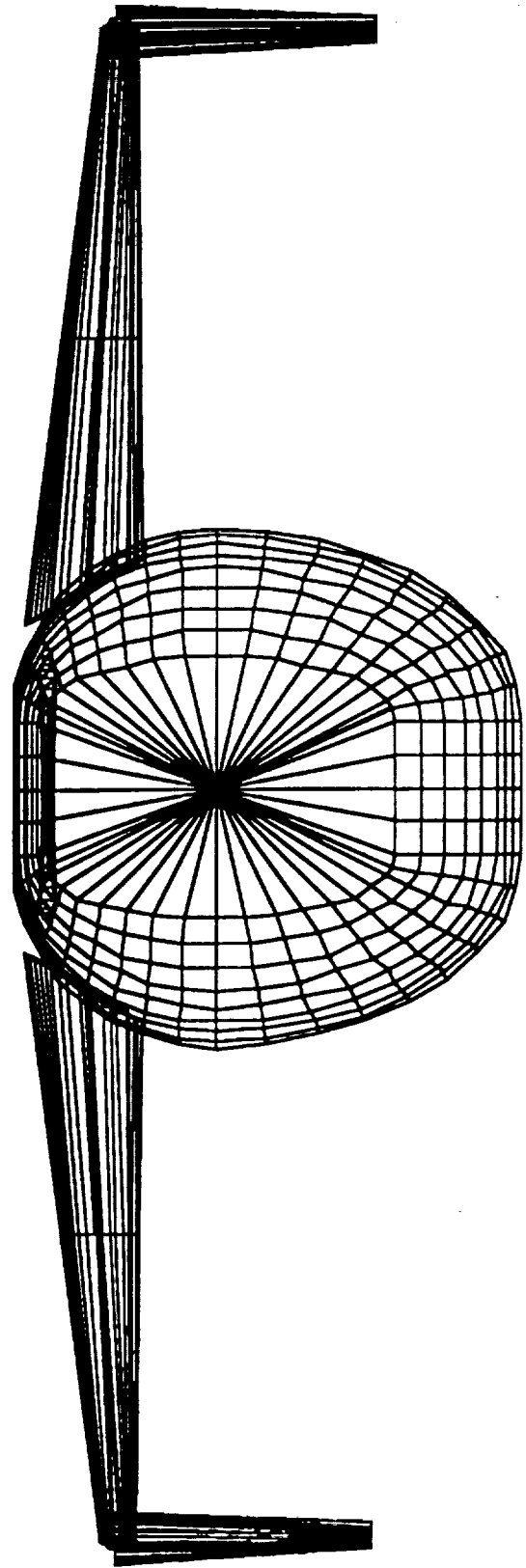


Figure 5-37 Rear View

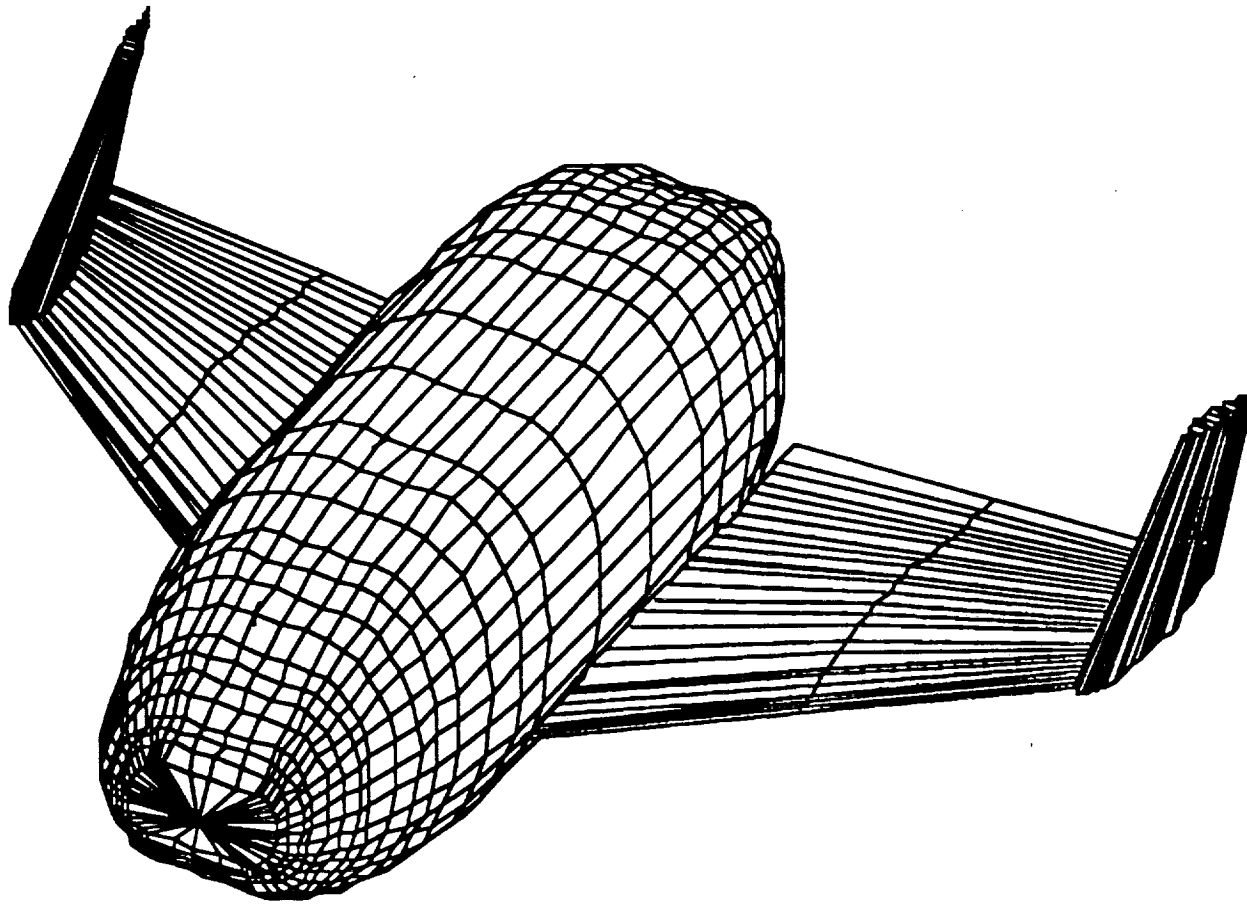


Figure 5-38, Final Configuration - No Strake

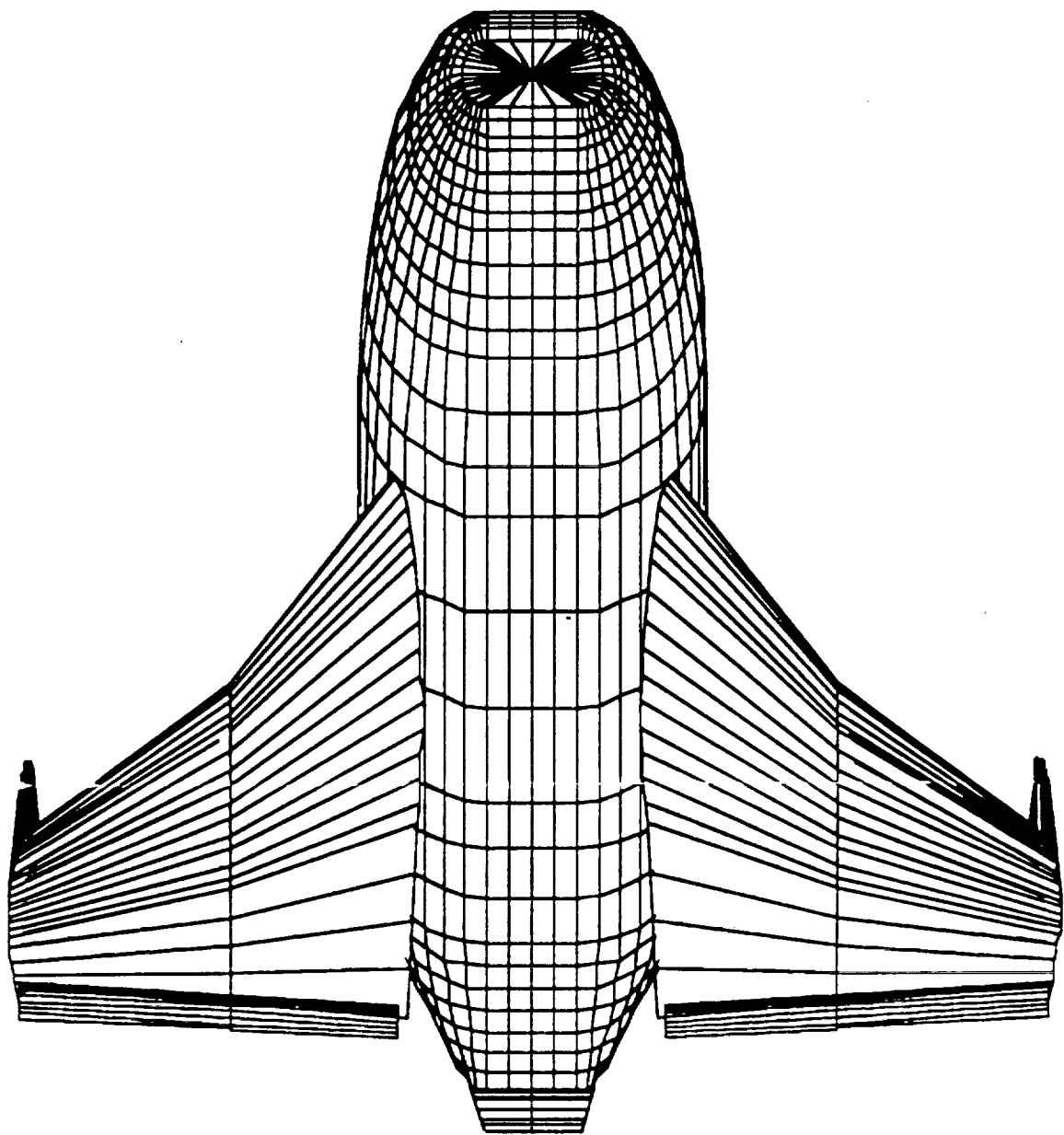


Figure 5-39, Final Configuration -35 deg. Angle Of Attack

THIS PAGE HAS BEEN LEFT INTENTIONALLY BLANK

6.0 STABILITY AND CONTROL

The stability and control analysis of the winged CRV involved a complex iterative process. The stability and control aspects for each of these flight regimes were very diverse and combining the separate requirements into a simple vehicle design, entailed compromises in each performance regime in order to provide adequate stability and control throughout the entire flight profile.

The hypersonic stability and control analysis of winged vehicles was based almost entirely upon simple approximations of contributions from each part of the vehicle (i.e. wings, underbody, etc.) and upon available Space Shuttle data fig. 6-1. Rotational stability is minimal at hypersonic velocities and methods used to improve this type of stability were very different than the supersonic/subsonic methods.

The subsonic stability and control analysis of the winglet vehicle was based on commonly available data and methods. The vehicle, however, is inherently unstable below Mach one. This is due to hyper/supersonic constraints dictating the center of gravity location. With modern active automated control systems readily available, similar to the space shuttle's, this unstable situation would not be a problem.

6.1 STABILITY AXES

Stability axes were defined so as to conform to standard practice. As can be seen in figure 6-1. The origin is at the aerodynamic center and a right handed coordinate system is used with the positive axis pointing out of the vehicle's nose.

Generalized Configuration Geometry for Hypersonic Stability Derivative Approximation

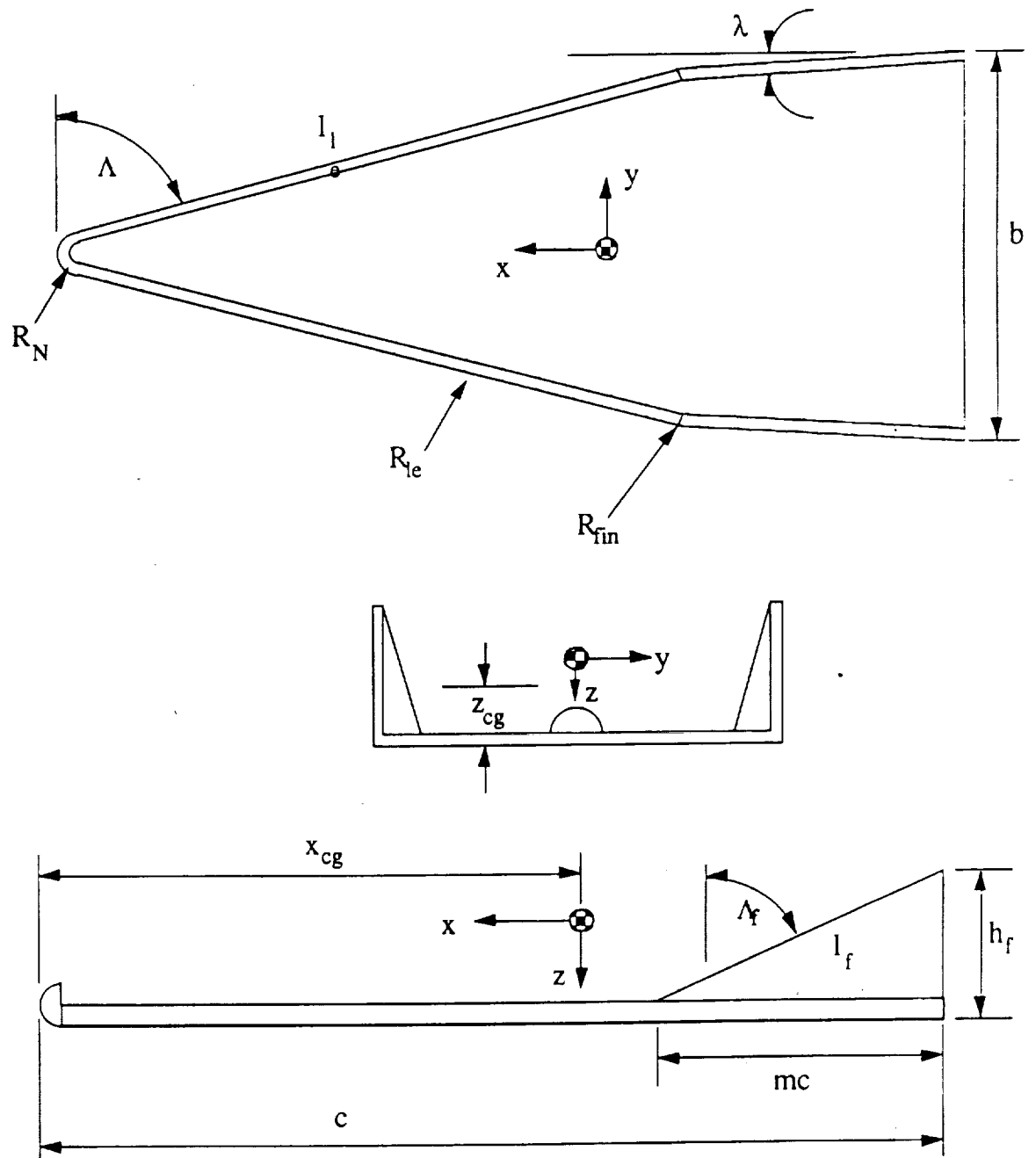
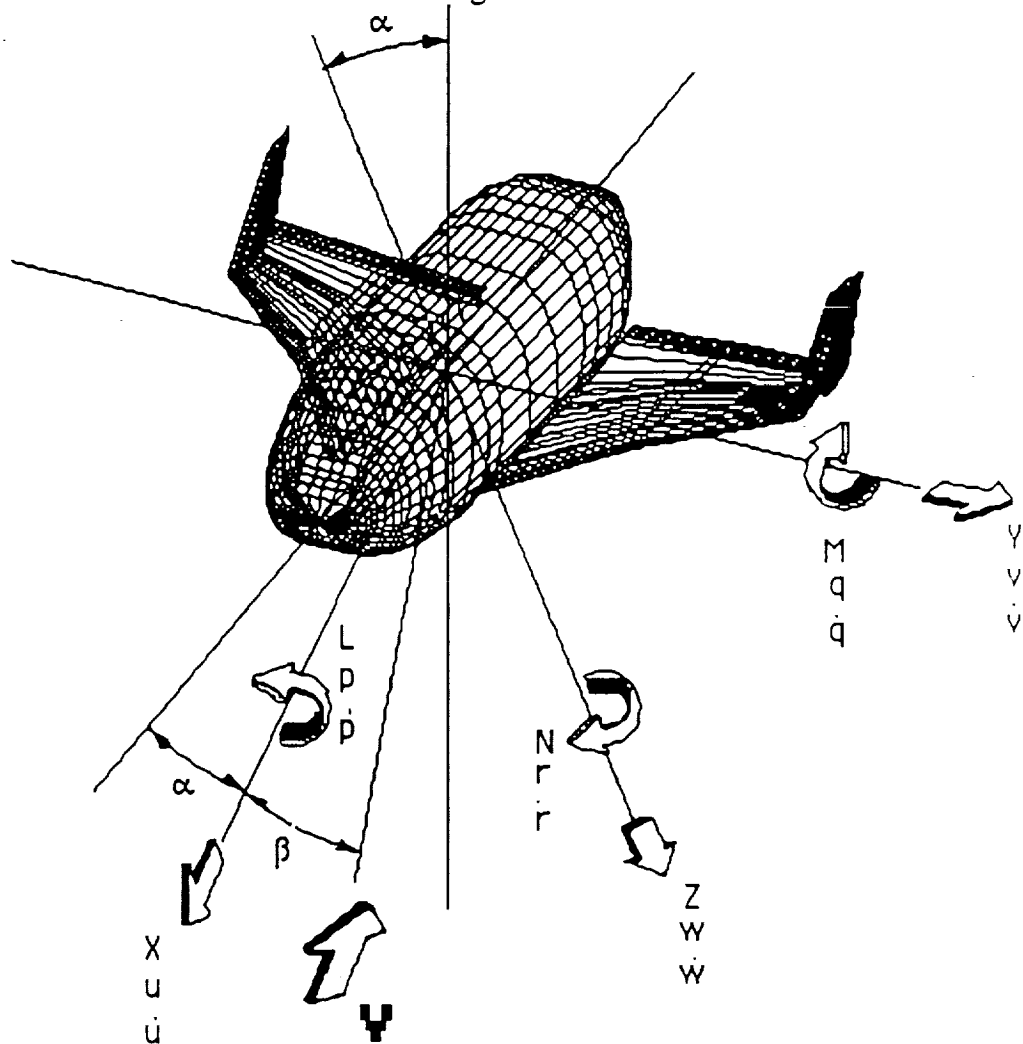


Figure 6-1 Generalized Configuration Geometry for Hypersonic
Stability Derivative Approximation

Figure 6-2 Axes used for atmospheric stability analysis of the winged CRV.



6.2 EXPLANATION OF S.A.P. AND TECHNIQUES

The approach taken to analyze the stability of the CRV was similar to the stability analysis for a low-speed vehicle, except, the relative importance of the various forces required for the analysis was different. Rotary derivatives such as C_{lb} , C_{nb} and C_{yb} become vanishingly small at hypersonic speeds. This greatly simplifies the stability analysis in the hypersonic region. The consequences of this condition, however, are extremely important. Since the rotary derivatives produce the damping of the vehicle, undamped or neutral oscillations should be anticipated (Ref. 6.5). The Stability Analysis Program (SAP) was written to compute the approximate stability derivatives for hypersonic and subsonic flight. Many stability derivatives such as $C_{n\dot{\beta}}$ and $C_{l\dot{\beta}}$ could not be accurately

calculated without the assistance of wind tunnel data. This was especially true for hypersonic flight. Therefore, much of the analysis for hypersonic derivative approximation was based on references 6.5, and subsonic/supersonic theory was taken from references 6.9, 6.13, and 6.17. The program SAP calculated derivatives using data inputted in the form of vehicle dimensions, control surface sizes, weights, altitude, density and velocity. Figure 6-2 displays the generalized configuration geometry used for approximating vehicle contributions needed for evaluating the stability derivatives. The resulting output provided the derivatives needed to complete a stability matrix to evaluate short period and phugoid modes for both the longitudinal and lateral modes. A program called MINNEMAC written by Professor B. Liebst at the University of Minnesota, which computes the different modes of stability and plots their resulting root loci, was used in the analysis of the vehicle.

The results of SAP were also used to make for comparisons between the various iterations of the CRV. Stability derivatives such as C_{Lb} and C_{nb} were graphed as a function of mach number and angle of attack and then compared against minimum values needed to remain within the boundaries of the stability and control requirements. This method was used to minimize control surface sizes and deflections.

6.3 STABILITY AND CONTROL REQUIREMENTS

6.3.1 Stability and Control Standards

Stability and control requirements are defined by many standards for different types of aircraft and their applications. Military requirements (MIL-F-8785C) were used as the main standard for outlining the stability and control parameters for the atmospheric flight analysis. It must be noted however, that these requirements are based on the flying qualities of piloted aircraft, whereas the CRV is an automatically controlled unmanned vehicle. The commercial and military requirements for the corresponding transport categories are very similar and also applied to the analysis. Though not specifically falling under either of these categories, reference performance and stability derivative data in the reentry hypersonic flight regime for the space shuttle has been applied to the CRV due to the close similarity of the vehicle styles.(Ref. 6.15)

6.3.2 Lateral and Longitudinal Stability

The CRV must maintain adequate controllability in the lateral and longitudinal axis and to complete its mission within a pre-determined flight profile. The ailerons (elevons) and rudder surfaces must be sized to provide complete roll, yaw, and pitch control in all atmospheric flight regimes.

6.3.3 Launch Integration Stability

The integrated static launch vehicle/CRV assembly must withstand wind effects during assembly and prelaunch preparation on the launch pad. These wind effects include gust and shears common to launch locations. Included in wind effects is the phenomenon of buffeting. Vortices are shed behind the launch vehicle assembly creating alternating side forces.

During the launch to orbit phase, the sideslip and attack angles of the entire assembly must not be so large as to create excessive loads on the structure or be beyond the capabilities of the control system to maintain controlled flight.

6.3.4 Control Requirements

Control of the vehicle will be maintained by an automated flight control system. Commands from either the Space Station or ground, control, however, have been, placed in the control loop.

The automated flight control system must be able to orient and maintain of the vehicle in a specified direction. The tools that the system has to work with consist of NTO/MMH reaction control jets, N2 cold gas thrusters, elevons, rudders, and a body flap.

6.3.4.1 Control Requirements During Ascent

On ascent the flight control system of the CRV would remain dormant until separation, at which point the vehicle's Orbital Maneuvering System (OMS) would insert the vehicle in the proper orbit. As a result, the Liquid Rocket Booster's flight control system must include commands to reduce ascent loads on the CRV structure and the CRV/Launch Vehicle Interface.

6.3.4.2 Control Requirements On-Orbit

The on-orbit flight control system would be utilized after the orbit insertion and would be terminated after the de-orbit maneuver. It will have to support all orbital missions with the space station or Orbital Maneuvering Unit. This would be accomplished by the 52 reaction control jets (28 NTO/MMH, 24 N2).

Attitude determination would rely on a star tracker and the Global Positioning System. Rotation rates would be determined by differentiating the attitude angles.

6.3.4.2.1 Control Requirements in Space Station Control Zone

Maneuvering within the space station's control zone would be done using the N2 cold gas thrusters. This requirement is specified by mission operations to prevent damage to the space station's optics and habitation module. Use of the N2 thrusters, however, will increase the time responses of the vehicle. Within the control zone the CRV is required to be controlled by space station personnel.

6.3.4.3 Control Requirements During Reentry

Aerodynamic control surfaces would control the vehicle through much of the atmospheric re-entry flight regime. Nominal aerodynamic control effectiveness is attained at 10-15 psf dynamic pressure. Therefore, at lower dynamic pressures the RCS system would be employed for vehicle control.

6.4 CONTROLS

6.4.1 On-Orbit Controls

Each of the 28 NTO/MMH jets supply a specific impulse of 289 seconds. Whereas the specific impulse of the N2 cold gas thrusters is 68. The cold gas thrusters are used for fine rotational control and maneuvering within the space station control zone. Figure. 6-3 illustrates the NTO/MMH jet locations and thrust directions (Ref. 6.11).

Attitude adjustment commands would be inputted and differentiated in the maneuver module. The resulting rate commands would be

summed along with the rate errors and then integrated to attain new position vectors. These position vectors would be summed with the attitude errors and inserted into the dead-band controller. From the controller, rotation commands would be sent to a jet select logic where proper control jets would be used for the specified maneuver. Figure 6-4 displays a simplified control law of the RCS.(Ref. 6.11)

Rate and attitude error commands stem from the state estimator. The estimator compares attitudes and rates against the rotation commands and values calculated by the maneuver track function to produce the rate and attitude errors. Inputs from either the star tracker or Global Positioning System would be used in the state estimator.

Attitude commands could be sent from space station personnel, ground operations, or AFC.

6.4.1.2 Mission Criterion

In order for the CRV to accomplish its mission it must either dock directly with the space station or rendezvous with the OMV.

The AFC must select the best attitude deadband ranges for each specific mission. Table 6-1 shows deadband ranges taken from the Space Shuttle's on-orbit FCS (Ref. 6.10). These deadband ranges are applicable to the CRV since they each have similar mission requirements.

Table 6-1 DeadBand Ranges

RCS Jets/thrusters	Rate Limit Range (deg/sec)	Attitude Deadband Range (deg)
NTO/MMH jets	0.2 to 4.0	1.0 to 20.0
N2 thrusters	0.01 to 0.5	0.1 to 20.0

6.4.2 Ascent Controls

Separation between the CRV and LRB would be achieved by detonating explosive charges between the CRV and CRV/LV interface. Initial attitude states and rates are inputted into the state estimator from the GPS and IMU. The attitude states and rates would then be compared with nominal attitude characteristics for orbital insertion. Proper jets would be selected and fired to

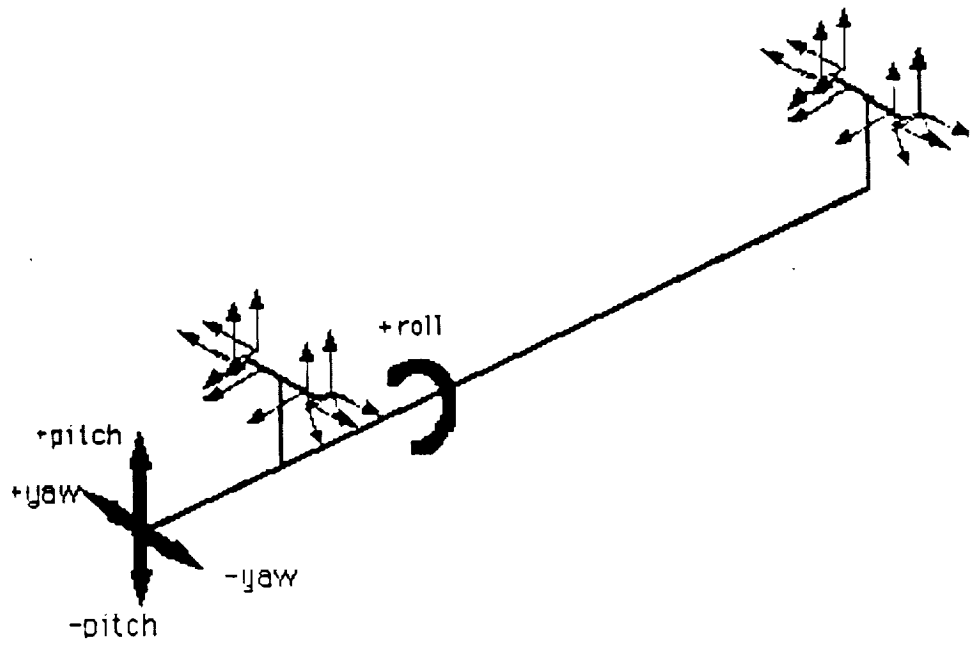


Figure 6-3 Thrust location of RCS

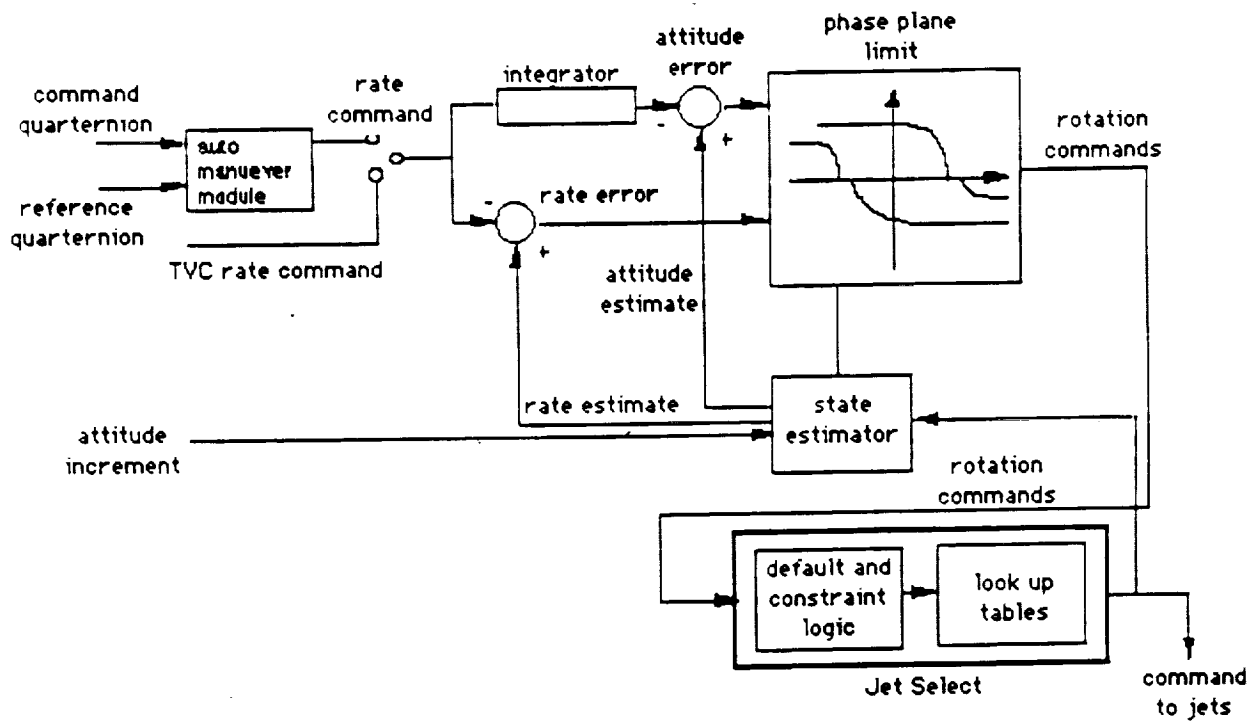


Figure 6-4 On-orbit Control Law

position the vehicle for the OMS burn. The OMS engine has the ability to gimbal 15 degrees in the longitudinal direction, which enables the thrust vector to point through the vehicles center of gravity.

6.4.3 Re-entry Controls

Re-entry controls are maintained by the aerodynamic control surfaces once the dynamic pressure increases to 10 psf. The reaction jets would control the CRV at lower dynamic pressures. The control surfaces consist of a body flap, elevons and two winglet rudders.

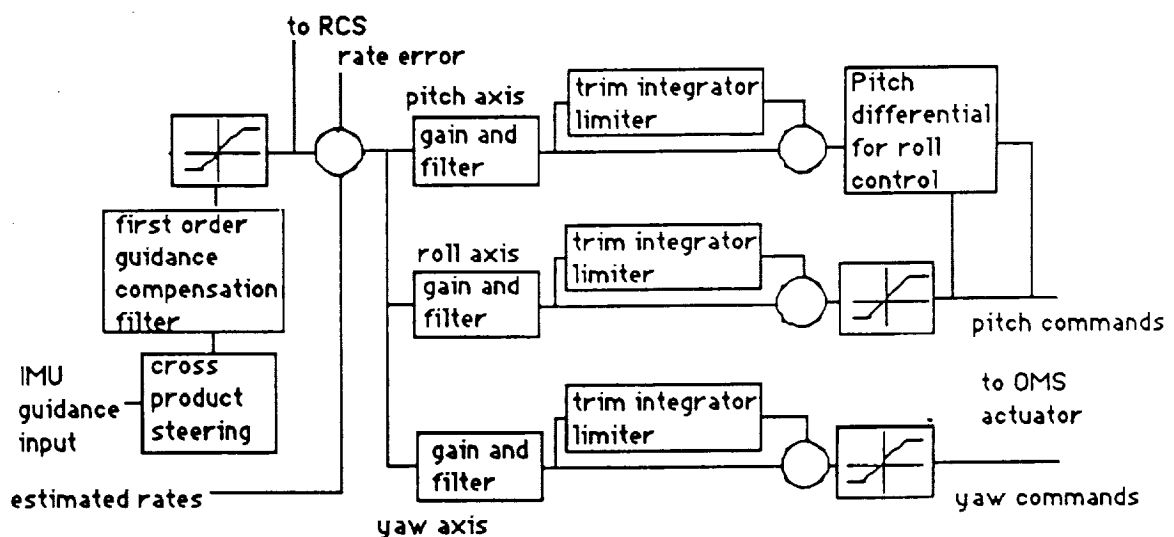


Figure 6-5 Ascent OMS control Law

Rate and attitude errors would be computed from the state estimator by comparing states obtained from the IMU. The errors would then be fed into the controller where steering commands would be formed for each of the respective axis.

At the beginning of re-entry, the RCS jets would be used to control the vehicle. At 10 psf dynamic pressure elevon roll effectiveness would be achieved and the roll thrusters would be deactivated. At 20 psf dynamic pressure the elevons would take over the pitch control. Rudder control would not become active until 170 psf.

IMU and GPS would be used for much of the re-entry sequence, but at mach 3, air data probes would deploy to measure the attitude states.

6.5 PERFORMANCE ANALYSIS

6.5.1 On-orbit Analysis

A rigid body model of the CRV was used to create the equations of motion (Ref. 6.13).

$$\alpha_1(I_{xz}^2 - I_1 I_3) = \omega_1 I_1 I_{xz} + I_{xz}(I_1 - I_2 + I_3)\omega_2 + (I_{xz}^2 - I_2 I_3 + I_3^2)\omega_2 + (-I_{xz} I_2 + I_3^2)\omega_3$$

$$\alpha_2 I_3 = \omega_2(2I_{xz} + I_3 - I_1) + \omega_3(-I_1 + 2I_3 - 2I_{yz})$$

$$\alpha_3(-I_{xz}^2 + I_1 I_3) = \omega_1(I_1^2 - I_1 I_2 + I_{xz}^2) + \omega_2[I_1^2 + I_{xz}^2 - I_1 I_2 + I_{xz}(I_1 - I_2 + I_3)] + \omega_3(I_1 I_{xz} - I_2 I_{xz} + I_3 I_{xz})$$

where $\alpha_{1,2,3}$ = angular acceleration for the roll, pitch and yaw axis respectively.

$I_{1,2,3}$ = moment of inertia for roll, pitch and yaw respectively.

$\omega_{1,2,3}$ = angular velocity for the roll, pitch and yaw respectively.

Analysis of the control system was accomplished by placing the linearized equations of motion into state space form. A root locus of the equations were then used to study the rotational rigid body motion. However, certain modes exist on the right side of the imaginary axis indicating rotational instability. The cause of this instability may be nutation. Nutation is the condition in which the instantaneous rotation axis is not aligned with the principal axis and the angular momentum vector is circumscribed by both the angular velocity vector and principal axis.

Design of a control system for an unstable system was attempted. A "bang-bang" control law with negative feedback was chosen and is shown in fig.6-7 (Ref. 6.22).

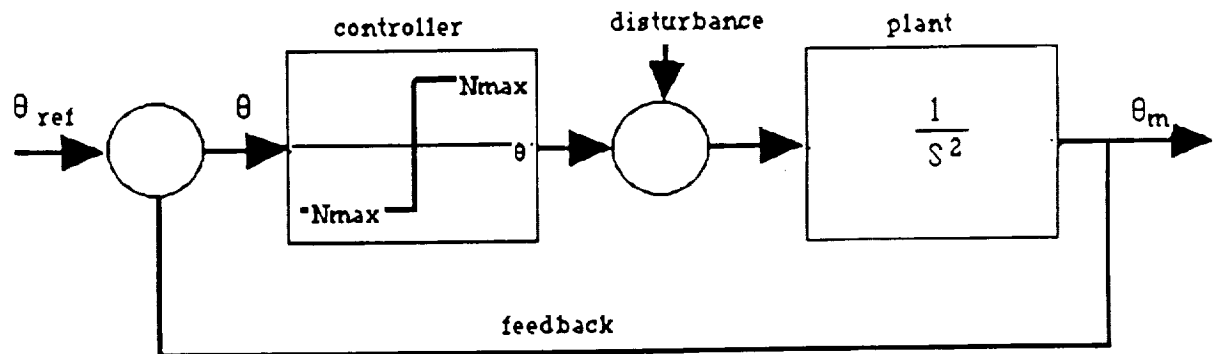


Figure 6-7 "bang-bang" control law with negative feedback

The control law is defined by:

$$N_c = \frac{-q}{|q|} N_{\max}$$

where N_c = control torque

N_{\max} = maximum control torque

q = angular error

Figure 6-8 shows the root locus of the transfer function of the equations of motion for a varying gain up to $1E+6$. This gain value is unpractical and demonstrates that a better estimator is needed. If desirable eigenvectors could be obtained then gains for the system could be computed and a stable system can be obtained.

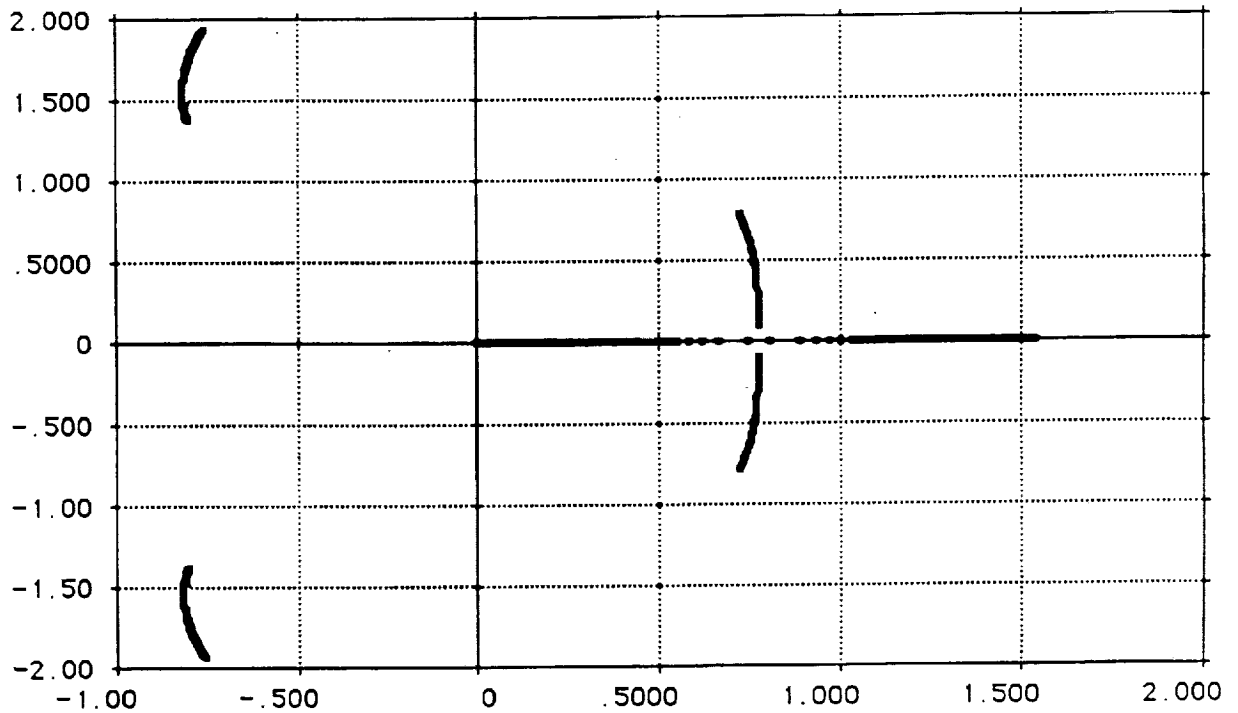


Figure 6-8 Root locus of transfer functions of varying gain

6.5.2 Static Longitudinal Analysis

6.5.2.1 Subsonic Neutral and Maneuver Points

The subsonic stick-fixed neutral point was derived using References 6.3, 6.13, and 6.18 (see fig. 6-10). Accounting for the wing/body and wing/winglets interference effects the total vehicle neutral point was found to be located 5.55 ft forward of the wing neutral point (45.05

ft aft of the nose). This location is 56% of the total vehicle length. The maneuver point was calculated at 1.03 ft aft of the neutral point. For the stability analysis, the stick-fixed neutral point was used instead of the stick-free neutral point as used in reference 6.3 to accommodate the automatic active control system.

$$h_{nw} = n + \frac{3(1+l)^2}{8(1+l+l^2)} \left(h_{cp} - \frac{1+2l}{3(1+l)} \right) A \tan L_n h_{cp}$$

6.5.2.2 Supersonic Neutral and Maneuver Points

For the lower supersonic region the stick-fixed neutral point for the wing was located at 50% of the wing mean aerodynamic chord as determined by supersonic center of pressure theory (Fig. 6-10). Accounting for the effects of aspect ratio, sweep angle and taper ratio (Ref. 6-18) and including the neutral point shift due to interference effects the analysis obtained a forward shift of 5.55 ft. The resulting total vehicle neutral point was 53.40 ft aft of the nose and corresponds 65% of the total vehicle length. The supersonic maneuver point was located 1.03 ft aft the supersonic neutral point at 10,000 ft. It should be noted that the supersonic maneuver point is a function of the relative mass parameter $\left(m = \frac{m}{rSI} \right)$. This parameter increases with altitude and hence the maneuver point approaches the neutral point as altitude increases.

6.5.2.3 Static Longitudinal Stability

The static stability and control analysis was broken into two flight regions: subsonic and supersonic/hypersonic. The main criterion for determining static longitudinal stability was the pitching moment of the entire vehicle. This moment must be negative for an inherently stable craft. In order to achieve this situation, the vehicle center of mass must lie ahead of the vehicle neutral point creating a positive (nose down) moment. Figure 6.9 indicates that Cm_a is negative for the entire flight regime indicating the vehicle would be stable longitudinally.

Unfortunately, the CRV must operate at supersonic, as well as, subsonic velocities resulting in two operational neutral points. Optimally, the center of mass would be shifted to accommodate the

Cm alpha vs Mach number

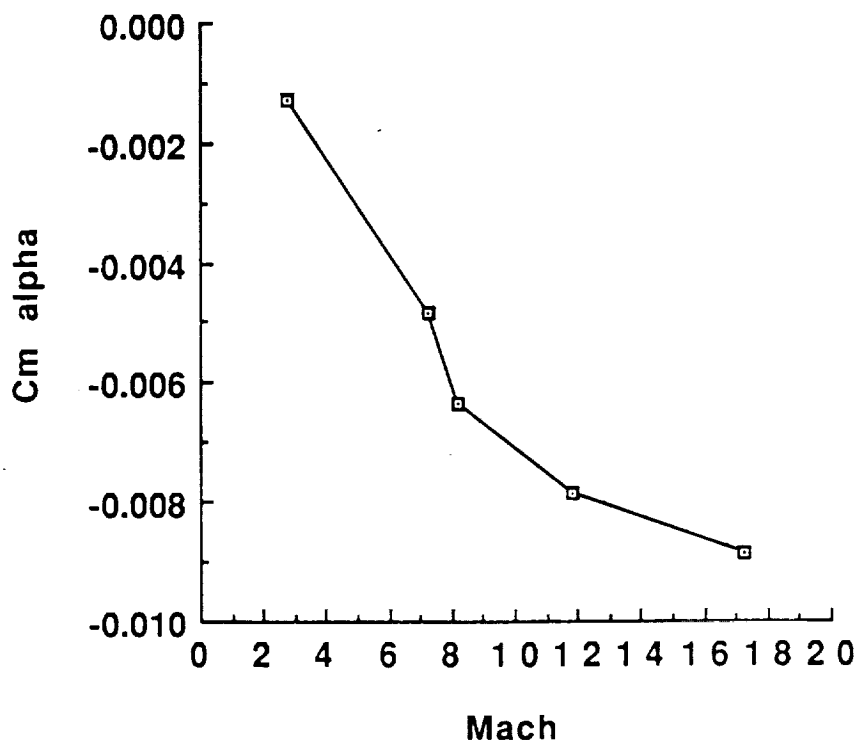


Figure 6-9 Cm_a vs Mach

changing neutral points and achieve a trim condition. However, the CRV has few items that can be shifted to produce trim. Instead, the CRV would operate in an unstable mode in the subsonic region with the center of mass behind the subsonic neutral point. This condition is tolerable if active automatic control systems are used. In the supersonic regime the vehicle would be positively stable with the center of mass placement ahead of the neutral point (fig 6-10).

6.5.3 Longitudinal and Lateral Derivative Approximations

The hypersonic stability derivative approximations are based largely upon methods defined in reference 6.5. These methods were also applied to the higher supersonic flight regime. The analysis was based on individual contributions from different vehicle components (fig. 6-2).

These contributing areas are:

1. Nose
2. Leading Edge
3. Lower Surface
4. Vertical Fin (winglets or single vertical fin)

Location of subsonic and supersonic vehicle neutral and maneuver points

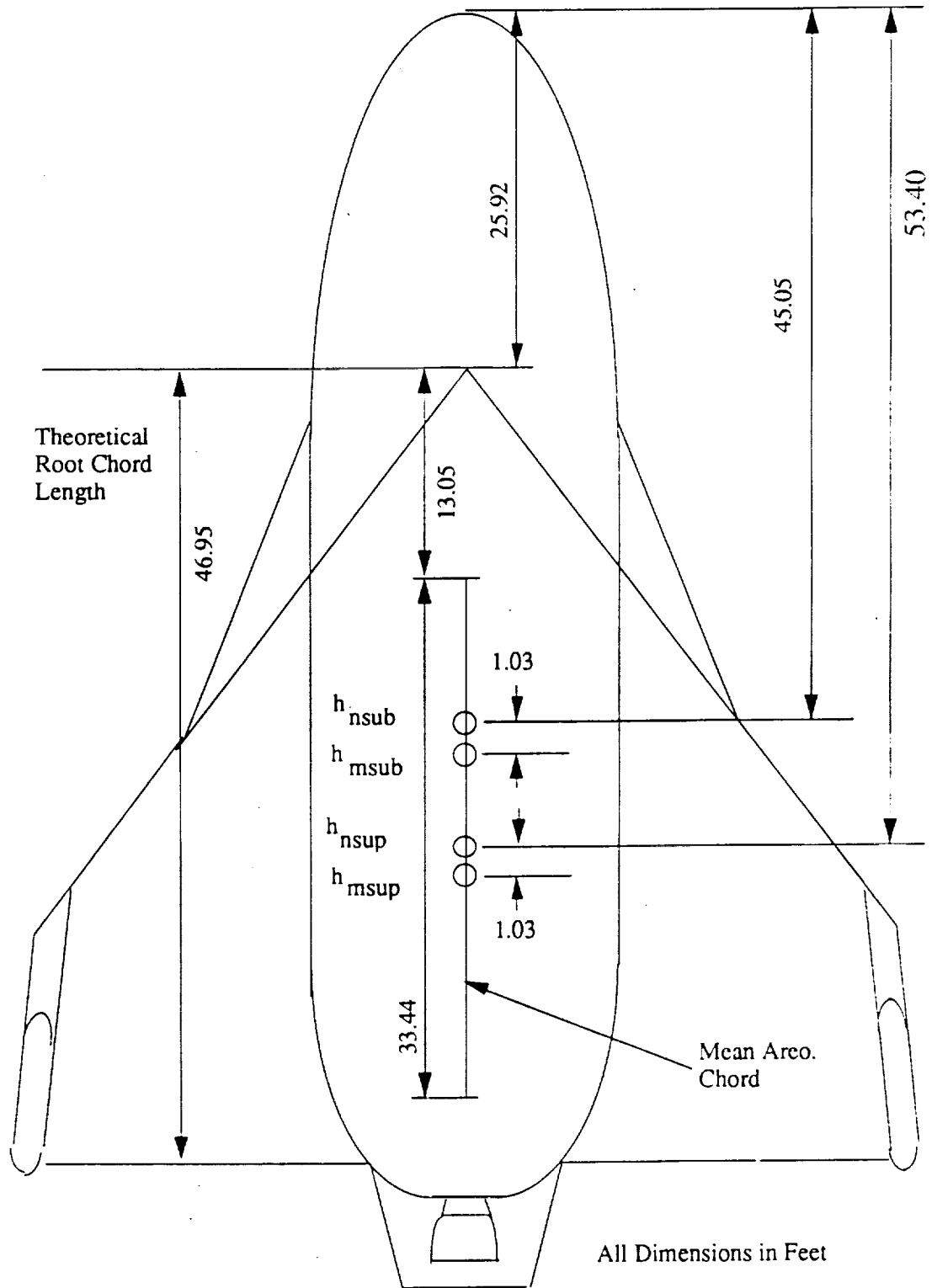


Figure 6-10

The vehicle parameters used in the SAP program for this analysis are defined in table 6-2.

6.5.4 Longitudinal Dynamic Analysis

MINNEMAC was used to analyze the stability of the final configuration for uncontrolled motion in the longitudinal axis. The results are shown in the Table 6-3 below.

Table 6-2 Parameters for analysis of the three configurations:

PARAMETERS	FIRST CONF.	SECOND CONF.	FINAL CONF.
L _w Wing Sweep	0.8491	0.8491	0.8491
L _F Fin Sweep	0	0.7854	0.7854
L _T Tail Sweep	0.8203	0.8203	0
S _T Area Tail	277.04	277.04	0
S _{T'} Area Tail P.	932.43	932.43	0
z _v	15.652	15.652	0
AR _T Tail	1.072	1.072	0
x _v	-38.07	-38.07	0
AR _w Wing	1.9032	1.9032	1.9032
AR _F Fin	0	0.815	0.815
W Weight	105,000	105,000	105,000
R _N	3.8	3.8	3.8
R _L	2.0	2.0	2.0
P _T	0.17	0.17	0.17
b Span	58	58	58
S _w Wing Area	1767	1767	1767
S Total Area	2287.6	2287.6	2287.6
S _F Fin Area	0	110.67	110.67
z _{LE}	5.5	5.5	5.5
z _N	0.95	0.95	0.95
z _F	0	5.29	5.29
z _L	5.5	5.5	5.5
y _{LE}	11.88	11.88	11.88
c _{bar}	33.44	33.44	33.44
x _N	39.2	39.2	39.2
x _L	-8.53	-8.53	-8.53
x _F	0	-10.61	-10.61
y _F	0	29	29
x _{LE}	-8.53	-8.53	-8.53
k _n	0.30	0.30	0.30

Table 6-3 Minnemac results
Mach 2.8

Mode 1 Phugoid Mode	
Period	9715.1122
z	0.0127
T 1/2	84249.1
N half	8.6720
Mode 2 Short Period Mode	
Period	55.0621
z	0.0057
T 1/2	1061.2086
N 1/2	19.2729

Mach 7.2

Mode 1 Phugoid Mode - UNSTABLE	
Period	10656.6688
T 1/2	32742.7073
N 1/2	3.0725
Mode 2 Short Period Mode	
Period	44.5059
z	0.0033
T 1/2	1484.4505
N 1/2	33.3541

Mach 17.2

Mode 1 Phugoid Mode - UNSTABLE	
Period	1472.3635
T 1/2	937.3591
N 1/2	0.6366
Mode 2 Short Period Mode	
Period	5.0063
z	0.0004
T 1/2	1382.6614
N 1/2	276.1868

At Mach 2.8 the vehicle would be stable in both phugoid and short period modes with $T_{1/2} > 1000$ secs. The values of the damping ratio are very small; $z=0.0127$ for the Phugoid mode and $z=0.0057$ for the short period mode. Therefore, at this velocity, the vehicle is very stable. At Mach 7.8 the vehicle is unstable in the Phugoid mode. The time to half, however, would be large enough to allow the control

system of the vehicle to correct perturbations in the flight path of the vehicle ($T_{1/2} > 3200$ sec). The vehicle would also be stable in the short period mode at Mach 2.8. At Mach 17.2 the vehicle is unstable in the Phugoid mode, but the time to half would again be large enough to allow the control system to correct the instability ($T_{1/2} = 937$ sec.). Overall the final configuration possesses adequate inherent stability in the longitudinal axis. In instances where it is not stable, the $T_{1/2}$ of the oscillations are large enough to allow the control system of the vehicle to correct the oscillation.

The maximum and minimum angles of attack for the CRV throughout atmospheric flight were estimated using space shuttle constraints (i.e. control and heating).

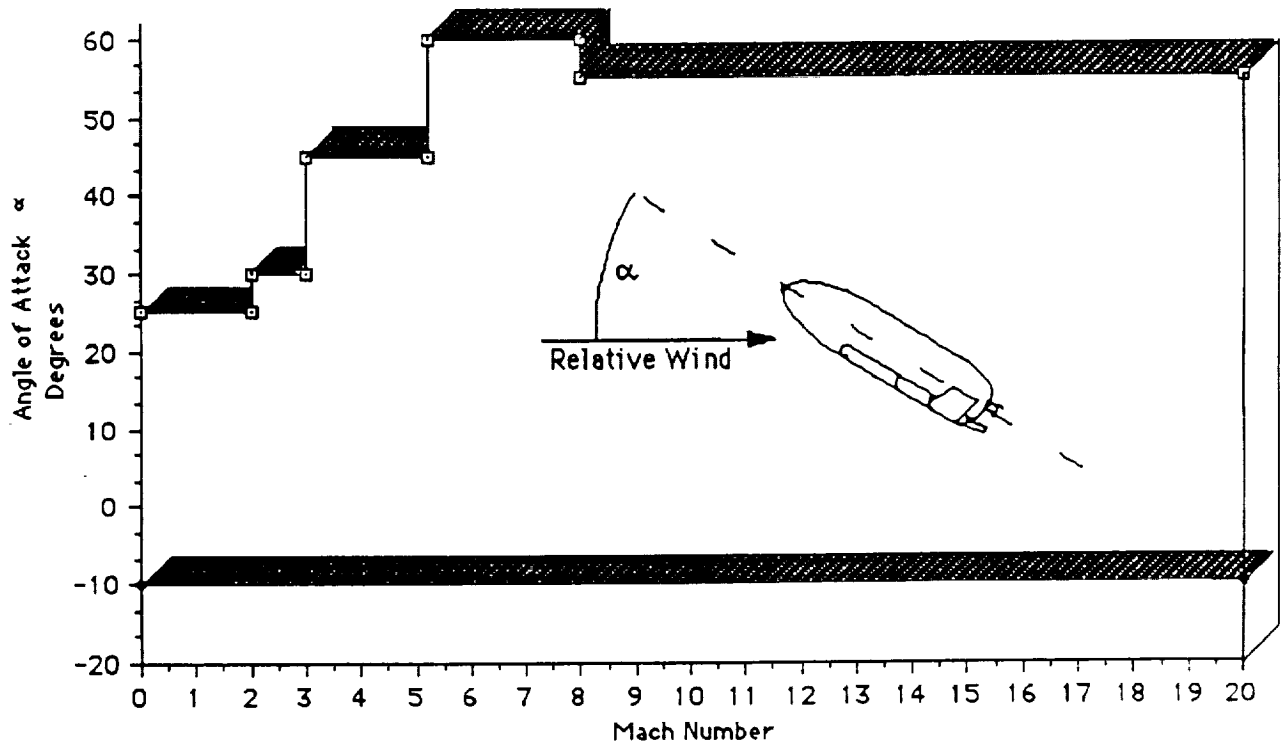


Figure 6-11 Angle of attack envelope vs. mach number.

6.5.5 Lateral Dynamic Analysis

The main criteria for the determination of the lateral dynamic stability were the rate of the change in the pitching moment with respect to the sideslip angle β , $\partial C_l / \partial \beta$ (also known as the dihedral effect) and the rate of change in the yawing moment with respect to the sideslip angle β , $\partial C_n / \partial \beta$ (also known as the weathercock stability).

6.5.5.1 Dihedral Effect

The dihedral effect is an important factor in determining how well the vehicle will respond to instability in the rolling and yawing axes. This derivative arises from the coupling of the rolling and yawing of the vehicle and is a function of the geometry of the wings and fuselage interface, as well as, the relative distances between the vehicle center of gravity and the aerodynamic centers of the wing and fins. At subsonic speeds the major contributor to the dihedral derivative was the wing sweep angle. The wing sweep angle contribution to the dihedral Effect becomes negligible above Mach 2.0.

An important constraint in calculating this derivative is the Reynolds Number (Re) of the flow around the vehicle. High Mach numbers in conjunction with relative high angles of attack usually give rise to high Re which in turn produces turbulent flow around the leading edge of the wing, the wing body interface, and the lower surface of the entire vehicle. This analysis considers a $Re = 500,000$ around the vehicle to produce a turbulent flow. The possibility of laminar flow around the body was also taken into consideration in the analysis of the dihedral derivative.

For a stable vehicle configuration, an increase in the sideslip angle b should cause a decrease in the moment coefficient about the rolling axis. This means that the derivative $\partial C_l / \partial b$ should be negative. SAP was used to calculate the $\partial C_l / \partial b$ for the three vehicle configurations considered by the Aerodynamics group at five points in the flight regime (Refer to Table 6-4). The results of SAP are presented in the following graphs (see Fig 6-13, to 6-17).

Table 6-4 Points for Analysis of Stability and Control

<u>H</u> Altitude (ft)	<u>Temp</u> (°R)	<u>a₀</u> speed of sound (ft/sec)	<u>ρ</u> density (slugs/ft ³)	<u>μ</u> viscosity (slug/ft s)	<u>V</u> velocity (ft/sec)	<u>M</u> Mach Number	<u>α</u> Angle of attack, (degrees)
100000	418	1001	.32x10 ⁻⁴	.32x10 ⁻⁶	3500	2.8	18
120000	451.4	1040	.12x10 ⁻⁴	.33x10 ⁻⁶	7500	7.2	25
150000	500	1095	.36x10 ⁻⁵	.36x10 ⁻⁶	9000	8.2	28
170000	508	1104	.17x10 ⁻⁵	.33x10 ⁻⁶	13000	11.77	31
200000	457	1047	1.7x10 ⁻⁵	.33x10 ⁻⁶	18000	17.2	33

DIHEDRAL EFFECT, M=2.8

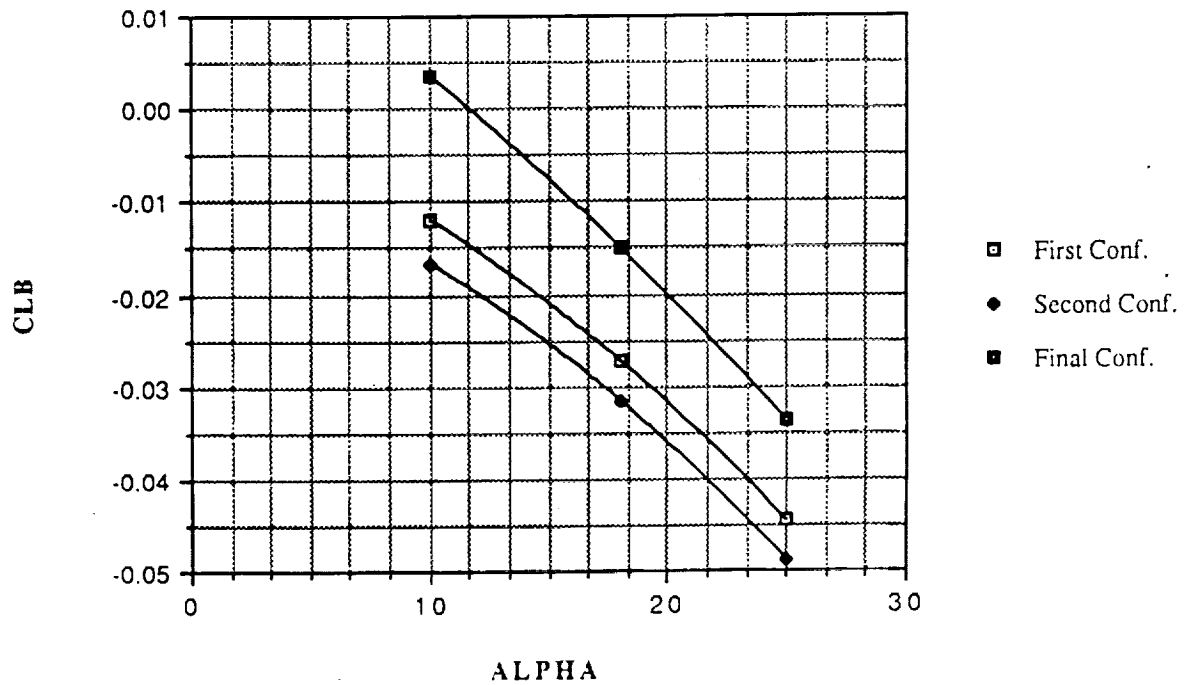


Figure 6-13

Dihedral Effect, M=7.2

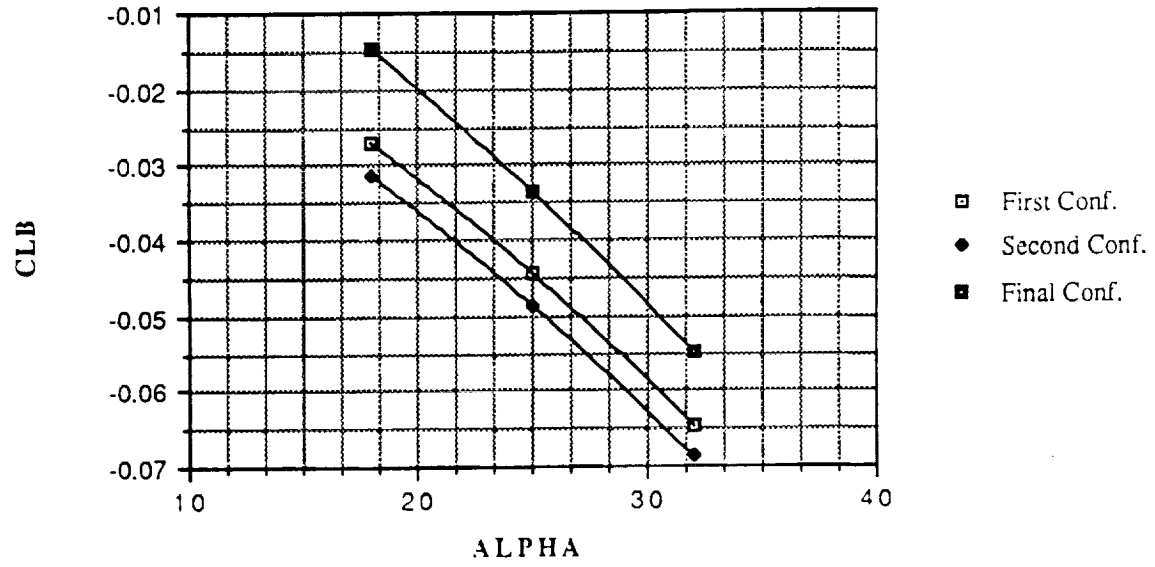


Figure 6-14

Dihedral Effect, M=8.2

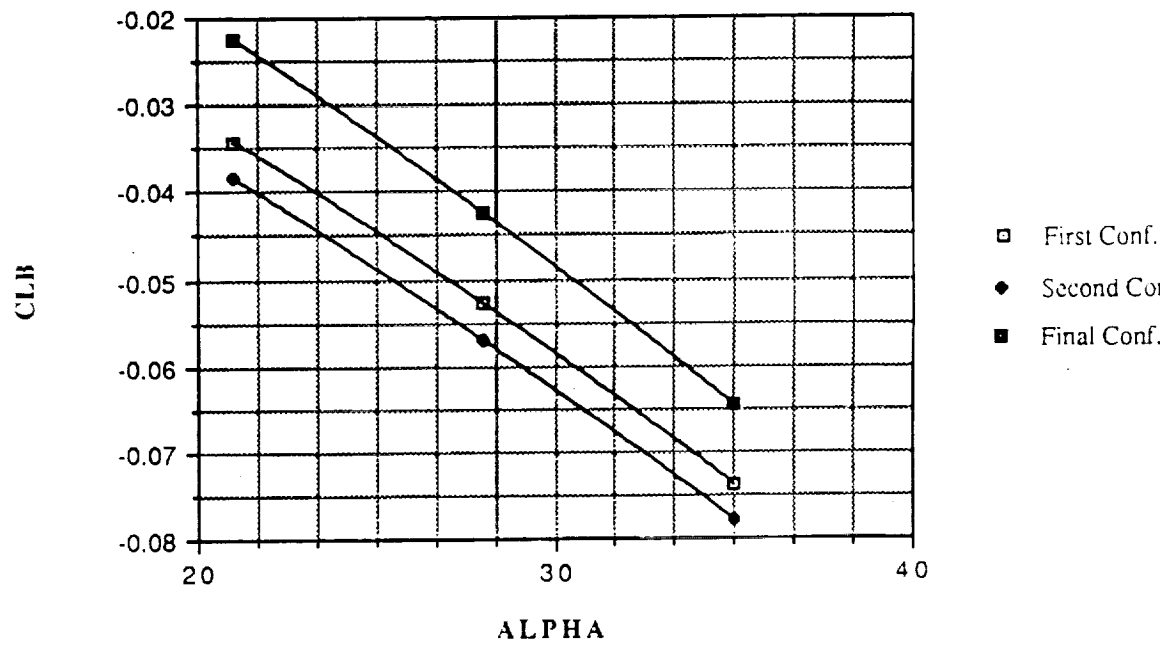


Figure 6-15

Dihedral Effect, M = 11.77

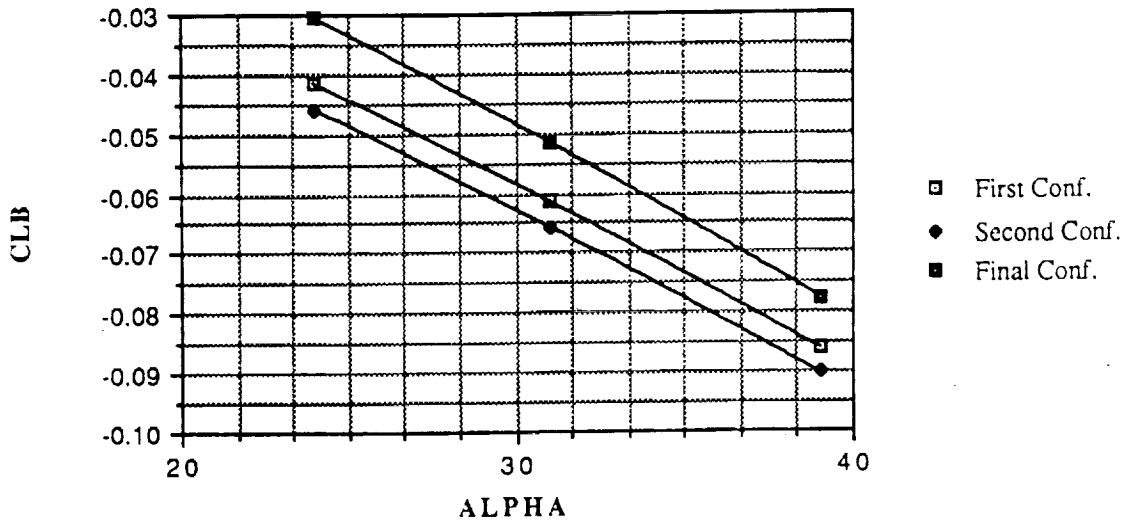


Figure 6-16

CLB vs. Alpha for entire flight regime

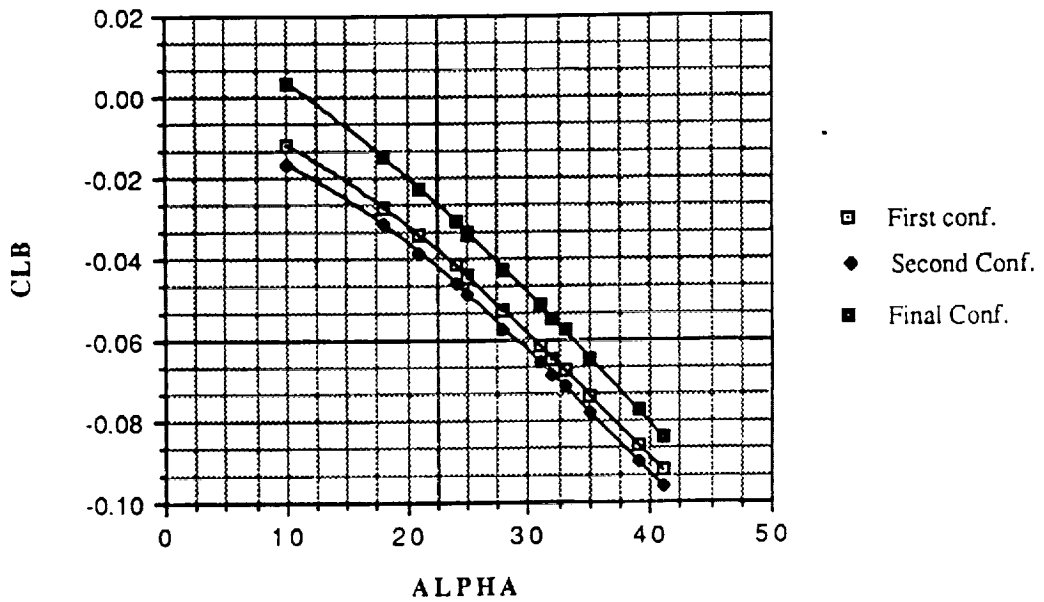


Figure 6-17

At M=2.8 the first and second configurations has a negative $\partial C_l / \partial b$ for an angle of attack range 10° to 25° . The final configuration had a positive $\partial C_l / \partial b$. The second configuration has the largest magnitude of -0.096226 for this derivative with the first configuration having the second largest value at -0.09211. Note that the relationship between $\partial C_l / \partial b$ and Alpha closely approaches linearity for Alpha=25°

to $\text{Alpha}=42^\circ$. At $M=7.2$ all three configurations were found to have negative $\partial C_1/\partial b$ with an angle of attack range of 18° to 32° . The first and second configuration again having the larger magnitude. At $M=8.2$, at an angle of attack range of 21° to 35° , all three configurations exhibit the same characteristic of having negative $\partial C_1/\partial b$ with the first and second configuration having the larger magnitude by approximately 21%. At $M=11.77$, at an angle of attack range of 24° to 39° all three configurations have a negative $\partial C_1/\partial b$, the second configuration has the largest $|\partial C_1/\partial b|_{\max}=-0.09622$ at Mach 17.2 and $\text{Alpha}=41^\circ$. At $M=17.2$ with an angle of attack range of 25° to 41° all three configurations were stable with the first and second configuration having a larger magnitude of $\partial C_1/\partial b$. It was noted that the magnitude of the total $\partial C_1/\partial b$ for all the configurations decreases in a linear fashion as Alpha is increased.

Table 6-5 Comparison of C_{1b}

	$ \partial C_1/\partial b _{\min}$	$ \partial C_1/\partial b _{\max}$
First Configuration	0.0119	0.09211
Second Configuration	0.01658	0.09622
Final Configuration	0.0035	0.0838

A separate analysis of the final configuration using SAP was performed in order to complete a more detailed stability and control analysis using MINNEMAC. The results are presented with the contributions to $\partial C_1/\partial b$ of each part of the vehicle: the nose, leading edge, lower surface, and the winglets. These contributions were analyzed as the Mach number was increased from Mach 2.8 to Mach 17.2 (see table 6-5).

The nose contributed a negligible amount to the total $\partial C_1/\partial b$. The winglet contribution varied very little with respect to the Mach number. The leading edge contribution changed from a positive $\partial C_1/\partial b$ to a negative $\partial C_1/\partial b$ at around Mach 7.5 to Mach 8. The lower surface contribution changed gradually from a minimum of -0.005081 to a maximum of -0.073494. A summary of the results of this analysis can be found in table 6-6 and figure 6-5.

CLBeta contributions vs. M, Final Configuration

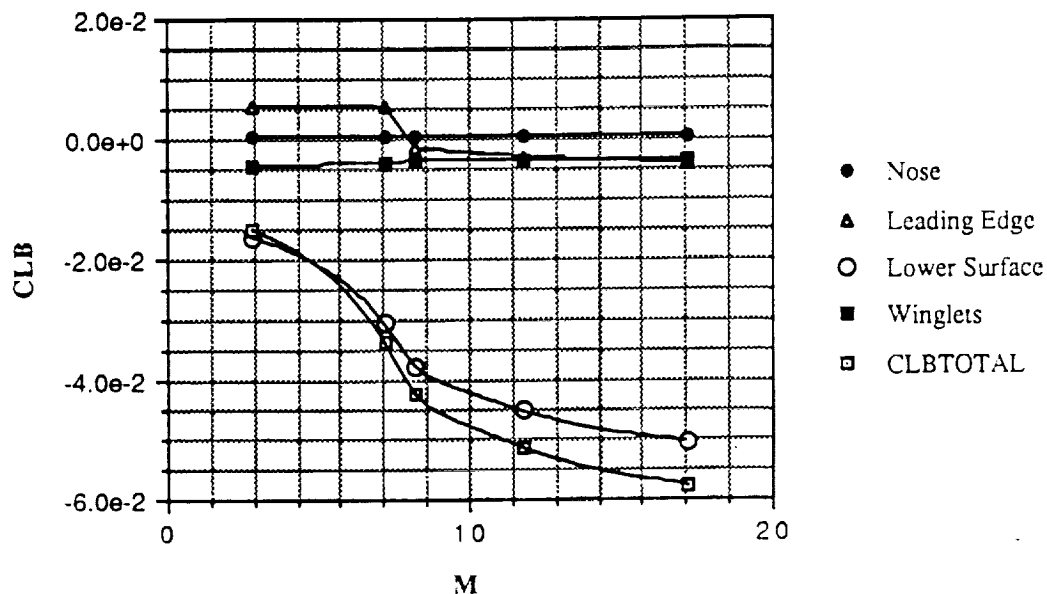


Figure 6-18 Breakdown of $C_{l\beta}$ contributions for Mach 2.8 to Mach 7.2

Table 6-6 Summary of $C_{l\beta}$ contributions from Mach 2.8 to Mach 17.2

	$ \partial C_{l\beta} / \partial b _{\min}$	$ \partial C_{l\beta} / \partial b _{\max}$
Nose	0.000363	0.0051
Leading Edge	0.013836	0.00766
Lower Surface	0.005081	0.073494
Winglets	0.003056	0.005716

6.5.5.2 Weathercock Stability

The weathercock stability derivative $\partial C_n / \partial b$ is an important factor in determining how well the vehicle responds to the instability in the yawing axis. When the vehicle is at a sideslip angle b relative to its flight path, the yawing moment produced must tend to restore the vehicle to symmetric flight. This implies that the weathercock stability derivative has to be positive. The winglets (or a center vertical fin) and the fuselage are the main contributors to this derivative. The hypersonic analysis of $\partial C_n / \partial b$ contributions for the three configurations takes into account the nose, leading edge, lower surface, and the winglets of the vehicle. This analysis takes into account the high Re and high angles of attack that would be encountered by the vehicle since the lower surface contribution

depends on the Re. A flow with $Re_{inf} 500,000$ was considered to be turbulent.

SAP was used to calculate the $\partial C_n / \partial b$ at the five points in the flight regime (Table 6-3). The results are presented in the following graphs.

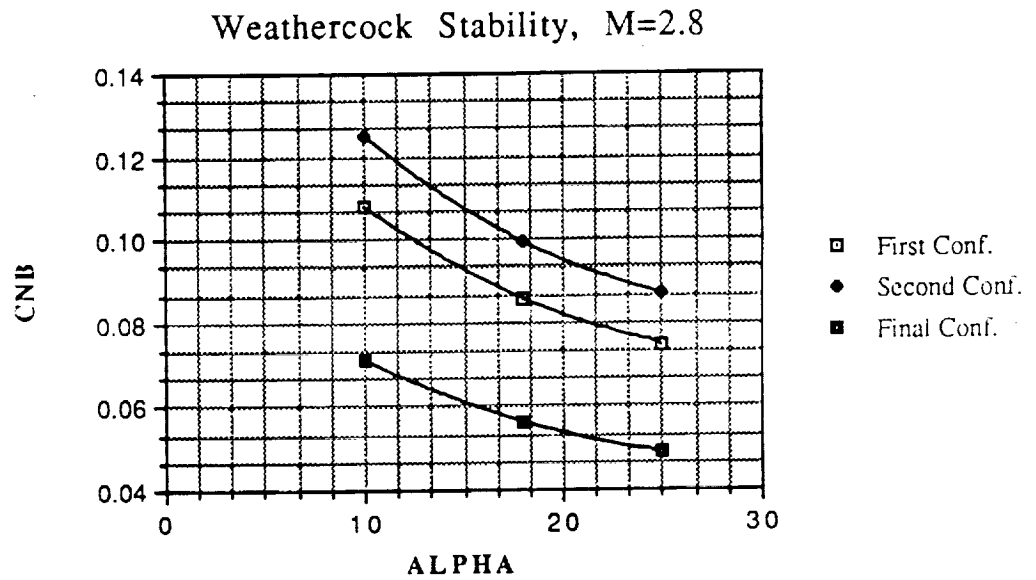


Figure 6-19

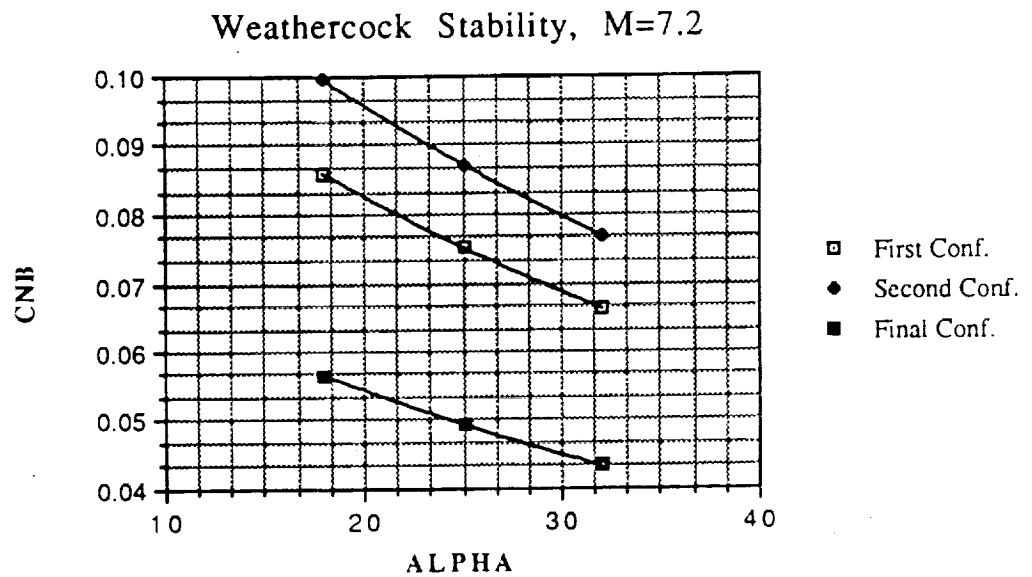


Figure 6-20

Weathercock Stability, M=8.2

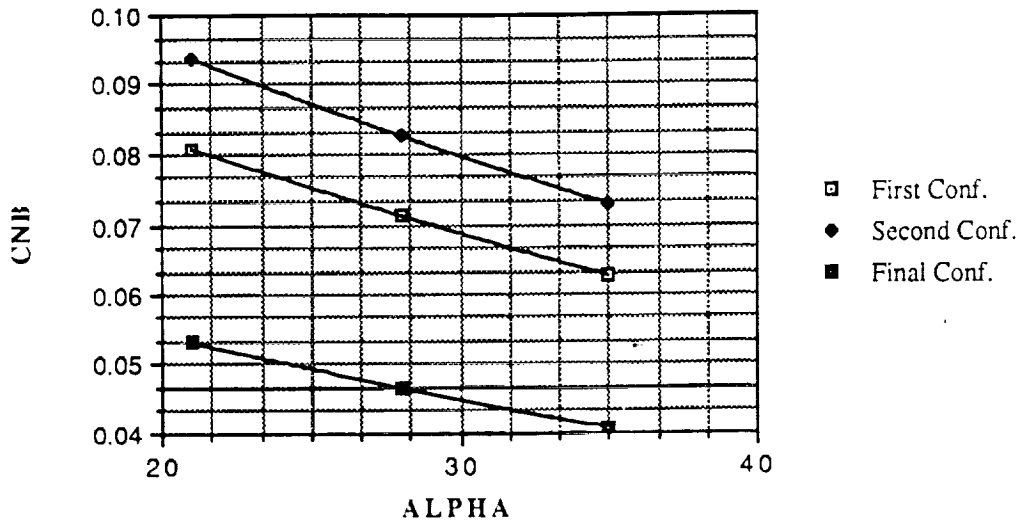


Figure 6-21

Weathercock Stability, M=11.77

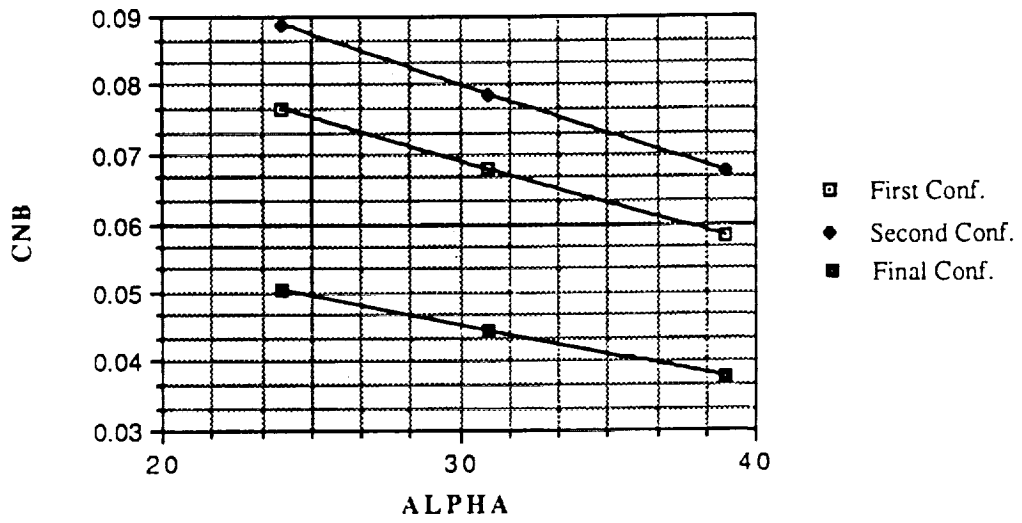


Figure 6-22

Weathercock Stability, M=17.2

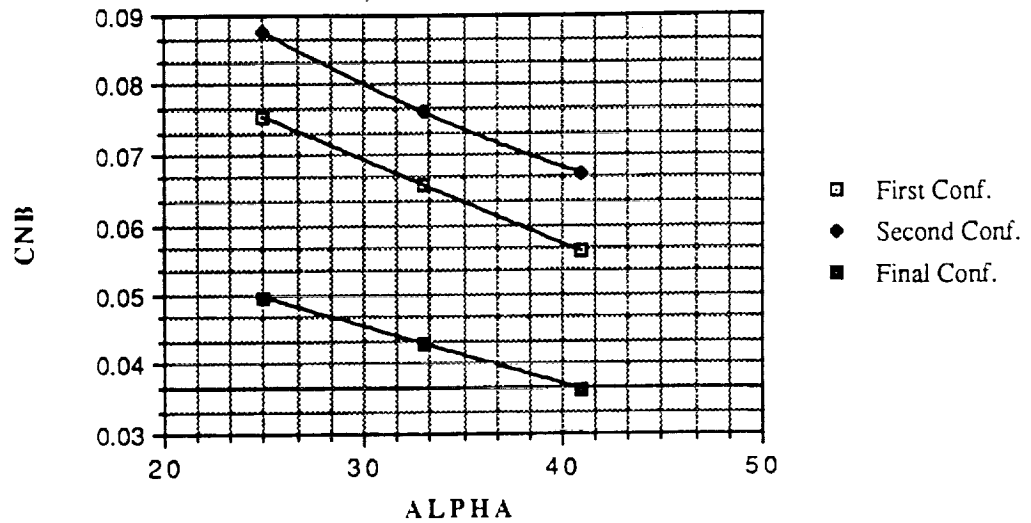


Figure 6-23

All three configurations have positive values for $\partial C_n / \partial b$. Throughout the entire flight regime the second configuration exhibited the largest $\partial C_n / \partial b$, typically 14% larger than the first configuration and 50% larger than the final configuration. This was due to its winglets plus a center vertical fin. The first configuration, with its single vertical fin has the second largest $\partial C_n / \partial b$. The final configuration, with winglets only, has the smallest $\partial C_n / \partial b$ (see table 6-7).

Table 6-7 Comparison of C_{nb}

	$ \partial C_n / \partial b _{\min}$	$ \partial C_n / \partial b _{\max}$
First Configuration	0.0561	0.1078
Second Configuration	0.06723	0.12482
Final Configuration	0.03646	0.07106

A more detailed analysis of the final configuration using SAP was performed in order to quantify the contributions to the total $\partial C_n / \partial b$ from different parts of the vehicle. The total $\partial C_n / \partial b$ was divided into the contributions from the nose, the leading edge, the lower surface and the winglets. The results are shown in Figure 6-24.

CNBeta Contributions vs. M, Final Configuration

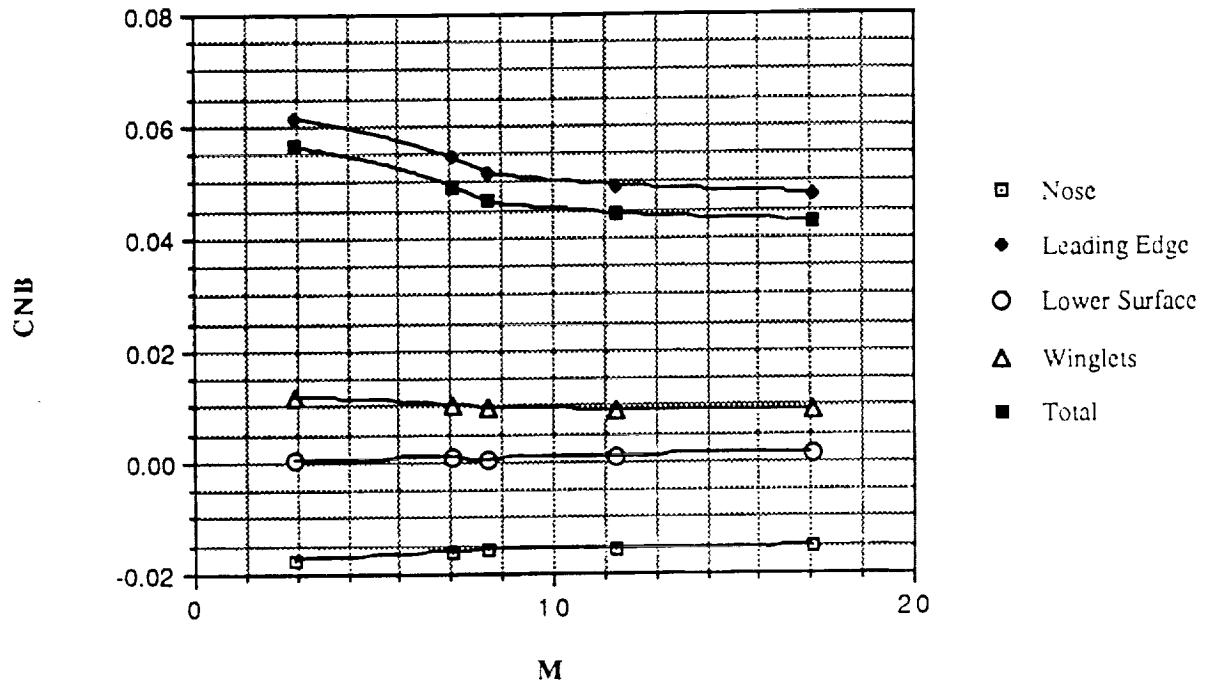


Fig. 6-24 Breakdown of $\partial C_n / \partial b$ contributions

The nose contributed a negative $\partial C_n / \partial b$, slightly increasing from $\partial C_n / \partial b = -0.02105$ at Mach 2.8 to $\partial C_n / \partial b = -0.08384$ at Mach 17.2. The winglets and the lower surface contribution varied very little as the Mach number was increased from Mach 2.8 to Mach 17.2. The largest contributor to $\partial C_n / \partial b$ was the leading edge. It decreased from a maximum value of $\partial C_n / \partial b = 0.07716$ at Mach 2.8 to $\partial C_n / \partial b = 0.0486$ at Mach 7.2 and then changes very little from Mach 8.2 to Mach 17.2.

MINNEMAC was used to analyze the stability of the final configuration for uncontrolled motion in the lateral axis at Mach 2.8, Mach 7.2, and Mach 17.2. The results are shown in table 6-8.

Table 6-8 Minnemac Dynamic Analysis
Mach 2.8

Mode 1, Spiral	
Period	383.217
z	1.000
T 1/2	42.085
N 1/2	0.1098
Mode 2, Roll	
T 1/2	166.00
Mode 3, Dutch Roll	
UNSTABLE	
T 1/2	17726.705

Mach 7.2

Mode 1, Spiral	
Period	537.0928
z	1.000
T 1/2	58.9836
N 1/2	0.1098
Mode 2, Roll	
T 1/2	232.2025
Mode 3, Dutch Roll	
UNSTABLE	
T 1/2	34298.337

Mach 17.2

Mode 1, Spiral	
Period	121.5689
z	1.000
T 1/2	13.3507
N 1/2	0.1098
Mode 2, Roll	
T 1/2	46.3577
Mode 3, Dutch Roll	
T 1/2	234.085

At Mach 2.8 the vehicle was stable in both the spiral and the roll mode, with the spiral mode having reached the critical damping ratio $z=1.00$. The Dutch roll mode was unstable with a $T_{1/2} > 4$ hours. At Mach 7.2 the vehicle was stable in both the spiral and roll mode, having large $T_{1/2, spiral}=58.9$ sec. and $T_{1/2, roll}=232.2$ sec. The damping ratio was $z=1.00$. The vehicle was unstable in the Dutch roll mode at mach 7.2. It has a $T_{1/2} > 8$ hours, which would be large enough time for the control system of the vehicle to correct the

perturbation. At Mach 17.2 the vehicle would be stable in all three modes of uncontrolled motion.

C_{Yr} is one of the coupling derivatives influenced by the size of the tail. Its variation with respect to the angle of attack and the Mach number is shown in Figure 6-25. It decreases linearly from 0.07515 at $\alpha=10^\circ$ and Mach 2.8 to 0.035779 at $\alpha=41^\circ$ and Mach 17.2.

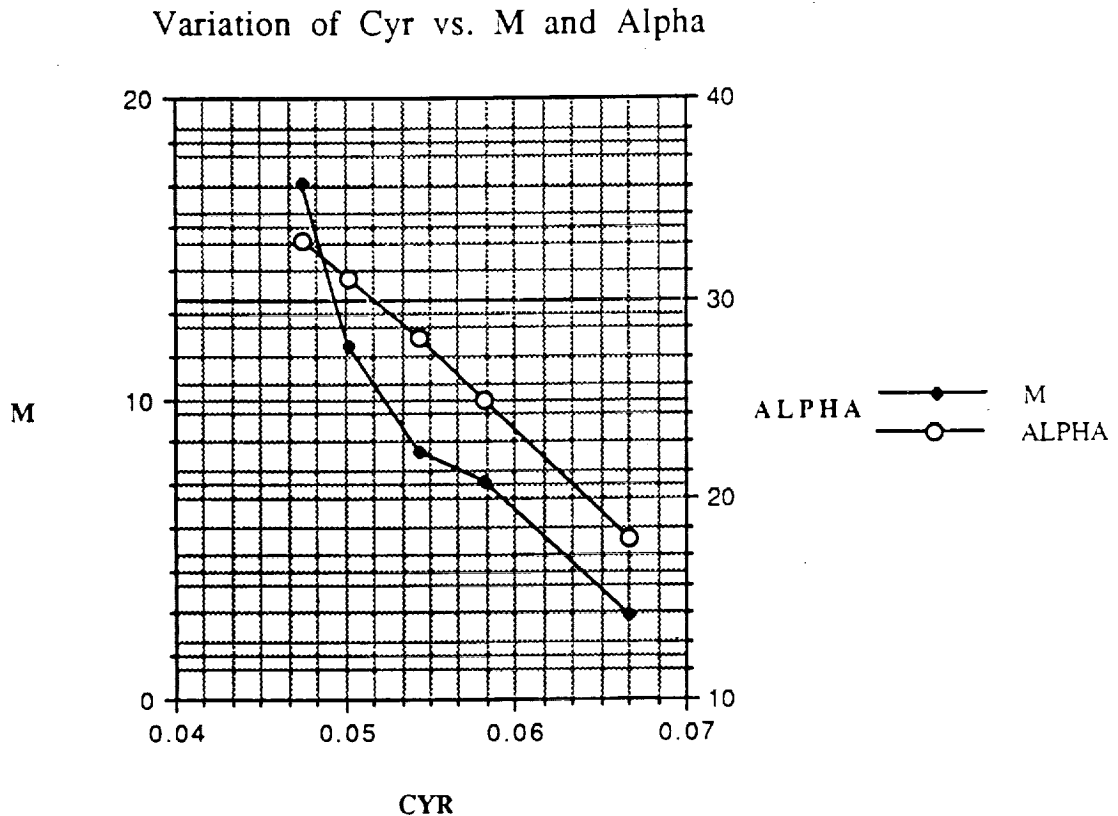


Figure 6-25 Variation of C_{Yr} vs M and Alpha

Hypersonic directional stability is improved by increasing the flat surface area on the rear of the vehicle or control surfaces. Edges above 4-6 inches in width greatly improve hypersonic stability performance when compared to a sharp trailing edge (Ref. 6.5). To integrate this advantage into the CRV, outward deflected winglet rudders were considered for hypersonic flight. However, the heating during re-entry on the rudders in the freestream flow was a major disadvantage. Instead, a toe-in angle of 6 degrees was employed resulting in an 'equivalent' trailing edge width of 1.43 ft. (Fig. 6-26). This toe-in creates an addition of $C_{nb \text{ toe-in}} = 0.838$ to the directional stability. The toe-in also improves subsonic L/D (see Aerodynamics, Sec. 5).

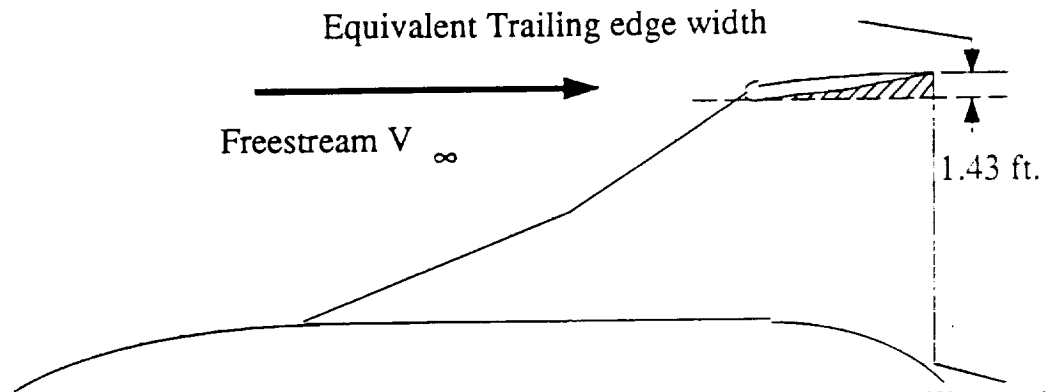


Fig. 6-26 Effect of 6 degree winglet toe-in on apparent trailing edge width.

The variable position body flap has three functions.

1. Shield OMS engine during re-entry
2. Increase lower hypersonic directional stability
3. Augment elevons to reduce control surface loads

The body flap would be deflected downwards during lower hypersonic velocities (figure 6-27). At the same time the elevons would be oppositely deflected. This contributes more 'equivalent' trailing edge width and improves directional stability. Additionally, the body flap would be employed to partially unload the elevons reducing concentrated control surface loads.

1. Mach 10 - 0.2 deflected downwards 16 degrees
2. Mach 0.2 - landing deflected upwards 11 degrees

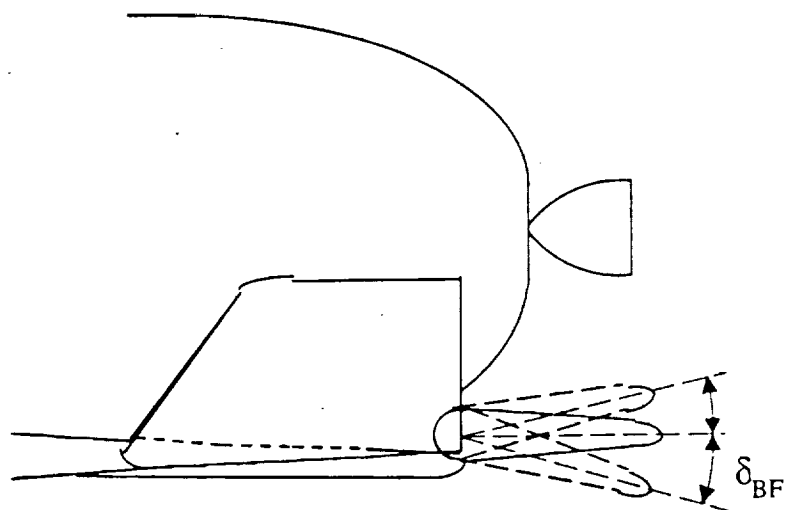


Figure 6.27 δ_{BF} (Body flap deflection, positive downwards)

The maximum and minimum sideslip angles for the CRV throughout atmospheric flight were estimated using available space shuttle constraints (i.e. control and heating) and the results of SAP (fig. 6-28).

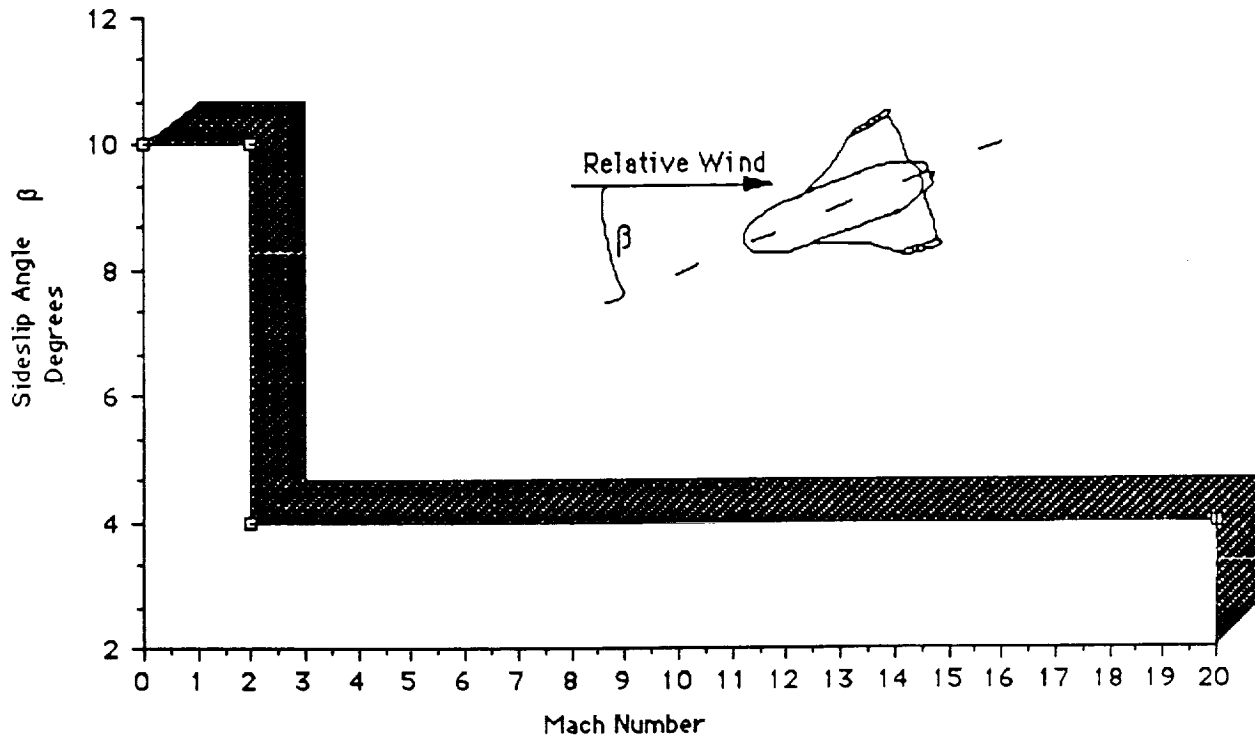
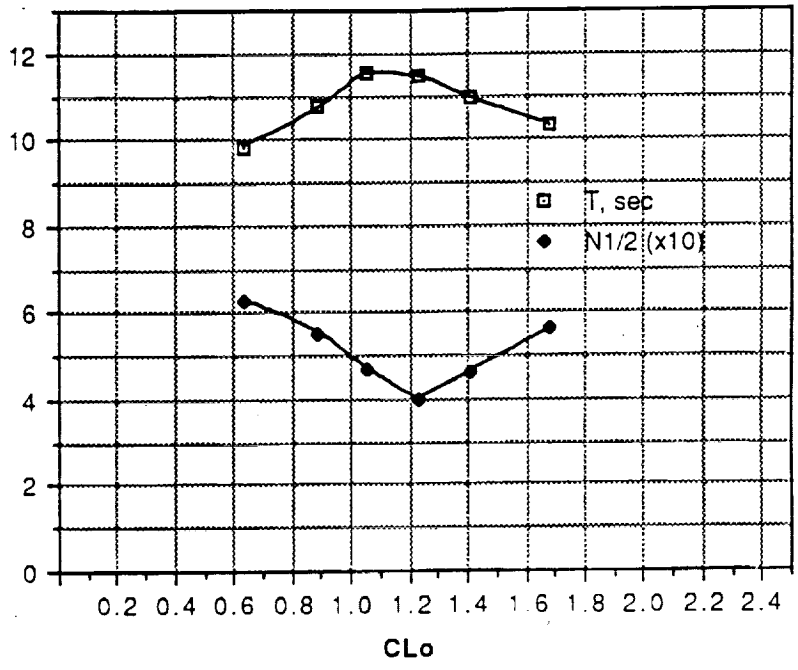


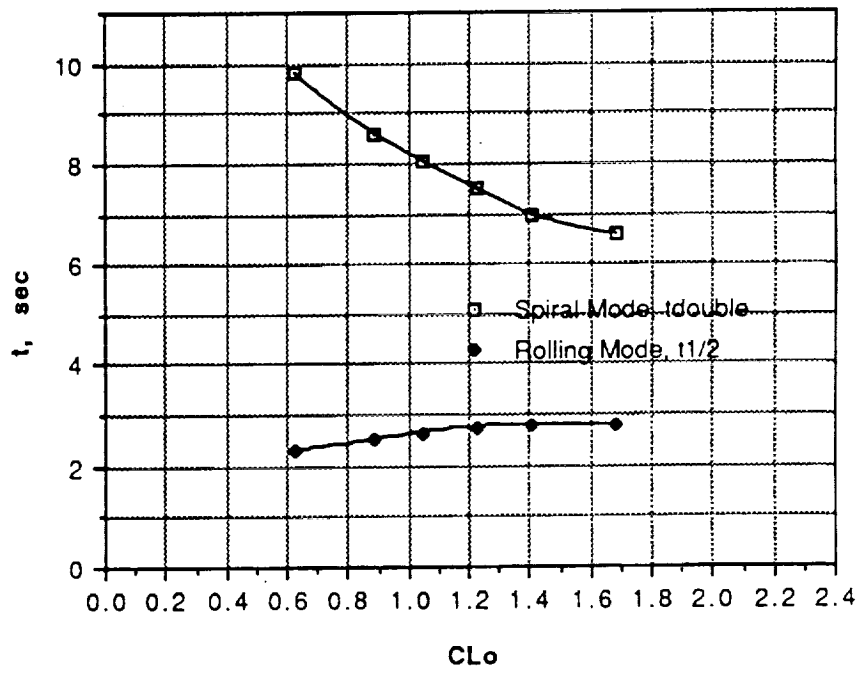
Figure 6-28 Side slip angle vs mach number

6.5.6 Center of Gravity Location

The center of gravity location for a winged re-entry vehicle would be compromised for all flight regimes. The winged CRV design c.g. envelope was found to be approximately 53-61% of the total vehicle length. For the Space Shuttle, the c.g. lies approximately within 65-68% of the total vehicle length. The CRV's c.g. location as compared to the Space Shuttle, is due to the lower aspect ratio and wing to body attachment location. The optimum forward c.g. location was determined by the maximum control surface deflection to trim and the resulting trim drag. The latter constraint was very difficult to approximate and will have to be determined more precisely using wind tunnel data. The maximum aft c.g. location was determined by longitudinal stability constraints.



Characteristics of Lateral Oscillation
Increasing alpha at V = 500 ft/s



Time Constants of Nonoscillatory Modes
Increasing alpha at V = 500 ft/s

6.5.6.1 Forward Center of Gravity

The forward center of gravity location was found to be 42.95 ft aft of the nose and 2.10 ft ahead of the subsonic neutral point (Fig.6.10). This location corresponds to the aft position of the vehicle and was determined by control surface deflection to trim and trim drag constraints. For the forward c.g. location, it was estimated that L/D would be lowered by 0.15% with a trim elevator deflection of 22 degrees at Mach 20.

6.5.6.2. Aft Center of Gravity Location

The aft center of gravity location was found to be 49.65 ft aft of the nose and 3.75 ft forward of the supersonic neutral point (Fig. 6.17). This location was determined by subsonic and supersonic control constraints. For the subsonic flight regime, this aft c.g. location would provide a static margin of -14% and +10% in the supersonic flight regime.

Operational c.g. envelope of final iteration vehicle including supersonic and subsonic neutral points.

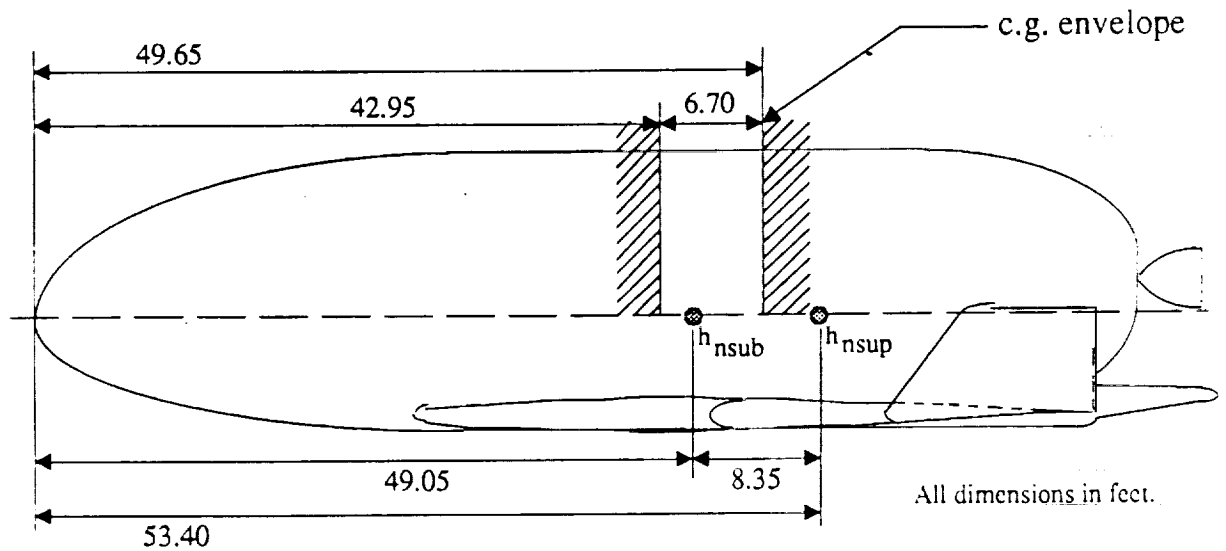


Figure. 6-29

6.5.7 Control Surface Sizes and Deflections

The final iteration control surface dimensions were refined from the original sizes scaled from the space shuttle. The elevons are rectangular at 17x13.9 ft.. Deflection angles are +35° for maximum forward c.g. location plus 10% and -20° as estimated from existing

space shuttle data. The winglet rudder dimensions are rectangular at 3.9x5.9 ft. Deflections were calculated at $\pm 25^\circ$ for acceptable rotary derivative values. The moveable body flap angles are 15° upwards and 25° downwards (fig.6-27).

6.5.8 Control Surface Moments

The control surface moments were calculated using the equations below (Ref. 6.3, 6.16). The aerodynamic force and moment reference dimensions are listed in table 6-9. The results of the analysis lie within the actuator and structural constraints.

$$P = A' + B' \frac{1}{2} \rho V^2$$

$$A' = G S e c_e C_{hd} \frac{F}{\frac{\partial C_{mo}}{\partial \delta_e}} w(h_n - h)$$

$$B' = G S e c_e \left(C_{ho} - C_{hd} \frac{F}{\frac{\partial C_{mo}}{\partial \delta_e}} C_{mo} \right)$$

$$F = 1 - \frac{C_{Ld} C_{hdt}}{C_{hd} C_{La}}$$

Table 6-9 Aerodynamic Force and Moment Reference Dimensions

PARAMETER	REFERENCE VALUE
Longitudinal and Lateral/Directional Coefficients	
Wing Area, S	1767 ft ²
Wing Span b	58 ft
Mean Aerodynamic Chord	33.444 ft
Hinge Moment Coefficients	
Elevon	
Area, S	108 ft ²
Chord c	46.8 in
Area Moment	5054.4 ft ² -in
Body Flap	
Area, S	133.5 ft ²
Chord c	80 in
Area Moment	10693.4 ft ² -in
Rudder	
Area, S	38 ft ²
Chord c	48 in
Area Moment	1824 ft ² -in

6.5.9 Effect of Center of Gravity Location on Range

The estimated hypersonic L/D reduction due to trim drag with the c.g. located 43 ft aft of the vehicle nose was 15%. This result was very approximate due to the difficulty in evaluating the control surface derivatives (i.e. C_{md} , C_{Ld}) of the CRV.

6.5.10 Pitch Break Instability

The pitch break stability of a highly swept tailless vehicle is an important concern in vehicle performance. Two parameters are used to establish pitch break stability as a comparison against guidelines outlined in (Ref. 6.17). These parameters were taper ratio and wing sweep angle at the quarter-chord. The addition of a highly swept strake also decreases pitch break stability. Using these guidelines, the CRV has a moderately stable pitch break.

6.6 Launch Integration

The static launch integration assembly encounters gusts, shears, and steady winds during pre-launch preparations. The main concerns from the static stability aspect are:

1. Moment generated at the base of the launch vehicle.
2. Resultant forces on the launch supports.
3. Individual moment of the CRV acting upon the launch vehicle mating mounts.
4. Buffeting due to vortex shedding behind the vehicle assembly.

6.6.1.1 Ground Wind Effects

For analysis, a steady wind case was investigated impacting upon the maximum flat plate area "seen" by the wind. The total moment forces on the assembly were calculated using flat plate momentum theory. The moment generated at the base of the launch vehicle for a 25 mph wind (X - axis) was calculated to be 4.4×10^6 ft-lb_f. The resultant forces due to wind effects on the base of the launcher are estimated to be $\pm 210,000$ lb_f. (see Fig. 6-31).

The moment created by the CRV upon the mating mounts due to these wind impacting directly upon the top or bottom side of the CRV would be 0.247×10^6 ft-lb_f.

6.6.1.2 Vortex Shedding and Natural Frequency of Assembly

Buffeting created by the shedding of vortices behind the launch assembly can create substantial side forces at a constant frequency and cause sway. For an onset flow velocity of 25 mph the frequency of the vortex shedding would be 20.32 rad/sec, approximating the launcher as a cylinder. This frequency is very low and, if nearly uniform along the height of the launch vehicle, can create alternating distributed side loads above 4,000 lbs. This is an ideal case as the shedding would actually be made irregular by the complex shape of the assembly.

6.6.2 Attack and Sideslip Envelopes

The pitch and sideslip angles of the integrated launch vehicle assembly during launch must lie within constraints determined by stability and control and the structural integrity of the entire assembly (figures 6-31a, 6-31b). These parameters were estimated using the space shuttle and the Boeing Dynosaur re-entry vehicle analysis as comparative models to the CRV because no wind tunnel data was available.

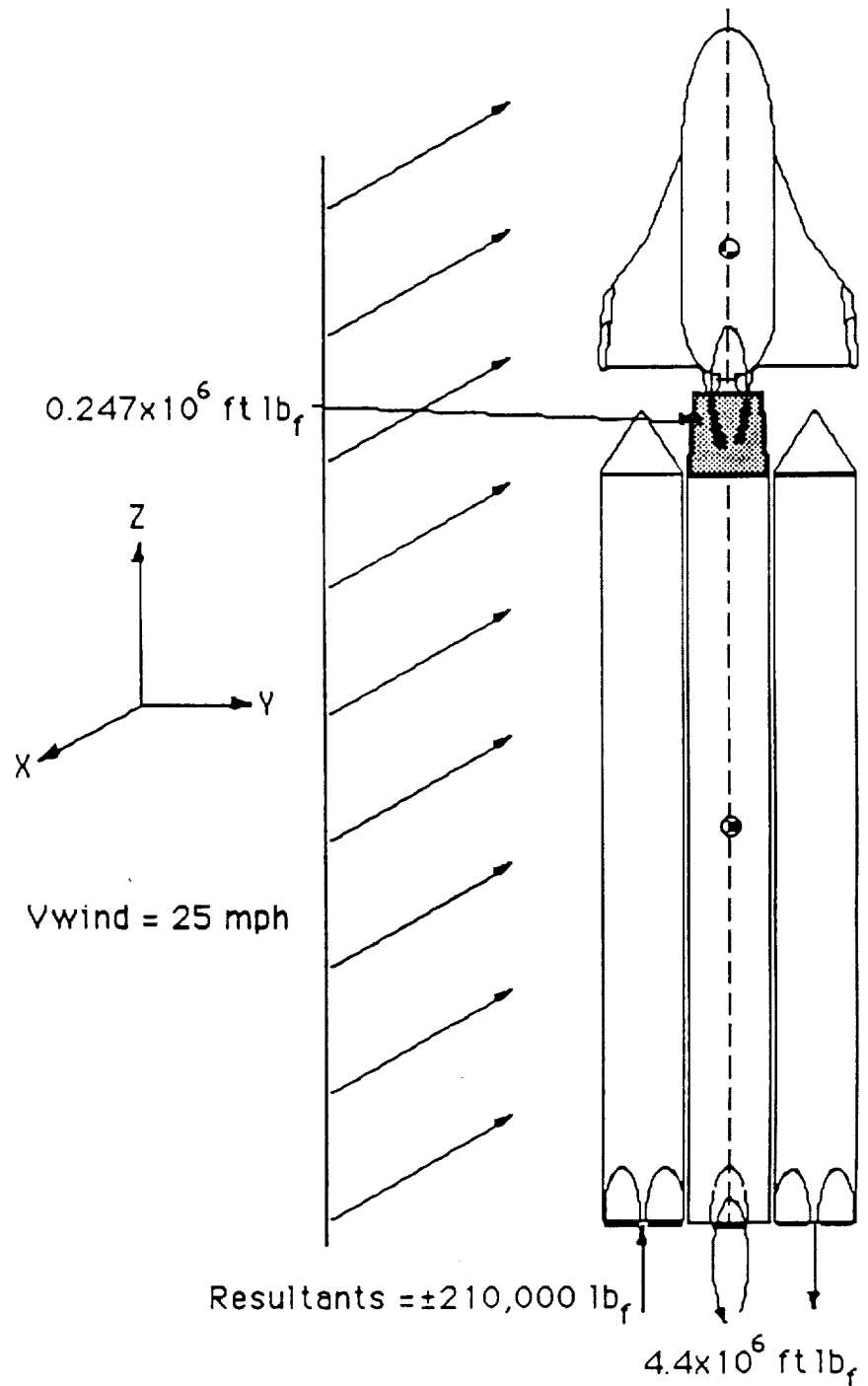
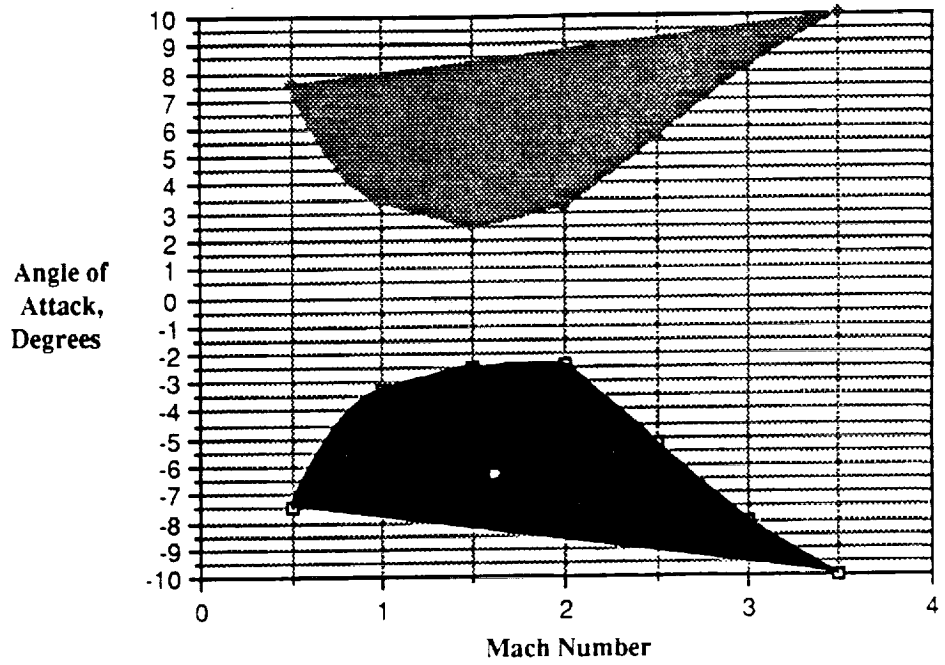
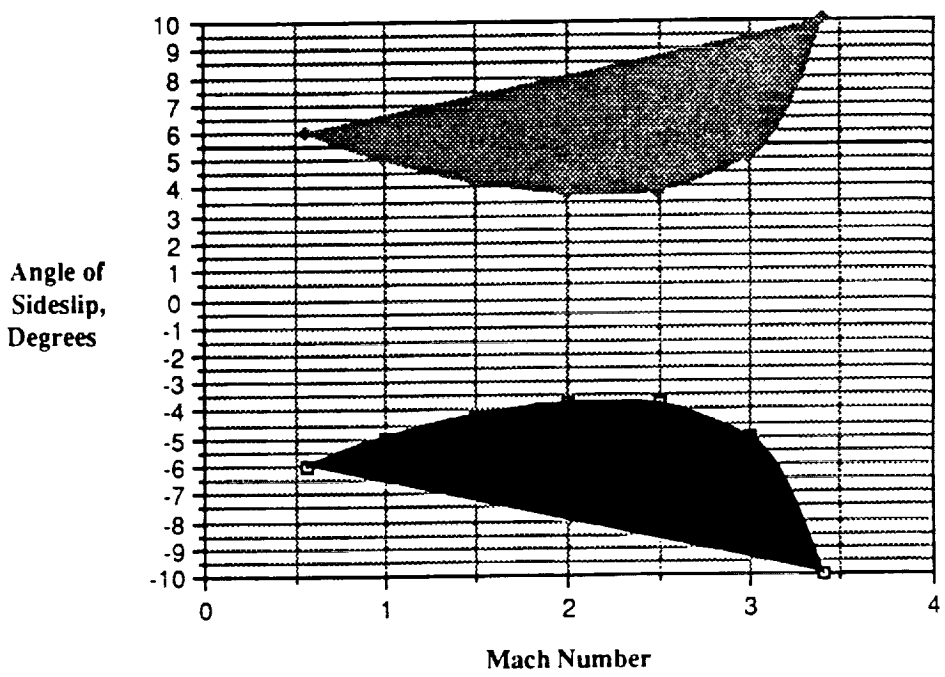


Figure 6-30 Resultant forces/moments generated at base of launch assembly and CRV mating mounts for a 25 mph wind impacting on maximum flat plate area of assembly



Angle of attack envelope of the integrated launch vehicle assembly vs. mach number.

Fig 6-31a



Sideslip envelope of the integrated launch vehicle assembly vs. mach number.

Fig. 6-31b

7.0 AVIONICS AND POWER SUBSYSTEMS

7.1 POWER SUPPLY

The power system on the Cargo Return Vehicle (CRV) must satisfy several requirements. Since this vehicles functions, including maneuvering, depend on the power supply the power supply must be highly reliable. The CRV would have varying mission times so the power supply would have to be flexible regarding to operating length. This vehicle would also have a fairly long life span so the power supply should be cost effective in the long run. Of the power systems available, fuel cells satisfy these requirements. The second choice would be batteries. Some comparisons between the fuel cells and batteries are found in figure 7-1.

This vehicles avionics would have a peak power usage of approximately 2.0 kw during thrusting maneuvers. of approximately. If a pressurized logistics module is on board then an additional 1.5 kw would be required. This produces a peak power need of about 6 kw depending on the type and number of other components in use. Current fuel cells produce 7 kw continuous and 12 kw peak.(Ref. 7.11) One fuel cell could supply all power required but the vehicle would have three cells included for system redundancy. The fuel cells are self-cooling units with their own fuel and oxidizer supply. They would be located in the bottom of the vehicle along with their fuel and oxidizer tanks. A separate fuel supply would be required because fuel cells need a much higher grade of fuel than the standard. The hydrogen/oxygen fuel exits the cells in water form at about 140 degrees Fahrenheit.(Ref. 7.5) This water could be used for heating or cooling other components or could be ejected out of the vehicle.

OPTIONS	COMPLEXITY	RELIABILITY	MAINTAINABILITY	REUSABLE	COST
BATTERY	LOW	HIGH	SIMPLE	YES	MEDIUM
FUEL CELL	MEDIUM	HIGH	SIMPLE	YES	HIGH

RECOMMENDATION IS FOR LIQUID HYDROGEN/OXYGEN FUEL CELLS

Figure. 7-1 Power Supply Decision Matrix

7.1.1 Servo Actuator Power Supply

A battery system that is separate from the main power system was chosen to power the servo actuators. It was believed that these servos would apply too high of a peak load to safely power them with fuel cells. The batteries used would be a high output rechargeable type. Nickel cadmium, nickel hydrogen, silver hydrogen, silver zinc and silver-oxide zinc are all types of rechargeable batteries.(Ref 7.1) The preferred type is the nickel cadmium because of its weight, volume and proven performance characteristics. Batteries are available with up to 12 kw-hr energy storage and up to 500 amp-hr discharge capabilities at about 30V which is comparable to the output voltage of fuel cells. The life of these batteries depends on factors such as operating temperature, number of charging cycles and depth of discharge. Life spans of up to several years can be obtained. The optimum operating temperature for the batteries is about ten degrees Celsius which would be close to the interior CRV temperature. Charging can be accomplished through the use of an umbilical during prelaunch and

at SSF. On-orbit charging by the fuel cells would also be a possibility. The depth of discharge would depend on the number of batteries on board, the amount of energy taken from them, and whether if they are recharged in orbit or not. All of this depends on how much power the servos would need which depends upon the mission.

The rechargeable nickel cadmium batteries weigh about 100 lb per cubic foot.(Ref 7.12) Approximately ten cubic feet or 1000 lbs would be needed. These could be placed in the nose of the CRV. This power supply has been chosen for several reasons which include:

- high output
- high energy storage amounts
- Rechargeable
- Expandable
- Eliminates a large power demand on fuel cells
- Long life expectancy

During high loading times on control surfaces if a fast movement is needed a high rate of power delivery may be required. Batteries can supply this if the correct number and configuration of batteries are used. During orbit and ascent no high loads would be experienced. The cargo doors would be near weightless, the OMS gimbaling would be minimal, and landing gear would be gravity assisted. The control surfaces would demand a high peak load, and this would only occur during descent. If a steady glide path is achieved then the power draw would decrease significantly. Batteries should have no difficulty in supplying what is needed.

Along with the rate of energy discharge the amount of energy storage was of interest. The amount of storage needed is directly proportional to the force required and amount of use of the servos. For moveable objects such as cargo doors, whose opening speed is not important, a slow power conservative servo could be used. The servos should also have some type of mechanism so that if they are not being used then no power would be required to keep them stationary. This would be useful in a gliding situation where if a steady glide is being maintained then no power would be needed to keep the controls at a locked position.

Since this battery system would be rechargeable it would be cost efficient and convenient to use. While in orbit all three fuel cells would be running even though only a small power supply would be

needed. This would prevent delays in start up times for the fuel cells. Since a KW-hr of energy per pound can be stored more efficiently for fuel than for batteries it makes sense to carry fuel on board to recharge the batteries while in orbit during low power demands on the fuel cells. This configuration would exploit the best features of both systems, a steady efficient power supply from fuel cells and a high output dependable burst from batteries.

Batteries are probably the most reliable form of a power supply. Like fuel cells they convert chemical energy to electrical energy but batteries do it in a more simplified manner. Battery systems are also the easiest power supply to expand. Additionally, this battery system would have a long life span with a range of years depending on operating conditions.

Another benefits of using batteries in conjunction with fuel cells is that it would provide yet another power supply to the CRV for emergencies and would eliminate a high peak load on the fuel cells. The fuel cell system on board outputs a max of 36 kw. This is 12 kw per fuel cell. A max operating load can be maintained for only 15 minutes after which the output must be brought down to 7 kw.(Ref 7.11) With other equipment operating at about 6 kw max this could leave only 15 kw for the servos. A single fuel cell failure could cause an unsuitable condition.

The battery and fuel cell systems could be interconnected not only for charging but also for output. If either of the systems should fail partially or totally the other could be used to back it up or take over completely. A simple schematic showing the power system configuration can be found in figure 7-2.

7.2 CONTROL ACTUATORS

Hydraulic systems are complicated and expensive. Electro-mechanical actuators are less expensive, simple and highly versatile. Servos, however, can require a large power supply. Landing gear and cargo bay door actuators would not be very power demanding compared to aerodynamic control actuators. These actuators, or servos, would be powered by high output rechargeable batteries. These batteries would be used for powering cargo bay doors and OMS actuators during ascent then be recharged by SSF or by the fuel cells and used again for OMS, control surfaces and landing gear actuators during descent. This electro-mechanical actuator system

should weigh about three to four thousand pounds including its power system.(Ref 7.3)

7.3 POWER VS. TIME

A major power usage change will occur after thrusting is complete during the ascent stage. Thrusting causes the highest load on the power system. The next jump would occur when the P-log is removed. The P-log uses 1.5 kw of power. The lowest power usages would occur when the CRV is docked to the SSF. During this time power needs could be supplied externally from the space station so the CRV power supply may be shut down completely. The next peak point would be during descent. This can be broken down into two stages: in atmosphere and out of atmosphere. The power usage in atmosphere would probably be larger of the two because of the high activity of the auto flight control system.

7.4 ORBIT TIME AND POWER CONSUMPTION

Increased time in orbit increases the kw-hr of energy the power system must have stored before take-off. Fuel cells produce kw-hr of energy in direct proportion to the amount of fuel on board. From Rockwell data on fuel cells it was found that approximately 1.1 lb of fuel/oxidizer produces 1 kw-hr of energy. The average power consumption of the CRV and P-log would be about 4.5 kw so a mission of five days would require about 600 lbs of fuel/oxidizer. The orbit time has little effect on the servos battery system since they are not used continuously. Their power supply requirements would be essentially the same for a long or short duration mission.

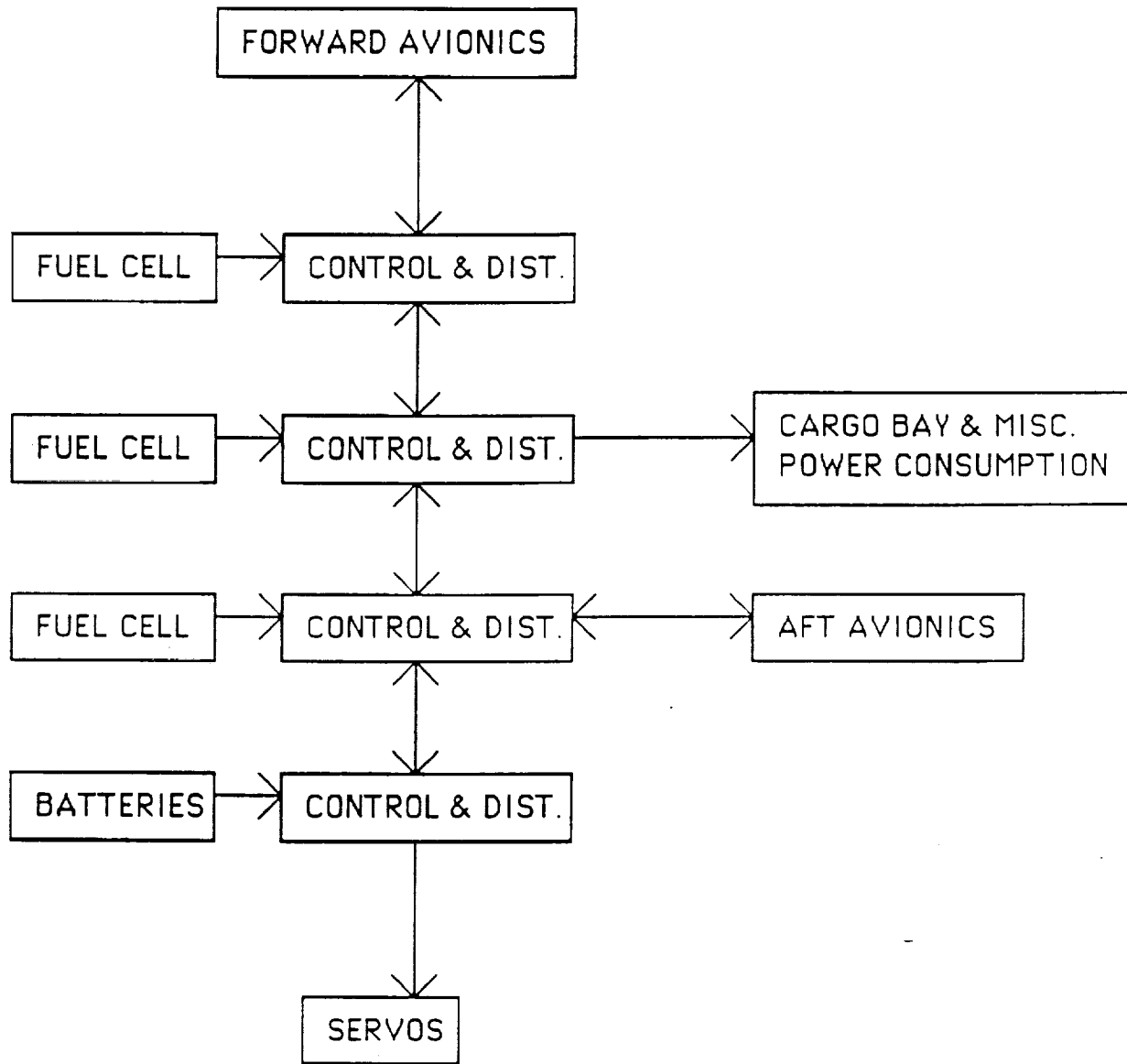


Figure. 7-2 Power System Schematic

7.5 AVIONICS

The primary function of the avionics systems is to provide guidance, navigation and control of the vehicle throughout all stages of the mission. The avionics also provides communication, telemetry and tracking. The avionics systems have been split into four subsystems which include:

- Guidance and navigation
- Flight control
- Autoland systems
- Communications and tracking

The first three all work closely together to provide the primary function of the avionics system. Some of the components of these subsystems interface with external and/or internal systems such as the payload for internal or TDRSS for external. The only major differences between the CRV avionics and the Space Shuttle's are the absence of flight instruments and verbal communications equipment, and an increase of telemetry. A simplified schematic of the avionics system can be found in figure 7-3

7.5.1 Guidance and Navigation

The major components of this subsystem are the GPS receiver, IMU's and star tracker. The global positioning system, GPS, has the function of determining the position of the vehicle relative to the Earth and SSF. The GPS works in either an arbitrary three axis system or with latitude, longitude and altitude. By giving a repetitive update of the position the GPS also provides a constantly updated velocity vector.(Ref 7.1)

The inertial measuring units, IMU's, are the primary sensor for the guidance and navigation system. They sense both lateral and rotational acceleration. They also detect rotational velocity. There could be a maximum of four and a minimum of two IMU's. The preferred unit is the Honeywell H700-3 Ring Laser Gyro Inertial Measuring Unit. It contains a ring laser gyro which measures angular velocity and three Sundstrand accelerometers used for linear acceleration measurements. The unit is 16.25 inches long, 11.25 inches wide and 5.9 inches high and weighs 42 lbs. This IMU has a projected life span of five years, has digital readout, can measure up to 800 degrees/sec. rotation, can measure 40 G linear acceleration, and operates between -65 and 160 degrees Fahrenheit. The star tracker would provide attitude update information. If the GPS were accurate enough it would be able to do the same thing using multiple antennas. The GPS system is currently being expanded and if it becomes feasible the star tracker would be eliminated. For now, the star tracker is required since it does the job well and is a compact and dependable unit. The star tracker would mount directly to the hull of the CRV and would have a small view port. Each of the

components would feed into a digital integrating unit and then be sent to the main data handling computers.(Ref 7.12)

7.5.2 Flight Control

A large portion of the flight control subsystem consists of mechanical devices to control the aerodynamic control surfaces, OMS gimbaling, and RCS control. The OMS and RCS would also need controls to start and shut down and to know which jets of the RCS to fire. These control systems would all work together with the main computer by feeding information to a digital integrating unit which then sends the information to the main data handling computers.

7.5.3 Automatic Landing System

The main components of the auto land system would involve the Microwave Scan Beam Landing System (MSBLS), a radar altimeter, the landing gear, steering and braking, and TV cameras for remote control. The main functions of this subsystem would be to capture and track the lateral guidance path, capture and track the vertical guidance path, provide sideslip maneuvers prior to landing, provide flare maneuvers prior to landing, drop landing gear automatically, and steer and brake while on the ground. The MSBLS would be the primary navigation device. It would be initiated at 10,000 to 14,000 feet when the vehicle is parallel to the runway and would provide the azimuth angle, elevation angle, and the distance during final approach and landing. The on-board radar altimeter would provide the height above the ground up to 5480 ft.

The MSBLS consists of an elevation group and an azimuth/distance measuring equipment group located on the ground and an RF assembly, decoder assembly, and antenna in the vehicle. The two ground antennas scan the approach volume constantly. They send out a set of elevation, distance and azimuth signals every 200 milliseconds which are processed by the on-board decoder when the vehicle is in range. Three things happen during the distance part of the transmission. First, the ground station sends 14 pulse pairs as a trigger for the on-board system to interrogate. Second, the airborne RF assembly interrogates the ground station then listens for a reply. Third, the ground station receives the interrogation, waits 80 microseconds then sends a reply. The on-board decoder measures the time from the interrogation to reply and finds the distance using

this information. This data is then sent to the auto flight subsystem every 200 milliseconds.(Ref 7.2)

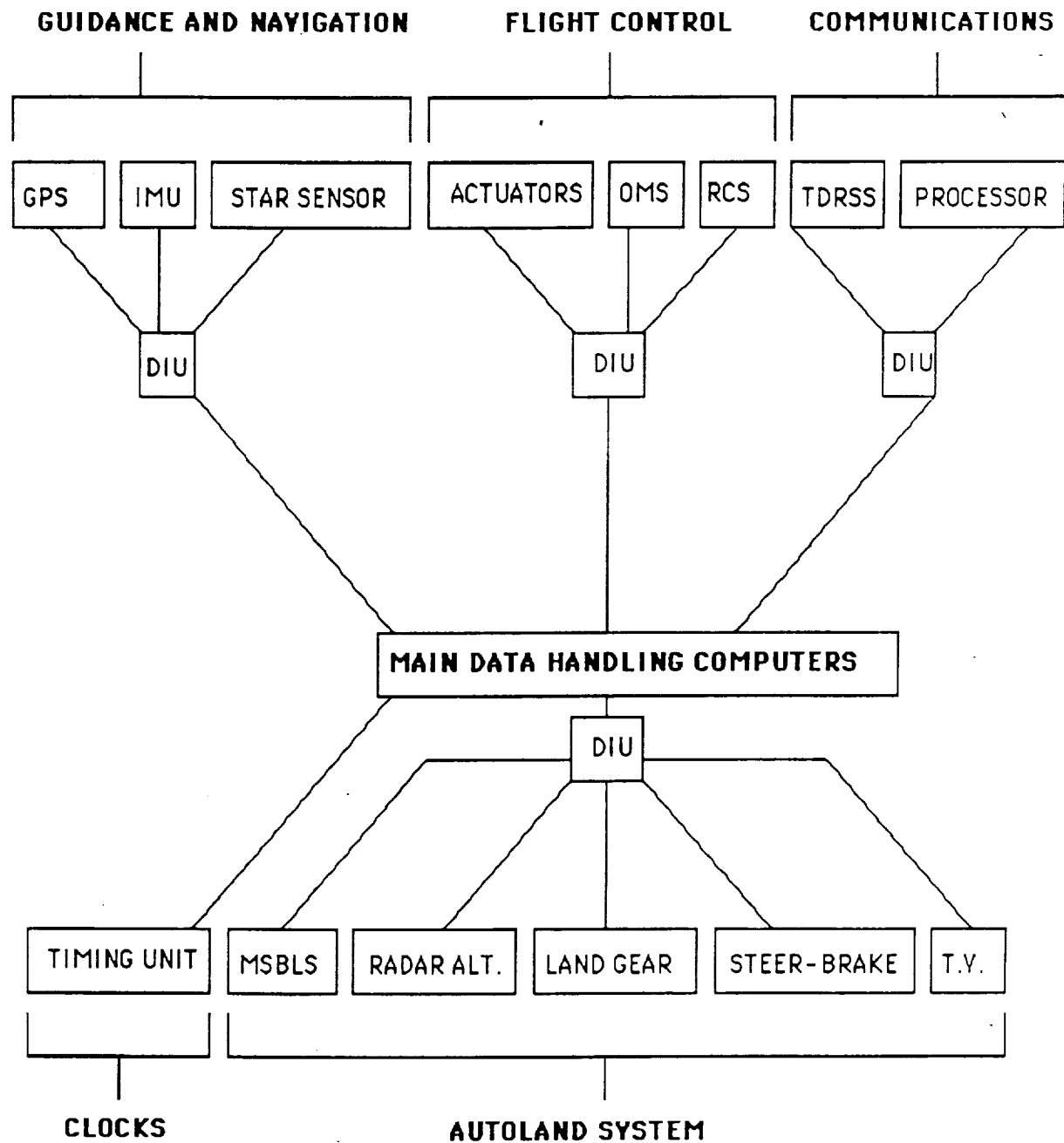


Figure 7-3 Avionic System Schematic

A TV camera system would be used for emergency remote control of the vehicle. It is also directly interconnected with the communication and tracking subsystem so that the camera pictures

could be sent out through the TDRSS network. Current technology for auto landing systems has come from several sources including:

- Blind landing experiment unit (British)
- All weather landing system program (Air Force and FAA)
- Boeing 767/757 program
- F/A 18A aircraft
- Digital integrated auto landing system
- HYMAT
- Area terminal automatic navigation, guidance and control using MSBLS

The Boeing aircraft listed above have full autoland except for flaps, landing gear and reverse thrust. The F-18 has fully automatic approach to land under all weather conditions for carrier recoveries.

7.5.4 Communications and Tracking

The main component of this subsystem is the Tracking Data Relay Satellite System (TDRSS). The TDRSS consists of a group of satellites that work together to track space vehicles. It is very effective for sending communications, data and position information throughout a vehicles entire orbit to and from the ground. Data can be sent from one satellite to another then to the ground to bring data from one side of the earth to the other. There are two satellites one at 41 and the other at 171 degrees west longitude, and a single ground control station at White Sands, New Mexico. There will also be two spare satellites, one in orbit and one ready for rapid replacement. The on-board unit would be the Motorola/NASA Second Generation TDRSS User Transponder.(Ref 7.12) It can be used for all receiving and transmitting functions for the TDRSS. TDRSS can support up to twenty spacecraft in the S band and an additional four in the KU band.

7.6 CAMERAS

There would be several cameras throughout the CRV with their number and location depending on mission requirements. Some would be permanently attached, such as in the nose and cargo bay while others would be easily removable. The capability for remotely moving the cameras would exist, and a VCR would be included for recording camera images for playback on earth. Two video channels would be used to transmitt camera images and would be relayed

through the TDRSS. There would also be a split screen capability so two camera views could be sent through the same channel.

7.7 CLOCKS

The clock system in the CRV would consist of a timing device that would be used as a reference for all other systems. This clock system is called the Master Timing Unit or MTU and provides several square wave frequency signals and time code signals. These produce two types of time: mission elapsed time and greenwich mean time. To keep the CRVs MTU in line with the time on the ground it would be updated periodically from the ground station.

7.8 MAIN DATA HANDLING COMPUTERS

The data handling system would consist of three to five general purpose computers that would receive input from onboard sensors and external sources, perform computations and processing, and generate output. The output would be for Guidance Navigation Control, communications and tracking, instrumentation, electric power distribution and control, other computers, performance monitors and payload handling and systems management. The data system would also contain several MDM and DI units to handle digital to analog and analog to digital conversions.

7.9 ENVIRONMENT CONTROL SYSTEM

Forced air and convection cooling would not be used. The only other common cooling techniques are cold plates and evaporators. Cold plates cool by mounting the avionics components directly to a plate that contains a heat transferring fluid. Evaporators do much the same thing but they use plates as evaporators in a refrigeration cycle. The cooling loop of the heat transferring fluid is in must be able to dissipate about 7000 watts(See fig 7-4).

Cold plates are generally constructed of aluminum or stainless steel. Total weight would be about ten kilograms depending on the size of the plate. Common practice is to have several plates and heat exchangers in one loop. Heat sinks could also be put in the loop to aid in dissipating heat during peak usages. Cold plate systems are highly reliable, virtually maintenance free, safe, inexpensive, and not very heavy.(Ref. 7.10)

Cold plates are made as large as .5 meters by .75 meters by 4.4 millimeters.(Ref 7.8) Their cooling capability depends on the size of the plate, the cooling fluid type, and the cooling fluid flow rate. Performance data can be found for the use of freon and water. Other fluids could be used but their performance would have to be researched. Figure 7.4 shows a common cold plate loop with heat exchangers, thermal capacitors and evaporators.

Evaporators, are efficient and compact. They are preferred when high amounts of heat must needed to be removed over an extended period of time. Disadvantages of evaporators are their weight, safety, complexity and cost.

A common type of heat exchanger is a heat pipe. In a heat pipe, heat is imposed and used to evaporate a working fluid. This vapor moves to any cooler spot and condenses, which transfers the heat to the condenser wall. The liquid then moves by capillary or gravity action back to the evaporator section of the heat pipe. These units are generally used for avionics applications which have a temperature range between -100 and +100 degrees celsius.(Ref 7.10)

Heat condensers are also sometimes used. These units have the working cooling fluid routed through a solid phase change material. Since the material is changing phase from solid to liquid it can absorb heat without a change in temperature. Common substances used are paraffins. Heat condensers are very effective during peak loads. The continuous operating temperature should be slightly less than the condenser material fusion temperature. Heat condenser units would prohibit a rapid increase in cooling fluid temperature and let the system operate more efficiently. Their main function is to assist in removing excess heat from the cooling loop under peak loads. After the peak was over the phase change material would be brought back down to its more solid continuous temperature through normal cooling. Typical condensers have 30-50Wh/kg capabilities.(Ref 7.10)

In this vehicle high heat loads are not predicted to be a problem. Reliability, safety and weight are major concerns. From these requirements cold plates were deemed to be the best choice.

During the descent and ascent phases of the mission the heat capacitors would be used to dissipate heat. During the orbit, the radiators would be used to dissipate the heat load.

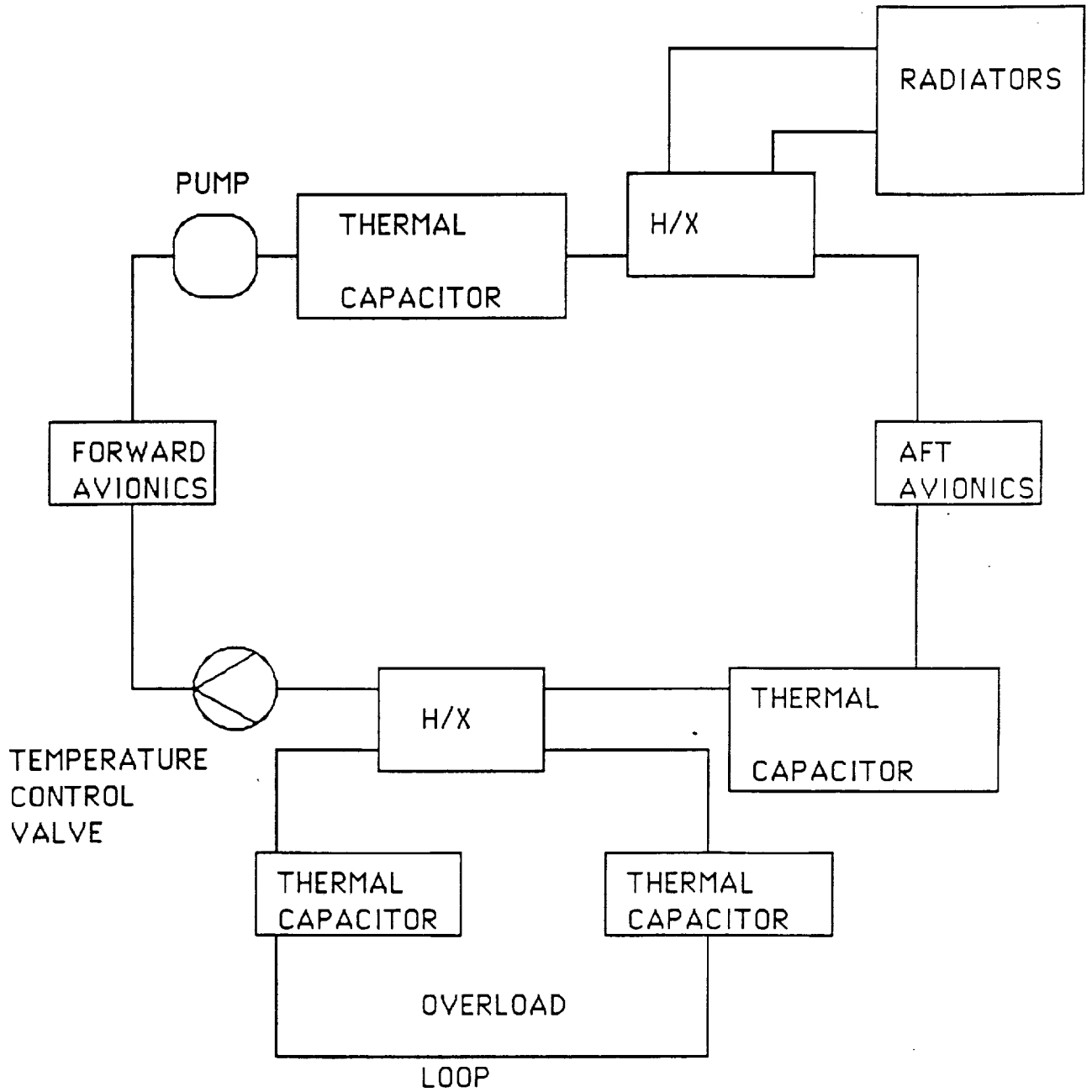


Figure 7-4 Cooling System Schematic

THIS PAGE HAS BEEN LEFT INTENTIONALLY BLANK

8.0 THERMAL PROTECTION SYSTEM

Based on the initial conceptual design for the Thermal Protection System (TPS) for a winged cargo return vehicle (CRV). The following materials were selected: reinforced carbon-carbon (RCC), Fibrous Refractory Composite Insulation (FRCI), and advanced flexible reusable surface insulation (AFSRI). Approximate thermal calculations were made to justify the TPS placement on the vehicle. This vehicle was similar to the Space Shuttle with the addition of winglets for a span of 58 feet and a length of 76 feet. A TPS weight of 6760 lb. was attained at a material cost of roughly \$ 4.8 Million. The report details further refinements and verifications of the TPS design and its relation to the other vehicle systems and operations. The design criteria was as follows:

1. Minimum weight
2. Refurbishability
3. Resistance to excessive expansion/compression
4. Resistance to debris damage
5. Low cost manufacturability, and protection of the substructure.
6. Restriction of temperatures and heat loads to the substructure and internal components.

8.1 AEROHEATING ANALYSIS

To effectively apply thermal protection to the Cargo Return Vehicle, accurate analysis of the temperature and heating rate along a trajectory was required. To fulfill this requirement, the program MINIVER was utilized. Using the trajectory established by the Re-entry Dynamics group, and models for the various body sections, the thermal environment encountered by the CRV was estimated. The CRV was split into five sections for modeling purposes. These sections consisted of the nose, body, wing tips, wing section one (sweep equals 68°), and wing section two (sweep equals 54°). The models for each of these sections was input into MINIVER and analyzed twice; once at laminar flow and once at turbulent flow. From the Reynolds number data in the MINIVER output, it was found that the air flow would remain laminar for this trajectory. This was based on transition beginning at $Re=3 \times 10^5$, and fully turbulent flow at 4×10^8 . The MINIVER data showed that transition does not begin

until about 3600 seconds into the trajectory. The final value for this trajectory was 1.415×10^6 at 3920 seconds, and was well below the fully turbulent criteria. From this information, the decision was made to use the data from the laminar analysis. For all of the body sections an emissivity of 0.8 was used. The atmospheric data used was the U.S. Standard Atmosphere option. An explanation of the models used and an interpretation of the results follows.

The nose of the vehicle is subject to the most extreme temperatures. The model for this section consisted of a two foot sphere. The Hemisphere Stagnation Point heat transfer option was employed. For this section we found a maximum temperature of 2811°F , and a maximum heat rate of 43.91 btu/ft-s . Both of these values occurred at 1760 seconds.

The windward side of the body was modelled after a flat plate. The Boeing Rho-Mu flat plate heat transfer option was used. The maximum temperature was found to be 1560°F , and occurred at 1280 seconds. The maximum heat rate was found to be 7.28 btu/ft-s , at 320 seconds.

For the wing tips and wing sections a swept cylinder was used as the model. The wing tips, which are parallel to the flow, were modelled as a cylinder with a 0.5 ft radius and 0° sweep angle. The Beckwith/Gallagher Swept Cylinder heat transfer option was used for the wingtip analysis. The maximum temperature was estimated to be 3092°F , which is high, due to limitations in the modelling. The maximum heat rate was 61.07 btu/sft-s . Both of these values occurred at 1760 seconds.

The wing was divided into two sections. Both sections were analyzed using the Beckwith/Gallagher Swept Cylinder method, with a radius of 2 ft. The first section was found to have a maximum temperature of 2547°F and a maximum heat rate of 31.34 btu/ft-s . Both of these values occurred at 1760 seconds. The second wing section had a maximum temperature of 2497°F and a maximum heat rate of 29.28 btu/ft-s . Both of these values occurred at 1760 seconds. Figures 7-1, 7-2, 7-3, and 7-4 show the temperature of each model section along complete trajectory.

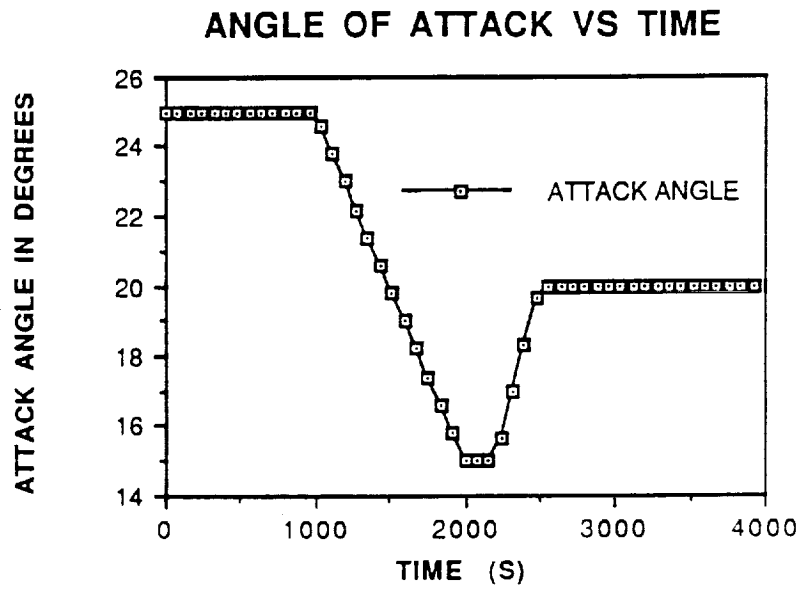


Figure 8-1 Angle of Attack vs Time

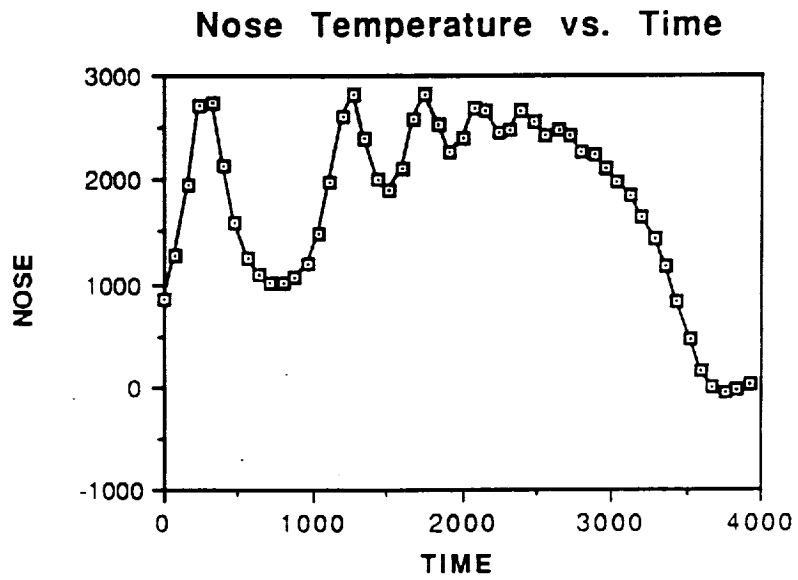


Figure 8-2 Nose Temperature vs Time

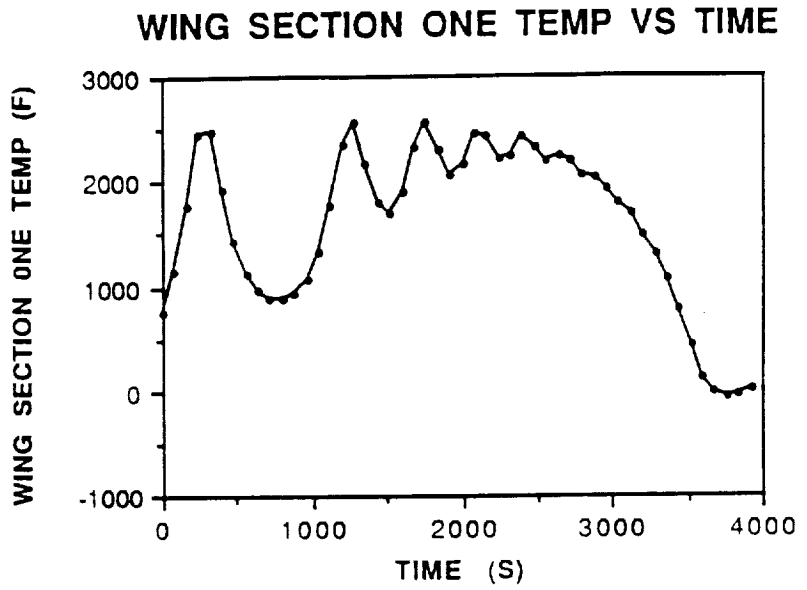


Figure 8-3 Leading Edge Temperature vs Time

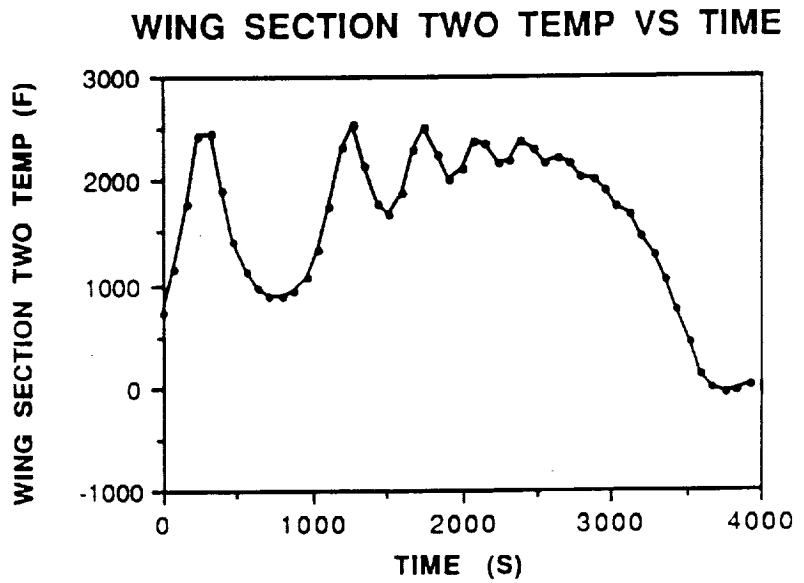


Figure 8-4 Bottom Wing Temperature vs Time

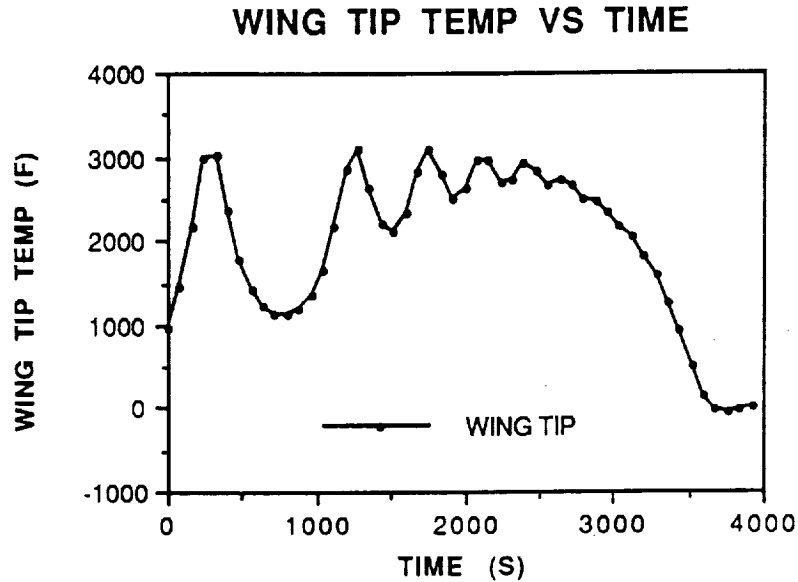


Figure 8-5 Wing Tip Temp vs.Time

8.2 THERMAL PROTECTION SYSTEM CHOSEN

There are four TPS outer shield types. An ablative system involves phase changes which absorb the incoming heat and return it to the surrounding flow. This type has full environment capabilities but would be difficult to refurbish quickly and cheaply. The Apollo ablatives cost around \$ 30,000 per square foot versus present non-ablative costs of under \$ 17,000. Thus, due to high costs and difficult refurbishability, the ablatives were not considered. The Shuttle-type heat sink tiles absorb the incoming heat without composition changes and can meet all the design criteria. The hot structure TPS would consist of multiple shields for structural strength with mostly radiation heat transfer. The structure can be constructed to withstand temperatures much higher than an aluminum substructure. Hot structures have benefits of competitive weights with minimal refurbishment. The fourth system consists of flexible blankets which can withstand moderate temperatures and provide insulation to the substructure. These are easily attached, easily refurbished, and have low weights.

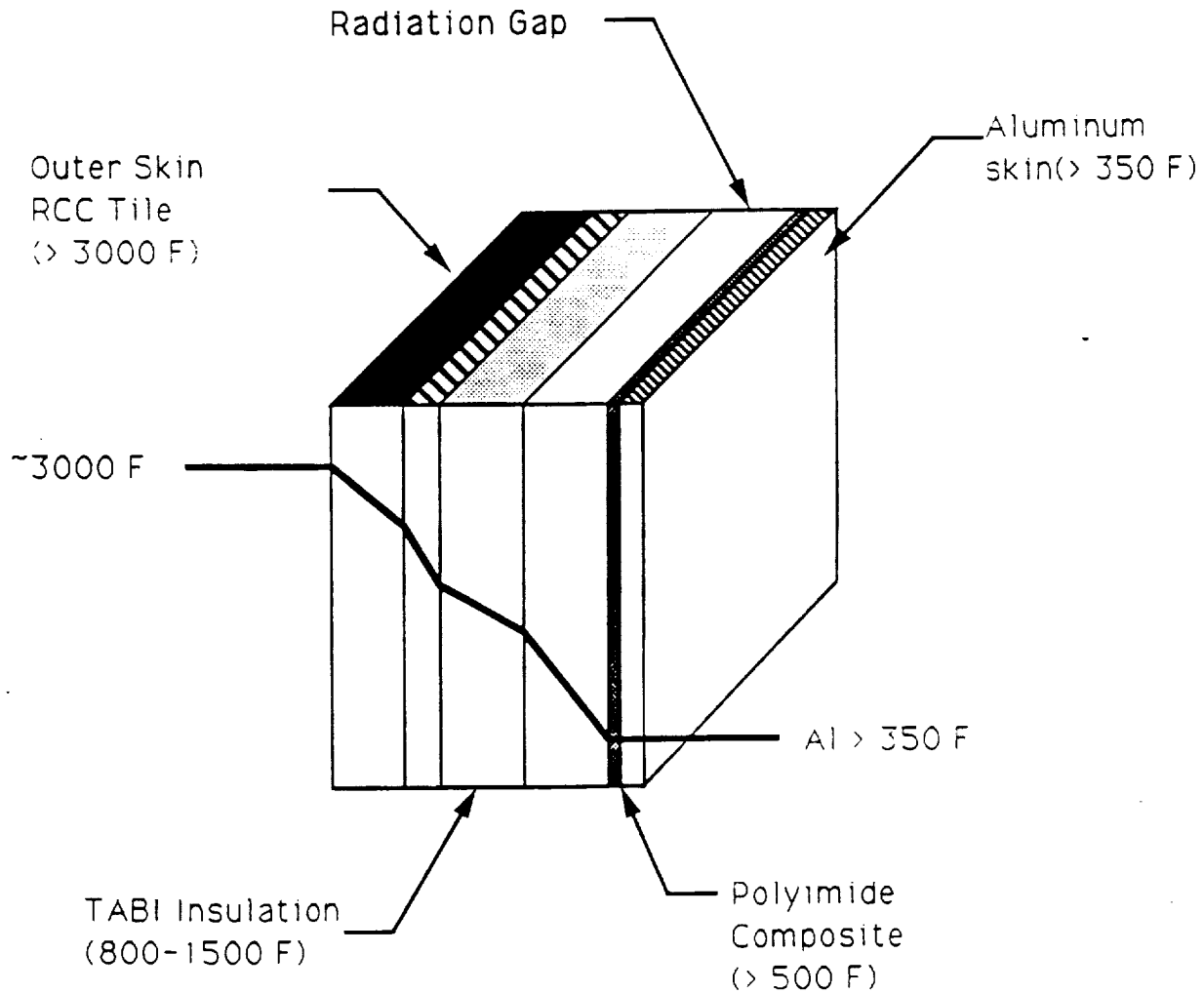
The hot structure Thermal Protection System appears to be very promising. A Rene' 41 tubular hot structure panel was considered for the lower side of the wing body. The panel design temperature is 1350 F beneath an outer heat shield like TD Ni-20. The panel weighs 2.1 lb/ft², has a buckling strength of up to 41000 lb., and can withstand pressures of up to 500 lb/ft². This system could be

supported by a gas convection cooling system in the higher temperature regions to 1350 F from gas cooled at low heating regions (the upper wing and connecting fuselage regions).(Ref. 8.1) This concept is being considered for the National Aerospace Plane (NASP) where the gas used is a bath of liquid hydrogen fuel. For the NASP, however, the highest thermal loads are likely during ascent when the fuel is present - not during reentry as is the case of the CRV. This hot structure was not utilized in the CRV design because the aluminum subsurface weight and the tile system weights would still be less than the panel and outer shield weight. Thus, the system chosen for the CRV consists of Shuttle-type heat sink tiles, flexible blankets, and carbon-carbon.

8.3 MATERIAL AND INSULATION DESCRIPTION

RCC continues to be the most applicable material for the nose cap and wing leading edge areas of maximum heating. The RCC thickness remains at the Shuttle thickness of 0.09 ft. An advanced carbon-carbon panel was used for the forward winglet sides in order to reduce the surface area required for RCC, which is nearly four times as heavy per surface area. The panel maximum temperature is not such that it can replace the RCC entirely. The panel thickness was taken as 0.207 ft for the back face temperature limit of 350 °F for aluminum. FRCI is used primarily because of its high maximum temperature which again lowers the carbon-carbon weight. There may be a much lighter carbon-carbon combination which covers the same temperatures, but references supporting this were not located. A superalloy honeycomb TPS panel was considered in an effort to reduce the FRCI weight. It consists of Inconel, titanium, Cerachrome, and Q-Fiber which weighs 1.5 lb/ft². This was not applicable since the weight was above that of FRCI. The FRCI-8 shield thickness of 0.15 ft was determined by data from MINIVER and Reference 8.2. The MINIVER output gave a total heat load on the rear body cylinder of 9530 Btu/ft². Reference 7.2 gives a FRCI thickness of 0.125 ft for a back face temperature of 350 F at an integrated heat load of 10,000 Btu/ft². The thickness chosen was 0.15 ft which provided nearly 20,000 Btu/ft². This considers the fact that the MINIVER heat load was not for nose cone surfaces. As of 1989, the AFRSI was found to be superior in minimum weight for maximum temperatures of up to 1800 F. The comparison materials were constructed of stainless steel and aluminum foils for reflective shields, Aluminoborosilicate (ABS) scrim cloth, and either ABS or silica felt insulations. The fact that the tailorable advanced blanket insulation

TEMPERATURE GRADIENT:



Schematic Diagram of Heat Transfer Through X-sect. of Laminate in terms of Max. Temp. Relative CRV Design.

Figure 8-6, Temperature Gradient

(TABI) has the same weight indicates that it should be compared further with AFRSI. From Reference 8.3, the silica fibers of AFRSI lost significant tensile strength around 1200 F while the TABI ABS fibers held to over 1500 F. Additionally, TABI has greater tolerance of aerodynamic loads due to the triangular fluted core design. For these reasons, AFRSI was replaced by TABI.

8.4 TPS VEHICLE PLACEMENT

Based on the initial design, aerothermal completed, and Shuttle temperature data the following vehicle protection regions were assigned:

Region	Temperature	Material
1	2000-3000F	RCC
1 Tile	2000-2700	Carbon-Carbon Tile
2	1500-2300	FRCI-8
3	800-1500	TABI
4	<800	TABI

These regions are illustrated in Figure 8-7.

8.5 TPS MOUNTING METHODS AND THERMAL SEALS

Holding the thermally resistive composites in place was one of the major problems faced in a CRV outer layer construction. The differences in the coefficient of thermal expansions of the various layers of material and the large temperature ranges involved during re-entry cause the mounting hardware technology to be extremely critical. The high temperatures encountered by the CRV required a need for adhesives and mechanical fasteners adequate to sustain the maximum heat load.

The current thin film technology, in terms of adhesives for high temperature applications, was applied to NASA methods of composite attachments for the Space Shuttle. The light-weight composites face extreme conditions and to properly attach the composite to the outer layer interface was a problem. The results of NASA research concluded on a few different material adhesives and fastening techniques.

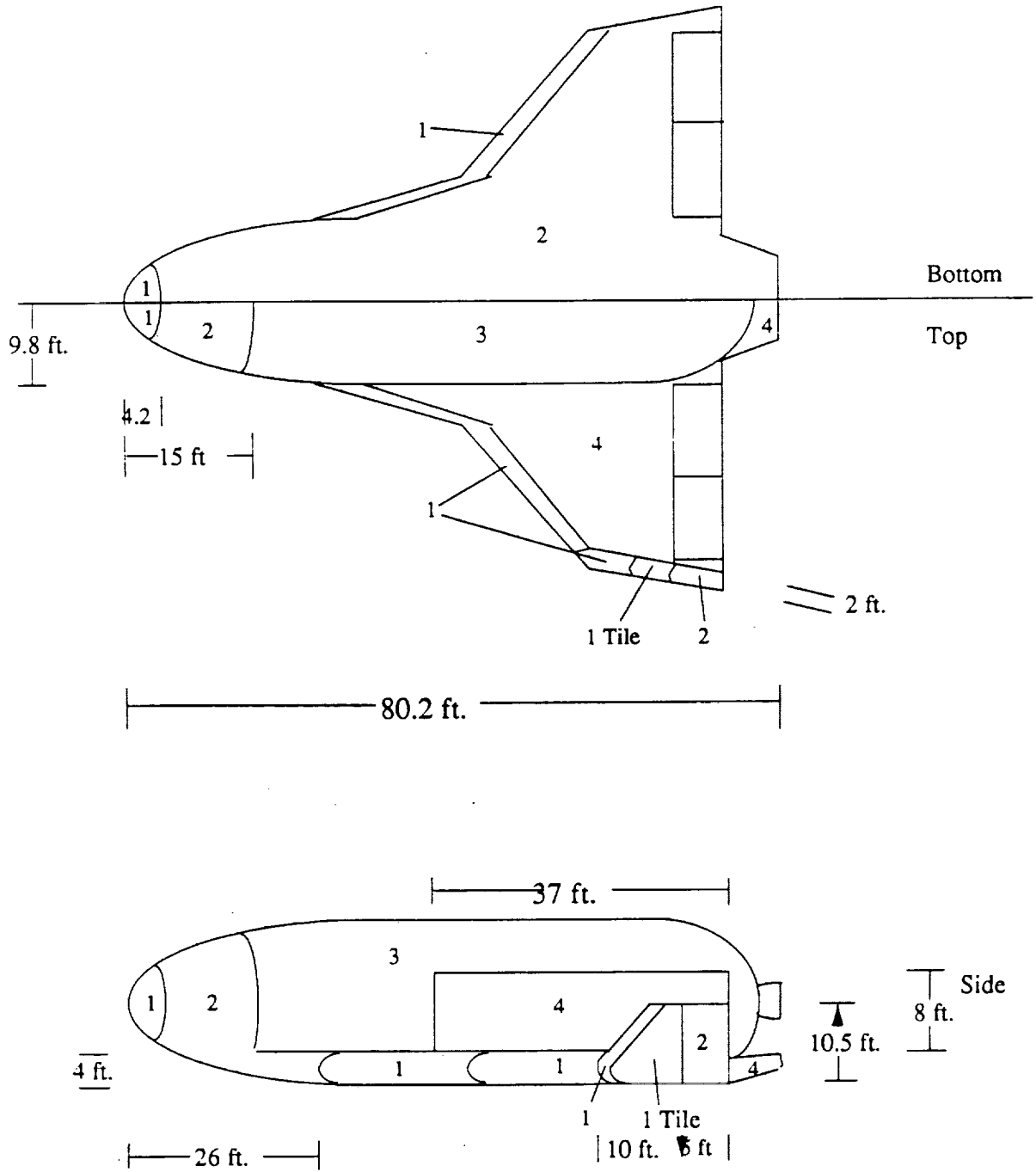


Figure 8-7, TPS Placement

8.5.1 Mechanical Fasteners

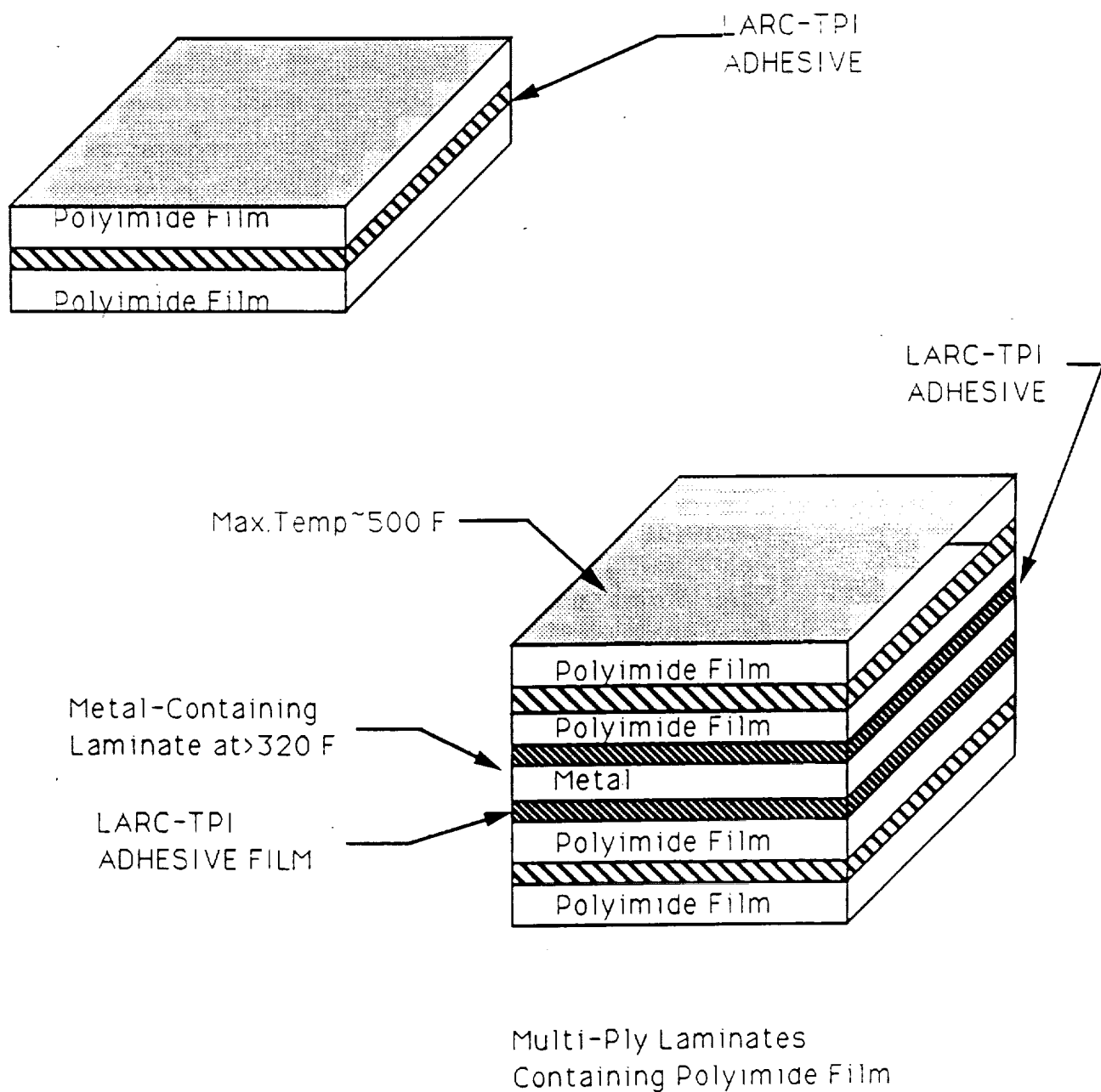
The material data that the research on mechanical fasteners was based on was provided by Johnson Space Center.(Ref 8.4) The Carbon-Carbon material, would be fastened to the outer layer (under-side) of the CRV. These panels are composed of a 12-ply carbon-carbon composite and are hexagonal in shape. The panels would be fitted together similar to a puzzle with matching edges in which no gaps present that could expose the substructure directly to the extreme temperatures of reentry.

The Carbon-Carbon panels would be fastened with a center (high temperature-resistant) mounting screw to the outer layer of the CRV. Thermally-insulating spacer bars support the interface involved when overlapping occurs. The interface between the substructure and the panel would be lined with a low-density batt insulation. This method will be used for the critical heat load areas on the CRV along with an adhesive coating on the interface (outer skin to tile). Each panel, initially in a dish configuration, is tightened centrally and flattened. The panel is to be placed in bending stress with the outer perimeter which surrounds the panel (Insulating spacer bar) being placed in compression. The center screw is tightened until flush with the outer layer. This method, along with silicone adhesives will secure the panel firmly onto the aluminum skin. The pre-stress created by the center-screw mechanism would be sufficient for normal operating loads and conditions. The screw, however, needs a carbon-carbon covering (plug) to protect it from harmful oxidation. The plug is held flush with the surface and secured in place with a ceramic cement applied on the perimeter of the screw cavity.

8.5.2 Adhesive Method

In developing a heat-resistant polymer for use on the CRV, one must consider the softening (T_s) and melting (T_m) points. This is important regarding the flexibility or rigidity of polyimide films which are often used in high temperature thin film adhesives (Fig. 8-8). One adhesive method (MSC-12619, U.S. patent #4124732), is where a tile is bonded to a Strain Isolation Pad (SIP), and then is attached to the aluminum structure. The interface between the aluminum skin and the tiles is coated with a silicone adhesive (RTV-560). This adhesive has a low glass transition temperature (-170 F) and remains flexible up to 500 F. This type of fastening concept

VOID-FREE LAMINATE CONSTRUCTION:



The LARC-TPI film and adhesive can form large-area, void-free bondlines that present good structural bonding in NASA composites. (Boeing Aerospace Co.)

Figure 8-8, Void-Free Laminate Construction

improves the overall bond strength performances of the Tile-RTV-SIP system.

8.5.3 Thermal Seal

A heat seal was used on the CRV to reduce the extreme temperatures in the gaps created by differences in thermal expansion coefficients of the composite material during reentry. A Bulb Seal, Flexible Sliding Seal, Flexible Heat-and-Pressure Seal and Heat/Pressure Seal for moving parts are some of the prototypes now in use by NASA.(Ref 8.4) The accepted temperature ranges for the seals to be used on the CRV fall within the following parameters:

1) Bulb Seals:

Designed for a wide temperature range (-423 to +500 F) composed of a thin-wall flow barrier which surrounds a layer composed of a Polytetrafluoroethylene or Polyolefin and outperforms conventional elastomeric seals used previously.

2) Flexible Sliding Seal:

A circular seal to accommodate engine gimbaling must be flexible and be able to absorb forward motion created by the thrust of the engine. The sliding seal is based on a silicone-nickel-on-graphite slider blocks. The flexible seal consists of an outside layer of silica-fiber fabric, a layer of thermal insulation, a layer of glass-fiber fabric for pressure sealing and structural support, a polyimide film for a pressure-seal backup, and an iron/nickel-alloy mesh for lightning protection. These were originally designed for the Space Shuttle but would be more than adequate to protect specific engine components of the CRV.

3) Flexible Heat-and-Pressure Seal:

A thermal/pressure seal-accommodates transverse and lateral motion between sealed surfaces. This particular seal withstands both heat and pressure. They can withstand temperatures up to 1950 F on one side while maintaining the other side at less than 350 F. This seal can also contain gas pressures

up to 5 lb/in² (34000 N/m²). The CRV components can be adequately protected in the high loading areas with this type of seal.

- 4) **Improved High-Temperature Seal:**
 The High-Temperature seals on the Space Shuttle Orbiter elervons have been improved and result in reduced leakage. It allows for thermal expansion, and reduces the weight by more than 66%. This seal is able to replace multiple high-temperature areas which have moving parts. This type of seal is constructed from Inconel metal foil. The outer foil (cylindrical shape) serves as an interface the secondary seal. The secondary seal is enclosed by the flexible seal which consists of a ceramic cloth sleeve wrapped around a foil tube containing an alumina mat filler. The use of this type of seal reduced the Thermal Protection System weight of the Space Shuttle by approximately 106 pounds (138 to 32 lbs.).

8.6 WEIGHT AND COST OF THE TPS

The following table describes the weight breakdown:

Table 8-1 Weight of the TPS

<u>Region</u>	<u>Temp.</u> °F	<u>Material</u>	<u>Thickness</u>	<u>Density</u> lb/ft ²	<u>Area</u> ft ²	<u>Weight</u> lb
1	2000- 3000	RCC	0.09	103	564	3495
1 Tile	2000- 2700	C-C Tile	0.207	11.2	218	504
2	1500- 2300	FRCI-8	0.15	8.0	2699	5351
3	800- 1500	TABI	0.15	5.4	2138	1732
4	<800	TABI	0.10	5.4	1714	926

Total Weight = 11609 lb.

Approximate Material Cost \$ 16.2 Million

8.6.1 Effects of TPS on Configuration

1. The TPS weight for a vertical tail would be 3% of the total while the winglets were 14.9%. This was an important factor when evaluating the practicality of each of the three configurations discussed in the aerodynamics section.
2. The use of canards was discouraged from the TPS viewpoint because they were projected to increase the TPS weight by over 10 %.
3. The use of strake was responsible for the large TPS weight of Region 1. A reduction of the area was promoted since it represented 20 % of the wing Region 1 protection.
4. The lower wing surface constituted over 20 % of the TPS weight.

8.7 THERMAL CONTROL OF THE CRV

8.7.1 Active Cooling System

An active TPS system based on a 2 X 20 foot Water/Glycol cooled aluminum panel was researched at the Langley Research Center. The water glycol cooling system consisted of a closed loop system which dispersed the aerodynamic heating from the exposed outer surface (i.e. the leading edge) and transferred it to the hydrogen fuel. This structural panel prototype was initially designed for a hypersonic vehicle with a speed range of Mach 5 to 7.

For high temperature regions (i.e. nose cap, wing leading edge) a forced convection system may aid in reducing the material weight. The radiation gap in the composite construction of the CRV was the area considered for the forced convection application. Heat transfer and circulation would be performed in a method similar to an automobile's turbocharger intercooler unit. The transfer medium to be used in the radiation gap would require further analysis.

The idea came from a radiator system used on the CRAY Supercomputer series. The CRAY-2 supercomputer has an active cooling system built into the ambient temperature within the system.

The computer circuitry is sealed and submerged in Fluorenert (by 3M) and regulated to transfer the heat dissipated from the components to an intercooler. Fluorenert is non-conductive electrically and is an efficient heat transfer medium (Fig. 8-9).

The maximum heat encountered would occur approximately 1/2 hour after the CRV lands. The major problem would be the differences in thermal expansion of the composites involved in the Thermal Protection System. If the temperature difference between the hot and cold regions of the CRV could be reduced the composites could be made to be more durable with time. A constant temperature could be maintained on the inner-side of the radiation gap by using the Fluorenert as the heat transfer medium. The fluorenert would then carry away the heat load and dissipate it to the intercooler, which would then send the heat to a radiator.

The increase in heat transfer through active cooling could be used to reduce some of the thicknesses of the insulating materials. A complete analysis, however, would have to be performed to determine if the use of an active cooling system would indeed reduce the overall TPS weight of the vehicle. Another consideration is whether the complexity of an active cooling system would outweigh the advantages of its use.

8.7.2 THERMAL CONTROL OF AVIONICS

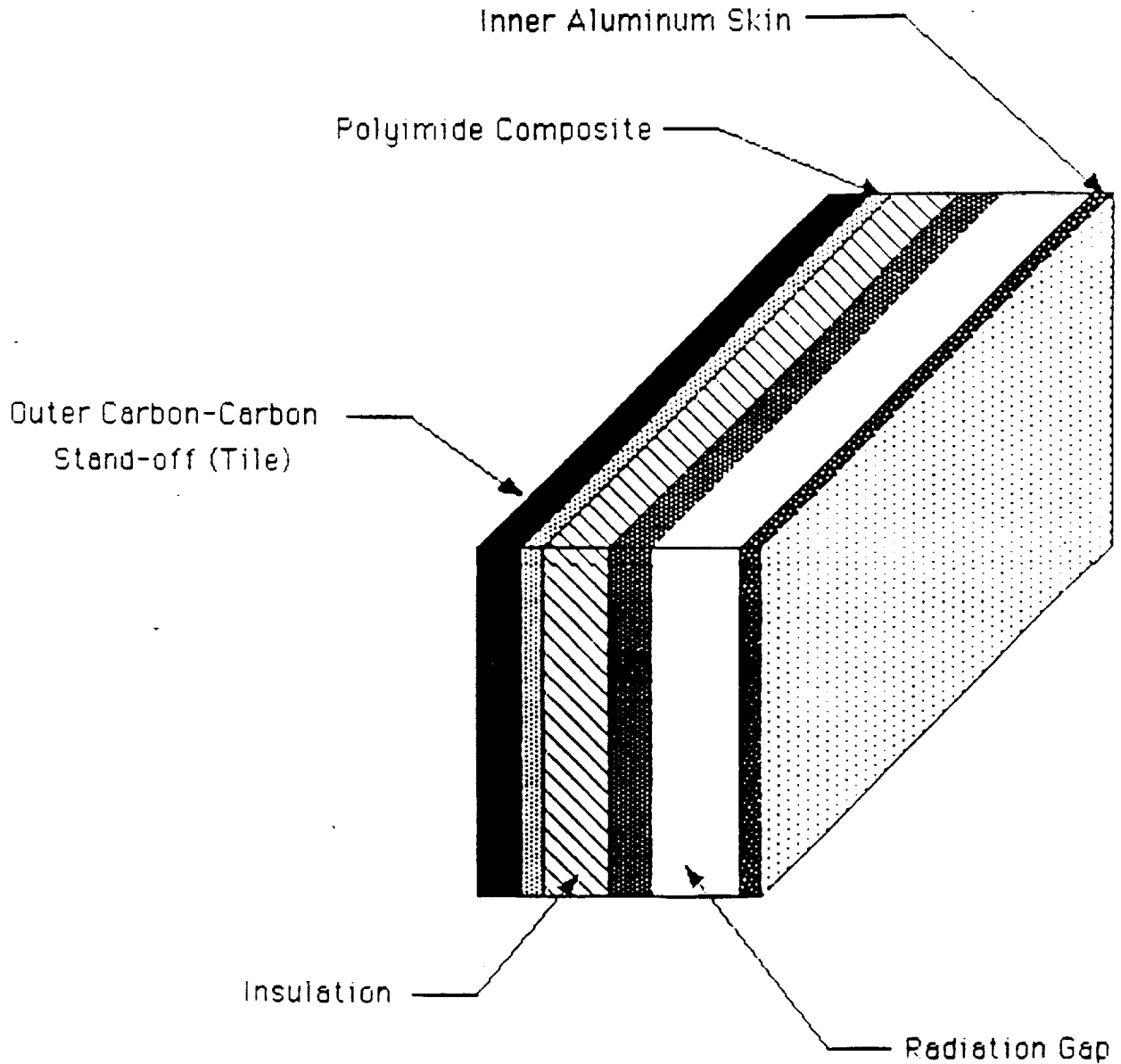
To maintain electronic-base equipment in proper working order the TPS must maintain a constant temperature. The Environmental Control System (ECS) consists of a cooling loop with cold plates, heat capacitors, heat exchangers, and radiation systems. The ECS would maintain all of the avionics hardware at the proper operating temperature determined by the manufacturers. The ESC would reduce temperature fluctuations which would in turn decrease the wear on avionics.

Avionic Components:

1) Avionics:

The avionics are located in the avionics bays at the front and rear of the cargo bay. The TPS in this area would keep the temperatures encountered relatively low. The avionics are self-cooling and the

FLUORINERT: Forced Convection Concept



**APPLICATION OF FORCED CONVECTION FLOW
OF FLUORINERT HEAT TRANSFER MEDIUM
THROUGH THE RADIATION GAP**

Figure 8-9, Forced Convection Concept

temperature would be maintained by the built in Environmental Control System (ECS).

2) Fuel Cells:

The fuel cells are located under the cargo bay floor and are self-cooling. The underside of the CRV is well protected by the TPS during re-entry and the temperatures encountered should be acceptable.

3) Servo Actuator Power Supply Batteries:

These batteries do not have a self-cooling system. Their optimum operating temperature is approximately 50° F. An acceptable variation in the temperature for these batteries 40-100 F. The Thermal Protection System approximated a median temperature of 70° F for this unit. The temperature was based on laminate construction using the MINIVER/EXITS program.

8.8 DEBRIS PROTECTION

All sources indicate that the tiles and blankets are sufficient to handle any damage caused by debris. Most damage to the TPS would probably occur during handling.

8.9 CONCLUSION

The Thermal Protection System for the winged cargo return vehicle was based primarily on the effective protection of the substructure while considering weight penalties. The aeroheating effects were defined from MINIVER data, approximate calculations, and Space Shuttle data. The protection materials chosen for use were reinforced carbon-carbon, carbon-carbon tiles, Fibrous Refractory Composite Insulation-8, and tailorable advanced blanket insulation (for the shuttle type heat sink and hot structure system). The placement of these materials was given in Figure 8-6, and the weight breakdown was given in table 8-1. The total material weight was 11609 lbs at an approximate material cost of \$16.2 million. Future use of an active cooling system appeared promising for use in connection with improved hot structures.

THIS PAGE HAS BEEN LEFT INTENTIONALLY BLANK

9.0 PROPULSION

The objective of the propulsion discipline was to design a propulsion system for the CRV which will meet all the mission requirements. The design methodology followed for the on board propulsion systems used empirical and theoretical methods to predict the needs of the CRV. The primary inputs were thrust level, delta-velocity requirements, and the total dry weight of the CRV. After theoretical values were found for each of the different systems considered, the data was reviewed and the most feasible system type was selected. A detailed analysis was then generated on that system to aid in sizing and tank placement.

The launch system design methodology consisted of researching the launch vehicle and methods that would be in use by the date of service, and based on the current information, deciding which should be adopted.

9.1 ORBITAL MANEUVERING SYSTEM

The Orbital Maneuvering System (OMS) of the CRV would serve two main purposes. First, the system would have to produce the necessary thrust and delta-velocity to propel the CRV from a 100 n.m. to a 210 n.m. orbit after booster shutdown. Second, the system would have to be able to produce sufficient delta-velocity for de-orbit. To accomplish this task two different systems were examined, Nitrogen Tetroxide/Monomethyl hydrazine (NTO/MMH) and cryogenic H₂/O₂. Both are bipropellants since monopropellants would not produce sufficient specific impulse for the CRV. The data generated on the two systems such as weights, specific impulse, tank volumes, etc, can be found in the tables below (Table 9-1, 9-2, 9-3).

9.1.1 OPTIONS RESEARCHED

NTO/MMH was the first option considered. This is the same type of propellant used on the shuttle. This system has exhibited great reliability and the technology is well developed. Additionally, the NTO/MMH system would require the least total tank volume to accomplish a typical mission. The main disadvantage is that it would be relatively massive when compared to other types of propellants.

Cryogenic H₂/O₂ was the second option considered. This is a "high performance" bipropellant. H₂/O₂ has a specific impulse that is

Propulsion Systems Specifications

Table 9-1 Cold Gas Data

Delta V =	30	Leng engine =	4.421
(ft/sec)		(ft)	
Vacuum Isp =	68	Leng nozzle =	1.913
		(ft)	
		Mass engine	15
		(lbm)	
		r =	0.1
		(in)	
rho bulk =	19.3	ullage =	0
		# engines =	24
Press Chamb =	100	C* =	1395
Area ratio =	10		
Thrust =	50		
(lbf)			
Mass vehicle dry	54716		
(lbf)			
Isp delivered =	68	Mass fuel =	830.989
(l/sec)			
Prop flow rate =	0.735	Vol fuel per tank	21.5282
(lbm/sec)		(ft ³) =	
Area throat =	0.318	Feedline dia fuel	0.59113
(in ²)		(in) =	
Area exit =	3.188	Pmax oper press	231
(in ²)		(lb/in ²) =	
Diam exit =	2.015	Feedline mass =	0.08718
(in)		(lbm)	
Mass prop used =	755.445	Misc. mass =	12.062
(lbm)		(lbm)	
Mass reserves =	75.545	Tank mass	22.4291
(lbm)		fuel(2) =	
		(lbm)	
Mass prop loaded	830.990	Tank diam f(2) =	3.45205
(lbm)			
		Sys. dry Mass =	417.645
		(lbm)	
t burn =	1027.405	Sys. wet Mass =	1270.162
(sec)		(lbm)	
		Diam throat =	0.63728
		(in)	

Table 9-2 Reaction Control System

Delta V =	40	Leng engine =	18.79
(ft/sec)		(in)	
Vacuum Isp =	289	Leng nozzle =	11.34
(1/sec)		(in)	
rho oxidizer =	89.9	Mass engine =	15
(lbm/ft ³)		(lbm)	
rho fuel =	54.8	r =	0.1
(lbm/ft ³)		(in)	
rho bulk =	74.1	ullage=	0.03
(lbm/ft ³)			
Mixture ratio =	1.65	# engines=	28
Press Chamb =	150	C*=	5675
Area ratio =	40	rho press=	2.9
Thrust =	400		
(lbf)			
Mass vehicle dry	54716		
(lbm)			
Isp delivered =	289	M fuel=	97.916
(1/sec)			
Prop flow rate =	1.384	M oxidizer=	161.561
(lbm/sec)			
Area throat =	1.628	Volume fuel per	0.920
(ft ²)		tank=	
Area exit =	65.102	Volume oxid per	0.926
(in ²)		tank=	
Diam exit =	4.553	Mlad fuel per	5.614
(in)		tank=	
Mass prop used =	235.888	Mlad oxid per	5.640
(lbm)		tank=	
Mass reserves =	23.588	M pressurant	0.805
(lbm)		per tank=	
Mass prop loaded	259.477	Volume press	0.278
(lbm) =		per tank=	
t burn =	170.429	Mlad press per	0.044
(sec)		tank=	
Feedline diam.	0.297	Tank mass fuel	2.250
oxygen (in) =		per tank	
Feedline dia fuel	0.254	Tank mass ox	1.23
		per tank	
		Tank mass pre	0.369
		pre tank	
P max oper press	341	Tank diam fuel	1.207
(lb/ft ²) =		per tank	
Feedline mass	0.024	Tank diam ox	1.209
feul (lbm) =		per tank	
Feedline mass	0.032	Tank diam pre	0.809
oxygen (lbm) =		per tank	
Feedline mass	0.015	System dry	462.284
press (lbm) =		Mass =	
Miscellaneous	12.005	System wet Mass	723.371
mass (lbm) =		=	

Table 9-3 Orbital Maneuvering System

Delta V =	802.1	Leng engine =	77.2	
(ft/sec)				
Vacuum Isp =	313	Leng nozzle =	50.5	
(1/sec)				
rho oxidizer =	89.9	Mass engine =	260	
(lbm/ft ³)				
rho fuel =	54.8	r =	0.1	
(lbm/ft ³)				
rho bulk =	74.1	ullage =	0.03	
(lbm/ft ³)				
Mixture ratio =	1.65	# engines =	1	
Press Chamb =	125	C* =	5675	
Area ratio =	55	rho press =	2.9	
Thrust =	6000	Mvehicle dry =	61596	
(lbf)				
Mass vehicle	54716			
dry (lbm) =				
				CALCULATIONS
Isp delivered =	313	M fuel =	1883.001	
(1/sec)				
Prop flow rate	19.169	M oxidizer =	3106.952	
(lbm/sec) =				
Area throat	27.049	Volume fuel =	35.392	
(in ²) =				
Area exit =	1487.717	Volume oxid =	35.597	
(in ²)				
Diam exit =	45.1	in.	Mlad fuel =	22.573
(in ²)				
Mass Prop =	4536.321		Mlad oxid =	22.600
(lbm)				
Mass reserves	453.632		M pressurant =	25.968
(lbm) =				
t burn =	4989.953		Volume press =	8.955
(sec)				
Feedline diam.	236.645		Mlad press =	16.187
oxygen (in) =				
Feedline dia	1.1035		Tank mass fuel	36.508
fuel (in) =				
Feedline dia.	0.946		Tank mass ox	39.705
feul (in) =				
			Tank mass pre	9.988
P max oper	286		Tank diam f	4.074
press (lb/ft ²) =				
Feedline mass	0.277		Tank diam ox	4.082
fuel (lbm) =				
Feedline mass	0.376		Tank diam pre	2.577
oxygen (lbm) =				
Feedline mass	0.013		System dry Mass	420.480
press (lbm) =			=	
Miscellaneous	12.254		System wet Mass	5436.401
mass			=	

approximately thirty-five percent higher than NTO/MMH. A cryogenic H₂/O₂ system would be relatively light compared to other systems. There are, however, several disadvantages in using a cryogenic system. Cryogenics would require the use of additional fuel to chill-down the engines before they are fired and to make up for boil-off losses. Even with current technology, these losses would stand at five percent per day in orbit.(Ref. 8.1) The amount of thermal control required to keep losses at five percent per day would add additional mass. Another problem with H₂/O₂ is that it would require approximately twice as much tank volume as NTO/MMH.

9.1.2 OMS PROPELLANT RECOMMENDATION

Based on the above discussion and the data listed in Table 9-3, it was determined that NTO/MMH was the best option. This propellant has the added benefit of being able to use existing shuttle hardware.

9.2 REACTION CONTROL SYSTEM

The Reaction Control System (RCS) system for the CRV would be responsible for fine orbital and attitude adjustments in space. This system would not be used in the lower atmosphere. The system would consist of 52 thrusters positioned as in the drawings included in figures 9-1, 9-2, and 9-3.

9.2.1 RCS Auxiliary

Recently, the availability of the OMV has been questioned. Therefore, it has been necessary to design for the possibility of hard-docking to SSF. One complication of hard-docking is that maneuverability must be available within the SSF control zone. SSF regulations prohibit all but the use of cold gas propellants within this zone.

To solve this problem an auxiliary RCS system in addition to the main RCS system has been designed. The auxiliary RCS system would only be used within the SSF control zone. This solution was chosen because, given the low specific impulse of current cold gas thrusters, a system capable of fulfilling total mission requirements would be too large in tank volume and mass to be efficient.

Since cold gas systems have such a low specific impulse it is important that the time required to perform the necessary maneuvers is not too lengthy. The total mission burn time necessary would be seventeen minutes. This encompasses over twenty burns during SSF control zone operations. This was calculated assuming the use of only one thruster in any direction. There are, however, two thrusters positioned in each direction, and in the event quicker maneuvers are required the additional thruster could be used.

9.2.1.1 OPTIONS RESEARCHED, RCS AUXILIARY

Two cold gas systems were researched. A third option, multi-propellant resisto-jet thrusters are described below but could not be integrated into a system due to a lack of available information.

Resisto-jet thrusters utilize electrical resistance to heat the gas before it is expelled. The power level required would be 200 watts but no figures were found for operating times in terms of Kilo-watt hours of power used. These thrusters can currently produce specific impulses of approximately 400 seconds and are very lightweight. Resisto-Jet thrusters are currently being developed for use with SSF and should be available in the future.(Ref. 8.5)

9.2.1.2 PROPELLANTS RESEARCHED

The propellants researched for use in the cold gas system were nitrogen and helium. Although helium provides a higher specific impulse than nitrogen it is the most voluminous of the two systems. Helium needs over twice the tank volume as nitrogen. This would require the tank to be extremely large and massive. A summary of the comparison follows:

	Table 9-4	
	<u>Helium</u>	<u>Nitrogen</u>
Engine mass(lbm)	15	15
Fuel Mass(lbm)	360	755
Isp(sec)	158	68
Fuel tank volume(ft ³)	61	22
Total system mass(lbm)	915	1270

9.2.1.3 COLD GAS RCS SYSTEM RECOMMENDATIONS

The above discussion and comparison indicates that a nitrogen system would require the least volume and as a result, was the final choice for the RCS auxiliary propellant. The higher mass of the nitrogen system was beneficial with respect to the center of gravity considerations for the vehicle.

9.2.2 OPTIONS RESEARCHED, RCS MAIN

There were two main categories of propellants researched, monopropellants and bipropellants. The main advantage of monopropellants are their simplicity due to the fact that they require less complicated control systems. The disadvantages of the monopropellants that they would require a high tank volume and do not supply a very high specific impulse. The main advantage of bipropellants are that they can deliver a high specific impulse while keeping tank volume to a minimum. The disadvantage of bipropellant systems is that they have a high mass when compared to monopropellants.

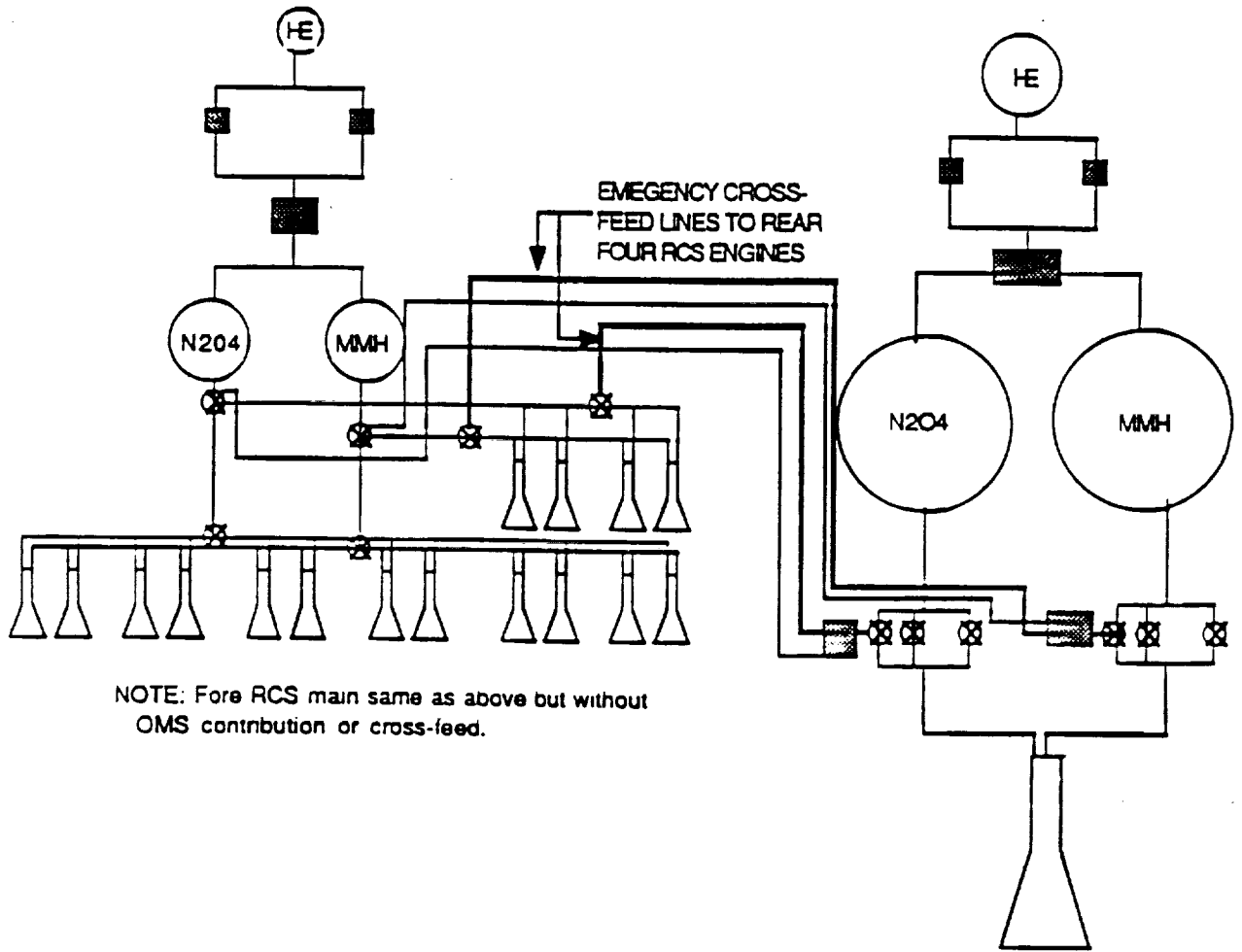
9.2.2.1 Propellants Researched

Four types of propellants were researched: NTO/MMH, cryogenic H_2/O_2 (bipropellants), N_2H_4 , and H_2O_2 (monopropellants). Cryogenics were discarded immediately for reasons mentioned in section 9.1.1. H_2O_2 , a cold gas monopropellant was discarded also due to the fact that it could not efficiently generate the required.

The thrust level required of the RCS system would be near the limit of N_2H_4 . Because of this the size of the thrusters would have to be unusually large, over twice the size of the others.

The thrust level needed by the CRV is well within the range of NTO/MMH. The thrusters are also about half the length of the N_2H_4 thrusters. Additionally there would be an advantage to using the same type of propellant for RCS and OMS. This would add an extra level of redundancy to each system. By routing extra feedlines there would be more ways to get fuel to an engine in the case of a feed system failure.

AFT RCS main / OMS SCHEMATIC



NOTE: Fore RCS main same as above but without OMS contribution or cross-feed.

FORE AND AFT COLD GAS SCHEMATIC

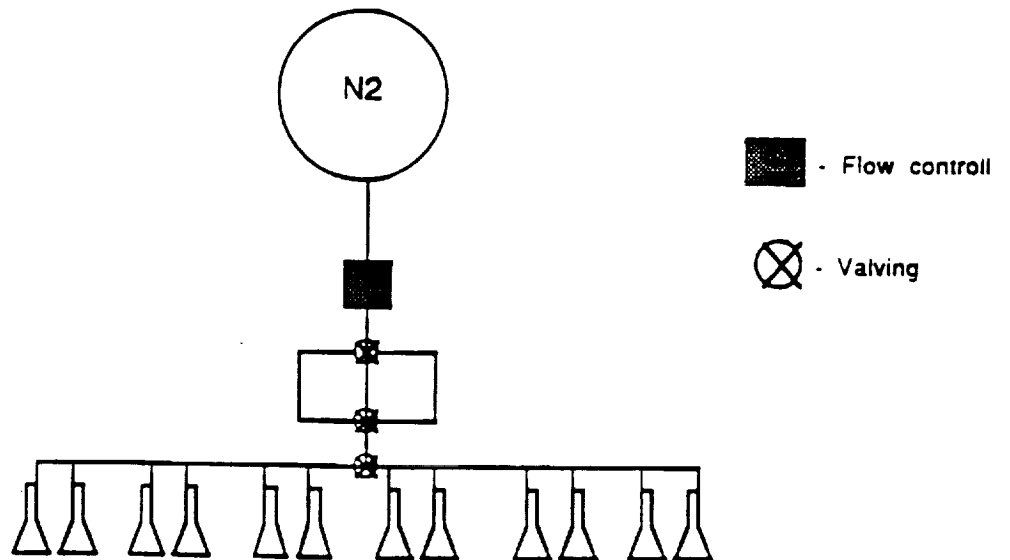


Figure 9-1 RCS/OMS Schematic

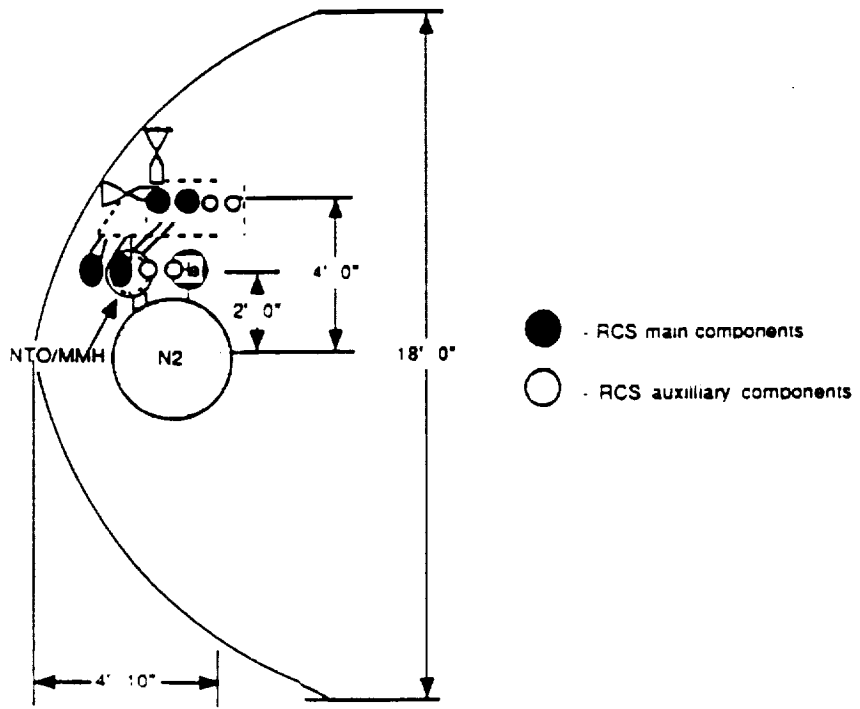


Fig 9-2 Side view fore RCS

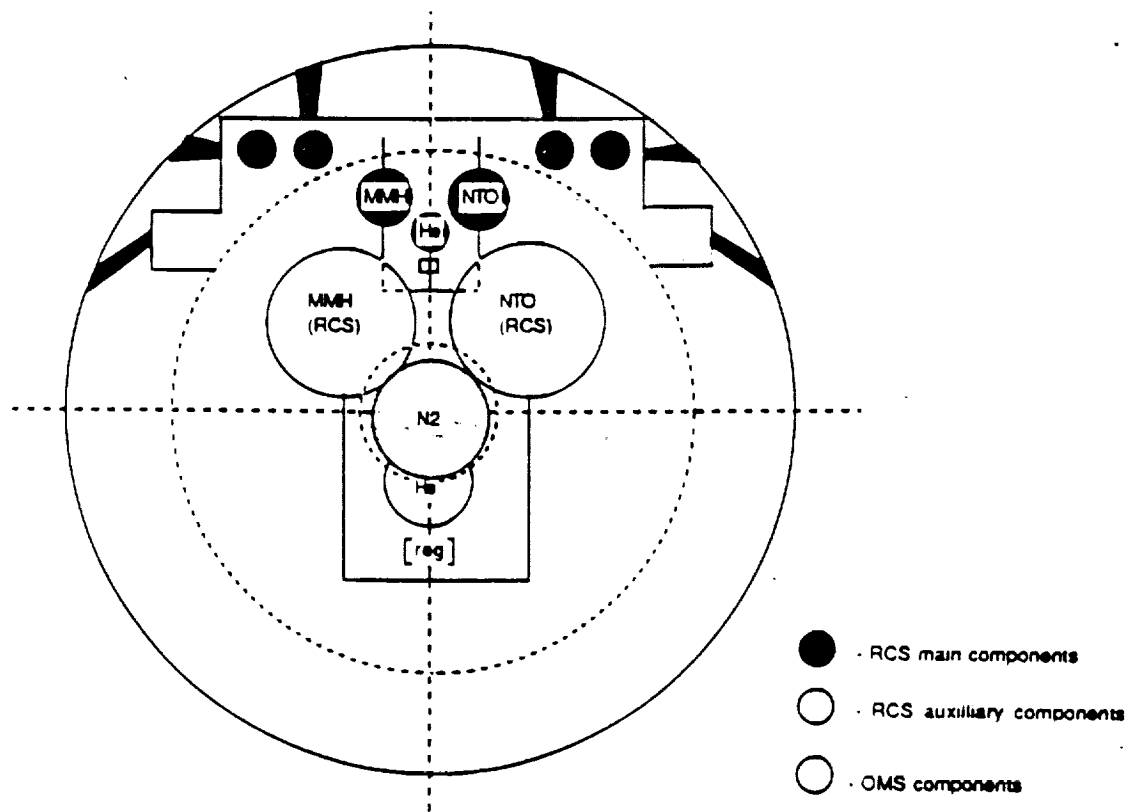
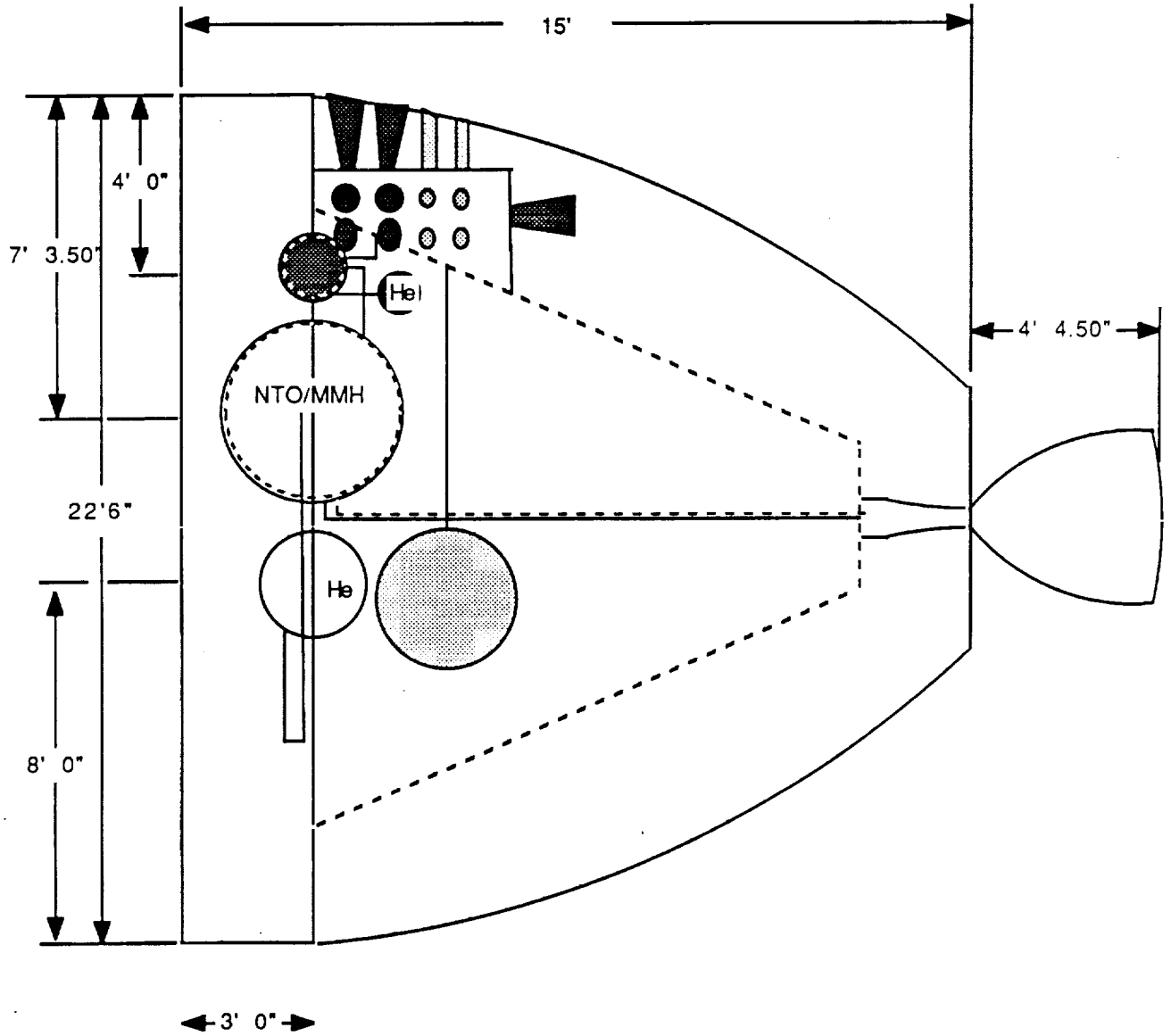


Fig. 9-3 Cross-sectional view, aft systems

Side view, aft systems



- - RCS main components
- ◐ - RCS auxilliary components
- - OMS components

Fig. 9-4 Side View aft systems

Table 9-6

<u>TANK</u>	<u>DIAMETER(FT)</u>
OMS fuel	4.07
OMS oxidizer	4.07
OMS pressurant	2.57
RCS main fuel	1.21
RCS main oxidizer	1.21
RCS main pressurant	.809
RCS auxiliary fuel	3.45

Note: For redundancy fore and aft RCS tanks are the same size.

9.4.3 Placement and Routing of Feed Systems

See figure 9-4 for a schematic of the routing. It should be noted that fail-safe valving was assumed but not specifically shown in the figures. The placement of the feed lines are shown in 9-1, 9-2, and 9-3.

9.4.4 Pressurization of System RCS and OMS

When a propulsion system is operated under low gravity or high acceleration conditions, a liquid acquisition device (LAD) is necessary to withdraw the liquid propellant.(Ref. 8.1) By using an inert pressurant the propellant can be forced to exit the fuel tank. For this application a surface tension device similar to the space shuttle's has been chosen. The LAD acts as a barrier between the incoming pressurant and outgoing fuel. These devices are the simplest and lightest type in use. Helium, an inert gas, has been chosen as the pressurant. These devices can be seen in figures Figure 9.1 and 9-4. Note that it would not be necessary to use either a LAD or a pressurant with a cold gas system.

9.5 POSSIBLE OMS ENGINE OUT

Originally a trade study on the number of OMS thrusters was performed. The conclusion of this study was that if the CRV could be de-orbited in the event of OMS engine out, one OMS engine would be advantageous for weight allowances.

In the unlikely event of an OMS engine failure, the aft four RCS thrusters could be used for an emergency de-orbit from any mission position. The extra fuel needed will be taken from the OMS tanks by

an independent system of feed lines. The mass of fuel needed for such a maneuver was calculated to be 1013.7 lbm, with a burn time of 680 seconds. There would be more than enough fuel on-board to accommodate this method of de-orbit.

9.6 NUMBER OF RCS THRUSTERS AND PLACEMENT

For effective six axis control, 24 cold gas and 28 NTO/MMH thrusters were placed as shown in Fig. 9-1, 9-2, and 9-3. Each main thruster would produce 400 lbs. of thrust. All thrusters would be fired individually except in emergencies. This number of thrusters allows for at least one degree of redundancy for each axis of motion. The thrusters would also be located to allow for paired-thruster operation if desired.

9.7 ENGINE SELECTION, OMS, RCS AND COLD GAS

Based on the theoretical engine size data of Table 9-3 for the OMS engine it can be seen that the current space shuttle OMS engine would satisfy all of the qualifications. It would be more efficient to use this existing engine than to design a new unit. Therefore, an Aerojet AJ10-190 was chosen for the use in the CRV. The dimensions of the engine are as follows:

Dia.. exit = 45.1 in,
Length nozzle = 50.5 in.
Total length = 77.2 in.
Thrust (vac) = 6000 lbf.

For the RCS system an engine suiting the thrust requirements of the CRV as shown in table 3-3 would have to be used. Lack of data concerning all of the engines currently available did not allow a choice to be made. Instead, the theoretical values of table 3-6 were used. If an engine suiting this application is not currently being produced, one would need to be developed on the specifications below.

Dia. exit = 9.44 in.
Nozzle length = 11.34 in.
Total length = 18.79 in.
Thrust (vac) = 400 lbf.

Current research indicates that the maximum thrust produced efficiently by cold gas systems is approximately 50 lbs.. This value

was chosen for the CRV application and a theoretical engine designed. A 50 lb. cold gas thruster could not be located, but the technology exists to develop one. Below are the specifications that this engine would be required to meet.

Dia.. exit = 2 in.
Nozzle length = 2.58 in.
Total length = 5.14
Thrust (vac) = 50 lbf.

9.7.1 System Mass Comparison

The two possible propulsion configurations for the CRV would include a system with Space Station Freedom (SSF) control zone capabilities, and one without. Whether or not the OMV is available or not would determine which is used. Below is a mass comparison of the two types of systems.

Cold Gas Included = 7429 lbm.
Cold Gas Not Included = 6159 lbm.

9.8 LAUNCH SYSTEMS

The launch system's responsibility for this application would be to deliver the loaded CRV to a 100 n.m. insertion orbit. It should be noted that the design of a new launch system was not attempted here. The choice of launch systems was limited to vehicles currently under design and those already in use. Currently, two systems would be available by the initial launch date that would meet the design requirement.

The first option consists of two Liquid Rocket Boosters (LRB) mounted on each side of one core unit each with its own engines and fuel. The core also carries all of the avionics and controls. The fuel used for this system would be liquid hydrogen(LH₂) and the oxidizer would be liquid oxygen(LOx). The engines used for this application would be Space Shuttle Main Engines (SSME). These were used because the current Space Transportation System Engines were designed to deliver a smaller a payload. Each booster would have five SSME's and the core would have two. This system is capable of delivering a payload of 113,000 lbs with one booster engine out. Which would be adequate for the CRV's design weight of 108,000

lbm.. The system can be recovered and research is currently being done by NASA to determine the most efficient way that this can be accomplished. This system was chosen for many reasons. It represents the long term solution for the problem. The LRB system was designed for multiple applications and payloads and can be easily modified and adapted. It also involves liquid booster technology which is more efficient than solid rocket boosters. Another factor involved in the decision to choose this launch system was abort capability. Since the LRB's can be throttled they allow for a high degree of control after launch. In the event of an emergency it would be possible to safely maneuver the booster to the Atlantic and detach the CRV for a safe landing at an alternate site. A detailed drawing of this system can be found in figure 9-6. The specifications of the booster can be found below.

**Launch System Specifications
SPACE SHUTTLE MAIN ENGINE DATA**

Expansion Ratio	35:1
Flow Rate (Oxidizer/Fuel) lb/sec	403.3/442.2
Isp sea level -sec.	403.3
Thrust sea level - lbs.	418,000
Weight - lbs.	6340
Length - in.	146
Length nozzle-in.	121
Diameter exit - in.	63
Mixture Ratio	6:1

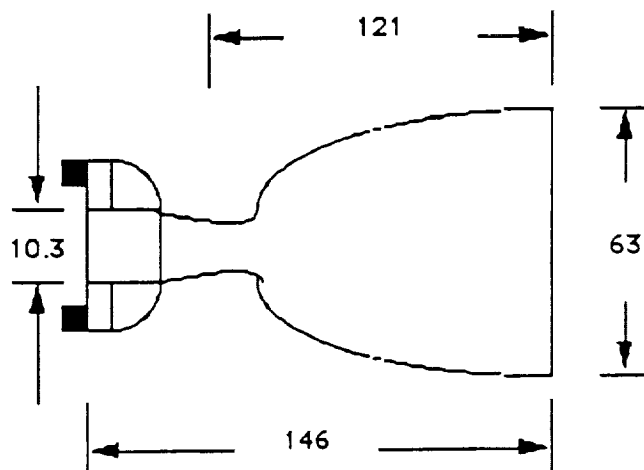


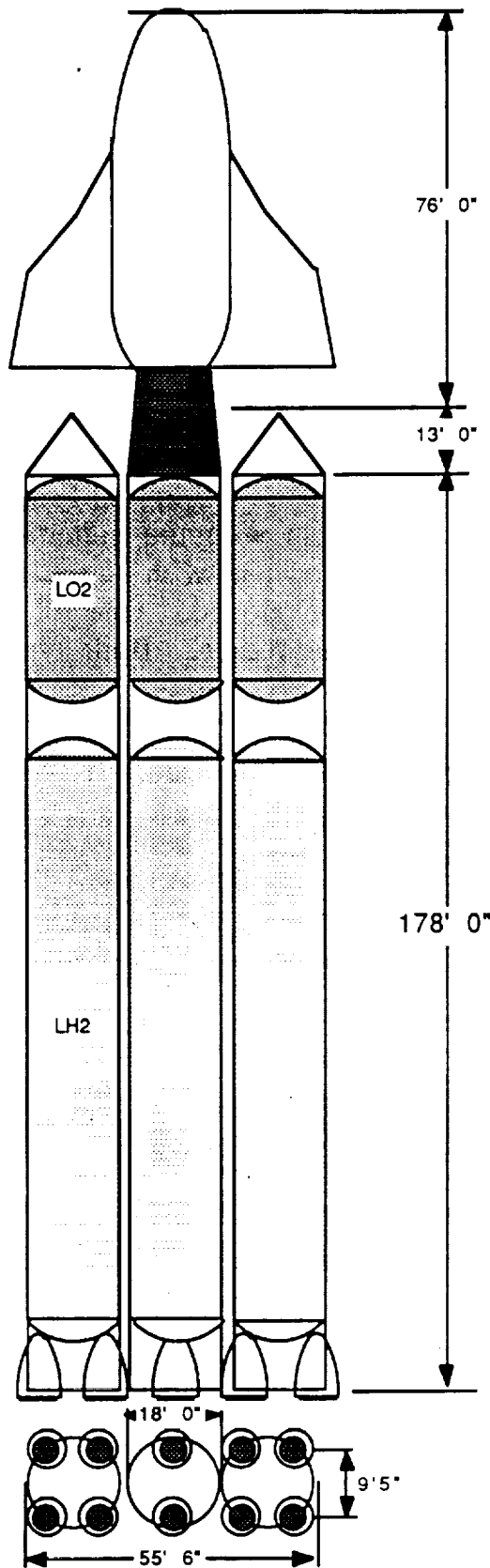
Fig. 9-5 SSME specifications

The second option is currently considered the back-up option in the event that the LRB system becomes unavailable. This system would

be similar to the shuttle's in all respects but one. Two SSME engines would be mounted on the bottom of the shuttle's external tank. The CRV would be mounted piggy-back in the same manner as the shuttle. This system currently exists with the exception of the modified external tank and would be able to fulfill all mission requirements.

9.9.1 Mounting of CRV on Booster

The CRV would be top-mounted to the LRB launch system. It has been determined that this would simplify orbital insertion and that ground wind loading would not be of major concern. The structures group has designed a mounting apparatus which would hard mount to the booster core. The CRV would then mate with the mounting structure via pins that have been developed for use with the LRB's. There are two types of pins that have been developed. One transmits axial forces and one transmits lateral forces. Both types of pins accommodate thermal expansion. The CRV would be mounted at eight points equidistant around the circumference of the mounting structure. This structure's placement can be seen in fig. 9-6 (Refer to Sec. 10.7 for more details).



3 LRB LAUNCH SYSTEM

10 SSME ENGINES

113.0 KLB PAYLOAD ONE BOOSTER
OUT

120.8 KLB PAYLOAD ONE CORE OUT

MAX ACCELERATION: 4.00 g's

Figure 9-6

THIS PAGE HAS BEEN LEFT INTENTIONALLY BLANK

10.0 STRUCTURAL DESIGN AND ANALYSIS

The front fuselage was based on a semi-monocoque design similar to conventional aircraft. This design utilized aluminum TA 2219 for the majority of the structure. The front fuselage houses the front landing gear, the avionics bays, and the docking module bay.

The wing used a conventional wing design consisting of spars, webs and honeycomb skin. The wing was constructed from aluminum TA 2219 except for the skin which used aluminum TA 2024. The aft landing gear base was placed within the wing structure.

The mid fuselage consists of a 30 foot long primary load-carrying structure housing the payload bay. The mid fuselage was a truss frame construction of aluminum TA 2219 which includes a wing carry through structure and the payload bay doors. The payload bay doors would be constructed entirely of graphite/epoxy.

The aft fuselage consists of an external shell structure and an internal thrust structure. Both are constructed primarily from aluminum TA 2219 and bonded boron epoxy laminates and titanium reinforcements. The aft fuselage houses the propulsion subsystem and was designed to transfer the launch and thrust loads to the mid fuselage.

These major structural components were joined together by several different methods including rivets, bolts, welding, and shear ties. The three fuselage sections interface by means of two supporting bulkheads.

10.1 WING STRUCTURAL LAYOUT

The wing structural layout was modeled after the NACA 64010 and NACA 64012 airfoils. Work involved in this design has included node and element coordinates, control surface structural layout, and winglet structural layout.

10.1.1 Materials and Construction

The wing structure would be constructed out of Aluminum TA-2219 alloy due to its strength to weight ratio, ability to withstand temperatures up to 600 deg. F, low cost, and welding characteristics.

Placement of the nodes in the structure was based on chord thickness calculations. A spread sheet was set up which calculated the chord lengths at two foot intervals from the root chord out to the span of the tip wing. Values were interpolated four feet from the trailing edge and then every three feet forward to the leading edge. This formed the elements of the wing structure(see Figure 10-1). Based on the lengths of all the elements, along with estimations for the cross sectional area the weight of the wing structure was determined.

Included in fig 10-1 are the structural dimensions of the control surfaces. Given the thickness of the trailing edges of the wing and winglet around the control surfaces (max 0.2 ft) solid aluminum plates were decided to be used, seen as shaded areas in fig 10-1. The leading edge spar would also be constructed of aluminum plate beginning approximately 1 ft back from the leading edge in order to provide for the Reinforced Carbon Carbon (RCC) thermal protection system.(Ref. 10.1)

10.2 FORWARD FUSELAGE STRUCTURAL LAYOUT

10.2.1 Design Dimensions and Requirements

The front fuselage structure was required to provide support and sufficient space for the front landing gear (see Figure 10-2). In addition, the front fuselage contains the avionics, guidance, and navigation systems.

Mounting support for these systems was required to be free of vibration and be accessible for maintenance. Also located in the front fuselage is the docking module bay. The purpose of this bay is to contain the docking module, docking module support structure, and any other equipment necessary for docking to Space Station Freedom. The forward structure consists of the fuselage up to the payload bay forward bulkhead. The width expands from the nose tip to 19.6 ft. at the bulkhead. Likewise, the height expands to the full payload bay height of 19.65 ft.

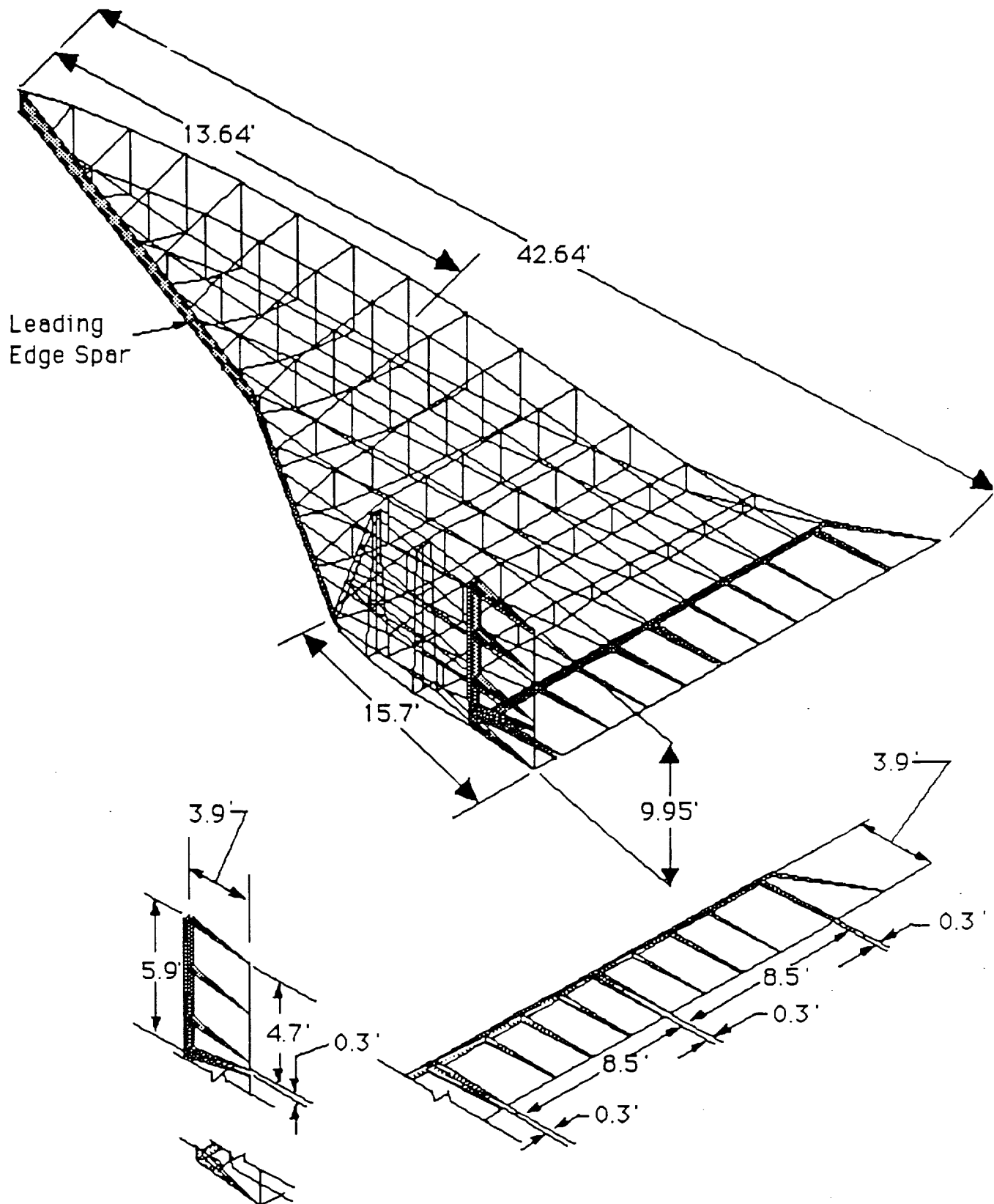


Figure 10-1 Wing Structural Drawing

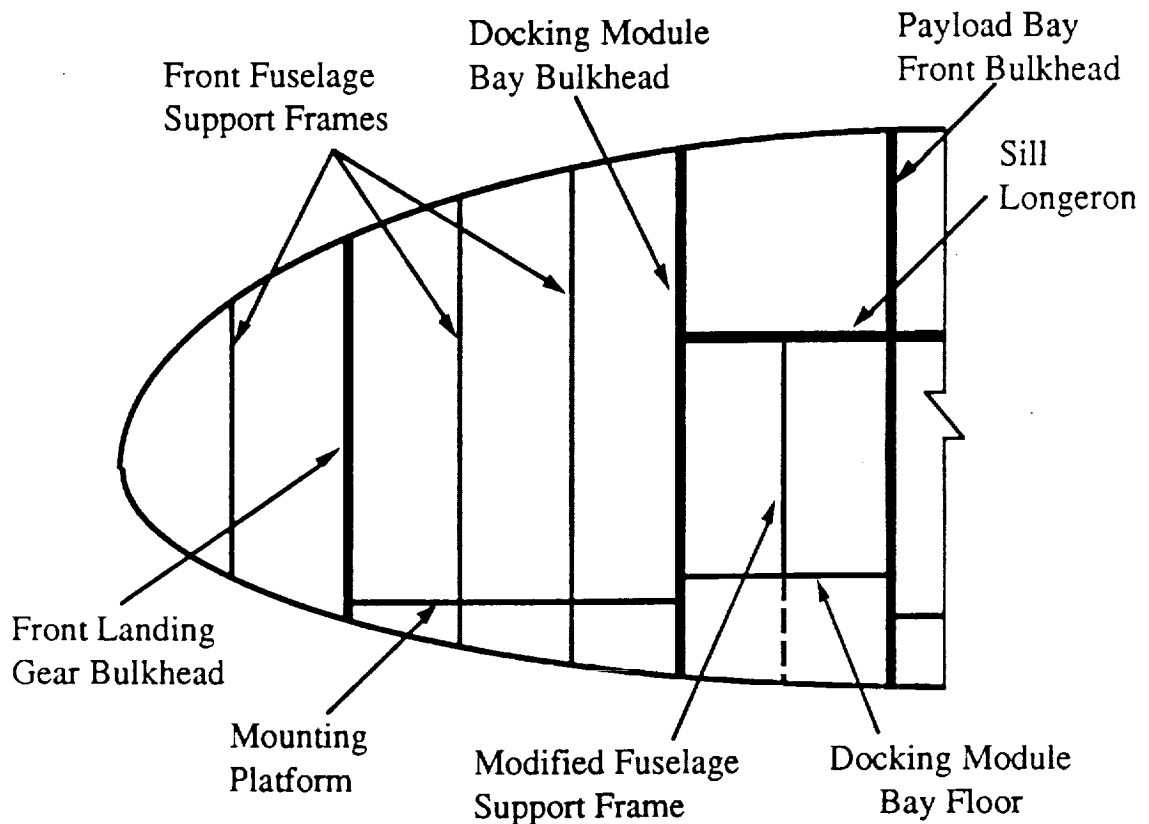


Figure 10-2. Front Fuselage Side-view

10.2.2 Fuselage Skin/Stringer

The entire front fuselage skin would be 2219 aluminum with stringers machined integrally in the skin. The integral skin/stringer technology is similar to what is currently used for the space shuttle skin. (Ref. 10.2) Using this method would reduce fastener points and weight, ensure skin to stringer integrity, and utilize an already existing system of machining and production. The preliminary design dimensions for the skin would be 0.0625" thick with 0.25" wide by 0.50" high stringers located 6.0" on center (see Figure 10-3). The TPS would be bonded to the outside of the skin/stringer combination.

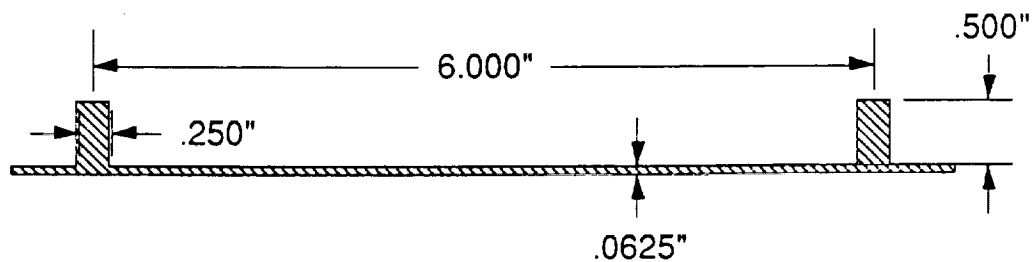


fig. 10-3. Skin/Stringer Combination

10.2.3 Front Fuselage Support Frames

The front fuselage support frames were designed similar to conventional aircraft and the space shuttle. (Ref. 10.2, 10.4) The frames have an aluminum I-beam cross-section (see fig. 10-4), to provide the necessary strength in the radial direction. Longitudinally, the support frames would be connected to the stringers of the skin/stringer combination. This would assure definite fastening to the skin and provide longitudinal strength and stiffness. Additional longitudinal strength may be determined

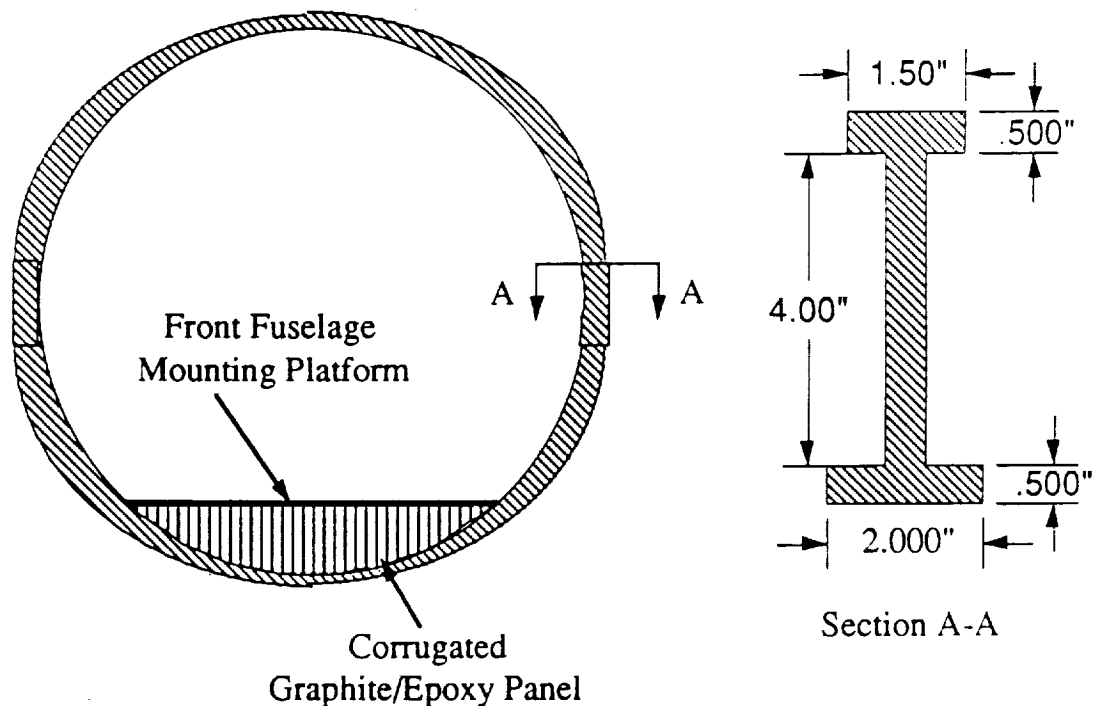


Figure 10-4. Front Fuselage Support Frame and Cross-Section

necessary after structural analysis is completed using a 3-dimensional finite-element method. Refer to vol. 3 for final design. More longitudinal stringers and/or an interior skin may be added to provide the additional strength. The support frames will be located at four foot intervals from the nose of the vehicle except where a bulkhead is required. This results in three support frames (see Figure 10-2).

10.2.4 Docking Module Bay and Doors

The docking module bay would be located directly in front of the payload bay (see Figure 10-2). Bulkheads would be placed at both ends of the bay to provide support to the bay and ensure satisfactory sealing of the bay doors. In addition, the sill longerons and corner longerons would extend into the docking module bay from the payload bay (see Figure 10-2). The payload bay forward bulkhead was used for the aft bulkhead in the docking module bay. The docking module bay doors would be constructed of graphite/epoxy and be the same design as the payload bay doors. The interior floor of the docking module bay would be fastened to both bulkheads and also have a support structure beneath it. The floor would be placed 4.0 feet above the bottom of the vehicle, be flat, and constructed of 0.50" thick aluminum honeycomb (see Figure 10-2). This floor would also add to the rigidity of the front fuselage. In the event that docking to Space Station Freedom is not required the bay has been designed to accommodate other types of miscellaneous payload. This was the primary reason for designing the docking module bay with a flat floor.

10.2.5 Modified Support Frame

A modified support frame was designed to allow access to the docking module bay (see Figure 10-5). The frame would be essentially a front fuselage support frame with its upper half removed. It is connected to the sill longerons which provide the major longitudinal support in the docking module bay and mid-fuselage. Tubular members between the bay floor and the support frame would provide the strength needed for the floor and docking module support structure. The tubular members would be made of 2219 aluminum and have the same cross-section as the tubular members in the payload bay truss frames (see Figure 10-6).

10.2.6 Front Fuselage Bulkheads

Two bulkheads constructed of 2219 aluminum would be located in the front fuselage (see Figure 10-2). The bulkheads have a preliminary design of 0.50" thick with four horizontal and four vertical stringers integrally machined into both sides. This preliminary design account for approximately 50% of the front fuselage weight and will be reduced after further analysis (see Vol.

3). The stringers would be T-section members identical to the T-section members in the payload bay truss frames (Figure 10-7). The docking module bay bulkhead would be located 20 ft. from the nose cone and would provide support for the bay and bay floor. This bulkhead would also help ensure a tight seal of the bay doors. The front landing gear bulkhead would be located 8 ft. from the nose cone. This bulkhead would provide the major mounting point for the front landing gear and support the front fuselage mounting platform.

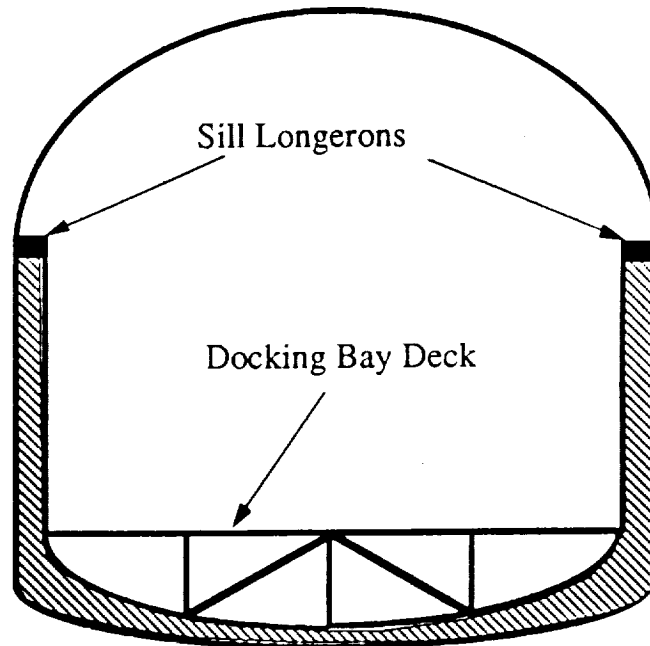


Figure 10-5 Modified Support Frame

10.2.7 Front Fuselage Mounting Platform

A mounting platform is necessary to provide the avionics, guidance, and navigation systems with a stable, vibration free structure. The platform would span the distance between the front landing gear bulkhead and the docking module bay bulkhead at a height of 3.0 ft. above the vehicle bottom (see Figure 10-2 and 10-4). Additional support for the platform would be corrugated graphite/epoxy panels between the front fuselage support frames and the platform. The main function of these panels will be to reduce vibration, but they would also contribute to the strength of the platform. Composition of the mounting platform itself will be aluminum honeycomb.

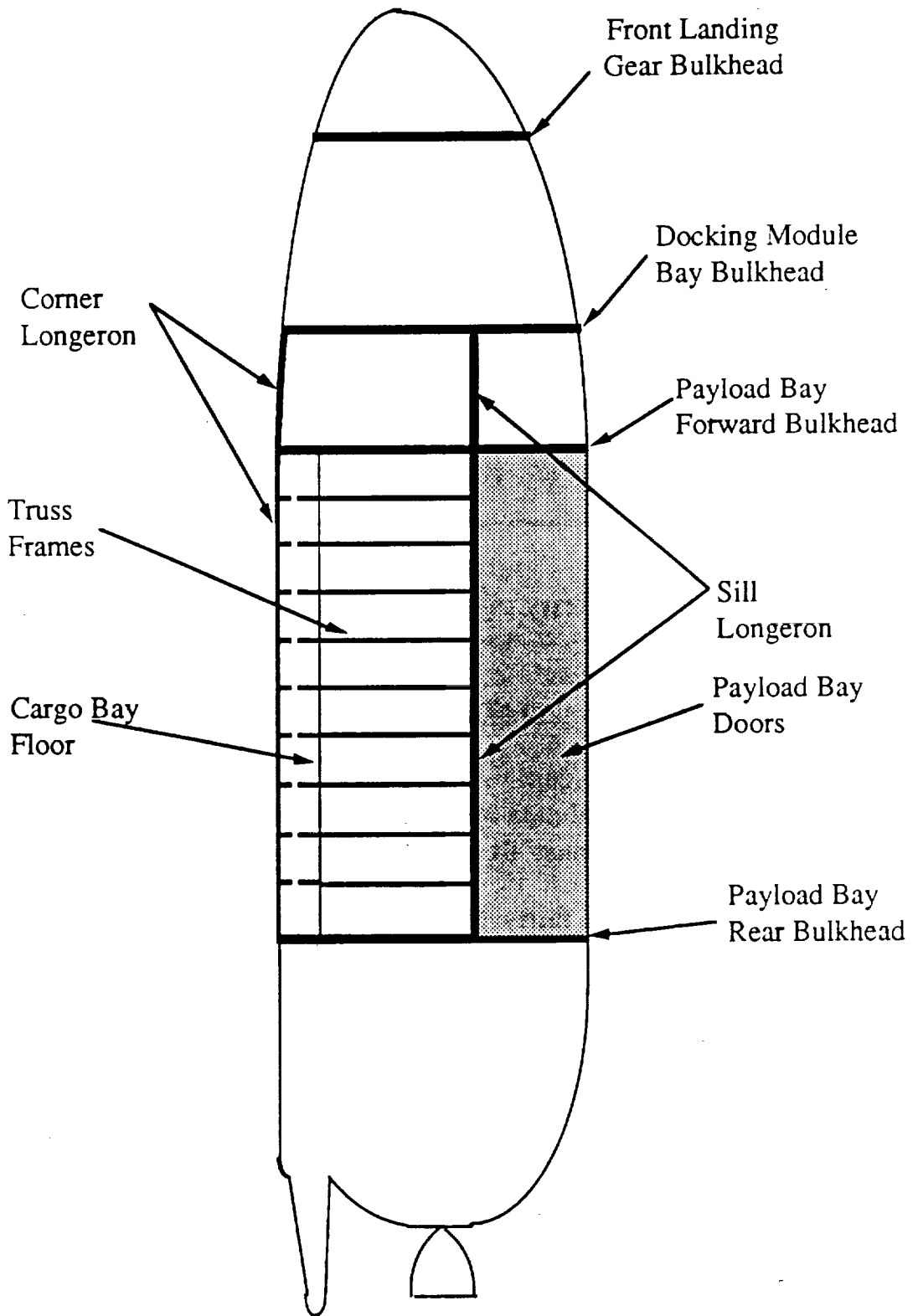


Figure 10-6 Mid-Fuselage Components

10.2.8 Weights of Front Fuselage Components

The following table lists the preliminary design weights of the major structural components in the front fuselage.

Table 10-1 Front Fuselage Component Weights

Front fuselage support frames (3 total)	630 lbs
Front fuselage skin/stringer	1200
Front landing gear bulkhead	1100
Front landing gear	800
Front fuselage mounting platform	200
Docking module bay support frame	190
Docking module bay bulkhead	2100
Docking module bay doors (2 total)	220
Docking module bay floor	60
	<hr/>
	6500 lbs

10.3 PAYLOAD BAY AND MID-FUESELAGE STRUCTURAL DESIGN

10.3.1 Design Dimensions and Requirements

The basic structural design requirement for the payload bay and mid-fuselage is that a pressurized logistics module (PLOG) and an unpressurized logistics module (UNPLOG) must fit inside the bay. The structure must also be able to accomplish its purpose of providing rigidity to the vehicle. The bay will be thirty feet in length and have a diameter of 16.6 feet. The depth of the bay from the still longerons to the payload bay floor would be 9.8 feet (see figure 10-6).

10.3.2 Payload Bay Design

The requirement of a cylindrical cargo bay with access from the top, in the mid-section of the vehicle where wing and fuselage bending moments are present, negated the use of support frames as used in the semi-monocoque construction of the forward fuselage. To maintain structural rigidity of the vehicle and the payload bay while also providing space for the bay, a truss frame was incorporated below the payload bay floor. The truss frame is very similar to the design currently utilized by the shuttle.(Ref. 10.3) Tubular 2219 aluminum members, T-section 2219 aluminum members, and graphite/epoxy shear panels would be used to construct the truss

frames (see figure 10-7). The truss frames would be placed at three foot intervals along the length of the mid-fuselage, which gives a total of nine truss frames. The tubular members would have an outside diameter of 1 inch and a wall thickness of 0.125 inches (see Figure 10-8). T-section members would be 1 inch in height and width with a thickness of 0.125 inches (see Figure 10-8). The composite shear panels would have a thickness of 0.25 inches to provide for sufficient distribution of transverse and shear loads. All dimensions are preliminary design estimates and are subject to change. Refer to Volume 3 for final design dimensions.

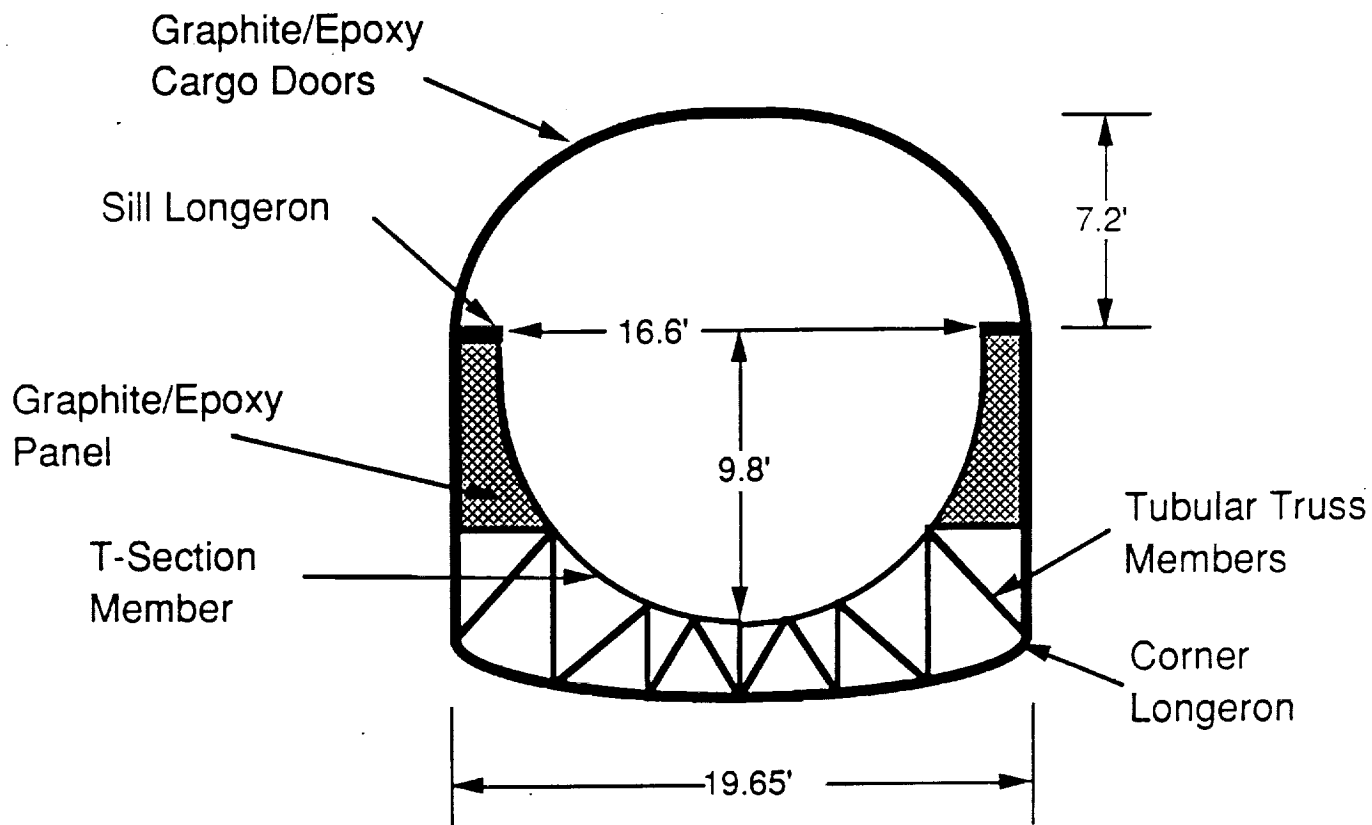


Figure 10-7 Payload Bay Truss Frame

Truss frames would provide the shape of the fuselage, provide the base for the payload bay floor, and distribute transverse loads applied to the fuselage. Longitudinal loading and fuselage bending moments, however, would not be sufficiently distributed by these frames. The fastening of sill longerons and corner longerons to the truss frames completes this function. The sill longerons would run longitudinally along the door/fuselage junction and also serve as a mounting point for the payload bay door hinges. They would use a

preliminary rectangular cross-section of 2 inches by 6 inches (see Figure 10-9). In addition to the two sill longerons there would be two corner longerons. The corner longerons would be located at the corner formed by the bottom of the mid-fuselage and the vertical skin panels. They would have a preliminary L cross-section, 1 inch by 1 inch with a thickness of 0.125 inches (see Figure 10-9). Both longerons will be fabricated from 2219 aluminum.

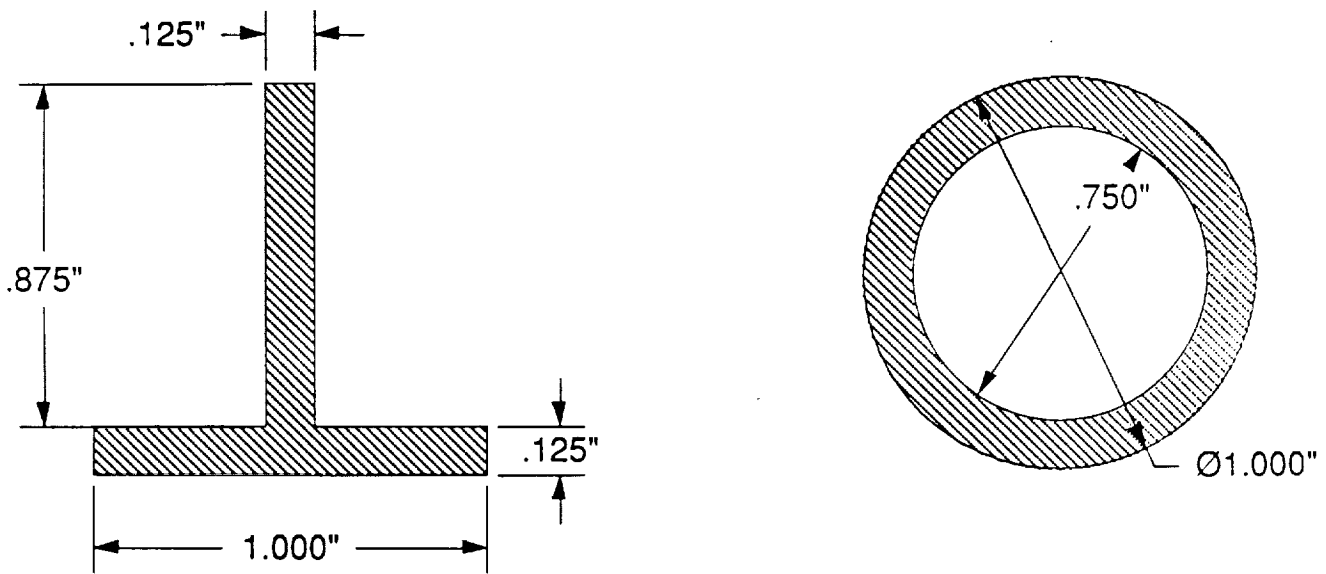


Figure 10-8 T-Section and Tubular Truss Members

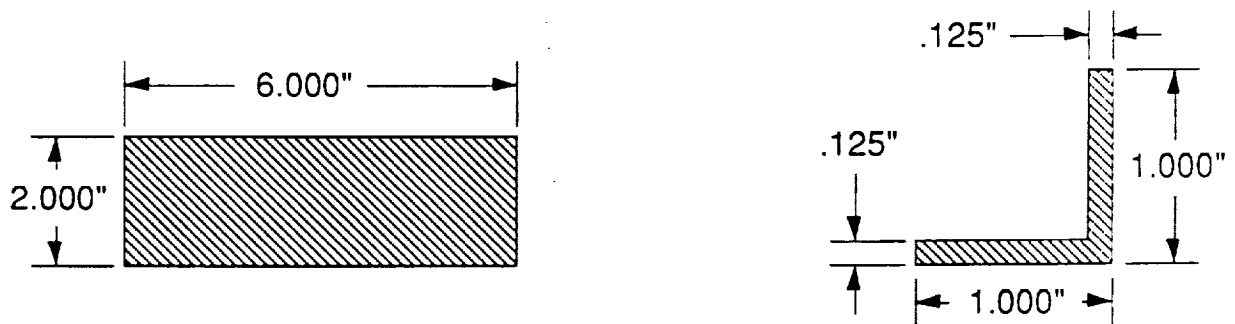


Figure 10-9 Sill Longeron and Corner Longeron Cross-Sections

10.3.3 Payload Bay Doors

The payload bay doors span the entire length of the payload bay and when fully opened provide easy access to the payload bay. Each has an approximate radius of 8.8 feet and a height of 7.2 feet above the sill longerons. Their primary construction would be of a graphite/epoxy sheet permanently bonded to a frame constructed of graphite/epoxy stringers. The stringers would run transversely from

top to bottom edge of the door and would be spaced at two foot intervals along the entire length of the door. The thickness of the sheets would be 0.125 inches and the stringers would utilize a preliminary rectangular cross-section, 0.5 by 0.25 inches. Composite materials were being employed exclusively in the design of the payload bay doors because of their low coefficients of thermal expansion in comparison to metal substitutes. Low coefficients of thermal expansion promote good sealing characteristics when enduring the extreme temperature differences in going from earth to orbit and back. The CRV payload bay door hinges would be constructed of the composite Inconel for the same reasons. Inconel was chosen because it is used on the space shuttle hinges also.(Ref. 10.2) Although composite materials provide very good strength to weight characteristics, the structure was designed to carry major structural loads away from the payload bay doors. This would decrease chances for failure of the doors or an unsatisfactory seal, either of which could result in damage to the payload.

10.3.4 Payload Bay Floor

The floor of the payload bay would be mounted directly on top of the semi-cylindrical area formed by the truss frames. This floor would be of an aluminum honeycomb design with a preliminary thickness of 0.5 inches. The floor must withstand loadings from the payload and will also carry structural loads from the mid-fuselage. The honeycomb design is ideal for these purposes.

10.3.5 Fuselage Skin/Stringer

The fastening of stringers to the truss frames and skin will be accomplished as is done in the forward fuselage, by machining the skin and stringers as one unit (see Figure 10-3). The skin/stringer combination will be used on the bottom of the mid-fuselage and on the vertical sides of the fuselage above the wing/fuselage junction.

10.3.6 Payload Bay Forward Bulkhead

Because the mid-fuselage is fastened directly to the forward fuselage, this connection should be rigid and provide a means by which large loadings can be dissipated between the forward fuselage, mid-fuselage, and the payload bay. This is accomplished by using an aluminum bulkhead to interface between the forward and mid-fuselage. This bulkhead, the payload bay forward bulkhead, will be

machined from aluminum to the exterior dimensions of the fuselage minus the thickness of the skin/stringer combination. In addition, there will be four horizontal and four vertical T-section stringers machined integrally into each side of the bulkhead. The preliminary maximum thickness of the bulkhead will be 0.5 inches and the T-section stringers will have identical dimensions to the T-section members in the truss frames (see Figure 10-8). This results in a very bulky, heavy structural element that accounts for approximately 13% of the weight between the forward and mid-fuselages. This represents the preliminary design only. For the final dimensions see Volume 3.

10.3.7 Mid-fuselage Weights

The following table lists the weights of the major structural components in the mid-fuselage.(Ref. 10.4)

Mid-fuselage truss frames (9 total)	900 lbs.
Payload bay forward bulkhead	2400
Sill longerons (2 total)	1100
Corner longerons (2 total)	20
Main landing gear	2400
Mid-fuselage skin/stringers	1550
Payload bay doors (2 total)	1000
Payload bay interior skin	350
	<hr/>
	9720 lbs.

10.4 AFT FUSELAGE STRUCTURAL LAYOUT

The aft fuselage structure consists of an outer shell, an outer skin, and an internal thrust structure. The aft fuselage is 19.6 feet wide, and 19.65 feet high where the aft fuselage meets the forward fuselage and is eighteen feet in length. Ten feet forward of the base heat shield the fuselage structure begins to curve until the cross-sectional shape is roughly circular. The three mid horizontal support frames would attach to the base heat shield which is five feet in diameter. A movable body flap would be attached to the bottom of the aft fuselage approximately 4.5 feet forward of the base heat shield. The body flap would be roughly ten feet long and can be deflected through 30 degrees. The aft fuselage supports and interfaces with the mid fuselage, four wing spars, the body flap, the CRV/launch vehicle interface, the orbital maneuvering system, and if

necessary a vertical fin. The aft fuselage shell structure transfers the launch loads to the mid fuselage and houses the propulsive subsystem (i.e., fuel tanks and feed systems).

The aft fuselage would consist of integrally machined aluminum TA 2219 skins and frames. The aft fuselage outer shell would be fully machined to decrease manufacturing costs. Diffusion bonded titanium or bonded boron epoxy laminates could be employed in the highly loaded areas if additional strength is needed. In the less highly loaded areas, conventional aluminum skin-stringer construction was utilized. The aft fuselage forward bulkhead closes off the aft fuselage from the mid fuselage with the payload bay and the base heat shield protecting the aft fuselage and its interior equipment from the re-entry environment. The aft fuselage skin could be either aluminum TA 2024 with honeycomb construction approximately one inch in thickness or aluminum TA 2219 approximately one-sixteenth inch thick. If a vertical fin is employed it would utilize the aluminum honeycomb skin construction. The combined weight of the aft fuselage shell structure and the thrust structure (including skin) would be approximately 10,000 pounds.

The major structural assemblies would be mated and joined together with rivets and bolts. The mid fuselage would be joined to the aft fuselage primarily with shear ties, with the mid fuselage skin overlapping the bulkhead caps. The wing would also be attached to the aft fuselage primarily with shear ties, except in the areas where the wing spars carry-through. These wing spars would be attached to the aft fuselage supporting frames with tension bolts. The body flap would attach to the bottom of the aft fuselage by four rotary actuators. If needed, a vertical fin could be attached to the aft fuselage with bolts which work in both shear and in tension.

Initially the CRV design utilized a vertical fin to facilitate stability and control of the spacecraft. The vertical fin, however, was dropped in favor of using winglets. This did not have a large effect on the overall structural weight of the vehicle, since, there were other benefits involved in this design change that made it the more feasible of the two choices. The final CRV structural layout does not include a vertical fin, but the structural design and analysis involved with a vertical fin was considered. This will allow easy implementation of a vertical fin in the event that the design reverts back to a shuttle type layout in the future. Figure 10-10 shows the

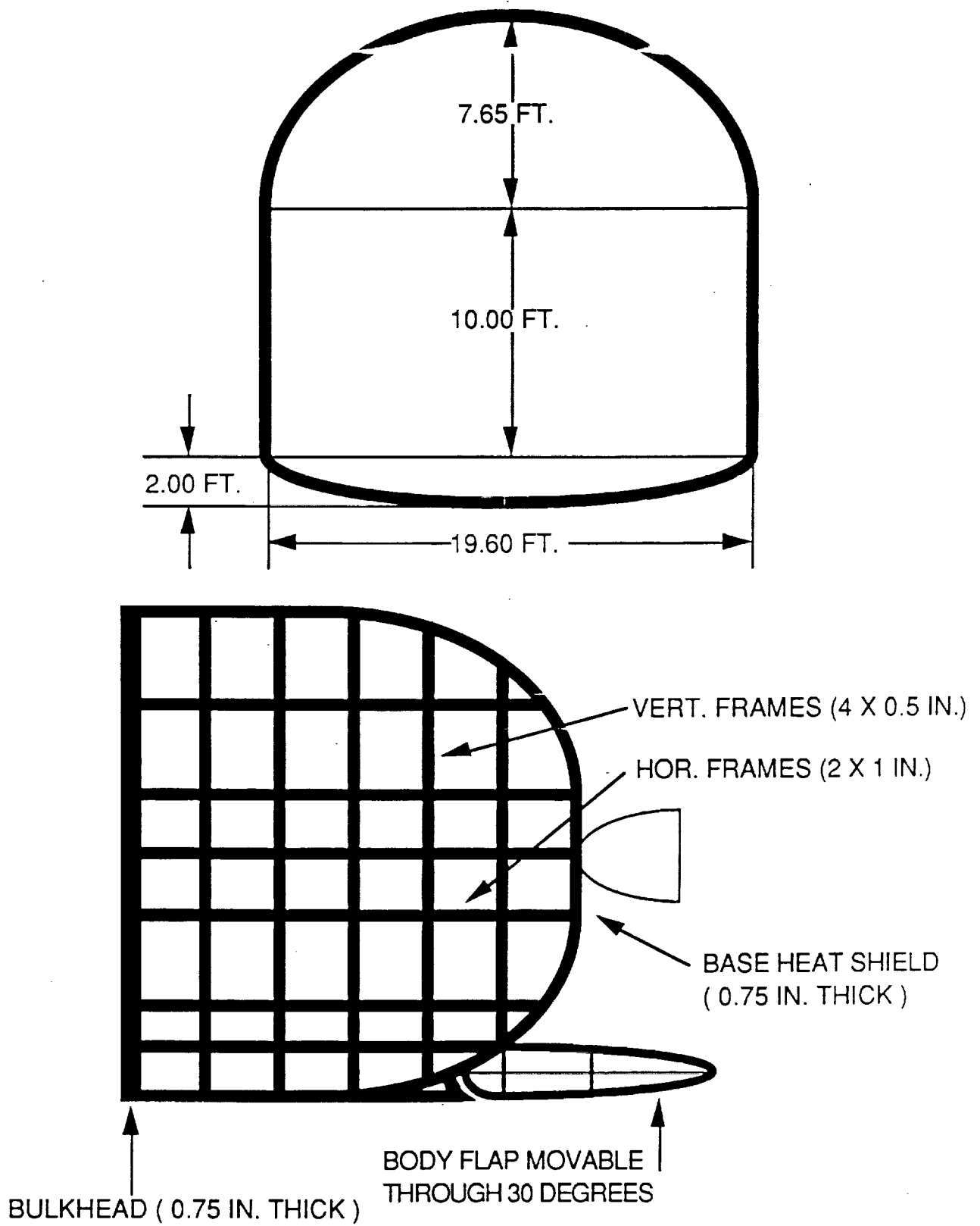


Figure 10-10 AFT FUSELAGE STRUCTURAL DIMENSIONS

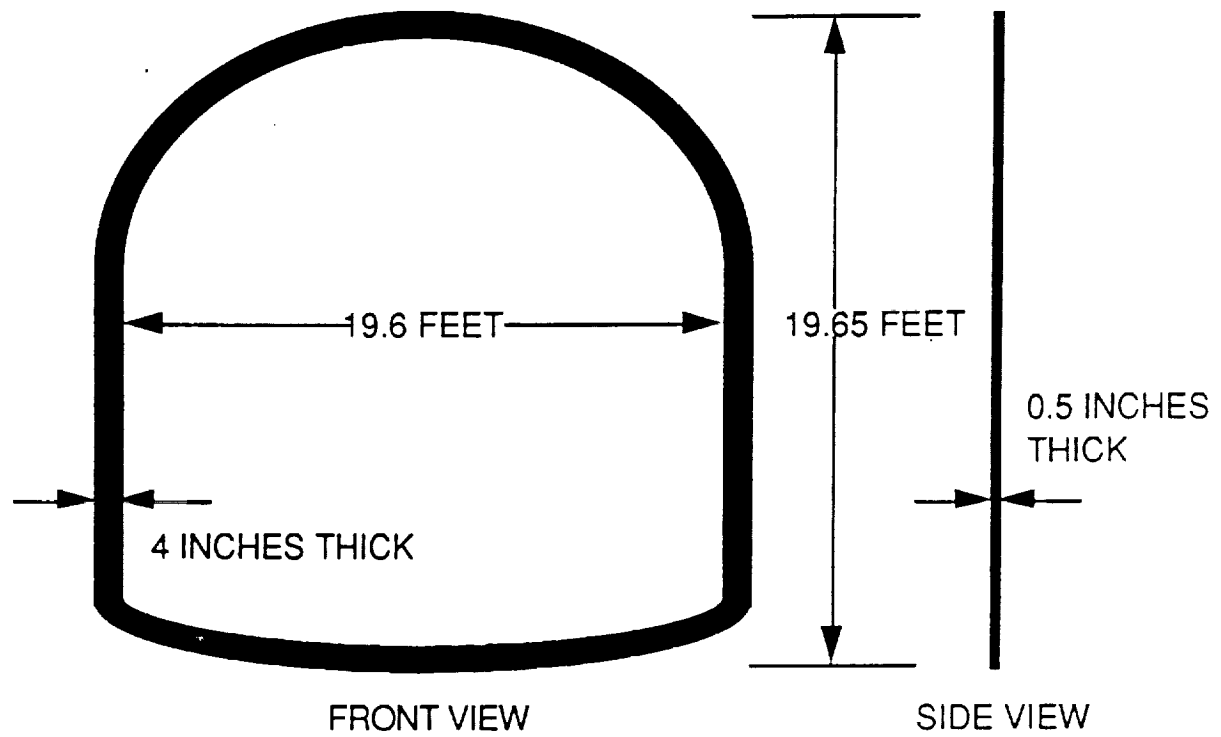
structural layout of the aft fuselage along with a cross-sectional view of the aft fuselage at the mid fuselage interface.(Ref. 10.2)

10.4.1 Horizontal and Vertical Support Frames

The aft fuselage support structure consists of five vertical support frames and nine horizontal support frames. The vertical support frames were all placed three feet apart with the first vertical frame located three feet aft of the aft fuselage forward bulkhead and the last vertical frame located three feet forward of the base heat shield. The vertical frames act as stringers along the length of the aft fuselage. These stringers would be integrally machined directly to the aft fuselage skin and welded to the horizontal frames. Each horizontal support frame would be attached to the forward bulkhead at both ends; except for the two centerline frames, the top frame, and the bottom frame, which all attach to the base heat shield at one end. The horizontal frames would be located at varying distances in the vertical direction depending on where structural support is needed. The cross-sectional shape of the horizontal frames was not fixed, however, for structural integrity, the cross-sectional area of these frames are planned to be at most 0.014 square feet (2 square inches) with a T-shape section. As with the vertical frames, the horizontal frames are to be machined directly to the aft fuselage skin and welded to the vertical frames. Figure 10-11 shows different views of the vertical and horizontal aft fuselage support frames. The dimensions given in the diagrams are for the three forward vertical frames and the two horizontal frames on either side of the centerline of the vehicle. The remaining two vertical frames are approximately circular in shape with the smaller diameter frame being closer to the base heat shield. The horizontal frames were all the same shape with varying sizes depending on the vertical location of the individual frame. The vertical and horizontal frames comprise the primary structure of the aft fuselage. The main purpose of these aft fuselage support frames is to transmit the launch loads to different sections of the mid fuselage and to support the CRV propulsion subsystem.

10.4.2 Aft Fuselage Forward Bulkhead and Base Heat Shield

The aft fuselage forward bulkhead was positioned at the front of the aft fuselage structure. This bulkhead would be of solid, aluminum TA 2219 construction and would have a constant thickness. The forward bulkhead could be reinforced with machined diffusion-



VERTICAL FRAME

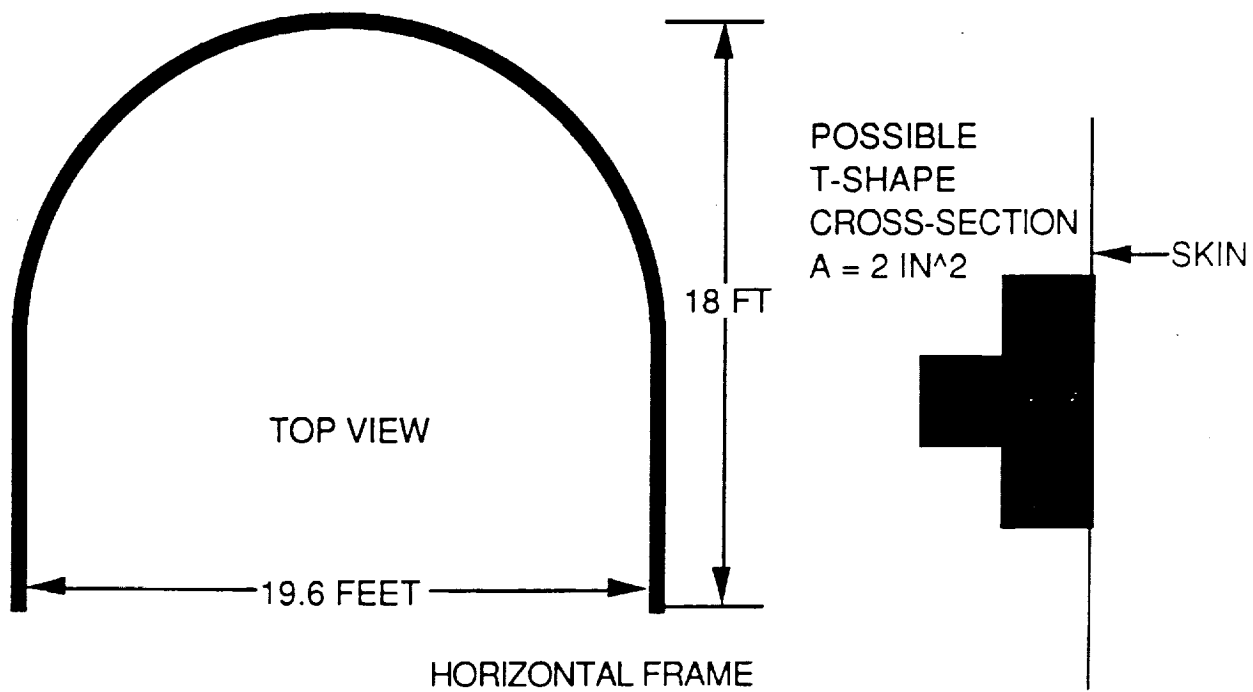


Figure 10-11 AFT FUSELAGE FRAMES

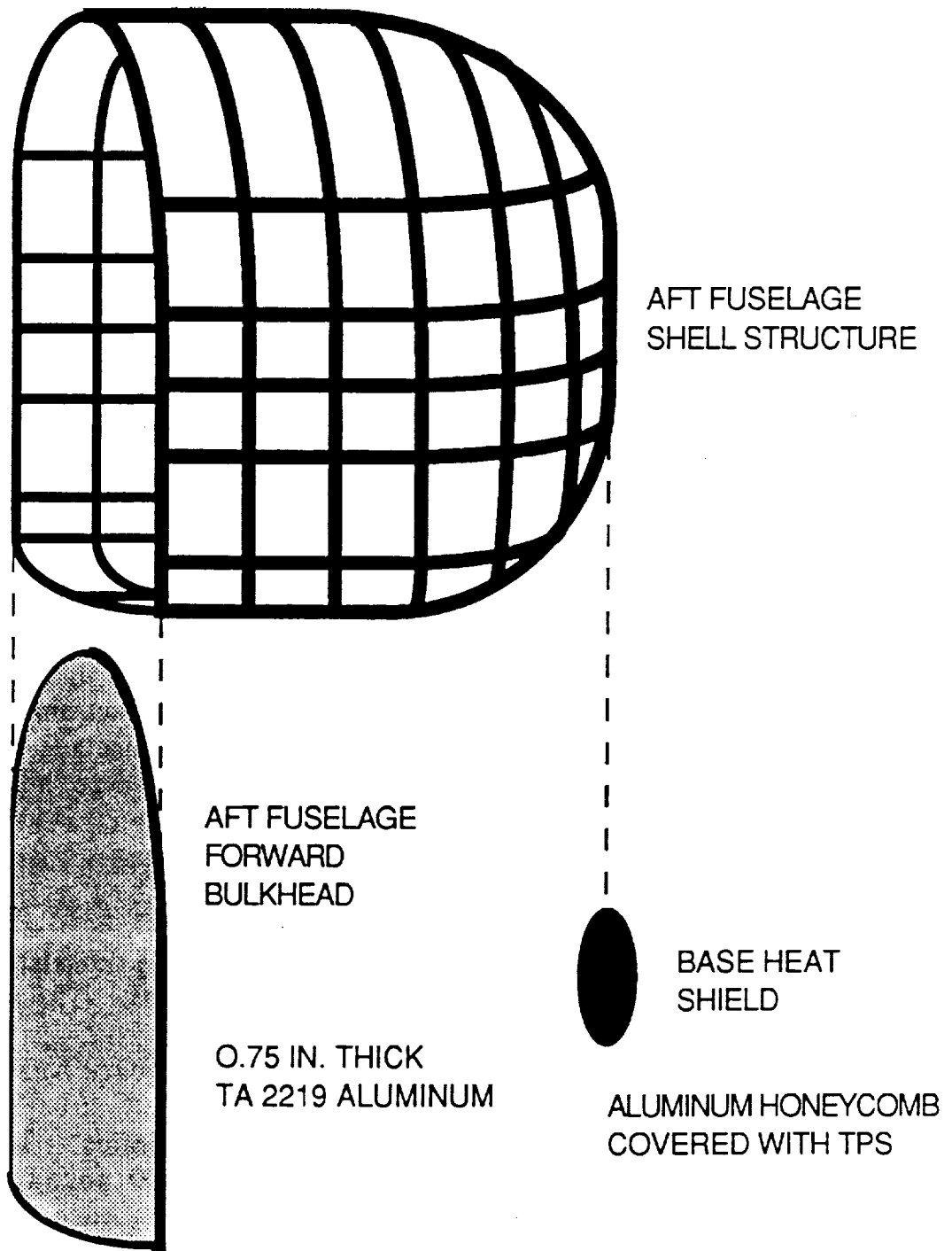


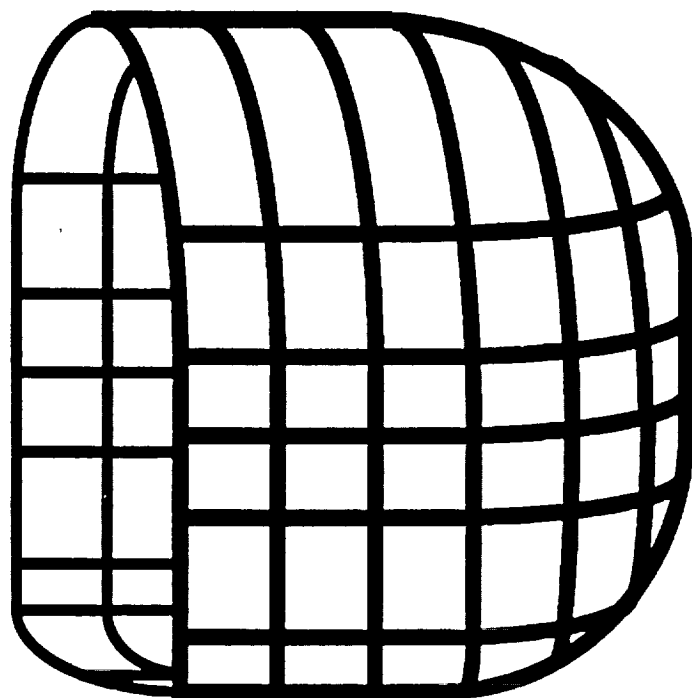
Figure 10-12 FORWARD BULKHEAD AND BASE HEAT SHIELD

bonded titanium members for increased strength or weight reduction. The bulkhead is the main interface between the mid fuselage and aft fuselage sections of the CRV. It also interfaces with the payload bay doors, the thrust structure, and the aft fuselage horizontal support frames. The aft fuselage forward bulkhead joins the mid and aft fuselage sections primarily through the use of shear ties. Welding would also be used locally for fitting attachments and the propulsion subsystem thrust structure would be bolted to the bulkhead at five different locations.

The base heat shield would be located at the aft end of the CRV and is five feet in diameter. The centerline of the CRV coincides with the geometric center of the base heat shield. This heat shield would be of machined aluminum and honeycomb construction covered with TPS to protect it from the intense heat experienced during reentry. The two centerline horizontal aft fuselage frames, the top aft fuselage frame, and the bottom aft fuselage frame would all fastened to the base heat shield by welding methods. The base heat shield would be responsible for protecting the aft fuselage structure and its interior equipment from the ascent and re-entry environments encountered during flight. Figure 10-12a and 10-12b shows the aft fuselage shell structure along with the forward bulkhead and the base heat shield.

10.5 THRUST STRUCTURE DESIGN

The aft fuselage thrust structure is a multi-unit assembly consisting of members that are bolted together and to the outer shell. The main purpose of the thrust structure is to transmit the orbital maneuvering system thrust loads to the aft and mid fuselage shell structures. The thrust structure also helps react the shell structure loads with all interface loads carried through mono-ball joints. The maximum thrust load created by the OMS engine is 6,000 pounds, which is small compared to the launch and landing loads encountered by the vehicle. Because these thrust loads are small, the thrust structure is constructed of aluminum members. These members can be reinforced with bonded boron epoxy laminates for strength, stiffness, and weight reduction if needed. There are five hardpoints on the thrust structure bolted to the aft fuselage forward bulkhead and there are five hardpoints bolted to the aft fuselage aft bulkhead. This aft bulkhead is similar to the forward bulkhead in design (aluminum TA 2219) and is welded to the vertical frame just forward of the base heat shield. The bulkhead has a five foot



AFT FUSELAGE SHELL STRUCTURE

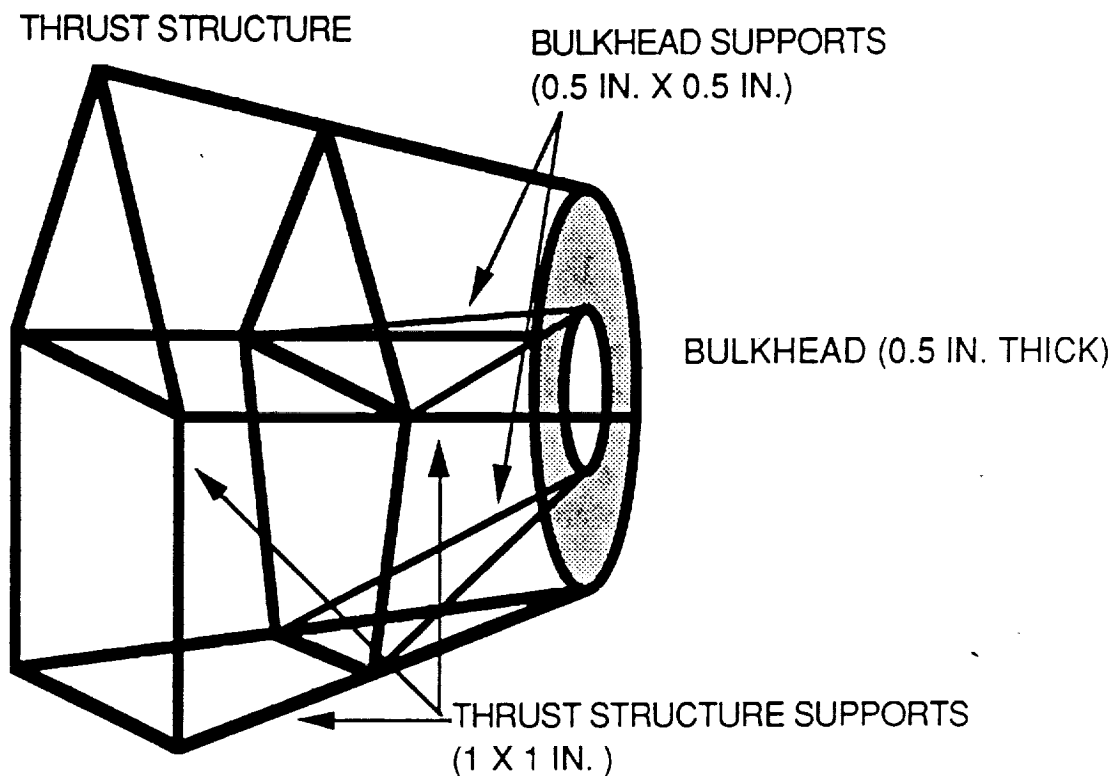


Figure 10-13 AFT FUSELAGE FRAME AND THRUST STRUCTURE

diameter hole for the propulsive system propellant feed lines. The main thrust structure supports should have cross-sectional areas of at most 0.007 square feet (1 square inch). There are also four bulkhead supports attached to the inner radius of the aft bulkhead, each should have cross-sectional areas of approximately 0.002 square feet (0.25 square inches). Figure 10-13 shows the aft fuselage shell and thrust structures. From this figure it can be seen how the thrust structure can be positioned in the aft fuselage shell structure.(Ref. 10.2)

The weight of the aft fuselage thrust structure is approximately 3,400 pounds. This value includes the aft fuselage aft bulkhead and all the supporting thrust structure members.

10.6 LANDING GEAR

The landing gear have been designed in such a manner so that the rear set will fold inward into the fuselage body and the front will buckle up into the nose. The rear sets have four tires each at 2.5 ft diameter, while the front landing gear has two tires at 1.8 ft diameter. The tire diameter in both front and back are constrained by the tight areas in which they recess upon their retraction. Landing gear dimensions and layout are presented in the following Figures 10-14 and 10-15

10.7 CRV/LAUNCH VEHICLE INTERFACE DESIGN

The CRV/launch vehicle interface is an eighteen member, eight hard point truss designed to mate the CRV to the launch booster. The interface consists of two circular support rings, one attached to the middle booster of the launch vehicle and the other attached to the aft fuselage vertical frame just forward of the base heat shield and to the aft bulkhead. Each support ring has eight attachment hardpoints located at equal distances around the ring and sixteen vertical members are attached to the rings by welding at these hardpoints. The interface is constructed of aluminum TA 2219 and can be reinforced with bonded boron epoxy laminates if additional strength is needed or if a weight reduction is necessary. The bottom support ring is eighteen feet in diameter and the vertical supports extend inward at small angles to attach to the top support ring which is 14.7 feet in diameter. the vertical distance between the two support rings is fifteen feet. The design for this interface is very simple due to the fact that each interface will be used for only one mission. The CRV

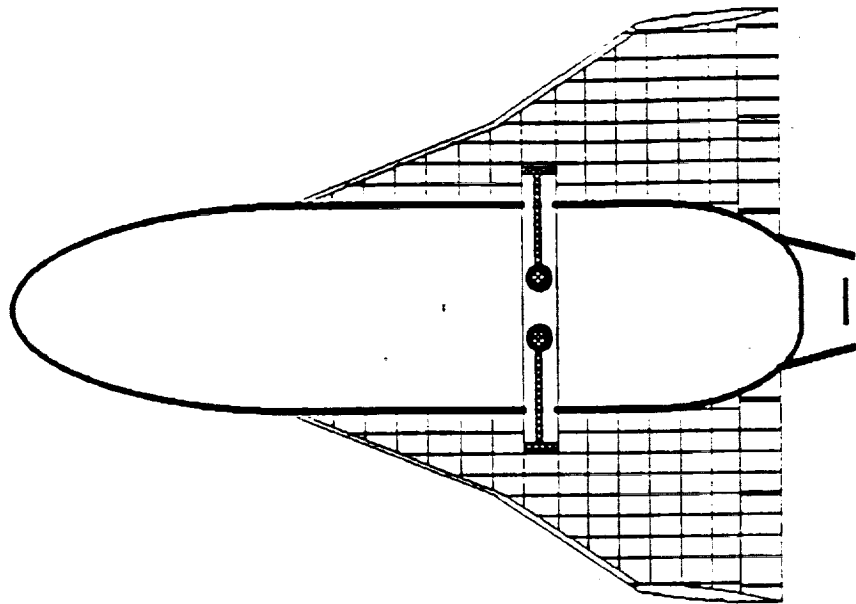


Figure 10-14 BOTTOM VIEW GEAR PLACEMENT

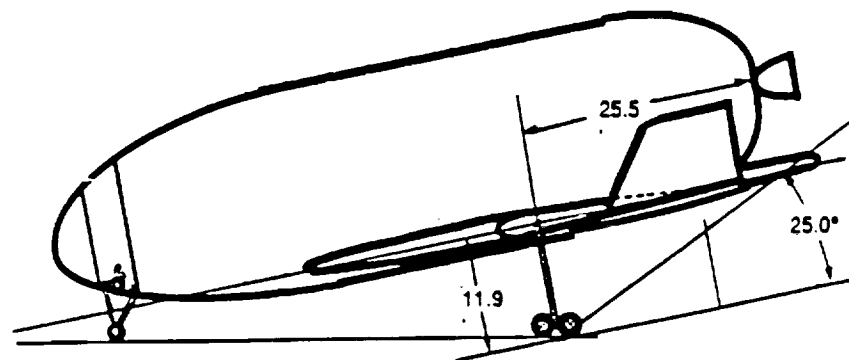
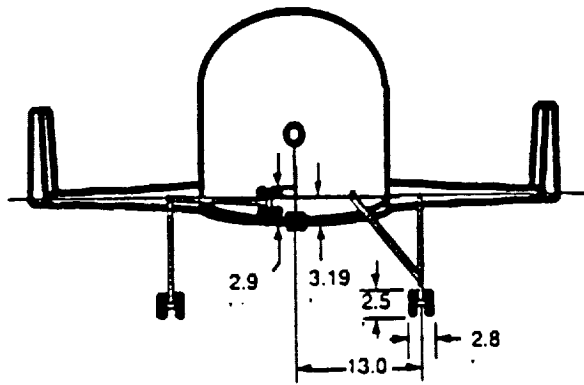


Figure 10-15 FRONT AND SIDE VIEWS GEAR DEPLOYED

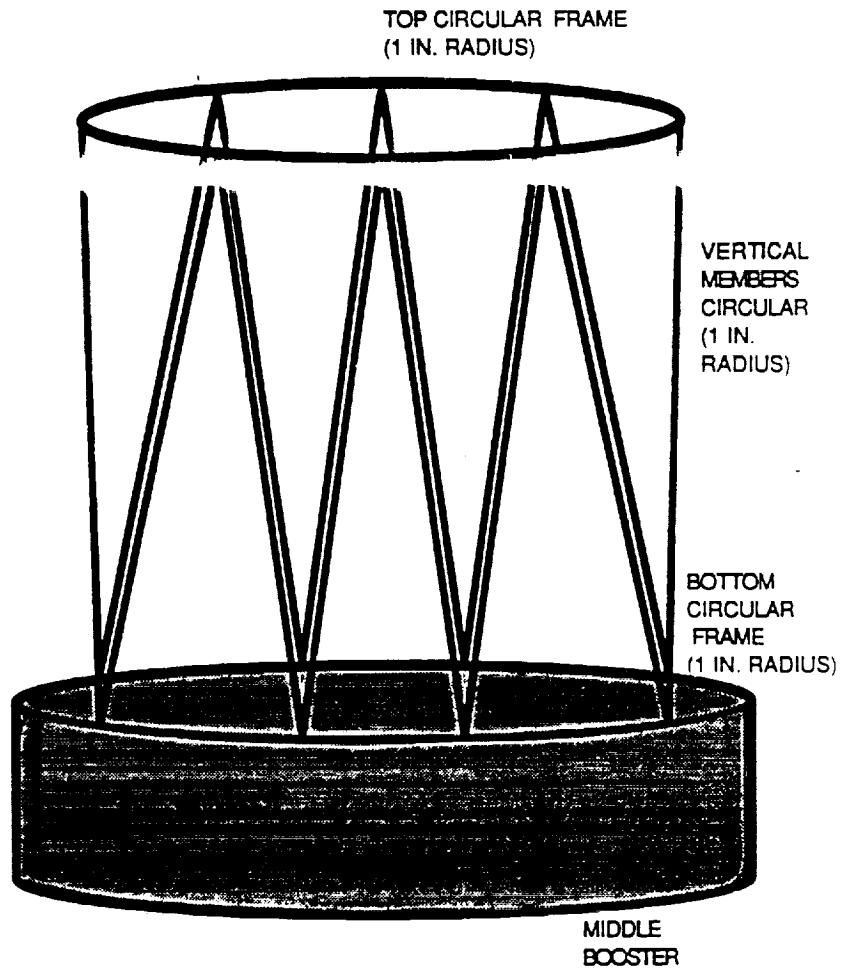


Figure 10-16 CRV/LAUNCH VEHICLE INTERFACE - SIDE VIEW

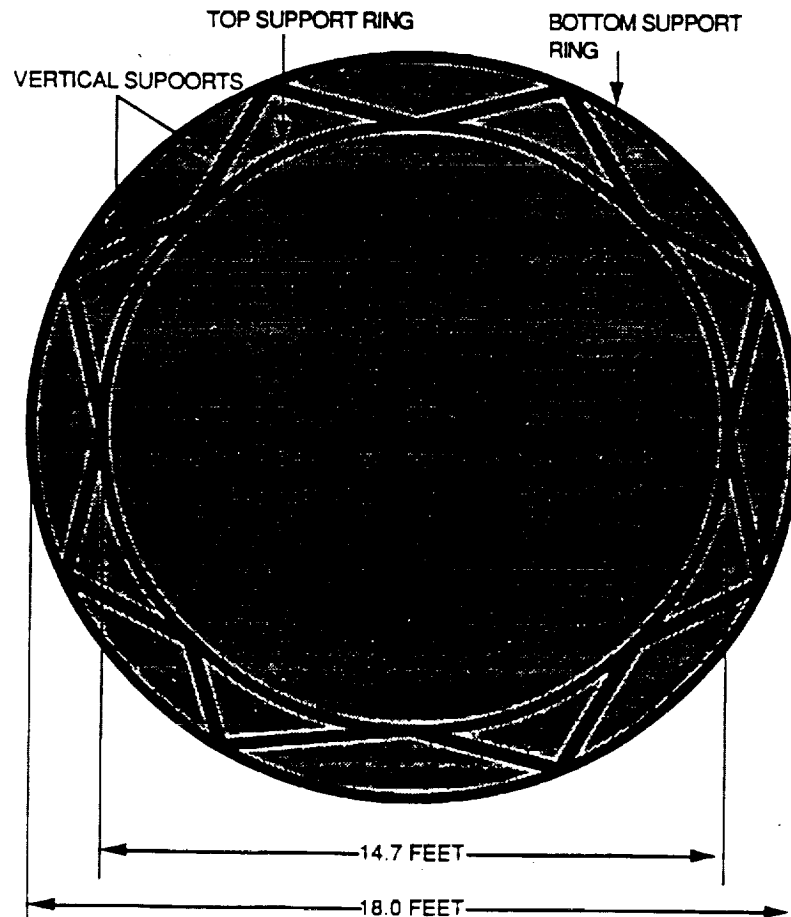


Figure 10-17 CRV/LAUNCH VEHICLE INTERFACE - TOP VIEW

will detach from the launch vehicle by employing explosive pyrotechnic pins to attach the CRV to the interface. After detachment the damaged interface will re-enter the atmosphere with the launch vehicle. Figure 10-16 shows a side view of the CRV/launch vehicle interface and Figure 10-17 shows a top view of the interface. It is easier to see the angles of the vertical members from this top view.

The weight of the CRV/launch vehicle interface is approximately 1,400 pounds.

10.8 DEBRIS PROTECTION SYSTEM

Debris protection for the CRV has been studied, but the necessity and type is yet to be finalized. The basic configuration would consist of a thin sheet of impact absorbing material bonded between the TPS and the aluminum skin. If debris does impact the TPS and puncture it, the layer of debris protection will absorb the kinetic energy of the debris and fragment it into smaller pieces which will not have enough energy to damage the aluminum skin. Ideally, the best material to use would be beryllium because of its high strength to weight ratio. Second to beryllium are honeycomb type materials that rely on multiple layers to remove energy from the debris.(Ref. 10.5)

Types of space debris can basically be divided into two broad categories, debris that can be detected and avoided and debris that will not cause significant damage to the vehicle. For smaller size debris, small particles and dust, the most feasible solution is to not include any debris protection. Most particles will be effectively stopped, slowed, or fragmented by the TPS. Replacing damaged TPS material and tiles as compared to covering the entire vehicle in a sheet of beryllium is much more cost effective. Perhaps the greatest reason for not including a debris protection layer is that the possibility of impacting space debris is extremely remote. A greater understanding of the probability involved should become available when the results of the LDEF(Long Duration Exposure Facility) are determined. Further study of debris protection will be completed next quarter, upon which recommendations will be made concerning the necessity of such a system.

10.9 STRUCTURAL ANALYSIS

Structural analysis of the mid-fuselage was accomplished by determining a distributed loading on the truss frame from the maximum dynamic pressure on the vehicle. Also included was a transverse loading determined from approximate wing moments. The truss frame was approximated as a two-dimensional pin-joint truss, with the sill longerons fixed. The analysis was performed using a Macintosh PC program entitled Truss Solver, which is currently used in the Structures I course, AEM 5515. Modification of the program was necessary to accommodate our entire truss. The sill longerons, the most rigid structural members, were fixed in one position to provide the required program boundary conditions.

The output from the program lists nodal displacements, bar forces, and bar stresses. With these, we used tensile yield values and critical buckling forces to determine the minimum safety factors in the members. Nearly all truss members were determined to be in compression, thus, the critical buckling force was our predominant constraint. Minimum safety factors determined for the tubular members were approximately two, while for the T-section members the minimum safety factors were approximately four.

The analysis of the truss frame included many approximations to allow the use of a 2-Dimensional program. Approximations that contributed to increasing the safety factors include fixed sill longerons and conservative applied wing moments. Approximations that contributed to decreasing the safety factors include neglecting the skin/stringer combination, neglecting the graphite/epoxy shear panels, using pin-joints, and neglecting vehicle angle of attack in determining applied dynamic pressure.

Structural analysis of the wing was performed by analyzing the third spar forward of the trailing edge as follows:(See Figure 10-18)

The load was calculated by multiplying the vehicle dry weight by a safety factor of 1.5 and taking 1/2 of this value for each wing. The distributed load was then calculated by dividing the load by the total length of the spars. The results of this analysis was that the structure failed under the previous combinations of cross sectional area and structural layout. This can be solved with a new combination of cross sections and by inserting diagonal members into the spars to more evenly distribute the load.

A preliminary structural analysis was performed on the aft fuselage section and also on the CRV/launch vehicle interface. An approximate static analysis was used to determine if the structural design is safe and if the weights and the structural dimensions are feasible. A safety factor of 1.5 was used throughout the analysis to account for the approximate methods used and the uncertainties in the numerical data.

Structural analysis of the third spar
forward from the trailing edge

nodes # 1 and #2 are locked

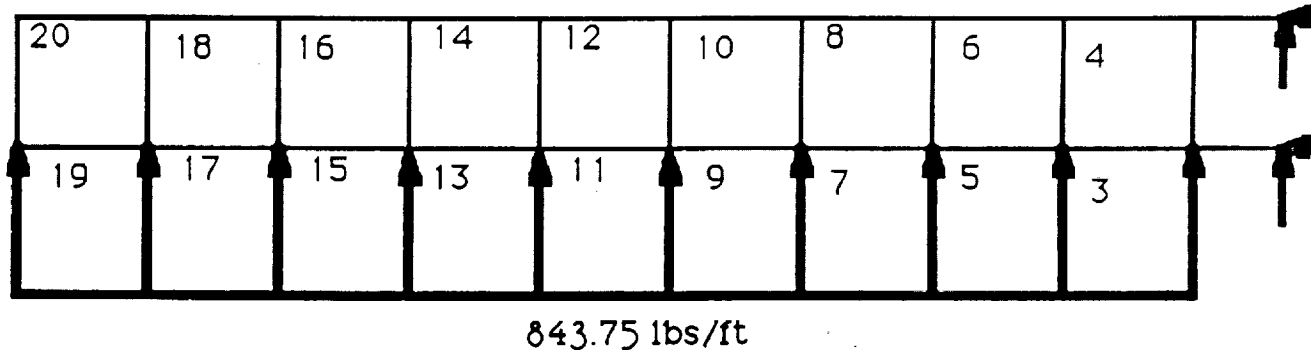


Figure 10-18 STRUCTURAL ANALYSIS MODEL

The CRV/launch vehicle interface was analyzed by assuming that the vertical support members are all perfectly vertical and that the launch loads are purely compressive. This analysis gave static stresses that were 5.56 % of the yield stress and 4.74 % of the ultimate yield strength.

The aft fuselage and thrust structure were also analyzed by approximating pure compression loads. The static stresses incurred on the thrust structure were 14.7 % of the yield strength and 12.5 % of the ultimate yield strength. The static stresses incurred in the aft fuselage members were 7.35 % of the yield strength and 6.27 % of the ultimate yield strengths.

Overall, the structural analysis performed concluded that the fuselage sections of the CRV are structurally sound, but the wing structure will have to be strengthened to support the loads encountered during flight. See Volume 3 for further structural analysis.

11.0 DESIGN OPTIMIZATION AND COST ANALYSIS

Optimization is an attempt to find the best design of a system given certain variables and constraints. Cost analysis involves taking the data from optimization and finding the best value taking into account all considerations such as materials, labor, fabrication, tools, and service and maintenance. There are many different methods of optimizing. The simplest method of optimization is: his intuition. One tends to choose the least complex and expensive components within design tolerances or constraints. This is a simple matter when there is only one or two variables involved, but when the problem becomes more complex there is a need to use optimizing methods based on mathematical analysis.

11.1 OPTIMIZING BACKGROUND

Before discussing the more complex optimizing methods, a background of optimizing must be discussed. Monotonicity entails the determination of how a function increases or decreases with a change in a single variable. For a constraint bound design, there are "exactly as many strict equalities as there are variables" at the optimum. A constraint is an implicit requirement of the design. Constraint bound designs are the easiest type to optimize. In this case, only the monotonicity of the design for optimization is needed to be known. The key to optimizing methods is to create lower bounds involving inequalities derived from estimations. Posynomials are sums of positive power function terms and are required for advance optimizing methods.

11.2 METHODS OF OPTIMIZING

In this report, only three methods of optimization will be discussed: partial optimization, simple lower bounds, and geometric lower-bound constants. For systems with ten or more variables, these methods become difficult to use. Those systems must be optimized by use of computerized numerical methods.

11.2.1 Partial Optimization

Partial optimization uses only the simplest of algebraic manipulations to optimize the design variables. Cost equations are minimized with

respect to a single variable at a time, with the other variables remaining constant. Partial cost will then depend upon all variables except the variable that was minimized out. The minimized total cost is then obtained by minimizing the partial minimum of the optimized variable with respect to the other variables. The advantages of using this method are that only the cost of the minimized variable needs to be considered and that a very simple constraint can be used, such as a design parameter.

11.2.2 Simple Lower Bounds Method

The simple lower bounds method does not necessarily seek the minimum, but finds a lower bound of the system. A lower bound is a constant but a lower bounding function is variable dependent. The first step is to eliminate the small terms of the first approximate function. Then a lower bound is found without the small terms being considered. Total cost is then determined and constrained by the lower bound. The true cost is found by adding in the neglected terms. This cost is the upper bound of the minimum cost. If the cost is determined to lie between the upper and lower bounds of the minimum cost, the the system does not need to be further optimized. A problem arises when the results are lower bounding functions. A better method must then be applied.

11.2.3 Weighted Geometric Mean Method

The weighted geometric mean method is the most accurate of the three bounding methods. The weights can be defined by dividing the terms by the total cost. This method, however, runs into problems when it yields bounding functions instead of constants. This is an indication that the weights were incorrectly chosen and is resolved by finding linearized equations relating the weighted terms. Semilogarithmic derivatives can be used to linearize the function. The sum of the weights must equal unity and be chosen so that the geometric mean is a constant instead of a function. This is done by setting the variables exponents equal to zero.

11.2.4 Summary of Optimization Methods

The optimization method used may depend upon the level of accuracy needed for the system and the level of precision of parameter coefficients. The design is satisfactory when it is indistinguishable from the ideal optimum. The ideal optimum isn't

strictly adhered to, however, for a realistic design. This is in large part affected by standardized sizes available for a given system. From determining the ideal optimum, the optimum standard size is found.

11.3 CRV/Booster Interface Optimization

The CRV/Booster interface will attach the aft of the CRV to the launch vehicle. The interface must be a rigid structure, allowing for no pitch, yaw, or roll of the CRV with respect to the launch vehicle. The proposed design for the interface used a triangular truss structure to hold the CRV mating ring to the Booster mating ring (Figure 11-1).

The vertical members of the interface tend to buckle rather than yield in compression. Therefore, it was determined to increase buckling resistance by varying the outer radii of the circular members without changing the cross-sectional area (ie. by making the members hollow). Since yielding in compression is only dependent upon yield strength (which is a constant for a given material) and cross-sectional area of the individual member, the force required to cause yielding would not change. As illustrated by the following equation, however, buckling is dependent upon the polar moment of inertia which does vary with the outer bar radius:

$$F(\text{buckling})=2.04\pi^2EI/L^2$$

where: E = modulus of elasticity
I = $\pi(R_o^4-R_i^4)/2$ = polar moment of inertia
L = length of bar

$$\text{weight [lbs.]} = \rho L N [R_o^2 - (R_o^4 - F L^2 / (N \sin(\Theta) \sin(\Phi) * 1.02 \pi^3 E))^{.5}] + Q \cdot 9$$

$$L = H \operatorname{cosec}(\Phi) \operatorname{cosec}(\Theta)$$

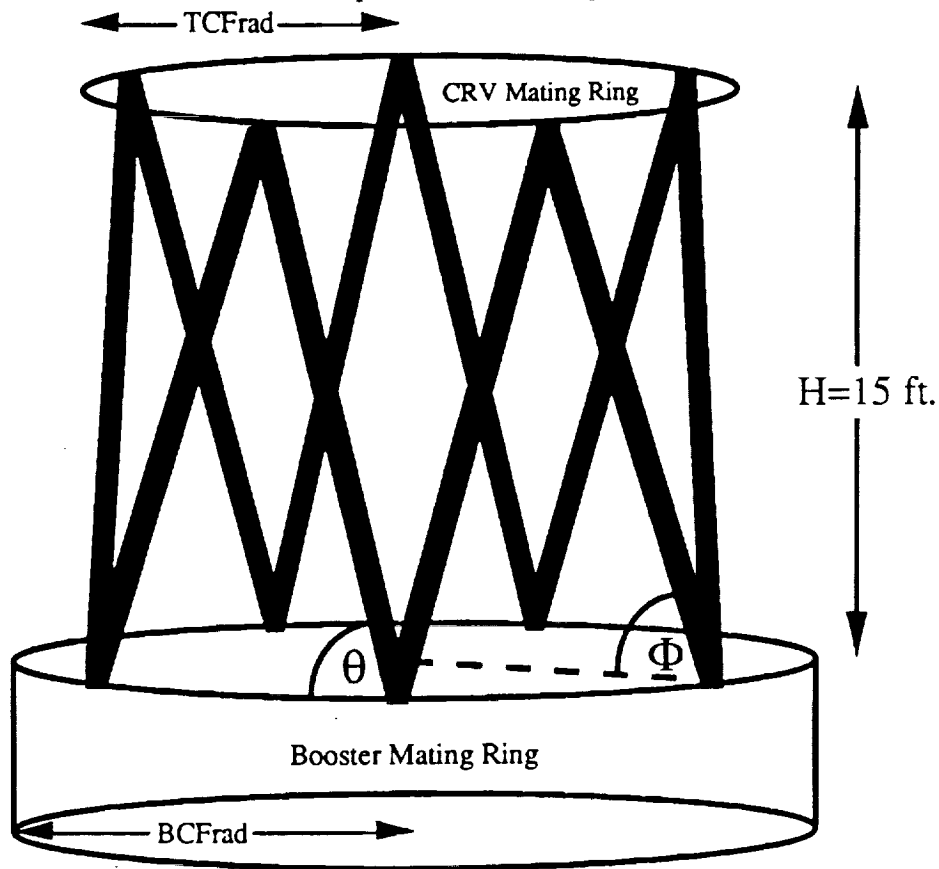
$$\Theta = \operatorname{atan}(BCFrad - TCFrad)^{-1} H$$

$$\Phi = \operatorname{atan}(H \operatorname{cosec}(\Phi) / (9 \pi N / 2))$$

where:

- ρ = density of material
- L = length of individual member
- N = number of members
- R_o = outer radius of member
- F = maximum downward force on interface
- Θ = (as shown in diagram above)
- Φ = (as shown in diagram above)
- E = elastic moduli of material
- H = 15 ft.
- TCFrad = 7.35 ft.
- BCFrad = 9.00 ft.
- Q = node weight coefficient

Figure 11-1 Vertical Members of CRV/Booster Interface and Optimization Equation



This buckling criteria requires that there be only longitudinal forces on the interface members. The nodes (where the members attach the the mating rings) will be rigidly connected (through a

combination of pinning and welding). Since the truss members are long relative to diameter, the nodes can be approximated by pin joints.

The costing equation for the interface is:

$$C = Lw + P_1w + P_2n$$

Where: C = total cost of vertical members and nodes

L = cost per pound for lifting weight of interface material

P₁ = price per pound of fabricated material

P₂ = price per bar of construction (bar and node

n = number of nodes

w = weight of interface

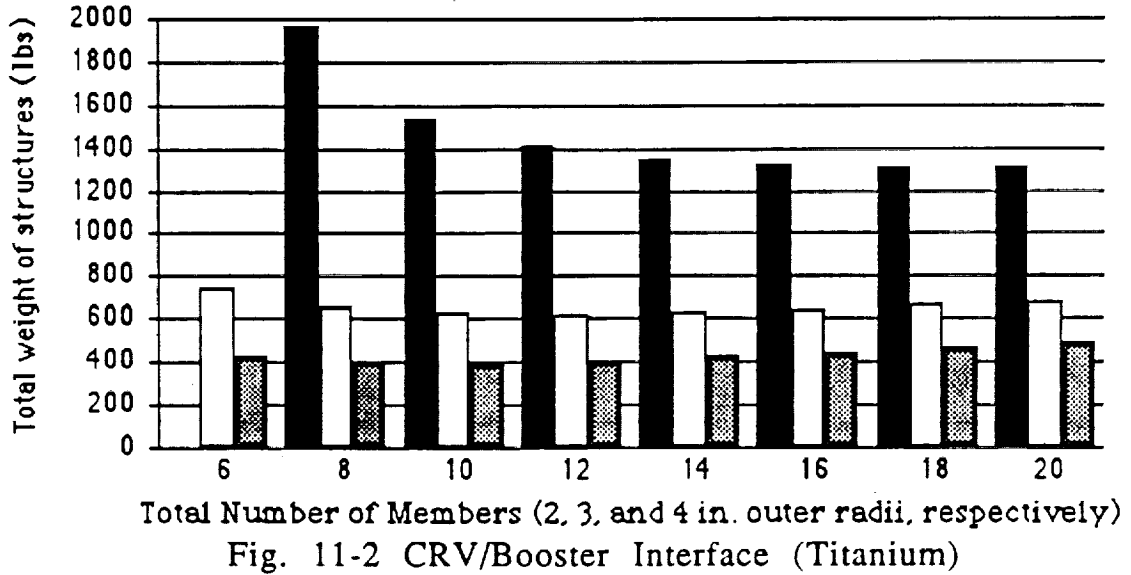
Because it was virtually impossible to determine what the lifting cost per pound will be for the CRV, at this stage of the design, the total weight of the interface will be minimized as weight is clearly the most important single variable involved on a weighted geometric mean basis.

The first stage was to determine how the overall weight of the interface was affected by changing the polar moment of inertia of the members. As shown in Figure 11.2, for a given total number of members, increasing the outer radii of each member decreases the required cross-sectional area to resist buckling and, thus, decreases the total weight of the interface.

In the weight equation, if the two terms are considered as functions of the number of bars only:

$$\text{weight [lbs.]} = \rho LN [R_o^2 - (R_o^4 - FL^2 / (N \sin(\Theta) \sin(\Phi) * 1.02 \pi^3 E))^{.5}] + Q \cdot 9$$

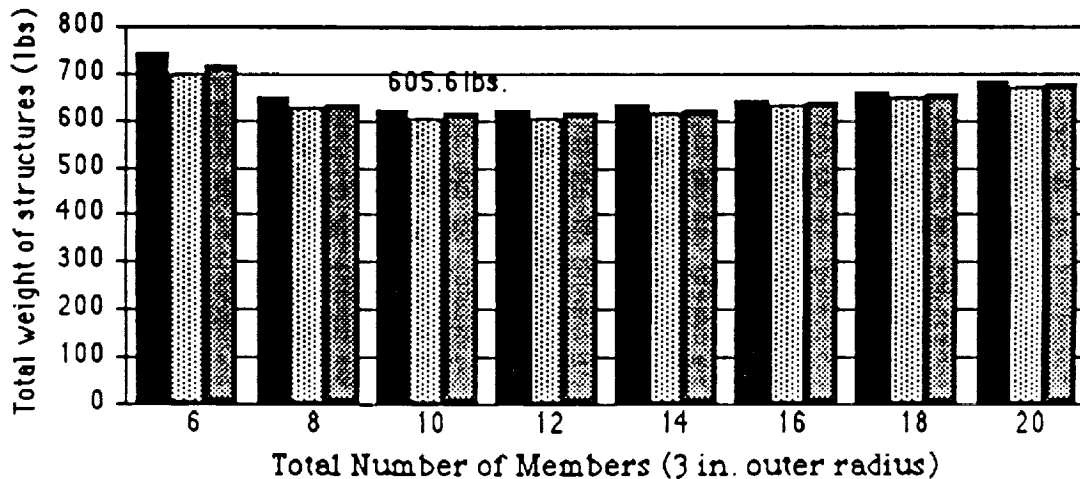
The first term of the weight equation decreases with increasing number of bars, and the second term increases with increasing number of nodes. Because this is a triangular truss, there is one node per member. The relationship between these two terms is illustrated in Figure 11.2. The weight added by the increasing number of nodes increase faster than the decrease in weight for the increasing number of bars.



Three commonly used aerospace materials were chosen for potential interface material:

	density (lb_f/ft^3)	elastic modulus ($10^9 \text{lb}_f/\text{ft}^2$)
Aluminum	172.8	1.440
Stainless Steel	494.2	4.176
Titanium	288.58	2.419

Further estimations required that the maximum force resulting from the CRV's weight ($\text{weight} = (\text{gearth} + \text{gacceleration})M_{\text{CRV}} + \text{Aerodynamic Drag of CRV}$) should not exceed 1,108,000 lb.



11.3.1 CRV/Booster Interface Summary

As shown in Figure 11.3, the optimal material was found to be steel and the optimal number of bars was ten. This yielded a total weight for the interface of 605.6 lbs. Of course, the weights of the terms in the costing function may make another material more cost efficient, but this is unlikely do to steel's relatively low cost and ease of use.

11.3.2 Propulsion System Optimization

Two component systems were chosen to be optimized; the propulsion tanks and the feedlines. On this vehicle, there were three types of engine systems used; OMS, RCS, and cold gas. There was only one OMS system, which consists of three different tanks and feedlines. These tanks were to contain the fuel, oxidizer, and pressurant. There were two RCS systems, which, like the OMS system, consists of three different tanks and feedlines containing the fuel, oxidizer, and propellant. There were two cold gas systems, which consists of only one tank and feedline. For both of the optimization problems, the optimum thickness was found. After finding the ideal optimum, the design optimum was found by using standard sized hardware that most closely matched the ideal.

11.3.2.1 Propulsion Tank Sizing and Materials

The problem was defined as finding the optimum shell thickness of the propulsion tanks. The shape of the tanks were chosen as spherical because this was the most volume efficient shape. The variables in this problem were determined as the radius and the shell thickness. The volume of the tank was dependent upon the amount of fuel required for a given mission. Another constraint was the maximum strength of the tank material. This constraint effects the thickness of the tank's shell. This optimization problem was solved by examining the monotonicity of the problem.

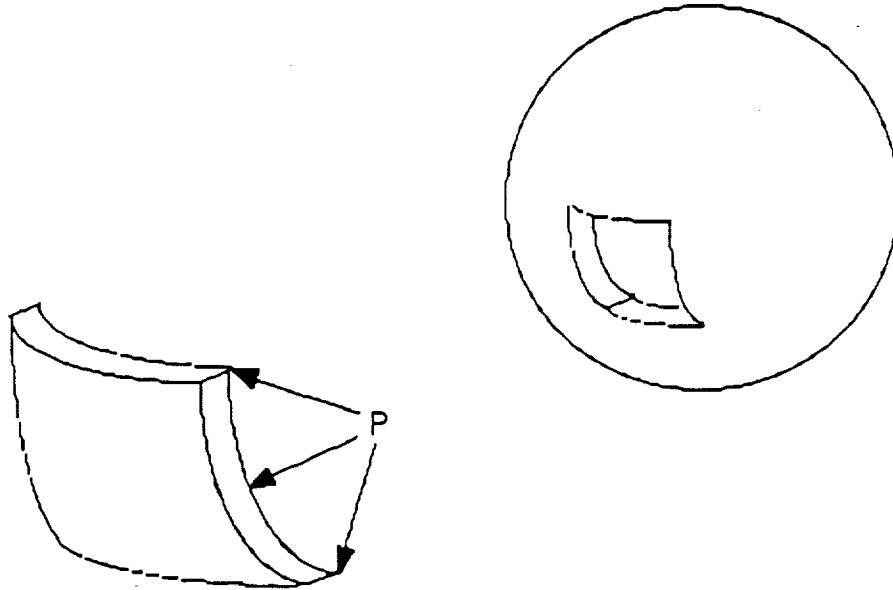


Figure 11-4 Propellant tank

Tank Volume:

$$V_{\text{tank}} = \frac{4}{3} \pi R^3 = M_{\text{prop}}(1+u)/\rho$$

where: V_{tank} = volume inside the tank
 R = inner radius
 ρ = density of the propellant
 u = usage factor = 0.3
 M_{prop} = mass of the propellant

Material Strength:

$$1 \geq 0.5PRt^{-1}\sigma^{-1}$$

where: P = maximum operating pressure inside the tank
 R = inner radius
 t = shell thickness
 σ = material strength (yield stress)

Table 11-1 OMS SYSTEM - tanks

<u>TANK TYPE</u>	<u>RADIUS</u>	<u>STAND. SIZE</u>		
Fuel:	(inches)	(inches)		
	24.441102	24 29/64		
	<u>MATERIAL</u>	<u>THICKNESS</u>	<u>STAND. SIZE</u>	<u>MASS</u>
		(inches)	(inches)	(lbm)
	Aluminum	0.478728	31/64	371.222729
Oxidizer:	Stainless Steel	0.161175	11/64	130.058962
	Titanium	0.233120	15/64	177.805750
	<u>RADIUS</u>	<u>STAND. SIZE</u>		
	(inches)	(inches)		
	24.488136	24 1/2		
Pressurant:	<u>MATERIAL</u>	<u>THICKNESS</u>	<u>STAND. SIZE</u>	<u>MASS</u>
		(inches)	(inches)	(lbm)
	Aluminum	0.479646	31/64	372.633282
	Stainless Steel	0.161484	11/64	130.556317
	Titanium	0.233567	15/64	178.484825
Pressurant:	<u>RADIUS</u>	<u>STAND. SIZE</u>		
	(inches)	(inches)		
	15.611576	15 5/8		
	<u>MATERIAL</u>	<u>THICKNESS</u>	<u>STAND. SIZE</u>	<u>MASS</u>
		(inches)	(inches)	(lbm)
Aluminum	0.305897	5/16	97.804058	
Stainless Steel	0.102987	7/64	33.791269	
Titanium	0.148958	5/32	48.417867	

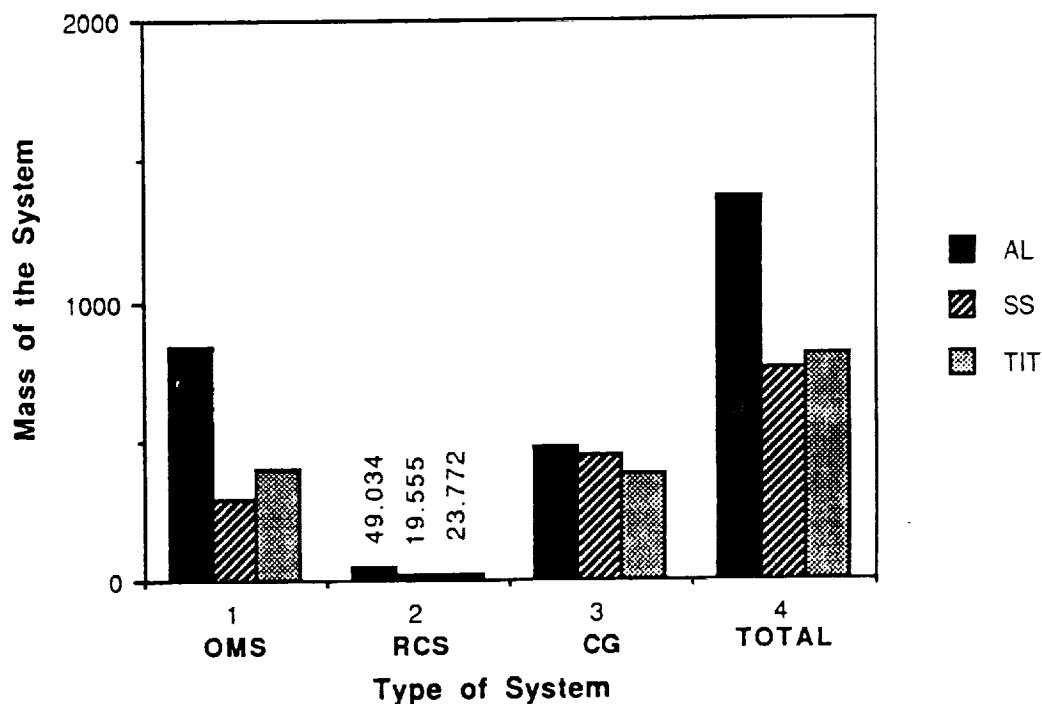
Table 11-2 COLD GAS SYSTEM - tanks

<u>TANK TYPE</u>	<u>RADIUS</u>	<u>STAND. SIZE</u>		
Propellant:	(inches)	(inches)		
	20.913824	20 59/64		
	<u>MATERIAL</u>	<u>THICKNESS</u>	<u>STAND. SIZE</u>	<u>MASS</u>
		(inches)	(inches)	(lbm)
	Aluminum	0.409596	27/64	236.767821
	Stainless Steel	0.137900	9/64	222.718068
	Titanium	0.199455	13/64	188.408524

Table 11-3 RCS SYSTEM - tanks

<u>TANK TYPE</u>	<u>RADIUS</u>	<u>STAND. SIZE</u>		
Fuel:	(inches)	(inches)		
	7.240660	7 1/4		
	<u>MATERIAL</u>	<u>THICKNESS</u>	<u>STAND. SIZE</u>	<u>MASS</u>
		(inches)	(inches)	(lbm)
	Aluminum	0.141936	5/32	10.544648
	Stainless Steel	0.047786	1/16	4.163940
	Titanium	0.069117	5/64	5.216118
Oxidizer:	<u>RADIUS</u>	<u>STAND. SIZE</u>		
	(inches)	(inches)		
	7.254594	7 17/64		
	<u>MATERIAL</u>	<u>THICKNESS</u>	<u>STAND. SIZE</u>	<u>MASS</u>
		(inches)	(inches)	(lbm)
	Aluminum	0.142242	5/32	10.589661
	Stainless Steel	0.047889	1/16	4.181830
	Titanium	0.069266	5/64	5.238504
Pressurant:	<u>RADIUS</u>	<u>STAND. SIZE</u>		
	(inches)	(inches)		
	4.904186	4 29/32		
	<u>MATERIAL</u>	<u>THICKNESS</u>	<u>STAND. SIZE</u>	<u>MASS</u>
		(inches)	(inches)	(lbm)
	Aluminum	0.096052	7/64	3.382774
	Stainless Steel	0.032338	3/64	1.431506
	Titanium	0.046773	3/64	1.431506

Fig. 11-5 Dry Tank Weights



11.3.2.2 Feedlines

The problem was defined as finding the optimum thickness and inner radius (the cross sectional area) of the feedlines. This problem was similar to the propulsion tanks problem but more complex. The constraints on this problem were not as apparent as in the tank problem. The thickness of the line was constrained by the strength of the material used for the feedline. The inner radius was constrained by the maximum allowable pressure drop in the lines and the ratio of the engine's required mass flow rate to the line's allowed mass flow rate. The only variables in this problem were the diameter, shell thickness, and the flow velocity. The mass flow is a fixed quantity because it is a function of the an engine parameter. The lengths of the feedlines were also fixed and were determined by the placement of the tanks and engines, which in turn was determined by the space available in the vehicle. This problem was solved as a constrained posynomial.

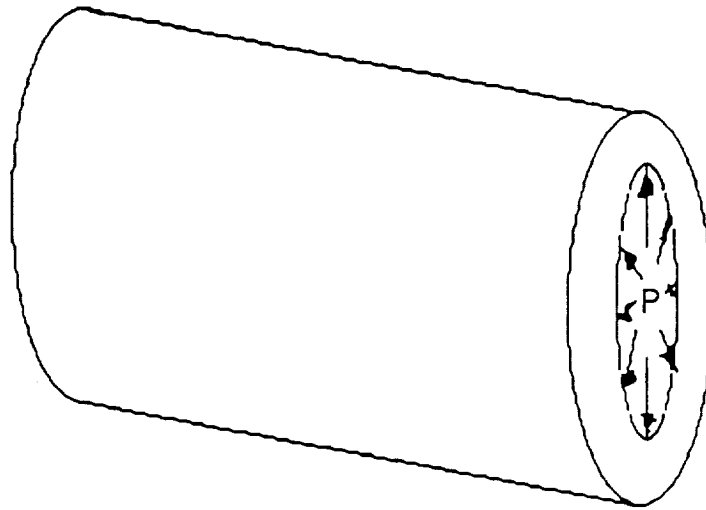


Figure 11-6 Feedline

Material Strength:

$$1 \geq PRt^{-1}\sigma^{-1}$$

where: P = maximum operating pressure inside the tank
 R = inner radius
 t = shell thickness
 σ = material strength (yield stress)

Pressure Drop in a Circular Pipe:

$$1 \geq 8\mu LVR^{-2}(P-P_{\text{chamber}})^{-1}$$

where: L = length of the feedline
 μ = propellant viscosity
 V = velocity of the flow
 P = pressure at the tank outlet
 R = inner radius
 P_{chamber} = pressure at the engine inlet

Mass Flow Ratios (required engine to pipe flow):

$$1 \geq 144m(\rho\pi)^{-1}R^{-2}$$

where: m = required engine mass flow rate

R = inner radius

ρ = density of the propellant

$$R_o t_o \geq \{8mLV(P-P_{chamber})-1R-2\}^{\lambda_1}(PRt-1s-1)^{\lambda_2}\{144m(\rho\pi V)^{-1}R-1\}^{\lambda_3}$$

where:

$$\lambda_1 + \lambda_2 + \lambda_3 = 1$$

$$R: 1 - 2\lambda_1 + \lambda_2 - \lambda_3 = 0$$

$$t: 1 - \lambda_2 = 0$$

$$V: \lambda_1 - 0.5\lambda_3 = 0$$

so:

$$\lambda_1 = 0.5, \lambda_2 = \lambda_3 = 1$$

Table 11-4 OMS SYSTEM - feedlines

<u>LINE TYPE</u>							
Fuel	<u>MATERIAL</u>	<u>R*t</u>	<u>RADIUS</u>	<u>ST. SIZE</u>	<u>THICKNESS</u>	<u>ST. SIZE</u>	<u>MASS</u>
		(inches ²)	(inches)	(inches)	(inches)	(inches)	(lbm)
	Aluminum	0.076919	1.230707	1 15/64	0.054879	1/16	7.156941
	Stainless Steel	0.025896	0.828665	27/32	0.018476	1/32	6.949301
	Titanium	0.037457	1.198616	1 13/64	0.026724	1/32	5.754711
Oxidizer:	<u>MATERIAL</u>	<u>R*t</u>	<u>RADIUS</u>	<u>ST. SIZE</u>	<u>THICKNESS</u>	<u>ST. SIZE</u>	<u>MASS</u>
		(inches ²)	(inches)	(inches)	(inches)	(inches)	(lbm)
	Aluminum	0.109356	1.399752	1 13/32	0.065435	5/64	10.21631
	Stainless Steel	0.036816	1.178108	1 3/16	0.022030	1/32	9.72902
	Titanium	0.053252	1.136044	1 9/64	0.031864	3/64	8.24473
Pressurant:	<u>MATERIAL</u>	<u>R*t</u>	<u>RADIUS</u>	<u>ST. SIZE</u>	<u>THICKNESS</u>	<u>ST. SIZE</u>	<u>MASS</u>
		(inches ²)	(inches)	(inches)	(inches)	(inches)	(lbm)
	Aluminum	0.001169	0.149686	5/32	0.006767	1/128	0.113208
	Stainless Steel	0.000394	0.050394	1/16	0.002278	1/128	0.134248
	Titanium	0.000569	0.072892	5/64	0.003295	1/128	0.096834

Table 11-5 RCS SYSTEM - feedlines

LINE TYPE							
Fuel:	<u>MATERIAL</u>	<u>R*1</u> (inches ²)	<u>RADIUS</u> (inches)	<u>ST. SIZE</u> (inches)	<u>THICKNESS</u> (inches)	<u>ST. SIZE</u> (inches)	<u>MASS</u> (lbm)
	Aluminum	0.01728 1	0.55298 1	9/16	0.026012	1/32	1.63461 0
	Stainless Steel	0.00581 8	0.37233 4	3/8	0.008757	1/64	1.54779 9
	Titanium	0.00841 5	0.53854 2	35/64	0.012667	1/64	1.30956 6
Oxidizer:	<u>MATERIAL</u>	<u>R*1</u> (inches ²)	<u>RADIUS</u> (inches)	<u>ST. SIZE</u> (inches)	<u>THICKNESS</u> (inches)	<u>ST. SIZE</u> (inches)	<u>MASS</u> (lbm)
	Aluminum	0.02060 5	0.65937 5	43/64	0.028404	1/32	1.94386 0
	Stainless Steel	0.00827 1	0.52935 3	17/32	0.010442	1/64	2.17955 4
	Titanium	0.01196 3	0.76565 3	25/32	0.015103	1/64	1.86290 3
Pressurant	<u>MATERIAL</u>	<u>R*1</u> (inches ²)	<u>RADIUS</u> (inches)	<u>ST. SIZE</u> (inches)	<u>THICKNESS</u> (inches)	<u>ST. SIZE</u> (inches)	<u>MASS</u> (lbm)
	Aluminum	0.00026 3	0.03362 8	3/64	0.003207	1/128	0.03589 5
	Stainless Steel	0.00008 8	0.01132 1	1/64	0.001080	1/128	0.03948 5
	Titanium	0.00012 8	0.01637 5	1/32	0.001562	1/128	0.04150 0

Table 11-6 COLD GAS SYSTEM - feedlines

LINE TYPE							
Fuel:	<u>MATERIAL</u>	<u>R*1</u> (inches ²)	<u>RADIUS</u> (inches)	<u>ST. SIZE</u> (inches)	<u>THICKNESS</u> (inches)	<u>ST. SIZE</u> (inches)	<u>MASS</u> (lbm)
	Aluminum	0.00005 7	0.00734 6	1/128	0.001499	1/128	0.00828 3
	Stainless Steel	0.00001 9	0.00247 3	1/128	0.000505	1/128	0.02369 1
	Titanium	0.00002 8	0.00357 7	1/128	0.000730	1/128	0.01383 3

Fig. 11-7 Dry Feedline Weights

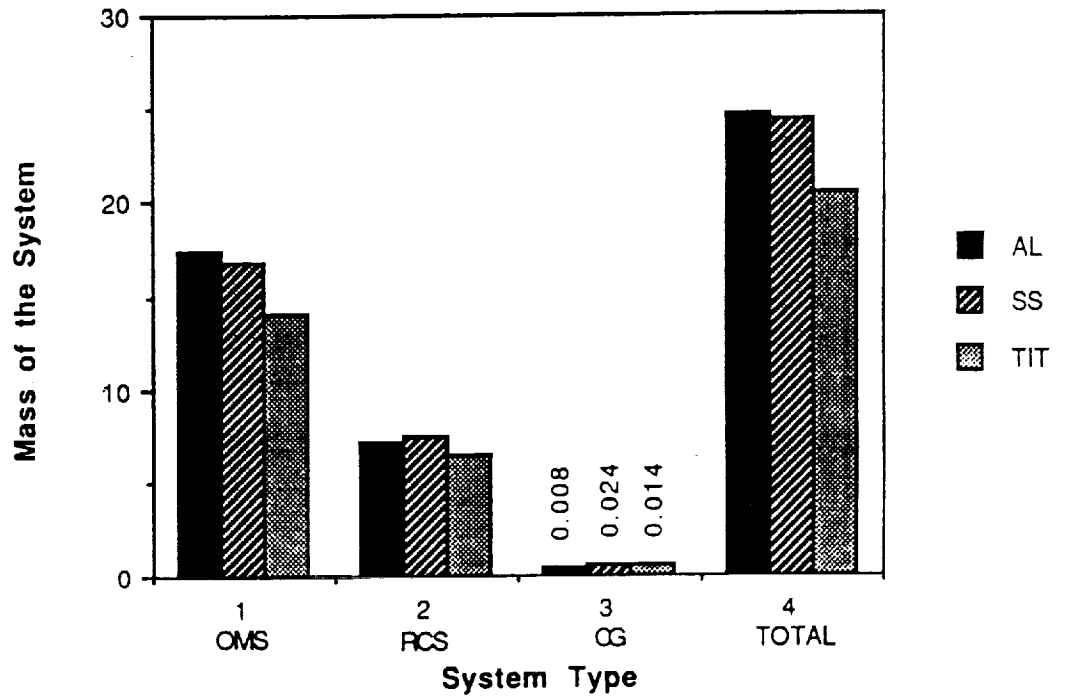
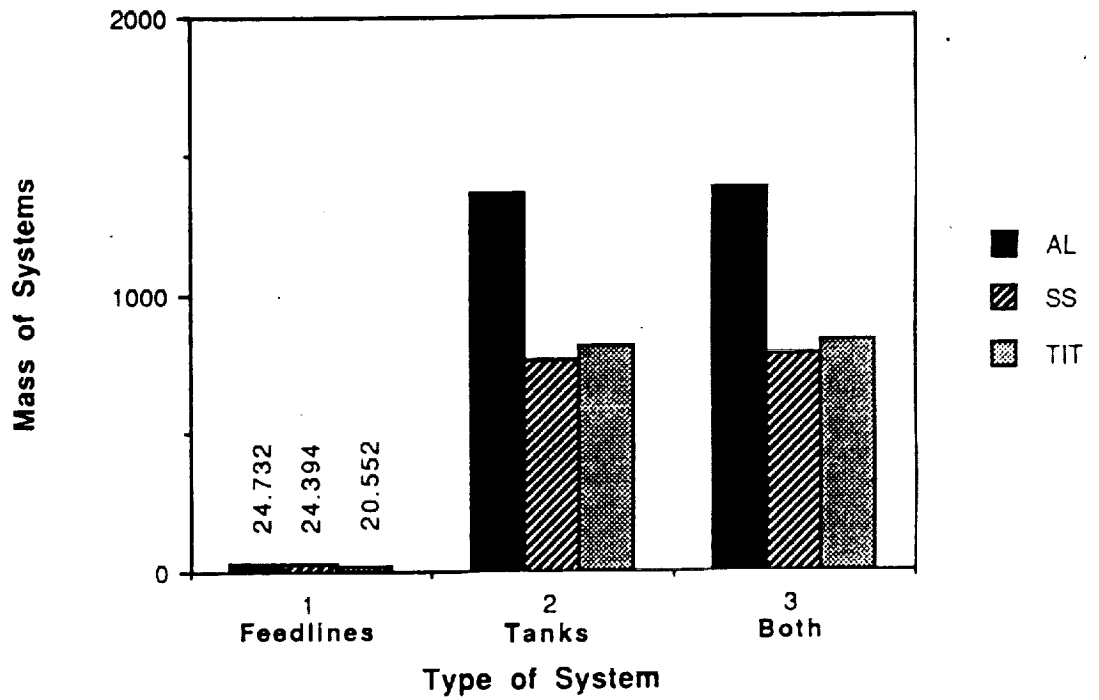


Fig. 11-8 Total Dry Weights of Systems



11.3.2.4 Propulsion System Summary

Only three types of materials were explored for both the propulison tanks and feedlines: aluminum, stainless steel, and titanium. These are the most common materials used in this kind of application. If the most important consideration in choosing material type is the weight, then the feedline material should be titanium. If the cost of the system was more important, then steel would be best. For weight considerations, the tanks should be made out of stainless steel because it is stronger than titanium and aluminum so the thickness of the shells can be made. Stainless steel would also be the least expensive materials to use for the tanks. The smallest standard size was taken to be 1/128th, so that in the case of the cold gas feedlines, aluminum would be the lightest. If the standard size could be less than this value, titanium would be the lightest just like all the other feedlines.

11.4 FURTHER OPTIMIZATION PROBLEMS

Future simple problems for optimization will be booster seperation altitude, thermal protection material, level of avionic redundancy, actuators, and aerodynamic surfaces. A more complex problem is that of the optimal fleet size. The fleet size will be dependant upon all the systems listed above, as well as all aspects of manufacturing and ground operations. As in all optimization problems, the analysis must be continually updated whenever there has been a change in any of the systems.(see Volume 5 for further information)

REFERENCES

- 3.1) Space Shuttle Payload Deployment and Retrieval System. JSC Report.
- 3.2) Space Station Operations Plan. NASA JSC 30201.
- 3.3) OMV User's Guide. MSFC Report .
- 3.4) CRV Payload Exchange.
- 3.5) CRV Alternate Mission Impact Study. NASA JSC 34009.
- 3.6) SSF Def. and Reg. Section 3 Space Station System Requirements. NASA SSP 30000.
- 3.7) Shuttle C/Space Station Assembly Operations Study. MSFC.
- 3.8) CRV Requirements for Docking at SSE. memo to Steve Cook from R.W. Browr..
- 3.9) OMV Quarterly Review 18 July 1989.
- 3.10) Stabilized Payload Deployment System (SPDS).
- 3.11) An Evaluation of Interactive Displays for Trajectory Planning and Proximity Operations. AIAA 88-3963-CP.
- 3.12) SAE Technical Paper Series - Space Station Cupola Definition. SAE 881124.
- 3.13) OMV Mission Operations. AIAA 89-0587.
- 3.14) Aerospace America Designing for Operations and Support. ISSN 0740-722X Vol. 26 Nov 1988 pages. 18-28.
- 3.15) OMV Support Study to ELV's in the Space Station Logistics Operations. TRW Report.
- 3.16) The Effect of Initial Velocity on Manually Controlled Remote Docking of an Orbital Maneuvering Vehicle to a Space Station. AIAA 89-0400.
- 3.17) Fundamentals of Astrodynamics. Bate, Mueller, White. 1971 Dover Publications, N.Y..

- 3.18) Information Summaries, Nasa Launch Vehicles and Facilites.
KSC PMS 018.
- 3.19) MSS Technical Summary. CSA/NASA Joint Program Review. 23
Jan 90.
- 3.20) Abort Capability Assessment of ther Langley Starr (CERV)
Vehicle. Talay, Dr. Theodore A., NASA Langley Research
Center.
- 5.1) Anderson, A. D., Hypersoic and High Temperature Gas Dynamcis.
McGraw-Hill, Inc., New York, 1989.
- 5.2) Calarese, W., Close - Coupled Canard - Wing Vortex Interaction.
AIAA-82-1369, AIAA 9th Atmospheric Flight Mechanics
Conference, San Diego, Ca, 1982.
- 5.3) Gailye, J. W., Kotker, D. J., Conceptual Desing and Analysis of
Hyervelocity Aerospace Vehicles. AFWAL-TR-87-3056,
Volume II, Boeing Aerospace, Seattle WA, February 1988.
- 5.4) Gailye, J. W., Kotker, D. J., Conceptual Desing and Analysis of
Hyervelocity Aerospace Vehicles. AFWAL-TR-87-3056,
Volume IV, Boeing Aerospace, Seattle WA, February 1988.
- 5.5) Gailye, J. W., Kotker, D. J., Conceptual Desing and Analysis of
Hyervelocity Aerospace Vehicles. AFWAL-TR-87-3056,
Volume VI, Boeing Aerospace, Seattle WA, February 1988.
- 5.7) Hale, Francis, Aircraft Performance, Selection and Design.
- 5.8) Kuchta, B. J., Spencer, B. Jr., Aerodyanmics and Flight
Characteristics of Several Variable Geometry Entry Spacecraft
During Subonsic Wing Deployment and Landing. AIAA Paper
No. 69-742, NASA Langley Research Center, General Dynamics
Corporation, 1969.
- 5.9) Powell, D. J., Space Transportation Architectural Study - Final
Phase Study Tasks - Book 3. GDSS-STASS-87-002, General
Dynamics Corporation, 1987.
- 5.10) Nicolai, Lelund, Fundamentals of Aircraft Design. METS Inc.,
San Jose, CA, 1975.

- 5.11) U. S. Standard Atmosphere, U.S. Government Printing Office, Washington D.C., 1962.
- 5.12) Moran Jack, An Introduction to Theoretical and Computational Aerodynamics. John Wiley & Sons, 1984.
- 6.1) Babister, A.W., Aircraft Dynamic Stability and Response. Frankfurt: Permagon Press 1980.
- 6.2) Babister, A.W., Aircraft Stability and Control. Frankfurt: Parmegon Press 1961.
- 6.3) Etkin, Bernard, Dynamics of Flight Stability and Control. John Wiley and Sons Inc. 1982 .
- 6.4) Franklin, G. Feedback Control of Dynamic Sytems. Massachusetts: Addison-West 1986.
- 6.5) Hankey, W.L., Re-Entry Aerodynamics. U.S.: Library of Congress 1986.
- 6.6) Kane, T.,Spacecraft Dynamics. New York: McGraw-Hill 1983.
- 6.7) Kaplan, M. Modern Spacecraft Dynamics and Control. New York: John Wiley & Sons 1976.
- 6.8) Larkin, D., The Space Shuttle Operators Manual. Ballantine Books: New York 1982.
- 6.9) McCormick, B.W., Aerodynamics, Aeronautics, and Flight Mechanics. New York: John Wiley and Sons 1979.
- 6.10) Mooij, H.A., Criteria for Low-Speed Longitudinal Handling Qualities of Transport Aircraft With Closed-Loop Flight Control Systems. Netherlands: Permagon Press 1985.
- 6.11) Nakano, M. M., and Williams, R.L., Space Shuttle On-Orbit Flight Control System. American Institute of Aeronautics and Astronautics, Inc. 1982.

- 6.12) Nelson, R.C., Flight Stability and Automatic Control. New York: McGraw Hill, Inc. 1989.
- 6.13) Nicolai, L.M., Fundamentals of Aircraft Design. San Jose, Calif.: METS, Inc. 1984.
- 6.14) Posbergh, T. A., Linearization of Equations of Motion. 1990.
- 6.15) Rockwell International. Space Shuttle Transportation System Aerodynamic Description and Data Usage, Volume 1.
- 6.16) Rockwell International. Space Shuttle Transportation System Launch Vehicle Airloads Data, Volume 4.
- 6.17) Roskam, J., Airplane Design Part VI: Preliminary calculations of Aerodynamic, Thrust and Power Characteristics. Lawrence, Kansas 1988.
- 6.18) Roskam, J., Airplane Design Part VII: Determination of Stability, Control and Performance Characteristics: FAR and Military Requirements. Lawrence, Kansas 1988.
- 6.19) Schleich, W. T., The Space Shuttle Ascent Guidance and Control. American Institute of Aeronautics and Astronautics Inc. 1982.
- 6.20) Selig, M.S., Airfoils at Low Speeds. Virginia Beach: H.A. Stokely 1989.
- 6.21) Stinton, D., Design of the Aeroplane. Great Britain: Van Nostrand Reinhold Company Inc. 1983.
- 6.22) Wertz, J.R., Spacecraft Attitude Determination and Control. Dordrecht: Kluwer Academic 1978.
- 7.1) Aeroassist Flight Experiment. MSFC Report.
- 7.2) In-House Transportation Studies: Winged Booster Def. MSFC Report.
- 7.3) Reentry Cargo Vehicle. Initial Def., MSFC Report.

- 7.4) Pace Trans. Arch. Study: Final Phase Study Tasks.
GDSSSTAS87002.
- 7.5) Orbiter and Subsystems. Rockwell Report.
- 7.6) Space Shuttle Elect. Power and Avionics. JSC Report.
- 7.7) A Historical Overview of the Elect. Power Systems. MSFC Report.
- 7.8) Cold Plate Specification. ESA Report.
- 7.9) Cold Plates for Spacecraft Applications.
- 7.10) Advanced Thermal Components for Cooling Avionic Syst.
- 7.11) Shuttle-C Avionics: In-House Study. MSFC Report.
- 7.12) Shuttle Orbiter Data. JSC Reports.
- 8.1) Buckling of Hypersonic Aircraft Tubular Panels with Comparison To Experimental Data. Presentation by Dr. William L. Ko.
- 8.2) Development of Ceramic Thermal Protection Materials for Aerobraking Orbital Transfer Vehicles.
- 8.3) High Temperature Properties of Ceramic Fibers and Insulations for Thermal Protection of Atmospheric Entry and Hypersonic Cruise Vehicles.
- 8.4) NASA Contractor Report 4227, Thermal Protection System of the Space Shuttle, June, 1989.
- 8.5) Procedure for Thermal Analysis of Launch Vehicles, MINIVER II.
- 8.6) Miniver II Upgrade for the AVID System.
- 8.7) 3M Flourinert Direct Contact Cooling Medium.
- 9.1) Bentz, M.D., Kotker D.J., Conceptual Design and Analysis of Hypervelocity Aerospace Vehicles. Volume 3-Propulsion. Boeing Aerospace Co., Feb. 1988.

- 9.2) Sutton, George P. Rocket Propulsion Elements, Wiley and Sons, N.Y., N.Y., 1986.
- 9.3) Propulsion Systems Data Book Vol's I, II. NASA Document.
- 9.4) Launch System Data Folder. NASA Document, January 16, 1990.
- 9.5) Journal of Propulsion and Power, February 1990, "Laboratory Testing of Multi-propellant Resisto-jet". Pg. 64-69.
- 10.1) Nayler, J.L, Advances in Space Technology, 1962.
- 10.2) Chun-Yung Niu, Michael, Airframe Structural Design, 1988.
- 10.3) Orbiter and Subsystems, SSV80-1, Rockwell International 1980.
- 10.4) Vaughn, Robert L., Space Shuttle, A Triumph in Manufacturing, 1985.
- 10.5) Abbott, Ira H., Albert, E. Von, Theory of Wing Sections, Duenhoff, 1959.
- 11.1) Wylde, Douglas, Globally Optimal Design, Wiley, 1987.
- 11.2) Warner, Dr. William, Univeristy of Minnesota Facult.